

© 1978

YANIS CHRISTOS YORTSOS

ALL RIGHTS RESERVED

ANALYTICAL MODELLING OF OIL RECOVERY BY
STEAM INJECTION

Thesis by

Yanis Christos Yortsos

In Partial Fulfillment of the Requirements
for the Degree of
Doctor of Philosophy

California Institute of Technology
Pasadena, California

1979

(Submitted August 17, 1978)

ACKNOWLEDGMENTS

The author wishes to express his sincere appreciation to his research advisor Professor G. R. Gavalas for his guidance, patience, thoughtful suggestions and encouragement during the preparation of this thesis. The moral support and valuable advice of Professors J. H. Seinfeld and L. G. Leal are gratefully acknowledged.

The author feels indebted to the California Institute of Technology and the Chemical Engineering Department for financial aid during the years of his graduate study.

The friendly atmosphere created by the graduate students and the personnel of the Chemical Engineering Department was thoroughly enjoyed. In particular, the daily companionship of the author's colleagues Ajit Yoganathan and Ken Bencala had a definite moral contribution to the accomplishment of the present work. Appreciation and special thanks are expressed to Ms. Kathy Lewis for her patient, understanding and skillful typing of this manuscript.

The friendly, stimulating and, at times, adventurous relationships with a number of the author's friends has been and will hopefully remain a source of human understanding and inspiration. Particular gratitude is expressed to Dora and Thanassis who have certainly shared with the author moments of happiness, concern and creativity.

Forever appreciating their love and concern, it is a natural and spontaneous thing for me to dedicate this thesis to my parents.

ABSTRACT

This dissertation is concerned with the mathematical modelling of oil recovery by steam injection using analytical techniques.

An integral method for generating approximate solutions to the one- and two- (three-) dimensional steam injection processes is presented. Due to the qualitatively different character of the problem the one- and two- (three-) dimensional cases are examined separately.

The applicability of the method for the determination of the rate of growth of the steam zone volume in one-dimensional systems is considered. An extensive study of the heat transfer in the surroundings and the hot liquid zone is carried out to complement the one-dimensional implementation of the technique. The resulting class of moving boundary problems and their methods of solution are discussed in detail. The results obtained are then combined with the integral technique to derive upper and lower bounds, asymptotic solutions and approximate solutions to the rate of growth of the steam zone. The important physical parameters are identified and their significance in the design of the process is outlined. In particular, the very important effect of heat transport in the surroundings and the hot liquid zone is fully accounted.

For two- (three-) dimensional systems, a more detailed version of the integral method is developed to account for the effect of gravity segregation in the determination of the steam front shape. A non-linear partial differential equation that describes the evolution of the steam front shape in gravity dominated systems is derived. The significance of the various physical parameters in the performance of a three-dimensional steam

injection process is discussed by providing a solution to the equation derived, in the limit of predominantly viscous flows.

A critical evaluation of the existing analytical models is presented and the regions of their validity established. The potential of the techniques developed, particularly in the heat transfer area, to treat a class of in-situ thermal methods is also clearly indicated.

Table of Contents

	<u>Page</u>
ACKNOWLEDGMENTS	<i>i</i>
ABSTRACT	<i>ii</i>
Chapter I. Introduction	1
Chapter II. Mathematical Formulation. The Integral Balance Approach	21
2.1 Introduction	21
2.2 Some Basic Definitions and Description of the Process	21
2.3 Mathematical Formulation	26
2.3.1 The Differential Equations	26
2.3.2 The Boundary Conditions	31
2.3.2.1 Interfacial Conditions	31
2.3.2.2 A Pressure Dynamic Condition	36
2.3.2.3 Boundary and Initial Conditions	38
2.4 The Integral Balances	39
2.4.1 Introduction	39
2.4.2 Volume (Area) Integration	41
2.4.3 The Constant Steam Zone Temperature Approximation	44
2.4.4 Area (Line) Integration	47
2.5 Dimensional Analysis	52
2.6 Conclusions	55
Chapter III. Heat Transfer Considerations	56
3.1 Introduction	56
Part A. Heat Transfer in the Surrounding Formations	56
3.2 Method of Approach	56
3.2.1 Calculation of the Heat Flux	58
3.2.2 Hot Water Injection	62

	<u>Page</u>
3.2.3 Steam Injection. Continuously Advancing Steam Front	62
3.2.4 Steam Injection. Arbitrary Propagation of the Steam Front.	64
3.3 Derivation of Bounds on the Heat Fluxes	66
3.3.1 Bounds on the Heat Losses to the Surrounding Formations.	66
3.3.2 Bounds on the Heat Fluxes to the Hot Liquid Zone	68
Part B. Heat Transfer in the Hot Liquid Zone.	69
3.4 Method of Approach	69
3.5 One-Dimensional Heat Transfer in the Hot Liquid Zone by Conduction, Convection, with a Steady or Moving Boundary but with No Lateral Heat Losses.	72
3.5.1 Constant Boundary Velocity.	73
3.5.1.1 Constant Boundary Velocity, Linear Geometry.	73
3.5.1.2 Constant Boundary Velocity, Cylindrical Geometry	76
3.5.2 Convective Term a Function of Time.	78
3.5.2.1 A Particular Solution. Linear Geometry.	78
3.5.2.2 Cylindrical Geometry	81
3.6 One-Dimensional Treatment of the Two-Dimensional Heat Transfer.	82
3.6.1 The Quasi-Steady State Approximation (No Lateral Heat Losses).	87
3.6.2 The Zero Net Convection Approximation (Includes Lateral Heat Losses).	88
3.7 One-Dimensional Heat Transfer in the Hot Liquid Zone by Convection, a Steady or Moving Boundary and Lateral Heat Losses (No Horizontal Conduction) . .	89
3.7.1 General Formulation	89
3.7.2 Solution of the Integro-Differential Equation (3.52)	91
3.7.3 Fixed Boundary.	96

3.7.4	Constant Front Velocity	99
3.7.5	Front Velocity of the form	
	$v_D(t_D) = \frac{\alpha}{\sqrt{t_D} + \alpha^2}$	103
3.8	One-Dimensional Heat Transfer by Convection, Conduction, Lateral Heat Losses and a Steady or Moving Boundary	107
3.8.1	General Formulation	107
3.8.2	Fixed Boundary, Arbitrary R	109
3.8.3	Constant Boundary Velocity, Steady States for Arbitrary R.	114
3.8.4	R = 1, Arbitrary Velocity	122
	3.8.4.1 Fixed Boundary	124
	3.8.4.2 Constant Front Velocity.	124
	3.8.4.3 Front Velocity of the form	
	$v_D(t_D) = \frac{\alpha}{\sqrt{t_D}}$	127
3.9	Conclusions.	129
Chapter IV.	Application to One-Dimensional Reservoirs.	132
4.1	Introduction	132
4.2	General Considerations	133
	4.2.1 Reformulation of the Integral Balances.	133
	4.2.2 The Marx-Langenheim (1959) and the Mandl-Volek (1969) Approaches	137
4.3	Upper Bounds	140
	4.3.1 Upper Bounds Derivation	140
	4.3.2 Variable Injection Rates.	149
	4.3.2.1 Square Pulse Injection Rates	149
	4.3.2.2 Two-Level Injection Rates.	153
	4.3.3 Constant Injection Rates.	156
4.4	Lower Bounds	170
	4.4.1 Asymptotic Behavior of a Lower Bound at Constant Injection Rates	170
4.5	Asymptotic Solutions	172
	4.5.1 Introductory Remarks.	172
	4.5.2 Large Times Behavior at Constant Injection Rates.	172

	<u>Page</u>
4.5.2.1 Linear Geometries	176
4.5.2.2 Cylindrical Geometries	180
4.5.3 Small Times Behavior at Constant Injection Rates	182
4.5.3.1 Modified Upper Bounds. $R, Pe \gg 1$	184
4.6 Approximate Solutions.	185
4.6.1 The Quasi-Steady State Assumption	185
4.6.2 Numerical Solution at Constant Injection Rates	189
4.7 The Saturation Distribution Inside the Hot Liquid Zone.	194
4.7.1 Introduction.	194
4.7.2 Theoretical Considerations.	194
4.7.3 Oil Saturation at its Residual Value.	197
4.7.4 Heat Losses Bounded from Below.	202
4.7.5 Heat Losses Bounded from Above.	213
4.7.6 Additional Remarks.	218
4.8 Conclusions.	219
Chapter V. Application to Two-Dimensional Reservoirs.	221
5.1 Introduction	221
Part A. Integral Characterization of the Steam Zone Growth.	221
5.2 Three-Dimensional Reservoirs with Vertical Fronts (Thin Reservoirs).	221
5.3 Three-Dimensional Fronts with One Degree of Symmetry (Rectangular or Radially Symmetric Geometry)	225
5.3.1 Reformulation of the Integral Balances	225
5.3.2 The Assumption of Uniform Propagation	228
5.3.3 Vertical Fronts	231
5.3.4 Separable Fronts	231
5.3.5 Parabolic Displacement.	243
Part B. Determination of the Steam Front Shape.	248
5.4 Introductory Remarks	248
5.5 Mathematical Formulation	249
5.5.1 A Momentum Integral Balance	255

	<u>Page</u>
5.5.1.1 The Dupuit Approximation	255
5.5.1.2 The Dynamic Boundary Condition	256
5.6 Derivation of the Governing Partial Differential Equations	259
5.6.1 The Thermal Energy Equation	259
5.6.2 The Steam Mass Equation	265
5.7 Methods of Solution of the PDE for the Steam Front	269
5.7.1 Predominantly Horizontal Flows.	269
5.7.2 Stability Criteria. Stable Displacement.	271
5.7.3 A Viscous Solution Using Lower Bounds for the Heat Losses	276
5.7.4 Neuman's (1975) Model	287
5.8 Conclusions.	289
Chapter VI. Concluding Remarks	292
References	300
Nomenclature	310
APPENDIX I	316
APPENDIX II.	318
APPENDIX III	320
APPENDIX IV.	321
APPENDIX V	325
APPENDIX VI.	327
APPENDIX VII	330
APPENDIX VIII.	332
APPENDIX IX	334
APPENDIX X	339

Chapter I. Introduction

The upsurge of reservoir engineering activity can be associated with the year that the U.S. became a net importer of crude oil: 1948. The competition of relatively low cost foreign oil, together with the rising cost of finding and developing new reserves, led the oil industry to increase its research efforts to improve recovery from existing fields. Although these forces still play a role, an awareness of the coming hydrocarbon shortage has been a more dominant force, in recent years, not only in improving recovery efficiencies but also in obtaining fluid fuels from organic solids such as oil shale and coal. The importance attached to an increase in the low recovery efficiencies ($\sim 30\%$), that are so far obtained from the average oil reservoir (Figure 1), is emphasized in a recent study by Doscher and Wise (1976), who concluded that development of more efficient recovery schemes is seen to have comparable importance to exploration in frontier areas. Thus, they point out that the erstwhile new frontier, now peaking out, Gulf of Mexico, will contribute 6.3 billion bbl of estimated ultimate crude oil while an increase in recovery efficiency of only two percentage points would add a reserve of slightly more than 8 billion bbl.

During the production history of a newly discovered reservoir, the various steps that are commonly followed are shown in a chronological order in Figure 2. Initially, oil flows out of the reservoir under its own pressure (or some other inherent natural drive) until the production rates are reduced to levels of insignificant recovery. Under natural pressure (primary recovery), oil wells generally yield only about 20% of

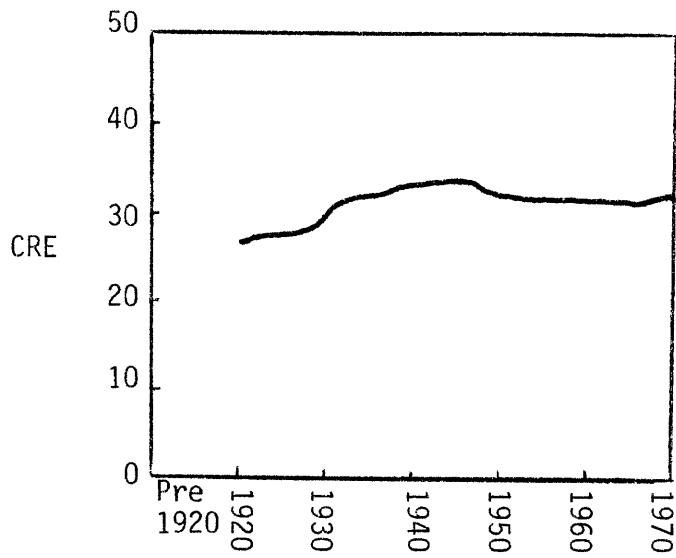


Figure 1. Cumulative Recovery Efficiency (CRE)
[Doscher and Wise (1976)].

the oil originally in place (OOIP). This yield can be further increased to about 30% by the subsequent injection of water, in a secondary recovery operation (waterflooding), that drives another portion of the oil out of the reservoir. Today, roughly half of all U.S. production depends on waterflooding [Bus. Week (1976)]. An estimated 70% of OOIP remains under the ground after the combined application of the above conventional recovery techniques. A very considerable challenge then exists to pinpoint factors that limit oil recovery and to find solutions that permit economic production of much of this unrecovered oil.

Although any improvement in production technology can lead to lower operational costs and thus to increased oil recovery, a great deal of research has been directed towards supplementary displacement processes which offer improvement over conventional primary and secondary techniques. To be of interest, such an "enhanced oil recovery (EOR)" process must satisfy the following requirements: (1) It must have the capability for mobilizing oil that does not respond to conventional methods. (2) It should provide a high volumetric sweep efficiency. (3) It must have an economically attractive application. Currently, the vast majority of EOR processes which satisfy these conditions are based on fluid injection. To understand the growth and applicability of fluid injection processes, we will briefly discuss the recognition and appreciation of factors controlling unrecovered oil.

Unrecovered oil may be left within individual pores, within clusters of pores containing relatively more oil than adjacent portions of the formation, and in bypassed volumes of the reservoir. When the oil within the pores is disconnected, it is trapped by capillary forces,

which in general correspond to pressure differences across the curved interface between two immiscible liquids, and are in turn affected by the physical properties of the liquid and the rock. Low recovery resulting from the bypassing of clusters of pores by an advancing front, is a consequence of capillary trapping and viscous fingering (unstable displacement due to inhomogeneities) and is more pronounced at higher values of the oil/water viscosity ratio. On a much larger scale, unrecovered oil exists in regions that remain unflooded at the time the flood is terminated. This gross bypassing is affected by the viscosity ratio, gravity and capillary forces. A detailed description of these phenomena can be found in any book on fluid flow through porous media [e.g., Bear (1972)]. For a concise literature review on the subject, the reader is referred to Prats and Miller (1973).

The prime target of the fluid injection based EOR processes is to eliminate the forces that control unrecovered oil. There is currently no exact procedure for predicting the magnitude of the above factors, for any given rock, and there is no assurance that a particular fluid injection will succeed in any one reservoir. But for any set of reservoir conditions, there are some processes that are more likely to succeed than others. Thus, depending on a combination of the reservoir characteristics, geometry and location, oil properties and operational availability, a variety of enhanced (tertiary) recovery methods have been developed such as miscible (CO_2) flooding, chemical (polymer or surfactant) injection and thermal flooding (Figure 2). With the exception of thermal methods, EOR production today exists on a small and

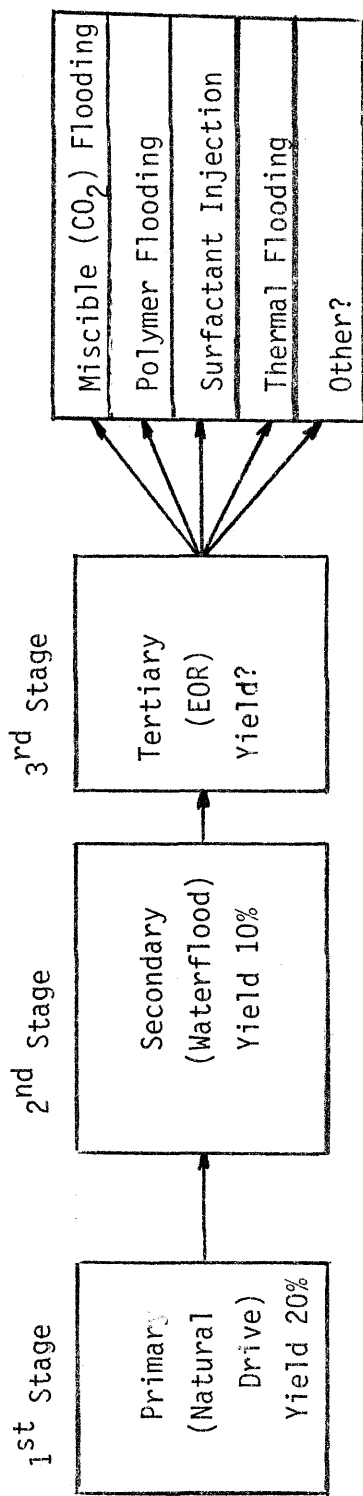


Figure 2. Oil Recovery Stages.

rather experimental scale. A good overview of the present status of EOR processes, and their applications in laboratory and field tests, is provided by the above-mentioned article of Prats and Miller (1973). A very considerable amount of research is still being conducted in the area of enhanced recovery. These efforts, prompted by continuously increasing concern about shrinking reserves and rising demand, aim, under optimal conditions, to double the U.S. present proved reserves of 32.7 billion bbl [Bus. Week (1976)]. (See also Figure 3.)

For the vast deposits of very heavy oils throughout the world, thermal recovery is the most efficient if not the only practical, enhanced recovery method. Because of the low mobility of the oil in such reservoirs, recoveries and production rates are generally low. Even in the early stages of the oil industry, it has been recognized that, due to the strong temperature dependence of oil viscosity (see Figure 4), heating heavy crude oils would enormously increase their mobility and significantly improve the performance of the recovery. With this objective, a variety of thermal techniques have since been developed, that can be generally classified into two broad categories:

- (1) Those in which the heat is injected into the reservoir from an external source.
- (2) Those in which the heat is generated in situ.

External heat injection can be carried out in two ways. The first is simple well heating to increase recovery rate, and consequently, the economic life of a well. The second method is the injection of a hot fluid, such as hot water (hot waterflood) or steam (steam injection and steam stimulation). The in situ method of heat generation (in situ

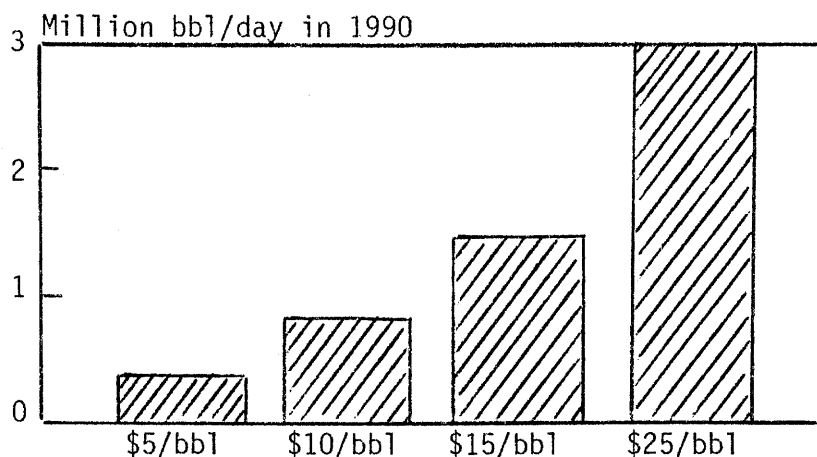


Figure 3. Potential EOR Rates from Known Fields.
 Notes: Oil prices in 1976 constant dollars.
 Recoveries calculated on 10% minimum rate of return. Figures shown represent mean of expected results. [Source: "tic facts", J. Pet. Tech. (May 1977) 520.]

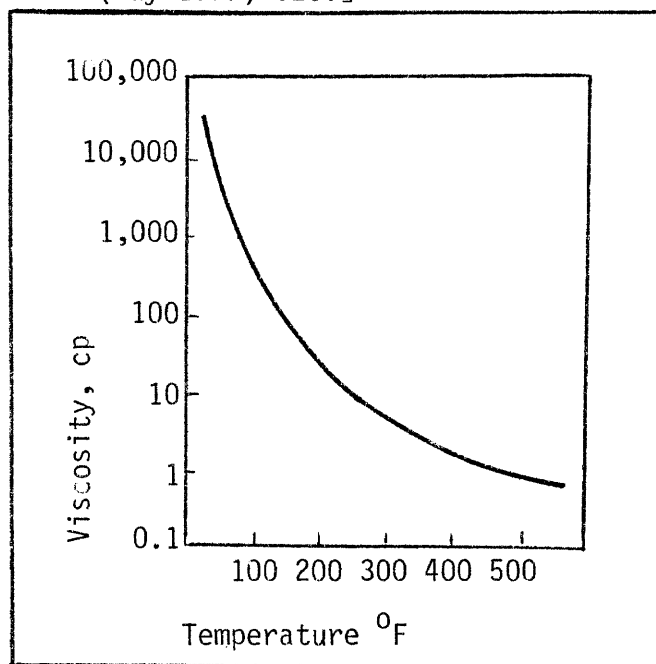


Figure 4. Universal Temperature-Viscosity Chart

[Source: "Thermal Recovery Handbook", World Oil, Houston (1969).]

combustion) involves injection of air (dry or wet) that burns a part of the hydrocarbons in place to provide the necessary heat. Combustion gases and a steam zone formed ahead of the combustion front displace oil to the production well. (Figure 5)

Thermal recovery techniques are currently being conducted in many parts of the world, including U.S., Canada, Venezuela and Holland. At today's prices of crude oil, they are considered to be the most economical EOR methods (see also Fig. 6). In numbers of 1973, at least 140,000 B/D, or 15 percent of California's production was attributed to these recovery processes. Steam stimulation (injection into and production from same well) has been the most popular among thermal recovery processes. However, experience has shown that the response to stimulation diminishes with successive cycles. Consequently, steam drive (injection and production at different wells) becomes of interest with decreasing economic attractiveness of the stimulation phase. Currently, steam injection is being applied on a commercial scale in California and Venezuela. By contrast, commercial interest in in situ combustion has remained at a relatively low level as compared to steam injection, although a modification that involves injection of air and water (wet combustion) is still receiving considerable industry attention.

From a fundamental viewpoint, the thermal recovery processes are perhaps the most complex, since their description entails, in addition to the usual hydrodynamic and interfacial phenomena common to other displacement processes, a detailed accounting for thermal energy and chemical reaction kinetics. These hydrodynamic, energy, and reaction kinetic factors are, in general, coupled together and a complete

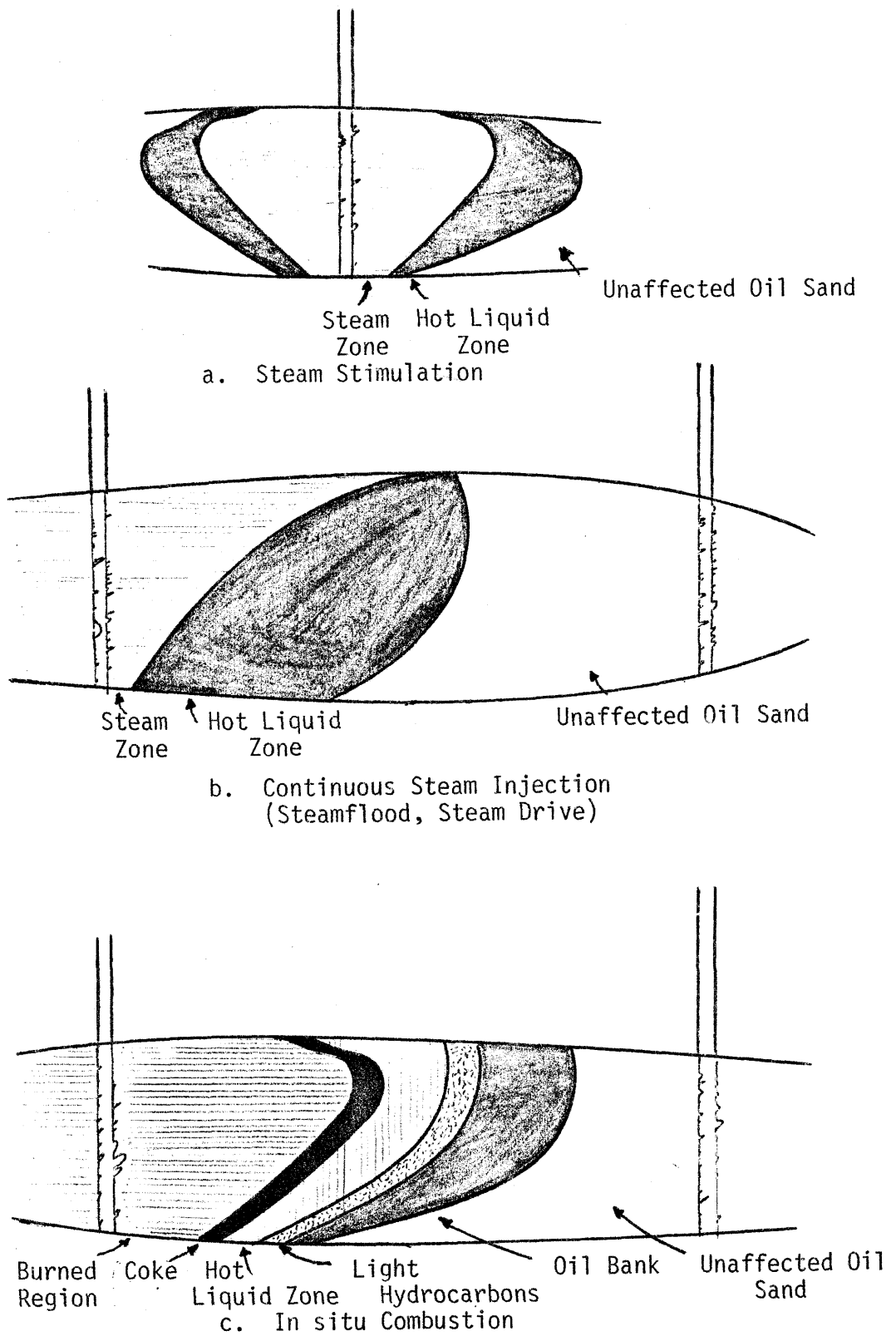


Figure 5. Schematic Representation of Thermal Recovery Processes.

description of the thermal recovery process would necessitate their simultaneous consideration. To elucidate basic mechanisms of thermal recovery, a large number of mathematical, laboratory and field studies have been undertaken [SPE Repr. Ser. (1972)]. A detailed discussion of the current status of steam injection follows. For the reader interested in the other thermal techniques, the articles by Wilson et al. (1958), Gottfried (1965), Dietz and Weijdema (1968) and Beckers and Harmsen (1970), in the area of in situ combustion, and by Boberg and Lantz (1966), Clossman et al. (1970) and Niko and Troost (1971) in the area of steam stimulation, are an excellent source of reference.

The steam injection process (steamflood, steam-drive) is quite complex, and defies an exact description. As soon as steam injection begins, the leading edge of the steam front starts advancing into the originally cool reservoir. Simultaneously, part of the steam condenses and a bank of water and displaced oil forms. The reservoir may then be divided in two regions separated by a moving boundary: (1) a region occupied by steam (steam zone) and (2) a region containing the displaced fluids, oil and water (hot liquid zone). The second region, in turn, consists of a hot zone and an initial cold zone [see Figure 7 and Wu (1977)].

The main elements of continuous steam injection, as a displacement process, were thoroughly analyzed in a landmark paper by Willman et al. (1961) who reported experimental studies and identified the principal mechanisms responsible for the enhanced oil recovery as: (1) thermal expansion of the displaced fluids, (2) viscosity reduction of oil and (3) steam distillation. They remarked that although the first two would

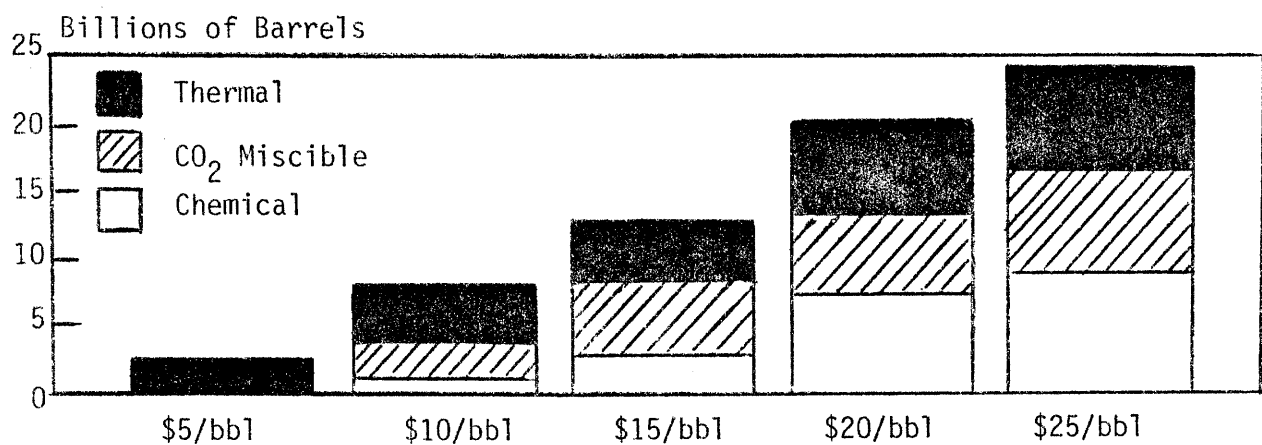


Figure 6. Incremental Ultimate EOR from Known U.S. Fields.
Source and Notes as in Figure 3.

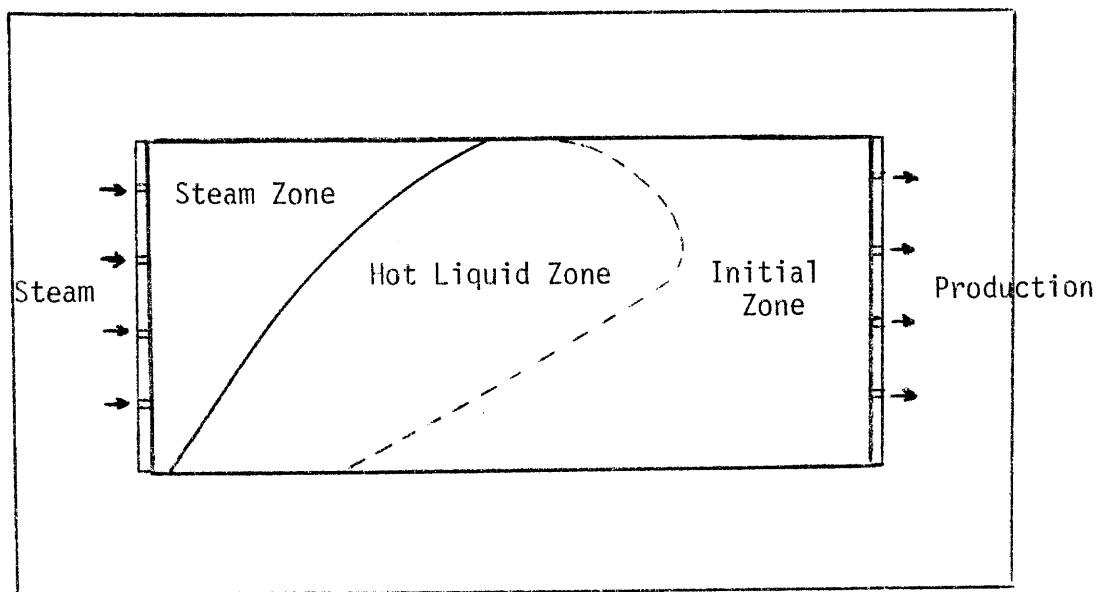


Figure 7. Regions of Two-Dimensional Steam Drive.

also enhance recovery in a hot waterflood, they are more effective with steam due to its lower density (see also Table 1). The displacement mechanism in the hot liquid zone was further elucidated by the investigations of Edmonson (1965), Poston et al. (1970) and Weinbrandt et al. (1975) concerning the temperature effects on the oil-water relative permeabilities. The results of Weinbrandt et al. (1975) indicated that the relative permeability to oil increases while the absolute permeability and the residual oil saturation decrease with temperature increase. The resulting effect on oil recovery has not yet been established. The significance of steam distillation on the performance of a steamflood is also still debatable. Willman's experimental work showed that distillation functions as a recovery mechanism within the steam zone, for light crude oils, and this conclusion was further supported by Johnson et al. (1971) and Wu (1977). By contrast, inclusion of distillation effects in a numerical simulation by Coats (1976) resulted in only moderately increased oil recovery, which was further shown to be very sensitive to the equilibrium values of the distillable component. In three-dimensional reservoirs of considerable thickness, the density difference among steam, water and oil generates another important steamflood mechanism, that was not detected by Willman et al. (1961), and is known as gravity segregation. As observed in field trials by Blevins et al. (1969) and Blevins and Billingsley (1975) and in laboratory experiments by Baker (1973), steam channels to the top and bypasses a large portion of the original oil (Figure 7) with a pronounced effect in the performance of a steam drive.

The aforementioned mechanisms that make oil displacement more effective were further validated and extended by the additional laboratory

Steam Injection Pressure (psig)	Recovery Percent OOIP			
	Core 11 Crude D		Core 12 Crude B	
	(520°F) 800	(327°F) 84	(520°F) 800	(327°F) 84
1. Hot Waterflood Recovery (includes viscosity reduction and swelling)	71.0	68.7	68.7	66.0
1a. Recovery Due to Gas Drive	3.0	3.0	3.0	3.0
2. Extra Recovery Due to Steam Distillation	18.9	15.6	9.3	4.9
3. Predicted Recovery Based on 1, 1a and 2	92.9	87.3	81.0	73.9
4. Actual Recovery by Steam	97.6	91.9	84.0	77.6
5. Recovery Improvements Due to Solvent-Extraction Effects	4.7	4.6	3.0	3.7

Evaluation of Mechanisms Contributing to Steam Recovery
[Willman et al. (1961)]

Table 1

experiments of Baker (1969) and Ozen and Farouq (1969) and the field tests of van Dijk (1968), de Haan and Shenk (1969), Bursell (1970), Volek and Pryor (1972), Hearn (1972), Hall and Bowman (1973) and Smith et al. (1973). In summary, one can presently identify the main steam-flood mechanisms as: steam displacement, steam distillation and gravity segregation, in the steam region; viscosity reduction, thermal permeability variation, thermal expansion and gravity segregation, in the hot liquid region.

Along with laboratory and field experiments, mathematical models were sought to aid in understanding and designing the complex steamflood process. A mathematical model can reveal the process dynamics and show the relative importance of various process variables, although this ability may be often limited by restrictive assumptions. Furthermore, the relatively high cost of the injected fluid and the risks involved in the large scale operation of steam injection requires a careful and imaginative project design. To a varying degree of success this can be achieved by the most useful tool of mathematical simulation.

The engineering evaluation of steamflood processes is based mainly on a simplified mathematical description of reservoir heating by hot fluid injection presented by Marx and Langenheim (1959). This theory was subsequently used by Willman et al. (1961) to determine the growth of the steam zone, provided the flow of heat from the steam zone into the hot liquid zone ahead of the condensation front is neglected. This method of solution, in spite of its restrictive assumptions, has found considerable applications in calculating steamflood performance. Mandl

and Volek (1969), in a combined theoretical and experimental study, were the first to call attention to the fact that neglect of heat transport into the hot liquid zone in the Marx-Langenheim model leads to over-optimistic results regarding the steam zone volume and the recovery rates. By further considering some aspects of the heat transport, they were able to develop a slightly improved approximate description of the steam zone growth based on approximate upper and lower bounds to the exact solution of the problem.

These early efforts in mathematical modelling of steam injection focused mainly on approximately simulating the heat flow in geometries where the process variables are allowed to vary along one direction. Thus, they did not account for the distribution of the various phases in the two regions and for the important effects caused by gravity segregation. To account for the fluid flow in the hot liquid zone, Shutler and Boberg (1972) developed an approximate technique that relies on the Marx-Langenheim model, for heat transfer calculations, and on the well known Buckley-Leverett (1942) method for calculating the distribution of the liquid phases inside the hot liquid zone. Although based on a number of assumptions (for example, viscosity reduction inside the hot liquid zone was neglected and fluid flow inside the steam zone was rather crudely approximated) this study gave fairly accurate results in predicting oil recovery rates.

The first theoretical effort that attempted to include the effects of gravity segregation was undertaken by Neuman (1975) who considered the problem of calculating the rate of growth of a three-dimensional steam zone that expands in both the horizontal and vertical directions.

Although this also was the first analytical study to include thermal effects on relative permeabilities, the validity of the derived model was limited by the underlying assumption that the mechanism of growth in the vertical direction is identical to the mechanism of areal growth, which in turn was approximated by the Marx-Langenheim model. A different approach was followed in a recent work by van Lookeren (1977). Based on segregated-flow principles such as previously used by Dietz (1953), he derived approximate analytical formulae that permit fast and simple, although approximate engineering, calculation of the performance of a steamflood in a three-dimensional reservoir. One should also mention the very interesting study of Miller (1975) on the stability characteristics of the steam front under idealized conditions.

In parallel to the analytical efforts, an increasing number of investigators concentrated on the development of fast and reliable numerical models that describe the physical phenomena of a steamflood with greater detail and make use of fewer restrictive assumptions. Within the past ten years a large number of papers studying the numerical modelling of the steam flood and other thermal methods has been published. Three-phase numerical steamflood models were derived by Shutler (1969), (1970) for one- and two-dimensional flow; by Abdalla and Coats (1971) for two-dimensional flow; and by Coats et al. (1974), Coats (1976) and Weinstein et al. (1977) for three-dimensional flow. The principal advantages of the last three models lie in the simultaneous solution of the mass and energy balances and in the implicit treatment of the various properties that are functions of the dependent variables. In addition, the last two models account for steam distillation. The development of such sophisticated numerical simulators was greatly aided by parallel

advances in the numerical solution of coupled, non-linear, parabolic partial differential equations in moving boundary regions, and by the increasing availability of faster and cheaper computers. In spite of their high degree of sophistication, however, the latest numerical simulators are still troubled by stability and reliability problems, and by large computational-time requirements. Towards improving upon these features, a considerable amount of industrial research is currently conducted.

Complementing physical and analytical models, the comprehensive numerical models find their primary utility as research tools. They serve as an aid in understanding the nature of the process and interpreting laboratory experiments, in optimization studies [Chu (1977)] and in evaluating and developing simpler mathematical models. On the other hand, the primary utility of the analytical models lies in their routine use as an aid in engineering design. It is the growth in the total volume of the steam zone that governs the amount of oil that can be produced, hence, the economics of the process. Therefore, if an analytical model adequately defines the volume of the steam zone as a function of steam injected, it provides us with an appropriate measure of how much oil can find its way to a producing well as a result of steam injection. In this context, the use of a reliable analytical model for the determination of the steam zone growth is much preferred over highly sophisticated and expensive numerical simulators, the latter being more apt in providing information regarding finer characteristics of the process. Favoring this view is the fact that the reliability of a numerical model is, more often than not, tested by checking numerical results concerning

integral characteristics of the process, such as the volume of the steam zone or the oil recovery rates, against existing analytical expressions. Furthermore, it should be kept in mind that the optimal application, in field cases, of the high-cost numerical simulators requires a detailed knowledge of the distribution of the various physical, geological and geometrical parameters. Such information is not always readily accessible.

The relative importance attached to the development of reliable and easily applicable analytical models is evidenced in a number of recent studies dealing with the engineering evaluation and economic appraisal of steam injection in actual field cases [Gomaa (1976), van Lookeren (1977), Myhill and Stegemeier (1978) and Doscher and Ershaghi (1978)]. It is also common knowledge that good theoretical models can be of great help in understanding and clarifying still unresolved issues about basic mechanisms of the process. Indirectly, they serve as a check for the validity of the numerical simulators which in turn provide useful information that cannot be otherwise obtained. In spite of the progress that has been made, it appears that an analytical model that accurately simulates the steam injection in one- and particularly in two- (or three-) dimensional systems has not yet been achieved. Additional research is, therefore, needed towards developing a more reliable model. In particular, this model should be capable to provide answers to two important unanswered questions:

1. What is the effect of the heat transport into the oil/water region ahead of the steam zone, on the rate of growth of the steam zone.

2. What is the vertical coverage of displacement and how does gravity affect the displacement front.

In the present study, we attempt to clarify both these topics by constructing analytical models that incorporate the above effects. More specifically, we concentrate on deriving an improved one-dimensional model that includes a detailed account of the heat transfer and a new two- (or three-) dimensional model that accounts for the effects of gravity. For this purpose, an integral technique is developed by means of which the basic conservation laws of the process are cast in an integral form for a reservoir of arbitrary geometry. The mechanism of heat transfer is further studied in detail. The arising moving boundary problems are then analytically solved and the solutions obtained are inserted in the conservation equations. According to the methods used in handling heat transfer, we obtain new expressions for bounds, asymptotic solutions and approximate solutions that, to a varying degree of accuracy, describe the one-dimensional steam zone growth. In the course of this pursuit the existing models are critically reviewed, the assumptions they are based upon reevaluated and the range of their validity delineated. In the novel area of modelling the three-dimensional steamflood two approaches are followed. In the first, upper bounds including the effects of gravity segregation are derived for the volume of the steam zone. These effects are further studied using a finer integral technique, by means of which we construct a new model for the shape of the steam zone in two- (or three-) dimensional systems. It should be noted that although we are primarily concerned with modelling the continuous steam injection process, some of the results obtained can be also applied to steam

stimulation. Similarly, due to common heat transfer characteristics, the heat transfer results can be very useful in analyzing other thermal recovery processes.

Because of the qualitatively different character of the displacement, we discuss the one- and the two- (or three-) dimensional steamflood separately (Chapters IV and V, respectively). In Chapter II we outline the integral techniques which form the basis for the construction, in Chapters IV and V, of the analytical models for the steam zone growth. The important topic of heat transfer is separately treated in Chapter III.

As a final note, it should be noted that in selecting symbols we followed the notation recommended by the Society of Petroleum Engineers (SPE) (1965), (1972) while all units employed in the numerical examples are SI units according to SPE directions (1977).

Chapter II. Mathematical Formulation. The Integral Balance Approach.

2.1 Introduction

In the first two sections of the present chapter we focus on the physical and mathematical description of the steam injection process. Part of Section 2.2 summarizes and outlines the definition of various terms that are commonly used in the area of oil recovery. In 2.3 follows a rigorous mathematical formulation of the process. The resulting moving boundary problem is, subsequently, treated by an approximate technique based on integral balances. The first part of Section 2.4 deals with the application of the technique to systems of one, two or three dimensions in order to derive information regarding average properties of the process. The second part of Section 2.4 outlines the implementation of the technique to two-dimensional, gravity dominated systems, in an effort to determine the finer structure of the propagating steam front. In the final Section 2.5, we attempt to derive, by dimensional analysis, the most important dimensionless groups of parameters and their significance in scaling.

2.2 Some Basic Definitions and Description of the Process

Before we start modelling steam injection (or steam drive) it is necessary to define some basic terms and concepts that are common in the area of thermal oil recovery and reservoir engineering in general. [See SPE Repr. Series (1972).]

An oil reservoir is a three-dimensional, porous geologic formation, R , permeable to fluid flow, that contains in its pore space, in addition

to water and a mixture of hydrocarbon (oil or gas), in a liquid or gaseous phase. The reservoir is characterized by the macroscopic properties of porosity and permeability which determine fluid flow and accumulation.

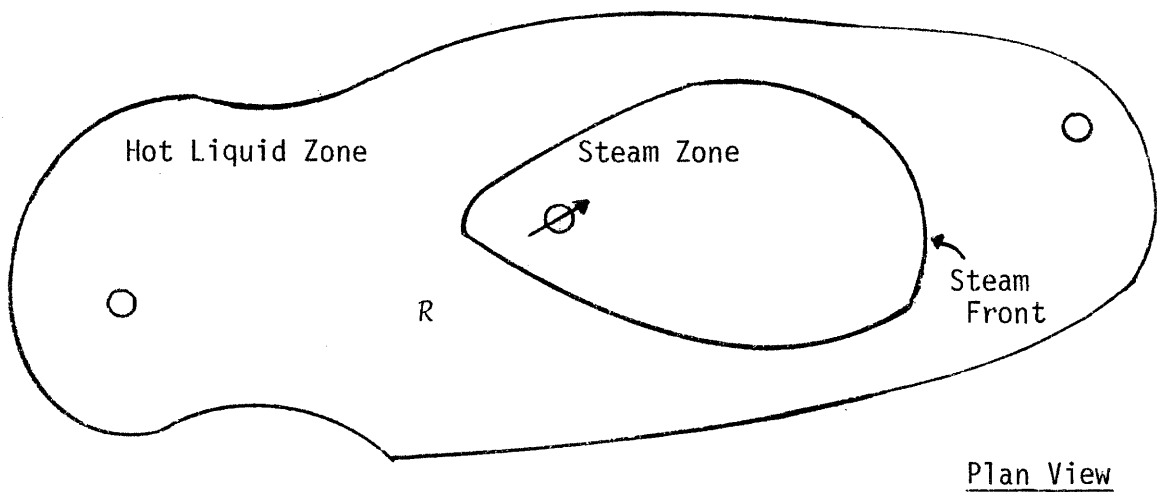
The reservoir is bounded by rock formations impermeable to fluid flow commonly referred to as the over- and under-burden (see Figure 8). Very often, due to geologic stratification, the reservoir is confined between two parallel planes, that are inclined with respect to the horizontal, in general.



An oil well represents a point, line or cylindrical (according to geometry) mass source or sink. It is characterized as a production or injection well according to its function in producing or injection fluids, respectively.

During a steam drive, steam of a certain temperature, pressure and quality is injected through one or more injection wells and displaces oil towards the producing wells. At any stage during the process, we can distinguish the following two distinct regimes inside the reservoir:

- a. A steam zone (S.Z.), which is that region of the reservoir which is occupied by the injected steam. The steam zone also contains liquid water (initially present and due to steam condensation) and oil at its residual saturation.

Mainly because of viscosity reduction due to the temperature increase, oil is continuously displaced ahead of the moving steam zone. The oil which is left behind is at a saturation (residual)



-  Injection Well
-  Production Well

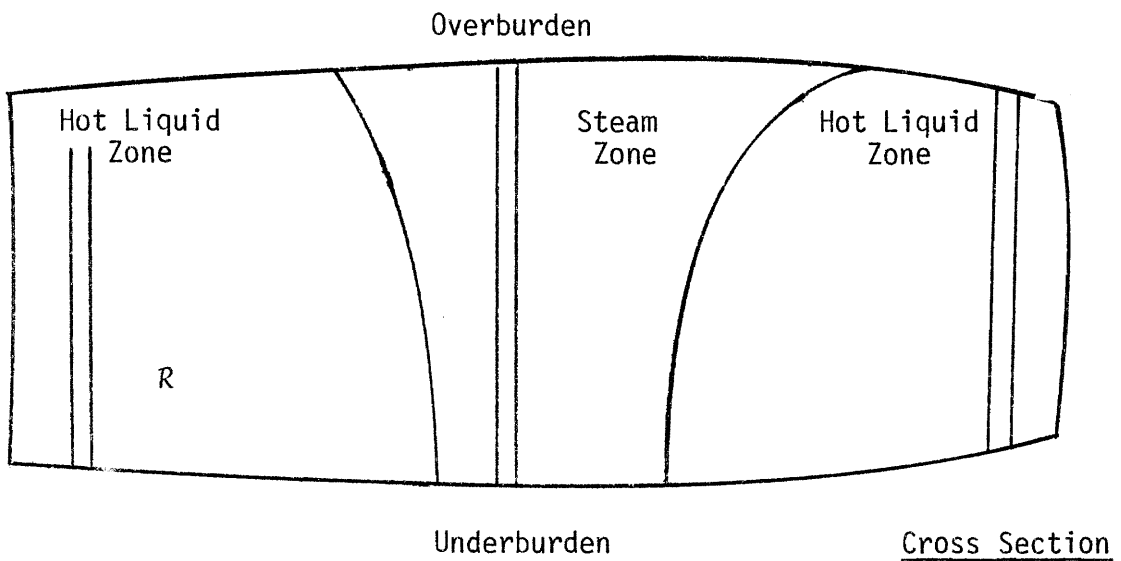


Figure 8. Schematic Diagram of a Reservoir Subject to Steamflooding.

that cannot be further reduced by steam or water drive.

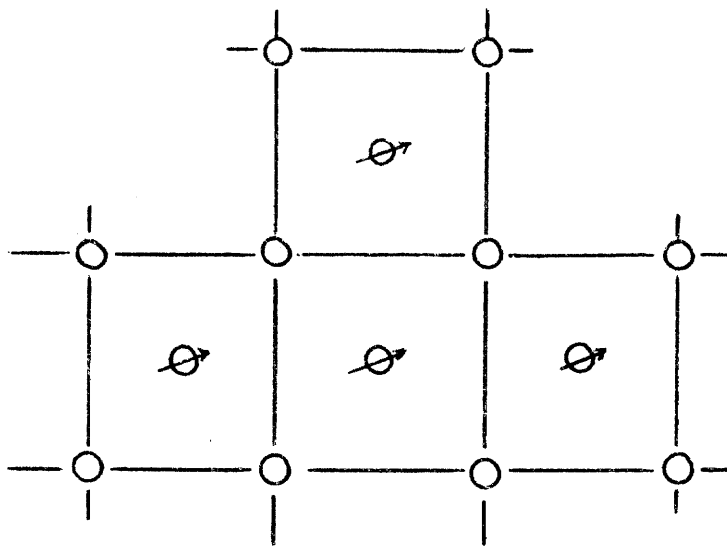
The steam zone is delineated by a moving surface called the steam front (S.F.), the dynamics of which play a most important role in determining the performance of a steam drive.

b. A hot liquid zone (H.L.Z.) in which water and oil pushed ahead of the steam zone flow towards the production wells.

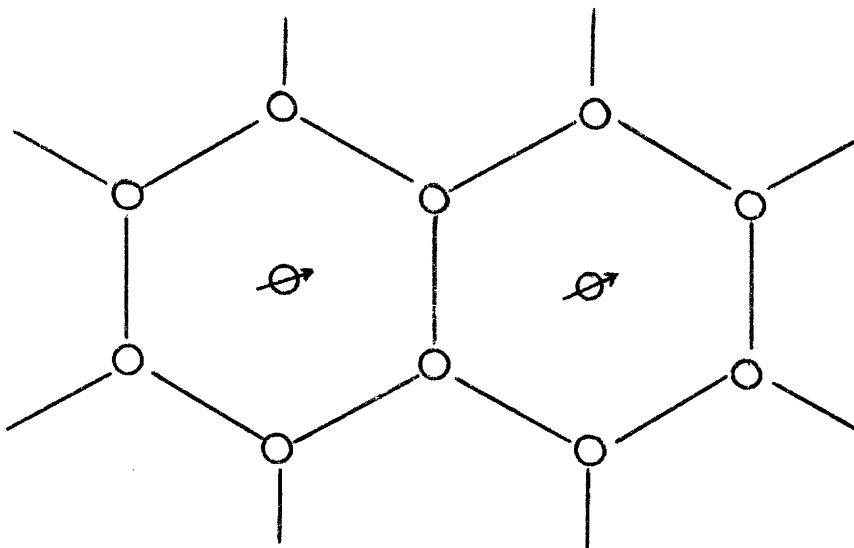
Very often due to density difference in the flowing phases, the steam zone tends to ride over the top of the hot liquid zone, thus forming a gravity tongue (see Figure 8). This gravity override, frequent in gravity dominated systems, severely limits the efficiency of the recovery along the vertical direction (vertical sweep efficiency).

The production pattern usually exhibits a periodic configuration consisting of repeated square or hexagonal unit cells, 5-spot or 7-spot, respectively (Figure 9). Due to this symmetry it is sufficient to focus our attention to a single unit cell, where a centrally located well is surrounded by 4 or 6 production wells, respectively.

The mathematical description, on a macroscopic scale of the phenomena associated with steam injection, makes use of the continuum hypothesis. According to this approach, the actual porous medium is replaced by a fictitious continuum: a structureless substance, at any point of which we can assign kinematic and dynamic parameters and variables that are continuous functions of the spatial coordinates and time. These variables averaged over a representative elementary volume (REV), enable us to describe transport and other phenomena in a porous



5-Spot



7-Spot

Figure 9. Schematic Diagram of 5-Spot and 7-Spot Production Patterns.

medium, in terms of partial differential equations [see Whitaker (1970), Bear (1972)].

2.3 Mathematical Formulation

2.3.1 The Differential Equations

We start the mathematical formulation by considering the partial differential equations that describe mass, momentum and energy transfer inside the reservoir. The well known Darcy's law for low Reynolds number flow in a porous medium provides expressions that relate the volumetric velocity vectors to the pressure gradients.

In the absence of steam distillation of oil, the equations read:

a. In the steam zone

steam, liquid water and oil mass balances:

$$\phi \frac{\partial}{\partial t} (\rho_s S_s) + \nabla \cdot (\rho_s \mathbf{u}_s) = M_g \quad (2.1)$$

$$\phi \frac{\partial}{\partial t} (\rho_w S_w) + \nabla \cdot (\rho_w \mathbf{u}_w) = -M_g \quad (2.2)$$

$$\phi \frac{\partial}{\partial t} (\rho_o S_o) + \nabla \cdot (\rho_o \mathbf{u}_o) = 0 \quad (2.3)$$

Volumetric balance:

$$S_s + S_w + S_o = 1 \quad (2.4)$$

Linear momentum balances (Darcy's Law):

$$\underline{u}_s = - \frac{k_{rs}}{\mu_s} \underline{K} \cdot (\nabla p_s - \rho_s \underline{g}) \quad (2.5)$$

$$\underline{u}_w = - \frac{k_{rw}}{\mu_w} \underline{K} \cdot (\nabla p_w - \rho_w \underline{g}) \quad (2.6)$$

$$\underline{u}_o = - \frac{k_{ro}}{\mu_o} \underline{K} \cdot (\nabla p_o - \rho_o \underline{g}) \quad (2.7)$$

Assuming thermodynamic equilibrium,

$$T_R = T_s(p_s) \quad (2.8)$$

In the above

1. The tensor \underline{K} is the second order symmetric permeability tensor, which for a homogeneous isotropic reservoir reduces to $k\underline{I}$, with k the scalar permeability and \underline{I} the identity tensor.
2. The relative permeability of each phase, k_{rj} , is in general a function of S_j , determined experimentally from laboratory tests. [Coats et al. (1974), Hagoort et al. (1977)].
3. The density ρ_j and viscosity μ_j , of each phase, are temperature dependent.
4. The pressure is different in each of the three phases due to the presence of capillary pressure terms.

For a water wet porous medium,

$$p_w = p_o - P_{cow}(S_w, S_s) \quad (2.9a)$$

$$p_s = p_o + p_{cos}(S_w, S_s) \quad (2.9b)$$

where again the dependence on S_i is to be established from experimental data. Except in regions of sharp saturation gradients, the capillary terms in (2.9) are much smaller than the absolute pressure terms and they can be safely neglected in our calculations.

5. Equation (2.8) is the usual thermodynamic equilibrium temperature-pressure relationship tabulated in steam tables [N.E.L. Steam Tables (1964)]. In reality, capillary pressure effects may result in a lowering of the vapour pressure at any given temperature [Calhoun et al. (1949)]. This effect is not significant, however, at the elevated temperatures and pressures of a regular steam drive, a fact that has been also confirmed in the work of Cady et al. (1972) concerning geothermal reservoirs. As a result, the thermodynamic equilibrium relation (2.8) is consistently employed in all reported mathematical models of steam injection and geothermal reservoirs. [Coats et al. (1974), Martin (1975), Weinstein et al. (1977)].
6. M_g is an interphase mass transfer term allowing for steam condensation. In some numerical models, an explicit expression which is T and P dependent is developed for M_g [Shutler (1969)]. Alternatively, it is more convenient to eliminate M_g by adding (2.1) and (2.2) in order to express the total water mass balance

$$\phi \frac{\partial}{\partial t} (\rho_s S_s + \rho_w S_w) + \nabla \cdot [\rho_s u_s + \rho_w u_w] = 0 \quad (2.10)$$

In writing down the energy equation, we assume that thermal equilibrium between the fluids and the rock matrix is instantaneously achieved [Bear (1972)], and that natural convection is not significant [Rubin and Schweitzer (1972)] for the prevailing conditions of rather high volumetric velocities. For small variations in pressure, inside the steam zone, the thermal energy balance becomes

$$\begin{aligned} \phi \frac{\partial}{\partial t} [\rho_s S_s h_s + \rho_w S_w h_w + \rho_o S_o h_o] + (1 - \phi) \rho_R \frac{\partial h_R}{\partial t} = \nabla \cdot k_{hR} \nabla T_R \\ - \nabla \cdot [\rho_s u_s h_s + \rho_w u_w h_w + \rho_o u_o h_o] \end{aligned} \quad (2.11)$$

Combined with Eqs. (2.1), (2.2), (2.3), the energy equation transforms into

$$\begin{aligned} \phi \rho_s S_s \frac{\partial h_s}{\partial t} + \phi \rho_w S_w \frac{\partial h_w}{\partial t} + \phi \rho_o S_o \frac{\partial h_o}{\partial t} + (1 - \phi) \rho_R \frac{\partial h_R}{\partial t} = \nabla \cdot k_{hR} \nabla T_R \\ - (\rho_s u_s \cdot \nabla h_s + \rho_w u_w \cdot \nabla h_w + \rho_o u_o \cdot \nabla h_o) - M_g L_v \end{aligned} \quad (2.12)$$

where $L_v = h_s - h_w$ is the water latent heat of vaporization.

b. Similarly, in the hot liquid zone, we have

Water and oil mass balances

$$\phi \frac{\partial}{\partial t} (\rho_w S_w) + \nabla \cdot (\rho_w u_w) = 0 \quad (2.13)$$

$$\phi \frac{\partial}{\partial t} (\rho_o S_o) + \nabla \cdot (\rho_o u_o) = 0 \quad (2.14)$$

Volumetric balance

$$S_w + S_o = 1 \quad (2.15)$$

The linear momentum balances are expressed through Darcy's Law [Eqs. (2.6), (2.7)], as before.

Thermal energy balance:

$$\begin{aligned} \phi \frac{\partial}{\partial t} [\rho_w S_w h_w + \rho_o S_o h_o] + (1 - \phi) \rho_R \frac{\partial h_R}{\partial t} \\ = \nabla \cdot k_{hR} \nabla T_R - \nabla \cdot [\rho_w u_w h_w + \rho_o u_o h_o] \end{aligned} \quad (2.16)$$

- c. In the surrounding formations which are permeable to fluid flow, the thermal energy balance is described by the pure heat conduction equation

$$(1 - \phi) \rho_f \frac{\partial h_f}{\partial t} = \nabla \cdot (k_{hf} \nabla T_f) \quad (2.17)$$

The systems of the nonlinear-PDE's (2.1) to (2.17), in each of the three different regions (steam zone, hot liquid zone, surrounding formations), are coupled to each other by means of the following interfacial, boundary, and initial conditions.

2.3.2 The Boundary Conditions

2.3.2.1 Interfacial Conditions

Let

$$S(\underline{r}, t) = 0 \quad (2.18)$$

define the moving boundary interface between any two regions (surrounding formation-steam zone, surrounding formation-hot liquid zone, steam zone-hot liquid zone). Since S is a material surface

$$\frac{DS}{Dt} = \frac{\partial S}{\partial t} + \underline{v} \cdot \nabla S = 0 \quad (2.19)$$

where \underline{v} is the velocity vector of any point of the interface.

Let, also

$$\underline{n} = \frac{\nabla S}{|\nabla S|} \quad (2.20)$$

be the outwards pointing unit vector normal to the interface (see Figure 10).

Then, the normal component of the velocity at the interface is given by

$$v_n = - \frac{\frac{\partial S}{\partial t}}{|\nabla S|} \quad (2.21)$$

Each of the equations (2.3), (2.10), (2.11), (2.13), (2.14), (2.16) (2.17) can be cast in the general conservation equation form

$$\frac{\partial \psi}{\partial t} + \nabla \cdot \underline{q} = 0 \quad (2.22)$$

where ψ is a conserved physical quantity with flux q . If ψ is conserved in any two different regions, it must also be conserved across the interface separating the two regions. Integrating (2.22) over an infinitesimal volume of the interface we obtain, in the absence of surface sources,

$$\psi^I \frac{\partial S}{\partial t} + \underline{q}^I \cdot \underline{\nabla} S = \psi^{II} \frac{\partial S}{\partial t} + \underline{q}^{II} \cdot \underline{\nabla} S \quad (2.23)$$

on $S(r,t) = 0$

(See Appendix I for derivation.) Here the superscripts I, II indicate inner and outer side of the surface, respectively, as defined by \underline{n} .

Substitution of (2.21) into (2.23) leads to:

$$q_n^I - \psi^I v_n = q_n^{II} - \psi^{II} v_n \quad (2.24)$$

Applying Eq. (2.24) successively to the mass and energy balances, Equations (2.10) - (2.13), (2.3) - (2.14), (2.11) - (2.16) we derive the following interfacial conditions:

i. On the steam zone-hot liquid zone interface:

water mass balance

$$\rho_s^I (u_{sn}^I - \phi S_s^I v_n) + \rho_w^I (u_{wn}^I - \phi S_w^I v_n) = \rho_w^{II} (u_{wn}^{II} - \phi S_w^{II} v_n) \quad (2.25)$$

oil mass balance

$$\rho_o^I(u_{on}^I - \phi S_o^I v_n) = \rho_o^{II}(u_{on}^{II} - \phi S_o^{II} v_n) \quad (2.26)$$

thermal energy balance

$$\begin{aligned} & \rho_s^I h_s^I u_{sn}^I + \rho_w^I h_w^I u_{wn}^I + \rho_o^I h_o^I u_{on}^I - \left(k_{hR} \frac{\partial T_R}{\partial n} \right)^I \\ & - \left[\phi (\rho_s^I S_s^I h_s^I + \rho_w^I S_w^I h_w^I + \rho_o^I S_o^I h_o^I) + (1 - \phi) \rho_R h_R^I \right] v_n \\ & = \rho_w^{II} h_w^{II} u_{wn}^{II} + \rho_o^{II} h_o^{II} u_{on}^{II} - \left(k_{hR} \frac{\partial T_R}{\partial n} \right)^{II} \\ & - \left[\phi (\rho_w^{II} S_w^{II} h_w^{II} + \rho_o^{II} S_o^{II} h_o^{II}) + (1 - \phi) \rho_R h_R^{II} \right] v_n \end{aligned} \quad (2.27)$$

Eq. (2.27) combined with Eqs. (2.25), (2.26) assumes the simpler form

$$\begin{aligned} \rho_s^I L_v^I (u_{sn}^I - \phi S_s^I v_n) &= \left(k_{hR} \frac{\partial T_R}{\partial n} \right)^I - \left(k_{hR} \frac{\partial T_R}{\partial n} \right)^{II} \\ &+ (1 - \phi) \rho_R (h_R^I - h_R^{II}) v_n \end{aligned} \quad (2.28)$$

ii. On the surrounding rock-steam zone (rock-hot liquid zone) interface, we have

$$v_n = 0, \quad u_{in}^{II} = 0 \quad i = s, w, o (i = w, o)$$

and the corresponding interfacial conditions become

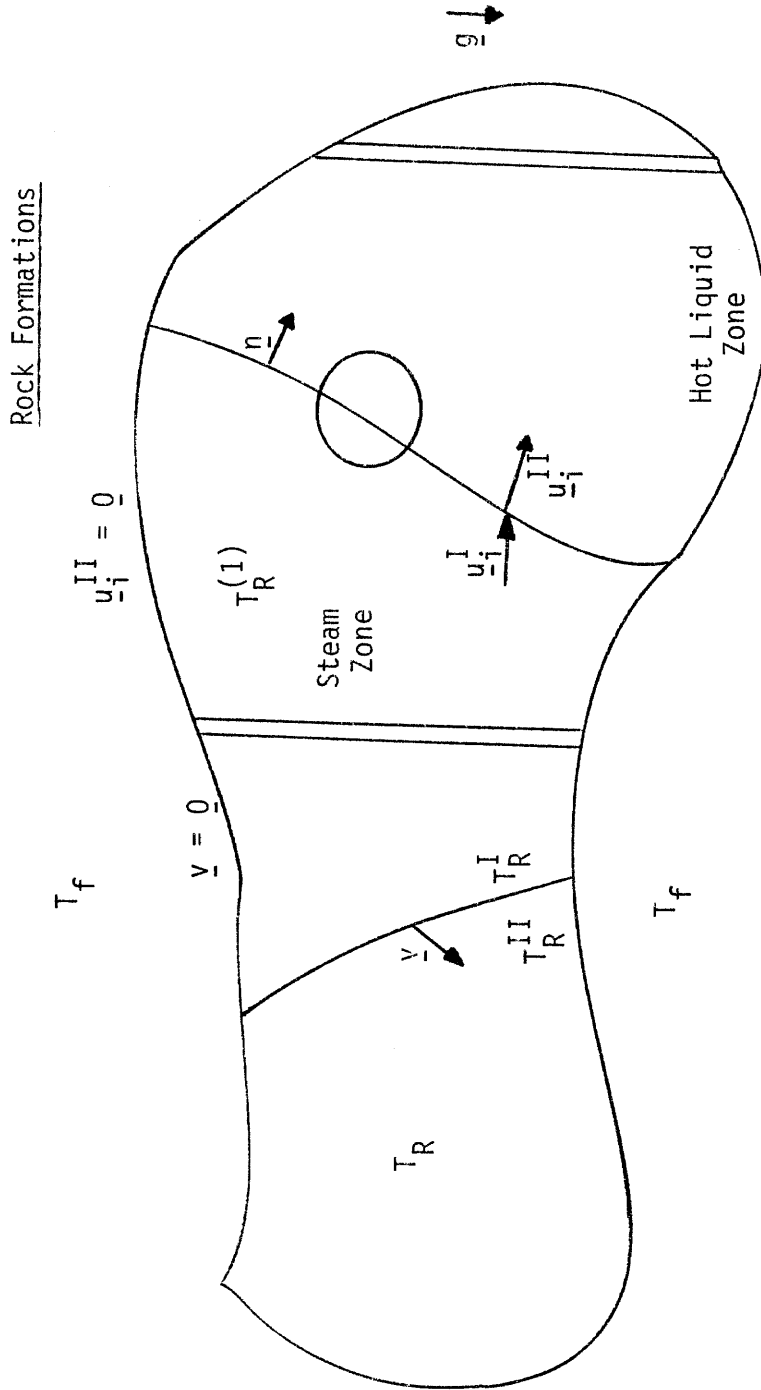


Figure 10a. Cross Section of a Reservoir Subject to Steamflooding.
 Notation for Subsection 2.3.2.

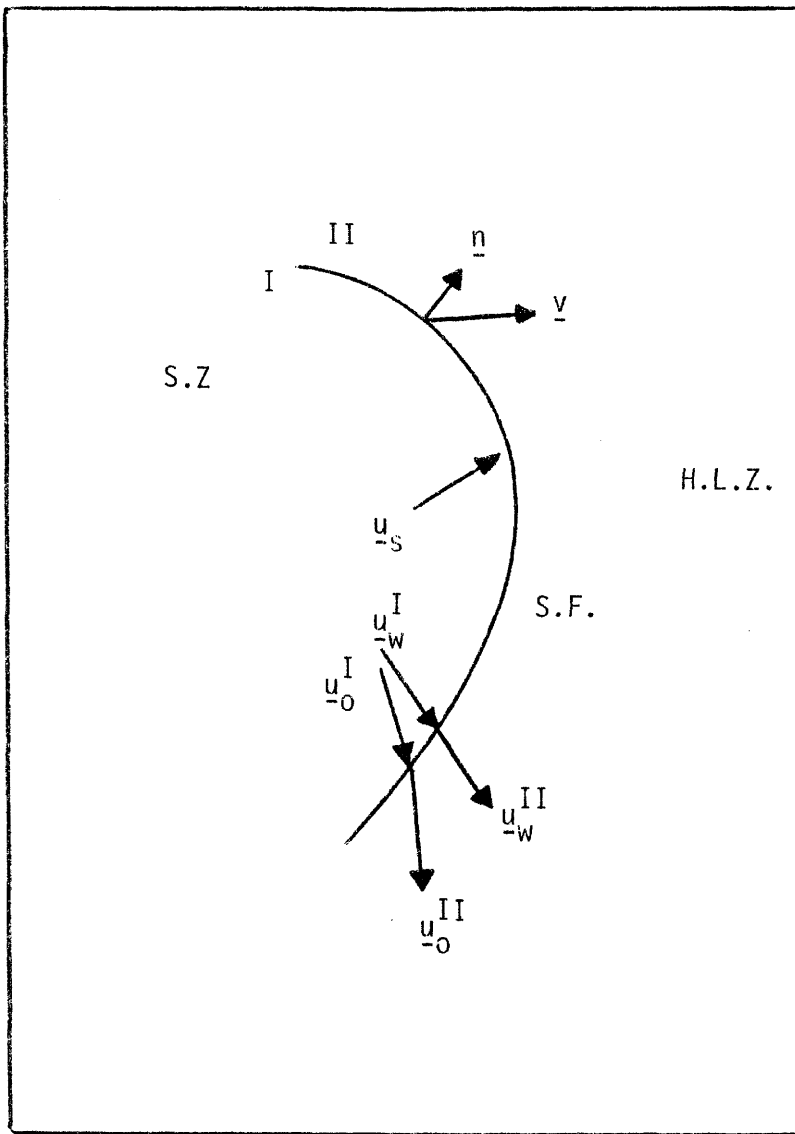


Figure 10b. Schematic Diagram of the Interface Between Steam Zone and Hot Liquid Zone. Enlargement of the Encircled Portion of Fig. 10a.

$$\rho_{su}^{II} + \rho_{wn}^{II} = 0 \quad (2.29a)$$

$$(\rho_{wn}^{II} = 0, \text{ for rock-hot liquid zone}) \quad (2.29b)$$

$$\rho_{on}^{II} = 0 \quad (2.30)$$

$$\rho_{su}^{II} = \frac{1}{L_v} \cdot \left\{ \left(k_{hR} \frac{\partial T_R}{\partial n} \right)^I - \left(k_{hf} \frac{\partial T_f}{\partial n} \right)^{II} \right\} \quad (2.31a)$$

$$\left(\left(k_{hR} \frac{\partial T_R}{\partial n} \right)^I - \left(k_{hf} \frac{\partial T_f}{\partial n} \right)^{II} = 0 \text{ for rock-hot liquid zone} \right) \quad (2.31b)$$

In addition, the absence of heat sources at the steam front dictates a continuity in temperature

$$T_R^I = T_R^{II} \quad (2.32)$$

At this point it should be noted that most of the previous analytical models [Marx and Langenheim (1959), Shutler and Boberg (1972)] consider a step temperature change across the steam front. This approximation violates the continuity condition (2.32) but does not contradict the conservation Equations (2.28), (2.31a).

2.3.2.2 A Pressure Dynamic Condition

Across the steam front the pressures in the oil and water phases are continuous and related to each other and the steam pressure by means of the microscopic capillary terms [Eqs. (2.9a), (2.9b)].

By its definition, the steam front is not the actual microscopic surface separating two phases but rather a macroscopic interface where fluctuations from pore to pore have been smoothed out over macroscopic unit distances. Therefore, it can be assumed that the pressure difference across this macroscopic interface is related to the capillary pressure through the familiar macroscopic expression

$$p_s^I - p_i^{II} = p_{ci} + (T_e(c_1 + c_2)) \quad i = w, o \quad (2.33a)$$

where c_1, c_2 are the principal curvatures of the macroscopic interface and T_e is a macroscopic "effective interfacial tension" [Chuoque et al. (1959), Outmans (1962)]. In other words, with relation (2.33a) we attempt to satisfy, in a macroscopic sense, the conservation of linear momentum across the steam front.

Although the validity of such a representation is questionable for a wide range of operating conditions, its adoption can greatly facilitate the analytical determination of the steam front shape, in gravity dominated reservoirs. By differentiating Eq. (2.33a) along the coordinate parallel to the interface, s , we get

$$\frac{\partial p_s^I}{\partial s} - \frac{\partial p_i^{II}}{\partial s} = \frac{\partial p_{ci}}{\partial s} + \frac{\partial}{\partial s} (T_e(c_1 + c_2)) \quad i = w, o$$

If we, furthermore, assume that the macroscopic curvature and capillary terms do not change considerably along the interface, we get the simple interfacial condition

$$\frac{\partial P_s^I}{\partial s} = \frac{\partial P_i^{II}}{\partial s} \quad i = w, o \quad (2.33b)$$

The above approximation very often employed in analytical modelling of two-dimensional, two-phase, immiscible displacement, [Sheldon and Fayers (1962), Beckers (1965)], is usually referred to as the pressure dynamic condition.

2.3.2.3 Boundary and Initial Conditions

i. Boundary Conditions

These involve the specification of steam injection rate, steam quality and temperature (pressure) at the injection well and pressure at the production well.

$$- \int_{A_{inj}} \rho_s u_{sn} dA = w_s(t) \quad (2.34)$$

$$- \int_{A_{inj}} \rho_w u_{wn} dA = w_w(t) \quad (2.35)$$

$$T_R(\underline{r}, t) = T_s, \quad \underline{r} \in A_{inj} \quad (2.36)$$

where A_{inj} is the injection area, w_i the mass injection rates.

Since there is no flow of oil at the injection well

$$u_{on}(\underline{r}, t) = 0, \quad \underline{r} \in A_{inj} \quad (2.37)$$

We finally consider the temperature condition at infinity

$$T_f(\underline{r}, t) = T_i \quad \text{as} \quad |\underline{r}| \rightarrow \infty \quad (2.38)$$

ii. Initial Conditions

Before steam injection begins, we have static and thermal equilibrium with no flow of either water or oil, constant saturations and temperatures inside the reservoir and the surrounding rock formations

$$S_w(\underline{r}, 0) = S_{wi} \quad (2.39a)$$

$$S_o(\underline{r}, 0) = S_{oi} \quad (2.39b)$$

$$T_R(\underline{r}, 0) = T_i \quad (2.39c)$$

$$u_w(\underline{r}, 0) = 0 \quad (2.39d)$$

$$u_o(\underline{r}, 0) = 0 \quad (2.39e)$$

$$T_f(\underline{r}, 0) = T_i \quad (2.39f)$$

The above sets of partial differential equations, interfacial and boundary conditions complete the description of a complicated but well-posed mathematical problem.

2.4 The Integral Balances

2.4.1 Introduction

The foregoing mathematical formulation indicates that in steam

injection we are dealing with momentum and heat transfer in two different regions coupled by interphase transport through a moving boundary and accompanied by a phase change. The last two features characterize a general class of problems known as Stefan problems [see Rubinshtein (1971), Ockendon and Hodgkins (1974)]. In this context our case, which in addition involves heat transfer to the surroundings (heat losses), can be classified as a generalized Stefan problem.

Unfortunately, the techniques developed for the analytical solution of Stefan problems, cannot be effectively applied in this situation, due mainly to the unique aspects of multiphase flow and heat losses. On the other hand, it is pretty clear that, aiming at an exact analytical solution, even for the simpler one-dimensional case, would be a rather fruitless project.

The complexity of the problem calls for a numerical solution. Indeed, detailed numerical simulators have been already developed [Shutler (1969), Coats et al. (1974), Weinstein et al. (1977) and used with increasing frequency. Despite substantial improvements during the recent years, however, they still suffer from large computational time, stability problems and in addition they are available at a rather high cost. It is also understood that optimal use of a numerical simulator in a field case, requires fairly accurate knowledge of the various geometric, geological and dynamic variables, their spatial distribution and their functional dependence.

Alternatively, one can use analytical techniques in order to extract as much information as possible regarding important integral aspects of

the process, such as the oil recovery efficiency or the oil (produced) to steam (injected) ratio. In addition, an analytical approach may result in a better understanding of the mechanisms that govern the process. This alternative, to be viable, should be based on two key steps:

1. Adoption of an Integral Balance Approach.
2. Decoupling of the heat and momentum transfer, whenever feasible.

We elect to follow this procedure with the two-fold objective to analytically determine the rate of growth of the steam zone volume and the steam front shape on a plane perpendicular to the reservoir bedding plane.

The integral balance approach involves integration over a volume or an area according to the geometry of the reservoir. The method bears a conceptual similarity to the integral techniques employed in boundary layer theory [see Schlichting(1955), for example], although the degree of complexity and the approximations to be used are different. The utilization of this approach allows us to shift our emphasis on the second step, which involves heat and momentum transfer (Chapter III). The combined application of the two steps provides rigorous analytical bounds or approximate solutions to the quantities of interest.

2.4.2 Volume (Area) Integration

Consider the volume $V(t)$ occupied by the steam zone at time t . Let $A(t)$ denote the surface enclosing $V(t)$, composed of $A_f(t)$, the interface with the surrounding formations, $A_f(t)$, the steam front area and A_{inj} , the injection area (See Figure 11). Integrating Eq. (2.11) over the

control volume $V(t)$ and using a modified version of the General Transport Theorem [Whitaker (1968)] we get

$$\begin{aligned} & \frac{d}{dt} \int_{V(t)} \left[\phi(\rho_s S_s h_s + \rho_w S_w h_w + \rho_o S_o h_o) + (1 - \phi) \rho_R h_R \right] dV \\ & + \int_{A(t)} \left[\rho_s h_s (\underline{u}_s - \phi S_s \underline{v}) + \rho_w h_w (\underline{u}_w - \phi S_w \underline{v}) + \rho_o h_o (\underline{u}_o - \phi S_o \underline{v}) \right. \\ & \left. - (1 - \phi) \rho_R h_R \underline{v} \right] \cdot \underline{n} dA = \int_{A(t)} k_{hR} \nabla T_R \cdot \underline{n} dA \end{aligned} \quad (2.40)$$

Employing the interface conditions Eqs. (2.29a), (2.30), (2.31a) and Eqs. (2.25), (2.26), (2.28) in evaluating the integrals over $A_f(t)$ and $A_f(t)$, respectively, and the boundary conditions Eqs. (2.34), (2.35) over A_{inj} , we obtain

$$\begin{aligned} & \frac{d}{dt} \int_{V(t)} \left[\sum_{i=s,w,o} \phi \rho_i S_i h_i + (1 - \phi) \rho_R h_R \right] dV + \int_{A_f(t)} \left[\sum_{i=w,o} \rho_i^{II} h_i^{II} (\underline{u}_{in}^{II} - \phi S_i^{II} \underline{v}_n) \right. \\ & \left. - (1 - \phi) \rho_R h_R^{II} \underline{v}_n \right] dA + \int_{A_f(t)} \left(- k_{hf} \frac{\partial T_f}{\partial n} \right)^{II} dA + \int_{A_f(t)} \left(- k_{hR} \frac{\partial T_R}{\partial n} \right)^{II} dA \\ & = h_s w_s(t) + h_w w_w(t) + \int_{A_{inj}} \left(k_{hR} \frac{\partial T_R}{\partial n} \right)^I dA \end{aligned} \quad (2.41)$$

which is a simpler version of the integral thermal energy balance over the moving control volume $V(t)$.

Similarly, working with the water mass balance (2.10), we obtain

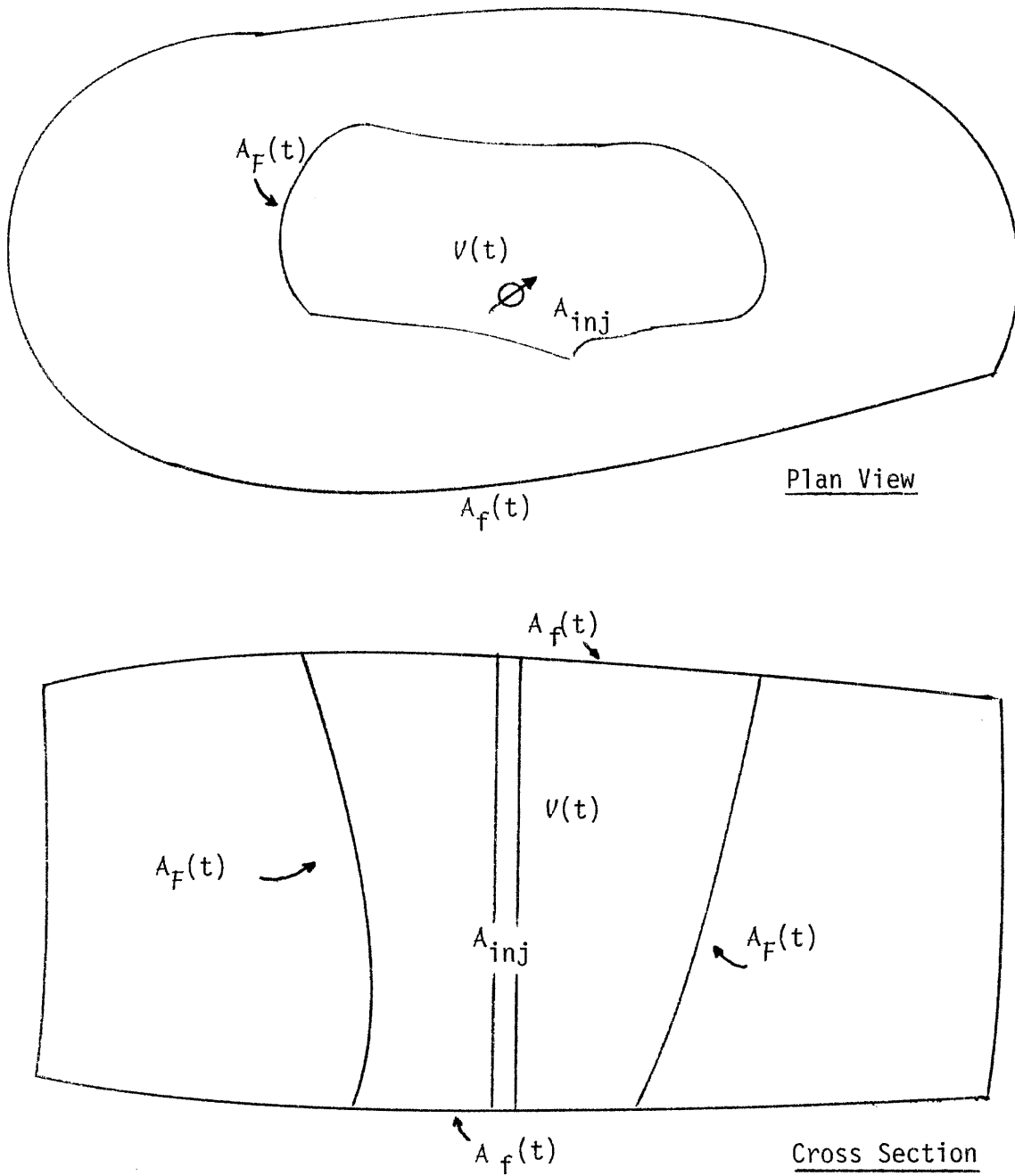


Figure 11. Geometries Examined in Subsection 2.4.2.
Notation for Area (Line) Integration.

$$\begin{aligned} \frac{d}{dt} \int_{V(t)} (\phi \rho_s S_s + \phi \rho_w S_w) dV \\ + \int_{A(t)} \left[\rho_s (\underline{u}_s - \phi S_s \underline{v}) + \rho_w (\underline{u}_w - \phi S_w \underline{v}) \right] \cdot \underline{n} dA = 0 \end{aligned} \quad (2.42)$$

which can be transformed through (2.25), (2.29a), (2.34) to

$$\begin{aligned} \frac{d}{dt} \int_{V(t)} (\phi \rho_s S_s + \phi \rho_w S_w) dV + \int_{A_F(t)} \rho_w^{II} (u_{wn}^{II} - \phi S_w^{II} v_n) dA \\ = w_s(t) + w_w(t) \end{aligned} \quad (2.43)$$

Eq. (2.43) represents the integral water mass balance over the volume $V(t)$. Finally, the integral oil mass balance becomes

$$\frac{d}{dt} \int_{V(t)} \phi \rho_o S_o dV + \int_{A_F(t)} \rho_o^{II} (u_{on}^{II} - \phi S_o^{II} v_n) dA = 0 \quad (2.44)$$

The above volume (area) integrals reduce accordingly to area (line) integrals when the reservoir exhibits an additional degree of symmetry.

2.4.3 The Constant Steam Zone Temperature Approximation

It is common practice, in steam injection, to consider the steam zone as a constant temperature region. The assumption, particularly useful for analytical purposes, has been verified by both experimental [Willman et al. (1961), Baker (1969), Baker (1973)] and numerical investigations [Shutler (1970), Coats et al. (1974)]. A theoretical proof

outlining the conditions under which the approximation is valid, can be provided by simple dimensional arguments.

For negligible temperature drop inside the steam zone, expression (2.41) simplifies to

$$\begin{aligned}
 & \phi \sum_{i=s,w,o} h_i^{(1)} \frac{d}{dt} \int_{V(t)} \rho_i S_i dV + (1 - \phi) h_R^{(1)} \frac{d}{dt} \int_{V(t)} \rho_R dV \\
 & + \int_{A_F(t)} \left[\sum_{i=w,o} \rho_i^{II} h_i^{II} (u_{in}^{II} - \phi S_i^{II} v_n) - (1 - \phi) \rho_R h_R^{II} v_n \right] dA \\
 & + \int_{A_f(t)} \left(- k_{hf} \frac{\partial T_f}{\partial n} \right)^{II} dA + \int_{A_F(t)} \left(- k_{hR} \frac{\partial T_R}{\partial n} \right)^{II} dA \\
 & = h_s^{(1)} w_s + h_w^{(1)} w_w
 \end{aligned} \tag{2.45}$$

where the superscript (1) refers to the steam zone.

Multiplying Eq. (2.43) by $h_w^{(1)}$, Eq. (2.44) by $h_o^{(1)}$ and subtracting their sum from Eq. (2.45) results to the integral steam mass conservation equation

$$\begin{aligned}
 & \phi L_v^{(1)} \frac{d}{dt} \int_{V(t)} \rho_s S_s dV + \int_{A_F(t)} \left[\sum_{i=w,o} (h_i^{II} - h_i^{(1)}) \rho_i^{II} (u_{in}^{II} - \phi S_i^{II} v_n) \right. \\
 & \left. - (1 - \phi) (h_R^{II} - h_R^{(1)}) \rho_R v_n \right] dA + \int_{A_f(t)} \left(- k_{hf} \frac{\partial T_f}{\partial n} \right)^{II} dA \\
 & + \int_{A_F(t)} \left(- k_{hR} \frac{\partial T_R}{\partial n} \right)^{II} dA = L_v^{(1)} w_s
 \end{aligned} \tag{2.46}$$

In both (2.45), (2.46) we have formally allowed a differentiation between $h_i^{(1)}$ and h_i^{II} . It is now obvious that, by assuming the step-temperature distribution [as in Marx-Langenheim (1959)] and choosing T_i as the reference temperature, the coupling convective and conductive terms in Eq. (2.45) vanish ($h_i^{II} = 0$). This results to a much simpler equation, the solution of which can be developed fairly easily.

The correct physical picture, however, involves a continuous change in temperature across the front. Regarding T as a continuous variable and with the convenient choice of T_i as reference temperature, we rewrite Eq. (2.45)

$$\begin{aligned} \Delta T \frac{d}{dt} \int_{V(t)} M_1 dV + \Delta T A_F(t) \left\{ W_F(t) + Q_F(t) \right\} + \int_{A_F(t)} \left(-k_{hf} \frac{\partial T_f}{\partial n} \right)^{II} dA \\ = [w_s(t) + w_w(t)] c_{pw} \Delta T + w_s(t) L_v^{(1)} \end{aligned} \quad (2.47)$$

where $\Delta T = T_s - T_i$. Here

$$M_1 = \sum_{i=s,w,o} \phi c_{pi} \rho_i S_i + (1 - \phi) \rho_R c_{pR} + \phi \frac{L_v^{(1)} \rho_s S_s}{\Delta T} \quad (2.48)$$

is the volumetric heat capacity of the steam zone,

$$\begin{aligned} W_F(t) = \left\{ \sum_{i=w,o} c_{pi} \int_{A_F(t)} \rho_i^{II} (u_{in}^{II} - \phi S_i^{II} v_n) dA - \right. \\ \left. - (1 - \phi) c_{pR} \int_{A_F(t)} \rho_R v_n dA \right\} / A_F(t) \end{aligned} \quad (2.49a)$$

is the net convective heat flux through the steam front and

$$Q_F(t) = \int_{A_F(t)} \left(-k_{hR} \frac{\partial T_R}{\partial n} \right) II \, dA / \Delta T A_F(t) \quad (2.49b)$$

is the conductive heat flux through the steam front.

Similarly, Eq. (2.46) can be recast in the form

$$\begin{aligned} \frac{d}{dt} \int_{V(t)} M_2 dV + \Delta T A_F(t) Q_F(t) + \int_{A_f(t)} \left(-k_{hf} \frac{\partial T_f}{\partial n} \right) II \, dA \\ = w_s(t) L_v^{(1)} \end{aligned} \quad (2.50)$$

where

$$M_2 = \phi \frac{L_v^{(1)} \rho_s S_s}{\Delta T} \quad (2.51)$$

is a modified volumetric heat capacity of the steam zone.

Notice that by subtracting Eq. (2.50) from (2.47) we recover the total water mass conservation Eq. (2.43), which indicates that only two out of the three Eqs. (2.43), (2.47), (2.50) are linearly independent. Together with the oil mass balance, Eq. (2.44), expressions (2.47) and (2.50) constitute our basic integral conservation equations. Further development on the heat transfer and the saturation distribution terms will lead to the determination of bounds and approximate solutions on the steam zone volume growth rate.

2.4.4 Area (Line) Integration

A three-dimensional averaging, such as the one described in the previous two sections, leads to the determination of volume averaged

quantities. In certain cases, however, it is necessary to obtain more information regarding the finer structure of the steam zone, for example, the steam front shape. A more accurate description towards this end necessarily requires a lower degree of integration.

For simplicity, we will consider a reservoir bounded by two parallel planes with a steam front of an arbitrary smooth shape (see Figure 12). We further assume that the reservoir is uniform along one of the Cartesian coordinates y , in rectangular geometries, or radially symmetric, in radial geometries.

Let us now integrate the thermal energy, steam mass, total water mass and oil mass balances along a vertical cross section of the steam zone bounded by the upper reservoir boundary from above and the steam front from below (see Figure 12). Using a two-dimensional version of the General Transport Theorem and the appropriate interfacial conditions, we get from the energy balance, Eq. (2.11):

$$\begin{aligned}
 & \frac{d}{dt} \int_0^{z(x,t)} \left[\sum_{i=S,W,O} \phi \rho_i S_i h_i + (1 - \phi) \rho_R h_R \right] dz \\
 & + \left[\sum_{i=W,O} \rho_i^{II} h_i^{II} (u_{in}^{II} - \phi S_i^{II} v_n) - (1 - \phi) \rho_R^{II} h_R^{II} v_n \right] |\nabla F| + \left(-k_{hR} \frac{\partial T_R}{\partial n} \right)^{II} |\nabla F| \\
 & + \left(-k_{hf} \frac{\partial T_f}{\partial n} \right)^{II} = - \frac{\partial}{\partial x} \left\{ \int_0^{z(x,t)} \left[\sum_{i=S,W,O} \rho_i u_{ix} h_i \right. \right. \\
 & \left. \left. + \left(-k_{hR} \frac{\partial T_R}{\partial x} \right) \right] dz \right\} \quad (2.52a)
 \end{aligned}$$

when the reservoir is uniform along the y -direction, and

$$\begin{aligned}
& \frac{d}{dt} \int_0^{z(x,t)} \left[\sum_{i=S,W,0} \phi \rho_i S_i h_i + (1-\phi) \rho_R h_R \right] dz \\
& + \left[\sum_{i=W,0} \rho_i^{II} h_i^{II} (u_{in}^{II} - \phi S_i^{II} v_n) - (1-\phi) \rho_R h_R^{II} v_n \right] |\nabla F| + \left(-k_{hR} \frac{\partial T_R}{\partial n} \right)^{II} |\nabla F| \\
& + \left(-k_{hf} \frac{\partial T_f}{\partial n} \right)^{II} = -\frac{1}{r} \frac{\partial}{\partial r} \left\{ \int_0^{z(x,t)} r \left[\sum_{i=S,W,0} \rho_i u_{ix} h_i \right. \right. \\
& \left. \left. + \left(-k_{hR} \frac{\partial T_R}{\partial r} \right) \right] dz \right\} \quad (2.52b)
\end{aligned}$$

in the radially symmetric geometry.

Here,

$$z - F(x,t) = 0 \quad (2.53a)$$

$$z - F(r,t) = 0 \quad (2.53b)$$

defines the steam front shape as a function of the coordinate x , or r and time. Clearly,

$$|\nabla F| = \sqrt{1 + \left(\frac{\partial z}{\partial x} \right)^2} \quad \text{or} \quad \sqrt{1 + \left(\frac{\partial z}{\partial r} \right)^2}.$$

We now invoke the constant temperature approximation of Section 2.4.2 and rewrite (2.52a), (2.52b) in a uniform notation:

$$\begin{aligned}
& \Delta T \frac{d}{dt} \int_0^{z(x,t)} M_1 dz + \Delta T W_F(x,t) |\nabla F| + \left(-k_{hR} \frac{\partial T_R}{\partial n} \right)^{II} |\nabla F| + \left(-k_{hf} \frac{\partial T_f}{\partial n} \right)^{II} \\
& = -\Delta T \frac{\partial}{\partial x} \left\{ \int_0^{z(x,t)} \left[\sum_{i=S,W,0} \rho_i c_{pi} \hat{u}_{ix} + \rho_s \frac{L_v^{(1)}}{\Delta T} \hat{u}_{sx} \right] dz \right\} \quad (2.54)
\end{aligned}$$

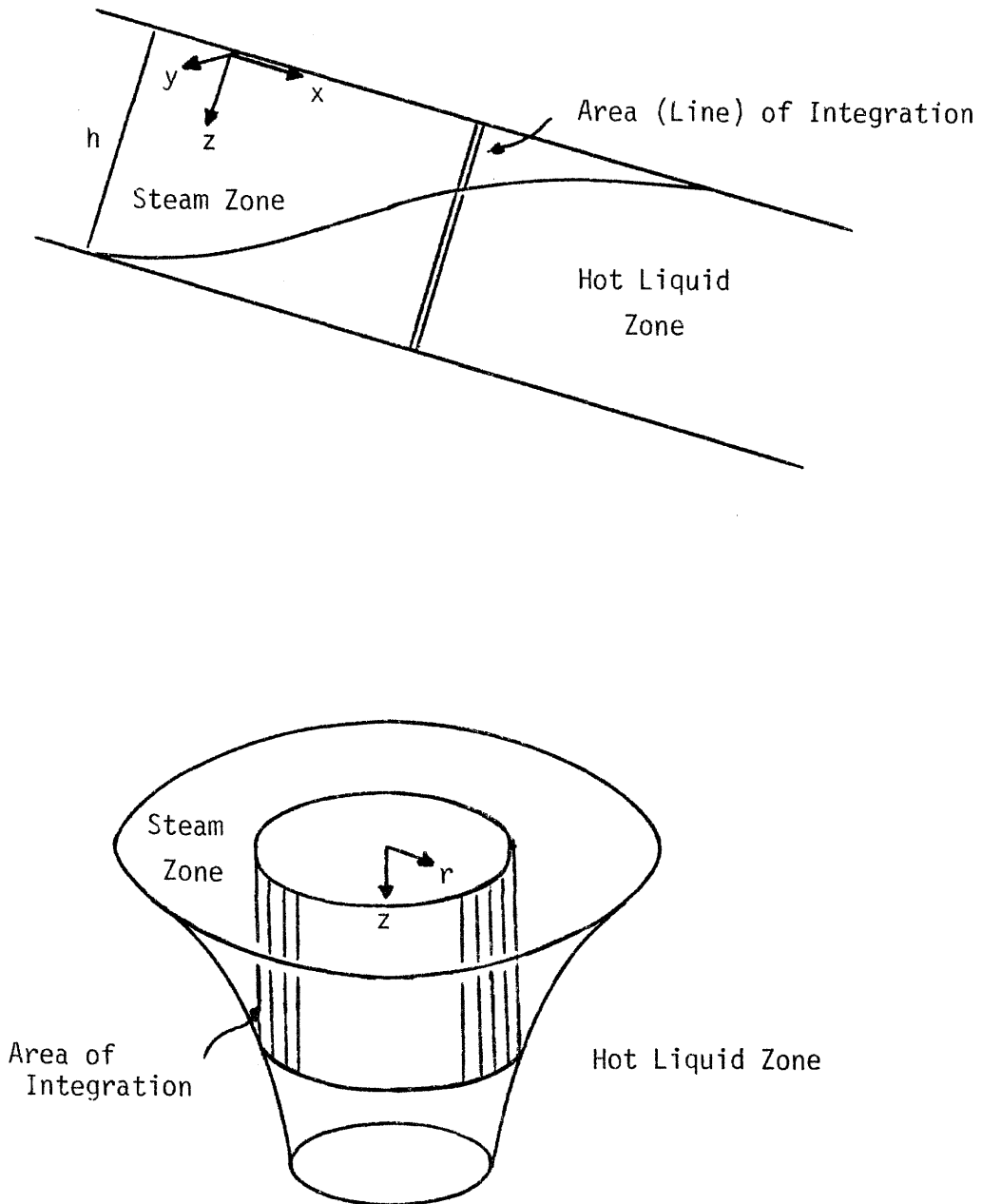


Figure 12. Geometries Examined in Subsection 2.4.4.
Notation for Area (Line) Integration.

where x stands for length or area, $\hat{u}_{ix} = u_{ix}$ or $2\pi r u_{ix}$ in rectangular or radially symmetric geometries, respectively.

Similarly, for the total water and oil mass balances in the steam zone

$$\begin{aligned} \frac{d}{dt} \int_0^{z(x,t)} (\phi \rho_s S_s + \phi \rho_w S_w) dz + \rho_w^{II} (u_{wn}^{II} - \phi S_w^{II} v_n) |\nabla F| \\ = - \frac{\partial}{\partial x} \left\{ \int_0^{z(x,t)} (\rho_s \hat{u}_{sx} + \rho_w \hat{u}_{wx}) dz \right\} \end{aligned} \quad (2.55)$$

$$\begin{aligned} \frac{d}{dt} \int_0^{z(x,t)} \phi \rho_o S_o dz + \rho_o^{II} (u_{on}^{II} - \phi S_o^{II} v_n) |\nabla F| \\ = - \frac{\partial}{\partial x} \int_0^{z(x,t)} \rho_o \hat{u}_{ox} dz \end{aligned} \quad (2.56)$$

Subtracting the proper linear combination of (2.56) and (2.55) from (2.54) we recover the steam mass balance:

$$\begin{aligned} \Delta T \frac{d}{dt} \int_0^{z(x,t)} M_z dz + \left(-k_{hR} \frac{\partial T_R}{\partial n} \right)^{II} |\nabla F| + \left(-k_{hf} \frac{\partial T_f}{\partial n} \right)^{II} \\ = - \frac{\partial}{\partial x} \left[\int_0^{z(x,t)} \rho_s L_V^{(1)} \hat{u}_{sx} dz \right] \end{aligned} \quad (2.57)$$

The analogy to the volume (area) averaged conservation Equations (2.47), (2.50) is obvious. Notice the convective term in the RHS of (2.54) - (2.57) in contrast to the source terms appearing in Eqs. (2.43)

(2.47), (2.50).

For the purpose of determining the steam front shape, it is necessary to integrate the water and oil mass balances inside the hot liquid zone as well

$$\frac{d}{dt} \int_{z(x,t)}^h \phi \rho_w S_w dz - \rho_w^{II} (u_{wn}^{II} - \phi S_w^{II} v_n) |\nabla F| = - \frac{\partial}{\partial x} \int_{z(x,t)}^h \rho_w \hat{u}_{wx} dz \quad (2.58)$$

$$\frac{d}{dt} \int_{z(x,t)}^h \phi \rho_o S_o dz - \rho_o^{II} (u_{on}^{II} - \phi S_o^{II} v_n) |\nabla F| = - \frac{\partial}{\partial x} \int_{z(x,t)}^h \rho_o \hat{u}_{ox} dz \quad (2.59)$$

Averaging along any other coordinate surface (line) is possible, of course. However, it seems that the above vertical integration is optimal, for it allows us to employ sound approximations in the modelling of the process. The technique of area (line) averaging is used in problems of two-dimensional, isothermal displacement [Sheldon and Fayers (1962), Beckers (1965)] and in ground water flow calculations [Bear (1972)]. In steam injection calculations, based on both volume or area integration, we have to deal with the additional coupling effect of interphase heat and mass transfer. This topic is studied in detail in later chapters.

2.5 Dimensional Analysis

To complete the study of the complex physical process of steam injection, before introducing any approximate techniques, we perform a dimensional analysis. The resulting dimensionless groups of parameters give rise to scaling rules for the design and comparison of laboratory and field projects and they help us obtain a first estimate on the

importance of various physical terms. The topic is not an integral part of the previous analysis and it is presented for the sake of completeness.

Dimensionally scaled models of oil reservoirs under conditions of isothermal and non-isothermal waterflooding are discussed by Geertsma et al. (1956) and van Daalen and van Damselaar (1972). In the area of steam injection, Niko and Troost (1971) provided a partial list of dimensionless groups together with the appropriate set of scaling rules.

To derive the important groups of parameters that are related to steam injection, one should proceed with a complete inspectional analysis of the relevant equations and boundary conditions derived in Subsections 2.3.1, 2.3.2. Details for this straightforward procedure are shown in Appendix II, where a compilation of the most important dimensionless groups is also presented.

Alternatively, an inspectional analysis of the integral balances would result to dimensionless groups that characterize the process in an integral sense. Thus, by nondimensionalizing the integral balances, Eqs. (2.47), (2.50), we recover the following groups shown in Table 2 (where asterisk denotes a characteristic dimensional quantity).

The groups in Table 2 also serve to define characteristic values for the two characteristic lengths and time. Thus, by letting $\Pi_1 = \frac{\pi}{16}$, $\Pi_5 = \frac{1}{2}$, we determine t^* , $L^{(1)*}$ (compare with Section 4.3). They can also provide a first estimate on the integral distribution of the heat injected into heat losses to the surrounding formations and to the hot liquid zone. Together with the mobility ratios (see Appendix II) they constitute a set of the most important dimensionless groups for steam injection. Since, however, a broader discussion falls outside the scope of the present study, we will not proceed on this subject any further.

Group

Name

Physical Meaning

$\Pi_1 = \left(\frac{\rho_f c_{pf}}{M_1^*} \right)^2 \frac{\alpha_f t^*}{h^2}$	Fourier Number	$\frac{[\text{Heat loss to surroundings}]}{[\text{S.Z. heat content rate of change}]}$
$\Pi_2 = \frac{c_{pw}^{(1)} \Delta T}{L_v^{(1)}}$	Stefan Number	$\frac{[\text{Sensible heat capacity}]}{[\text{Latent heat capacity}]}$
$\Pi_3 = \frac{M_2^*}{M_1^*}$	--	$\frac{[\text{S.Z. latent heat content}]}{[\text{S.Z. total heat content}]}$
$\Pi_4 = \frac{w_s^*}{w_s^* + w_w^*}$	Steam Quality	Steam Quality
$\Pi_5 = \frac{[(w_s^* + w_w^*) c_{pw}^{(1)} \Delta T + w_s^* L_v^{(1)}] t^*}{M_1^* \Delta T h [L^{(1)*}]^2}$	--	$\frac{[\text{Total heat injected}]}{[\text{S.Z. total heat content}]}$
$\Pi_6 = \frac{w_F^* t^*}{M_1^* L^{(1)*}}$	--	$\frac{[\text{Heat convection to H.L.Z.}]}{[\text{S.Z. total heat content}]}$
$\Pi_7 = \frac{w_F^* (L^{(2)*})}{k_{hR}}$	Peclet Number (H.L.Z.)	$\frac{[\text{Heat convection to H.L.Z.}]}{[\text{Heat conduction to H.L.Z.}]}$

Dimensionless Groups Arising from a Dimensional
Analysis of the Integral Balances (2.47), (2.50).

Table 2

2.6 Conclusions

In summary, the present chapter deals with the development of an integral technique the two versions of which, for one- and two- (or three-) dimensional systems, will be further utilized in the determination of the rate of growth of the steam zone volume and the steam front shape, respectively. The approach consists of a rigorous mathematical description of the steam injection process and a subsequent integration, along suitable coordinates, of the basic conservation equations. The region of integration varies, depending upon the particular purposes, from a three- to a two- (one-) dimensional domain. The resulting integral balances are exact. The unknown heat transfer and fluid flow terms that arise are further discussed and modelled in the chapters to follow. A preliminary analysis based on dimensional considerations has also been carried out in order to determine the important dimensionless groups of steam injection.

Chapter III. Heat Transfer Considerations

3.1 Introduction

The present chapter studies in detail the mechanism of heat transfer in the surrounding formations (Part A) and the hot liquid zone (Part B). As invoked from the integral formulation of Chapter II, modelling the heat fluxes that emanate from the steam zone is essential for the determination of the front dynamics. Since this is equally true for any other thermal method, the discussion is not restricted to steam injection exclusively but intends to cover a variety of other thermal methods.

In Section 3.2, we develop analytical expressions for the heat flux from the reservoir to the over- and under-burden (lateral heat losses) in terms of the temperature distribution inside the hot liquid zone. Various approximate solutions to the temperature distribution are obtained and the respective heat fluxes from the steam zone are computed in Sections 3.4 to 3.8. The intermediate Section 3.3 deals with the derivation of vigorous bounds on the various heat flux terms, with the objective of obtaining exact information regarding the front progress without recourse to approximate techniques.

Part A. Heat Transfer in the Surrounding Formations

3.2 Method of Approach

Heat is transferred to the surrounding formations by pure heat conduction as described by Eq. (2.17). This equation is coupled with

the convective and conductive heat transfer in the reservoir via the interface conditions, Eqs. (2.13a), (2.13b).

In most practical cases, convection dominates over conduction in the reservoir. Then, one can reasonably assume that heat transfer inside the surroundings occurs mainly through one-dimensional conduction along the coordinate vertical to the bounding surface of the reservoir. The effectiveness of the approximation depends upon the magnitude of the local Peclet number

$$Pe = \frac{L^{(2)*} \bar{w}_R}{k_{hR}} \quad (3.1)$$

where $L^{(2)*}$ is a characteristic length along the boundary and \bar{w}_R represents an average convective heat flux term. (See also Sections 3.7 and 3.8.)

For most steam injection processes, Pe is large enough, $O(10^2)$, (see Section 4.5) to justify the use of the above simplification, when calculating the amount of heat transferred from the reservoir to the surroundings. [Chase and O'Dell (1973), compare also with Lauwerier (1955), Marx and Langenheim (1959) and Avdonin (1964)].

The approximation has been tested by both analytical [Thomas (1967)] and numerical methods [Spillette (1965), Coats et al. (1974)] with the result that including horizontal conduction in hot water or steam injection calculations does not produce significant differences. The reservoir geometry plays also an important role, the assumption being better as the boundaries have a smaller curvature. Due to

stratification, most reservoirs have relatively uniform width and straight boundaries, hence this condition is usually satisfied.

Having made the above assumption, we can calculate the lateral heat losses, $-k_{hf} \left(\frac{\partial T_f}{\partial n} \right) II$, by considering the heat flux at the origin of a one-dimensional, semi-infinite, heat conducting medium with a surface temperature which is an arbitrary function of time and the horizontal coordinates, and an initial temperature, T_i , constant.

3.2.1 Calculation of the Heat Flux

Consider the Cartesian coordinate system x, y, z shown in Figure 13. Let $z' = -z$ be the coordinate along which heat is conducted, $T_f(x, y, z', t)$ the formation temperature. Then,

$$\frac{\partial T_f}{\partial t} = \alpha_f \frac{\partial^2 T_f}{\partial z'^2} \quad (3.2)$$

with

$$\begin{aligned} T_f(x, y, z', 0) &= T_i \\ T_f(x, y, 0, t) &= T_i + \phi(x, y, t) \\ T_f(x, y, \infty, t) &= T_i \end{aligned}$$

In calculating the heat flux at $z' = 0$, we can follow a straightforward Green's function approach [Stakgold (1968)] or make use of the following shortcut:

Define $T(x, y, z', t) = T_f(x, y, z', t) - T_i$ and rewrite (3.2)

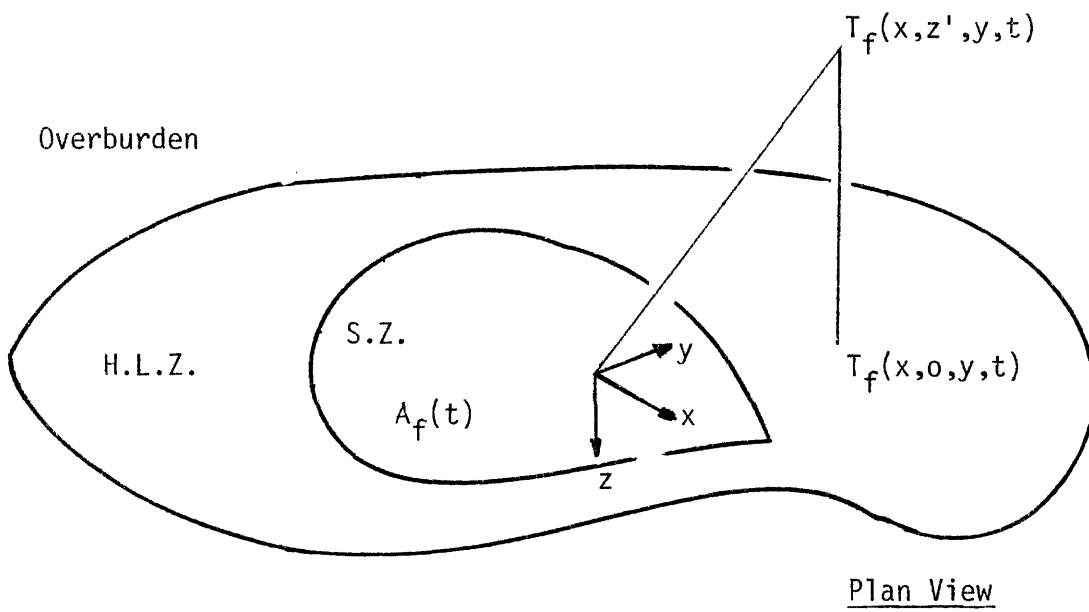


Figure 13. System of Coordinates and Notation for Subsection 3.2.1.

$$\frac{\partial T}{\partial t} = \alpha_f \frac{\partial^2 T}{\partial z'^2} \quad (3.3)$$

with

$$T(x, y, z', 0) = 0$$

$$T(x, y, 0, t) = \phi(x, y, t)$$

$$T(x, y, \infty, t) = 0$$

Let $L_t F$, $L_z F$ represent the Laplace Transform of the function F with respect to t and z' and denote the transform variables by s and ζ , respectively. Take the Laplace Transform of (3.3) successively with respect to z', t . Then,

$$\frac{\partial}{\partial t} [L_z T] = \alpha_f \zeta^2 L_z T - \alpha_f \zeta \phi(x, y, t) - \alpha_f q(x, y, t) \quad (3.4a)$$

$$s L_t L_z T = \alpha_f \zeta^2 L_t L_z T - \alpha_f \zeta L_t \phi - \alpha_f L_t q \quad (3.4b)$$

$$L_t L_z T = \frac{\alpha_f \zeta}{\alpha_f \zeta^2 - s} L_t \phi + \frac{\alpha_f}{\alpha_f \zeta^2 - s} L_t q \quad (3.4c)$$

where

$$q(x, y, t) = \left. \frac{\partial T}{\partial z'} \right|_0 \quad (3.5)$$

Inverting (3.4c) with respect to z' and recalling that L_t , L_z commute, one obtains

$$L_t T = \cosh \left(\sqrt{\frac{s}{\alpha_f}} z' \right) L_t \phi + \sqrt{\frac{\alpha_f}{s}} \sinh \left(\sqrt{\frac{s}{\alpha_f}} z' \right) L_t q \quad (3.6)$$

[Abramowitz and Stegun (1965)]. But $L_t T$ is a finite function of z' , for all z' , and this can only happen if, in (3.6),

$$L_t q = - \sqrt{\frac{s}{\alpha_f}} L_t \phi \quad (3.7)$$

Inversion of (3.7) for a continuous and piecewise smooth function $\phi(x,y,t)$ results to

$$q(x,y,t) = - \frac{1}{\sqrt{\pi\alpha_f}} \cdot \frac{\partial}{\partial t} \int_0^t \frac{\phi(x,y,\tau) d\tau}{\sqrt{t-\tau}} \quad (3.8)$$

and finally

$$- k_{hf} \left(\frac{\partial T_f}{\partial n} \right)^{II} = \frac{k_{hf}}{\sqrt{\pi\alpha_f}} \cdot \frac{\partial}{\partial t} \int_0^t \frac{\phi(x,y,\tau) d\tau}{\sqrt{t-\tau}} \quad (3.9)$$

In terms of fractional calculus notation [Oldham and Spanier (1974)]

$$- k_{hf} \left(\frac{\partial T_f}{\partial n} \right)^{II} = \frac{k_{hf}}{\sqrt{\alpha_f}} I^{(-\frac{1}{2})} \phi(x,y,t) \quad (3.10)$$

We thus expressed the local instantaneous heat losses from the reservoir to the surrounding formations, in terms of the temperature history at any point of the reservoir boundaries. Note that the above result is valid for any thermal recovery process and it may considerably facilitate heat transfer calculations [compare with Chase and O'Dell (1973), Weinstein (1972), Weinstein (1974)]. According to the functional form of $\phi(x,y,t)$, we consider the following subcases.

3.2.2 Hot Water Injection

Here, $\phi(x,y,t)$ is a continuously differentiable function of t (see Figure 14a) and (3.9) reduces to:

$$-k_{hf} \left(\frac{\partial T_f}{\partial n} \right) II = \frac{k_{hf}}{\sqrt{\pi\alpha_f}} \int_0^t \frac{\partial \phi(x,y,\tau)}{\partial \tau} \cdot \frac{d\tau}{\sqrt{t-\tau}} \quad (3.11)$$

3.2.3 Steam Injection. Continuously Advancing Steam Front

For a continuously advancing steam front ($v_n > 0$), a typical temperature distribution at the reservoir-overburden interface would be (see Figure 14 b)

$$\phi(x,y,t) = \begin{cases} \phi(x,y,t) & 0 < t \leq \lambda(x,y) \\ T_s - T_i & \lambda(x,y) \leq t \end{cases} \quad (3.12)$$

with $\phi(x,y,t)$, $0 < t \leq \lambda(x,y)$ a continuously differentiable function of t .

Therefore,

$$-k_{hf} \left(\frac{\partial T_f}{\partial n} \right) II = \frac{k_{hf}}{\sqrt{\pi\alpha_f}} \begin{cases} \int_0^t \frac{\partial \phi(x,y,\tau)}{\partial \tau} \cdot \frac{d\tau}{\sqrt{t-\tau}} & 0 < t \leq \lambda(x,y) \\ \frac{T_s - T_i}{\sqrt{t - \lambda(x,y)}} - \frac{1}{2} \int_0^{\lambda(x,y)} \frac{\phi(x,y,\tau)}{(t-\tau)^{3/2}} d\tau & \lambda(x,y) \leq t \end{cases} \quad (3.13)$$

Related to this case is the step temperature distribution assumed by Marx-Langenheim (1959) (see Figure 14c)

$$\phi(x,y,t) = \begin{cases} 0 & 0 < t < \lambda(x,y) \\ T_s - T_i & \lambda(x,y) < t \end{cases} \quad (3.14)$$

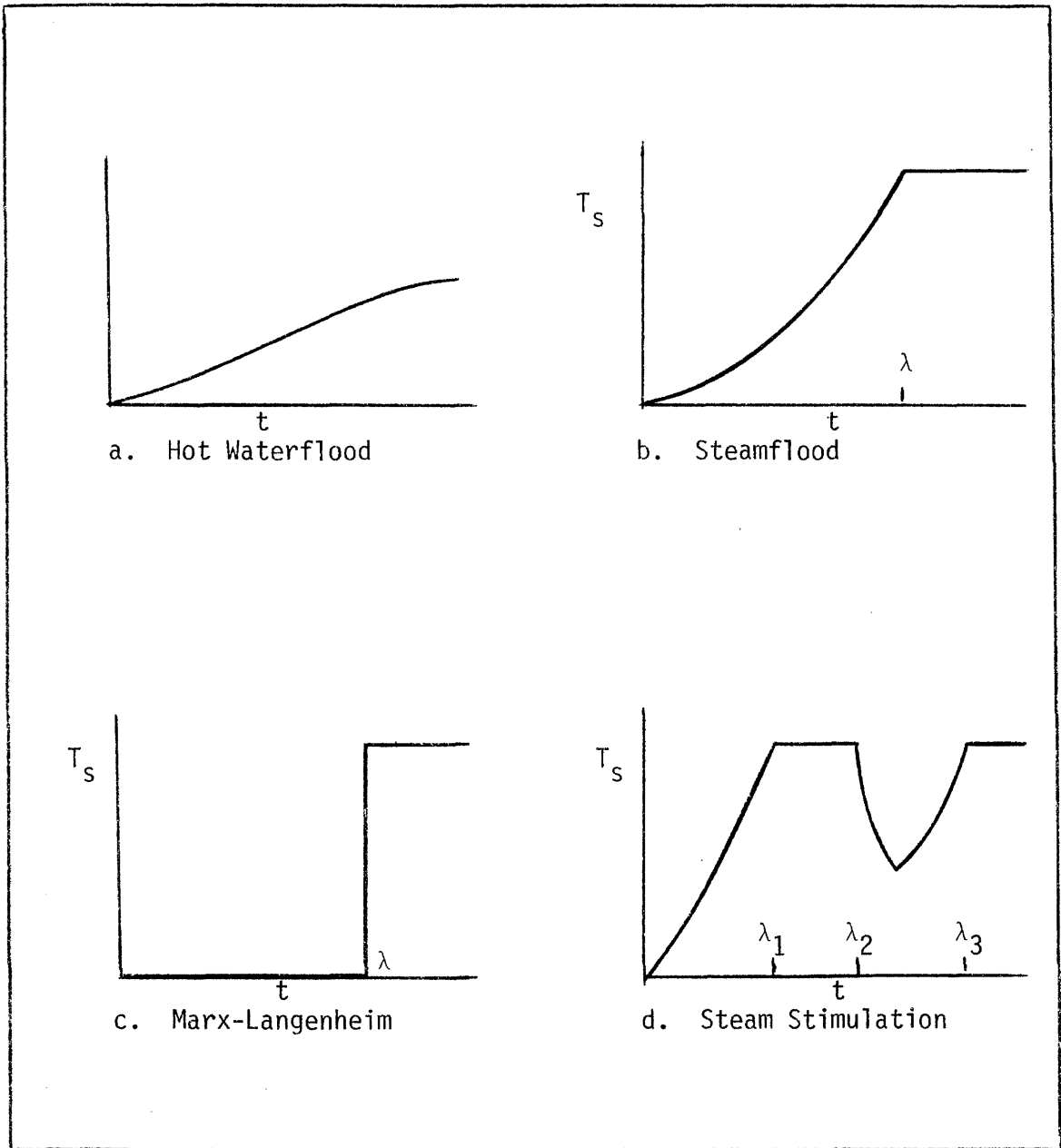


Figure 14. Typical Temperature Profiles at a Point at the Reservoir-Surrounding Formations Interface, for Various Thermal Recovery Processes.

Then, from (3.9)

$$-k_{hf} \left(\frac{\partial T_f}{\partial n} \right) II = \begin{cases} 0 & 0 < t < \lambda(x,y) \\ \frac{k_{hf}}{\sqrt{\pi\alpha_f}} \cdot \frac{(T_s - T_i)}{\sqrt{t - \lambda(x,y)}} & \lambda(x,y) < t \end{cases} \quad (3.15)$$

the well-known formula, widely used in previous analytical modeling of steam injection [see also Mandl and Volek (1969), Shutler and Boberg (1972)]. In both (3.13) and (3.15), $\lambda(x,y)$ represents the time it takes for the front to reach the point (x,y) , and is a single-valued function of (x,y) , for continuously advancing fronts.

3.2.4 Steam Injection. Arbitrary Propagation of the Steam Front

In arbitrary steam injection, the front is not necessarily advancing at all times. Depending on the injection rates and other reservoir characteristics, such as inhomogeneities, etc., the front may locally or globally recede on a certain time interval. The boundary temperature $\phi(x,y,t)$ follows an analogous variation (see Figure 14d).

$$\phi(x,y,t) = \begin{cases} \phi_{2k+1}(x,y,t) & \lambda_{2k}(x,y) \leq t \leq \lambda_{2k+1}(x,y) \\ & k = 0, 1, 2, \dots \\ T_s - T_i & \lambda_{2k+1}(x,y) \leq t \leq \lambda_{2k+2}(x,y) \end{cases} \quad (3.16)$$

where, now, $\lambda(x,y)$ is a multi-valued function of (x,y) .

Such a situation is most commonly realized in steam-stimulation operations where injection rates vary periodically between zero and constant levels [Boberg and Lantz (1966)]. It is also frequent in steam

injection, when injection rates cannot sustain a continuous rate of advance.

The resulting heat flux is given by the lengthy but simple expression:

$$-k_{hf} \left(\frac{\partial T_f}{\partial n} \right)_{II} = \frac{k_{hf}}{\sqrt{\pi \alpha_f}} \cdot$$

$$\left\{ \begin{aligned} & -\frac{1}{2} \sum_{k=0}^{m-1} \int_{\lambda_{2k}}^{\lambda_{2k+1}} \frac{\phi_{2k+1}(x,y,\tau) d\tau}{(t-\tau)^{3/2}} - (T_s - T_i) \sum_{k=0}^{m-1} \left[\frac{1}{\sqrt{t - \lambda_{2k+2}(x,y)}} \right. \\ & \left. - \frac{1}{\sqrt{t - \lambda_{2k+1}(x,y)}} \right] + \frac{\partial}{\partial t} \int_{\lambda_{2m}}^t \frac{\phi_{2m+1}(x,y,\tau) d\tau}{\sqrt{t-\tau}} \quad \lambda_{2m}(x,y) < t < \lambda_{2m+1}(x,y) \\ \\ & -\frac{1}{2} \sum_{k=0}^m \int_{\lambda_{2k}}^{\lambda_{2k+1}} \frac{\phi_{2k+1}(x,y,\tau) d\tau}{(t-\tau)^{3/2}} - (T_s - T_i) \sum_{k=0}^{m-1} \left[\frac{1}{\sqrt{t - \lambda_{2k+2}(x,y)}} \right. \\ & \left. - \frac{1}{\sqrt{t - \lambda_{2k+1}(x,y)}} \right] + \frac{(T_s - T_i)}{\sqrt{t - \lambda_{2m+1}(x,y)}} \quad \lambda_{2m+1}(x,y) < t < \lambda_{2m+2}(x,y) \end{aligned} \right.$$

(3.17)

Obviously, the lower part is used when the point (x,y) is located inside the steam zone, otherwise the top formula prevails. Analogous results are also obtained for other thermal processes, such as combustion, the detailed study of which is outside the scope of the present discussion.

3.3 Derivation of Bounds on the Heat Fluxes

The above equations express the heat losses from the reservoir to the overburden and underburden as function of the temperature at the reservoir boundaries, $\phi(x,y,t)$. The latter is an unknown function to be determined by the simultaneous solution of the heat and momentum transfer in the hot liquid zone and the surrounding formations. This problem will be treated by two methods. One is an approximate analytical solution developed in Part B. The other utilizes known properties of $\phi(x,y,t)$, in order to derive useful bounds for the heat losses to the surroundings and the heat flux to the hot liquid zone. These will eventually be used to obtain rigorous bounds for the rate of growth of the steam zone.

3.3.1 Bounds on the Heat Losses to the Surrounding Formations

In steam injection, the function $\phi(x,y,t)$ satisfies the constraints

$$0 \leq \phi(x,y,t) \leq T_s - T_i; \quad \forall (x,y) \in R, \quad t > 0$$

In view of this, the following inequalities result for any (x,y) inside the steam zone

$$\frac{k_{hf}}{\sqrt{\pi\alpha_f}} \cdot \frac{(T_s - T_i)}{\sqrt{t}} \left\langle -k_{hf} \left(\frac{\partial T_f}{\partial n} \right) \right\rangle^{II} \left\langle \frac{k_{hf}}{\sqrt{\pi\alpha_f}} \cdot \frac{(T_s - T_i)}{\sqrt{t - \lambda_{2m+1}^2(x,y)}} \right\rangle \quad (3.18a)$$

where $\lambda_{2m+1}(x,y) \leq t \leq \lambda_{2m+2}(x,y)$, m arbitrary. Recall that for continuously advancing front, $m = 0$ in (3.18a).

In physical terms, the upper bound in (3.18a) represents the instantaneous heat losses that would result out of a step temperature distribution

$$T_R(x,y,t) = \begin{cases} T_i & 0 < t < \lambda_{2m+1}(x,y) \\ T_s & \lambda_{2m+1}(x,y) < t \end{cases}$$

while the lower bound corresponds to the heat losses that would result if the temperature assumes the constant value T_s as soon as steam injection begins. When heat transfer in the hot liquid zone is conduction dominated, the actual heat losses approach the upper bound, whereas when convection dominates, the heat losses term is closer to the lower bound.

Integrating (3.18a), we establish bounds on the integral heat losses:

$$\begin{aligned} & \frac{k_{hf}(T_s - T_i)}{\sqrt{\pi\alpha_f}} \cdot \frac{1}{\sqrt{t}} \int_{A_f(t)} dA \left\langle \int_{A_f(t)} \left(-k_{hf} \frac{\partial T_f}{\partial n} \right) \right\rangle^{II} dA \left\langle \frac{k_{hf}(T_s - T_i)}{\sqrt{\pi\alpha_f}} \right\rangle \\ & \cdot \int_{A_f(t)} \frac{dA}{\sqrt{t - \lambda_{2m+1}^2(x,y)}} \end{aligned} \quad (3.18b)$$

3.3.2 Bounds on the Heat Fluxes to the Hot Liquid Zone

By the very definition of the hot liquid zone $T_R(\underline{r}', t) \leq T_s$, thus, the local conductive heat flux into the hot liquid zone is non-negative

$$\left(-k_{hR} \frac{\partial T_R}{\partial n} \right)^{II} \geq 0 \quad \forall t > 0 \quad (3.19a)$$

Integrating over the steam front,

$$\Delta T A_F(t) Q_F(t) = \int_{A_F(t)} \left(-k_{hR} \frac{\partial T_R}{\partial n} \right)^{II} dA \geq 0 \quad \forall t > 0 \quad (3.19b)$$

which serves to bound the total conductive heat flux from below.

In order to bound the net heat flux through the steam front we consider an entropy balance across the steam front. Recalling the second law of thermodynamics, for an irreversible process, we define,

$$\begin{aligned} & \left(-k_{hR} \frac{\partial T_R}{\partial n} \right)^{II} + \Delta T \sum_{i=w,0} \rho_i^{II} c_{pi} (u_{in}^{II} - \phi S_i^{II} v_n) \\ & - (1 - \phi) \Delta T \rho_R c_{pR} v_n = T_s \Delta_i > 0 \quad \forall t > 0 \end{aligned} \quad (3.20a)$$

and a fortiori

$$\begin{aligned} \Delta T A_F(t) \{W_F(t) + Q_F(t)\} &= \left\{ \Delta T \sum_{i=w,0} c_{pi} \int_{A_F(t)} \rho_i^{II} (u_{in}^{II} - \phi S_i^{II} v_n) dA \right. \\ &\quad \left. - (1 - \phi) \Delta T c_{pR} \int_{A_F(t)} \rho_R v_n dA + \int_{A_F(t)} \left(-k_{hR} \frac{\partial T_R}{\partial n} \right)^{II} dA \right\} \\ &= T_s \int_{A_F(t)} \Delta_i dA > 0 \quad \forall t > 0 \end{aligned} \quad (3.20b)$$

where Δ_i is a positive entropy source at the interface [see Delhaye (1974)]. The above inequalities state that the steam front must move in such a way so that the net heat flux through the steam front is positive.

Expressions (3.19b), (3.20b) provide lower only bounds for the heat fluxes to the hot liquid zone, in contrast to (3.18b) which bounds the heat losses from above as well. It is also easily verified that the bounds in (3.18b) and (3.19b), (3.20b) are independent from each other, which implies that in the process, we uncoupled the heat transfer in the hot liquid zone and the surroundings. This, in turn, suggests that we may be able to arrive at closer bounds, but only after a detailed study of the heat transfer in the hot liquid zone.

Part B. Heat Transfer in the Hot Liquid Zone

3.4 Method of Approach

The differential equations (2.13), (2.14), (2.16) coupled to Eq. (2.17) describe the momentum and heat transfer in the hot liquid region of any thermal method (steam flood, hot waterflood, combustion). Because the complexity of the problem prohibits a complete, analytic solution for an arbitrary geometry, we propose to proceed from simpler to more complex systems (depending on the approximations made and the dimensionality of the problem) as shown in Figure 15.

Our investigation starts with one-dimensional heat transfer with zero heat losses (Section 3.5). The resulting solutions form the basis for approximate solutions in harder two-dimensional systems (Section 3.6) and are also utilized in connection with exact solutions of one-dimensional

heat transfer including heat losses (Sections 3.7, 3.8). The underlying approximation in all cases involves decoupling momentum from heat transfer. Quantitatively, this amounts to considering the convective term in the heat equation as either constant or a known function of the independent (or dependent) variables. This assumption becomes better as the difference between the volumetric heat capacities of water and oil gets smaller. Indeed, from a linear combination of (2.13), (2.14) and for slowly varying heat capacities one obtains:

$$\phi \frac{\partial}{\partial t} (\rho_w c_{pw} S_w + \rho_o c_{po} S_o) + \nabla \cdot (\rho_w c_{pw} u_w + \rho_o c_{po} u_o) = 0$$

Now, the quantity $\phi(\rho_w c_{pw} S_w + \rho_o c_{po} S_o)$ is fairly insensitive to variations in liquid saturation [Prats (1969)] and then

$$\nabla \cdot (\rho_w c_{pw} u_w + \rho_o c_{po} u_o) = 0$$

In one-dimensional geometries this further implies

$$\rho_w c_{pw} u_{wx} + \rho_o c_{po} u_{ox} = \text{const.}$$

as postulated. In the spirit of this approximation, viscosity reduction plays an important role in determining the saturation distribution and oil recovery, but does not significantly alter the heat transfer mechanism.

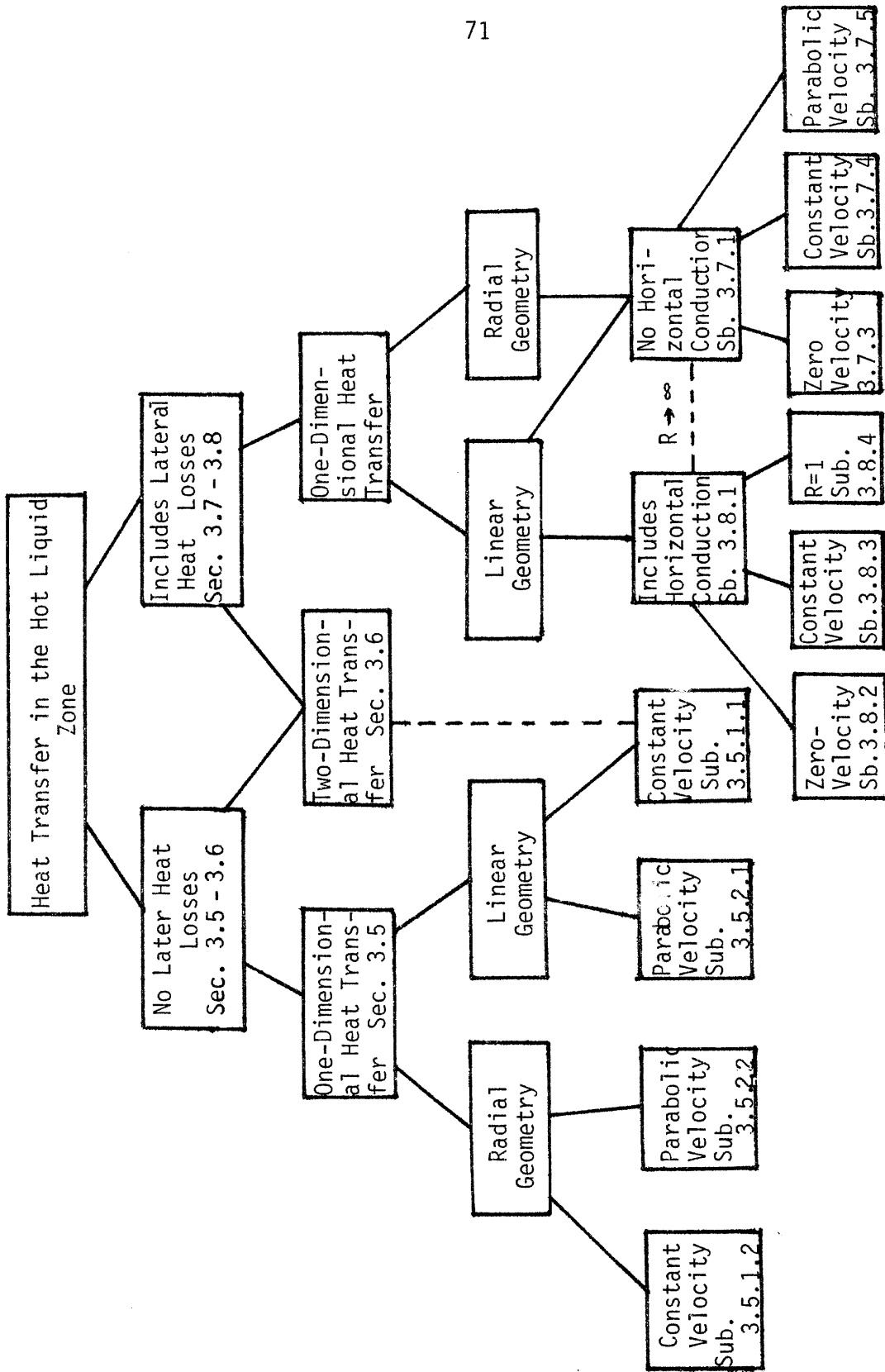


Figure 15. Approach Followed in Studying Heat Transfer in the Hot Liquid Zone.

3.5 One-Dimensional Heat Transfer in the Hot Liquid Zone by Conduction and Convection, with a Steady or Moving Boundary but with no Lateral Heat Losses

The one-dimensional thermal energy equation reads as follows:

$$\begin{aligned} & \left(\phi S_w \rho_w c_{pw} + \phi S_o \rho_o c_{po} + (1 - \phi) \rho_R c_{pR} \right) \frac{\partial T_R}{\partial t} \\ & + (u_{wx} \rho_w c_{pw} + u_{ox} \rho_o c_{po}) \frac{\partial T_R}{\partial x} = k_{hR} \frac{\partial^2 T_R}{\partial x^2} \end{aligned} \quad (3.21a)$$

in linear and

$$\begin{aligned} & \left(\phi S_w \rho_w c_{pw} + \phi S_o \rho_o c_{po} + (1 - \phi) \rho_R c_{pR} \right) \frac{\partial T_R}{\partial t} \\ & + (u_{wr} \rho_w c_{pw} + u_{or} \rho_o c_{po}) \frac{\partial T_R}{\partial r} = \frac{k_{hR}}{r} \frac{\partial}{\partial r} \left(r \frac{\partial T_R}{\partial r} \right) \end{aligned} \quad (3.21b)$$

in radially symmetric geometry. The boundary conditions involve a moving boundary:

$$\begin{aligned} t = 0; \quad T_R &= T_i \\ x, r \rightarrow \infty; \quad T_R &\rightarrow T_i \\ x, r &= \int_0^t v(\tau) d\tau; \quad T_R = T_s \end{aligned}$$

where $v(t) \neq 0$ for steamflood or combustion, $v(t) \equiv 0$ for a hot water flood. The domain of integration of (3.21) is $x, r \geq \int_0^t v(\tau) d\tau, 0 < t$. We can now examine the following cases depending on the functional form of $v(t)$.

3.5.1 Constant Boundary Velocity

3.5.1.1 Constant Boundary Velocity, Linear Geometry

Let

$$M^{(2)} = \phi S_w \rho_w c_{pw} + \phi S_o \rho_o c_{po} + (1 - \phi) \rho_R c_{pR} \quad (3.23a)$$

$$W_F = u_{wx} \rho_w c_{pw} + u_{ox} \rho_o c_{po} - M^{(2)} v \quad (3.23b)$$

For typical values of $\rho_w c_{pw}$, $\rho_o c_{po}$, $\rho_R c_{pR}$, the volumetric heat capacity term $M^{(2)}$ remains approximately constant and, as already shown, the same is true for the convective term. For a boundary moving with constant velocity, both $M^{(2)}$, W_F can be treated as constant.

Going over to a system of coordinates t , $\xi = x - vt$ and scaling $T_R - T_i$ with $T_s - T_i$, ξ with $x^* = \left(\frac{k_{hR}}{|W_F|} \right)$ and time t with $t^* = \left(\frac{x^{*2} M^{(2)}}{k_{hR}} \right)$, we get in dimensionless notation (subscript D indicates dimensionless quantity)

$$\frac{\partial T_D}{\partial t_D} + \frac{W_F}{|W_F|} \frac{\partial T_D}{\partial \xi_D} = \frac{\partial^2 T_D}{\partial \xi_D^2} \quad 0 < \xi_D < \infty, \quad 0 < t_D \quad (3.24)$$

with

$$t_D = 0 ; \quad T_D = 0$$

$$\xi_D \rightarrow \infty ; \quad T_D \rightarrow 0$$

$$\xi_D = 0 ; \quad T_D = 1$$

The solution of (3.24) is easily obtained by a Laplace transformation [see also Carslaw and Jaeger (1959)]

$$T_D = \frac{1}{2} \left\{ \operatorname{erfc} \left(\frac{\xi_D - t_D \frac{W_F}{|W_F|}}{2(t_D)^{1/2}} \right) + \exp \left(\frac{W_F}{|W_F|} \xi_D \right) \operatorname{erfc} \left(\frac{\xi_D + t_D \frac{W_F}{|W_F|}}{2(t_D)^{1/2}} \right) \right\} \quad (3.25)$$

Figure 16 shows typical profiles of T_D versus ξ_D , for various t_D , for constant boundary temperature. The quantity of most interest, for steam injection calculations, is the conductive heat flux through the moving origin:

$$\left. \frac{\partial T_D}{\partial \xi_D} \right|_0 = \frac{1}{2} \frac{W_F}{|W_F|} - \left\{ \frac{e^{-\frac{t_D}{4}}}{\sqrt{\pi t_D}} + \frac{1}{2} \operatorname{erf} \left(\frac{\sqrt{t_D}}{2} \right) \right\} \quad (3.26)$$

As $t_D \rightarrow \infty$,

$$\left. \frac{\partial T_D}{\partial \xi_D} \right|_0 \sim \frac{1}{2} \left(\frac{W_F}{|W_F|} - 1 \right) + o \left(\frac{e^{-\frac{t_D}{4}}}{t_D^{3/2}} \right) \quad (3.27)$$

The convergence, being exponential, is very rapid and we can, thus, deduce:

- (1) When $W_F < 0$, i.e., when the net convective heat flux through the front is negative, $\left. \frac{\partial T_D}{\partial \xi_D} \right|_0$ approaches exponentially -1.

One can easily show that the corresponding temperature distribution approaches the quasi-steady solution:

$$T_D \sim e^{-\xi_D} \quad (3.28)$$

[see Figure 16 and Miller (1975)]

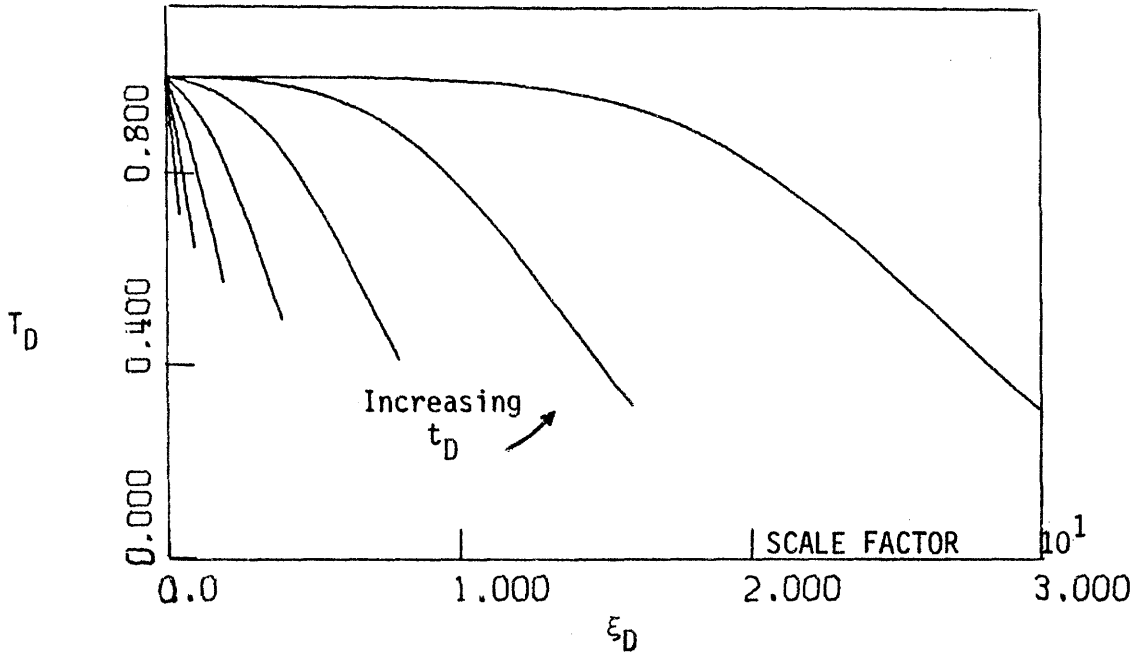


Figure 16a. Temperature Profiles of Eq. (3.25) for $W_F = 1$ and $t_D = 0.4, 0.8, 1.6, 3.2, 6.4, 12.8, 25.6$.

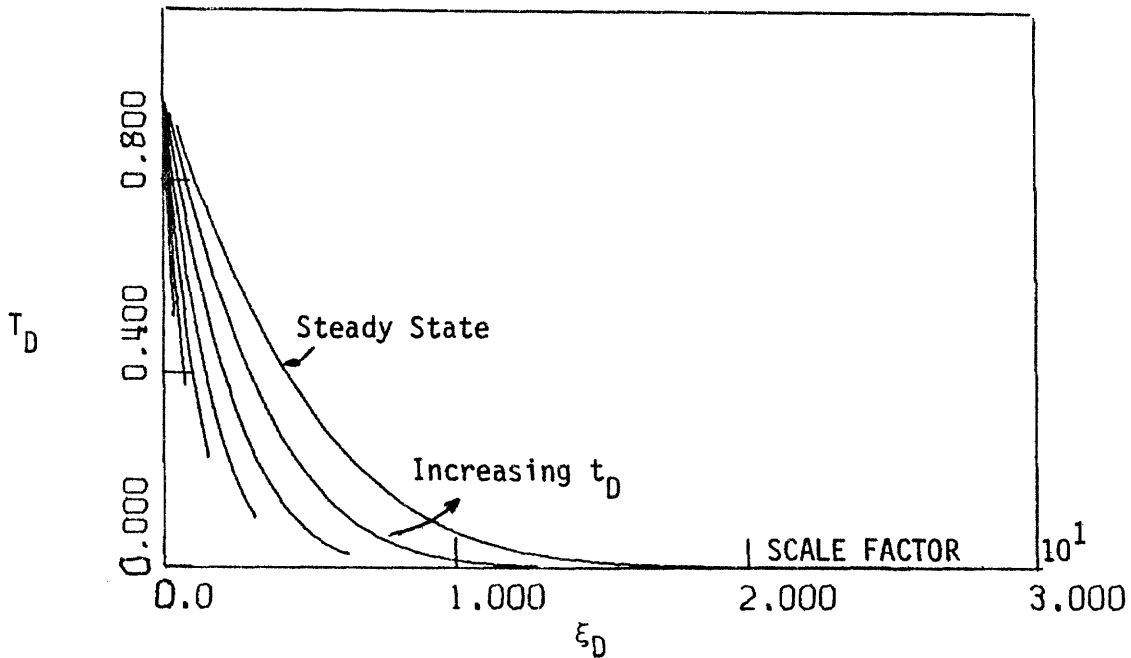


Figure 16b. Temperature Profiles of Eq. (3.25) for $W_F = -1$ and $t_D = 0.4, 0.8, 1.6, 3.2, 6.4, 12.8, 25.6$.

- (2) When $W_F > 0$, i.e., when the net convective heat flux through the front is positive, $\frac{\partial T_D}{\partial \xi} \bigg|_0$ approaches exponentially zero.

The corresponding expression for the dimensional conductive heat flux is

$$-k_{hR} \frac{\partial T_R}{\partial x} \bigg|_{x=0} = \int_0^t v(\tau) d\tau \sim \begin{cases} (T_s - T_i) |W_F| & W_F < 0 \\ 0 & W_F > 0 \end{cases} \quad (3.29)$$

The characteristic time for convergence to the steady state is $O(4t^*)$ and in dimensional variables $O\left(4 \frac{k_{hR} M^{(2)}}{W_F^2}\right)$. Accordingly, the larger

the absolute value of the net convective heat flux through the front, the faster the approach to the quasi-steady state conditions.

3.5.1.2 Constant Boundary Velocity, Cylindrical Geometry

In cylindrical coordinates, the constant convection approximation translates into:

$$u_{wr} \rho_w c_{pw} + u_{or} \rho_o c_{po} = \frac{q}{2\pi r} \quad (3.30)$$

where $q > 0$ is assumed constant. Scaling the independent variables by $\frac{t^*}{r^{*2}} = \frac{M^{(2)}}{q}$ we obtain the following dimensionless version of (3.21b), in fixed coordinates

$$\frac{\partial T_D}{\partial t_D} + \frac{1}{2\pi r_D} \cdot \frac{\partial T_D}{\partial r_D} = \frac{1}{Pe} \cdot \frac{1}{r_D} \frac{\partial}{\partial r_D} \left(r_D \frac{\partial T_D}{\partial r_D} \right) \quad 0 < r_D < \infty, 0 < t_D \quad (3.31)$$

with

$$t_D = 0; \quad T_D = 0$$

$$r_D \rightarrow \infty; \quad T_D \rightarrow 0$$

$$r_D = 0; \quad T_D = 1$$

In solving (3.31), we first note that when $Pe = \left(\frac{q}{k_{hR}} \right)$ is equal to 2π , Eq. (3.31) reduces to the thoroughly examined, pure heat conduction equation. When $Pe \neq 2\pi$ the similarity transformation $\eta = \frac{2\pi r_D^2}{t_D}$ leads

to the equation

$$(2 - \eta) \frac{dT_D}{d\eta} = \frac{4}{Pe} \left(\eta \frac{d^2 T_D}{d\eta^2} + \frac{dT_D}{d\eta} \right)$$

with solution

$$T_D = 1 - P\left(\beta, \frac{Pe r_D^2}{4t_D}\right) \quad (3.32)$$

where $P(a, x)$ is the incomplete Gamma function, $\beta = \frac{Pe}{4\pi}$.

When the radial velocity of the boundary is constant, the problem is not as easy to solve, except in the special case $Pe = 2\pi$. However, we can still obtain the steady state solutions. In the moving coordinates

$$t, \rho = r - vt$$

the dimensionless equation reads:

$$\frac{\partial T_D}{\partial t_D} + \left(\frac{1}{2\pi(\rho_D + v_D t_D)} - v_D \right) \frac{\partial T_D}{\partial \rho_D} = \frac{1}{Pe} \cdot \frac{\partial^2 T_D}{\partial \rho_D^2} + \frac{1}{Pe} \cdot \frac{1}{(\rho_D + v_D t_D)} \cdot \frac{\partial T_D}{\partial \rho_D} \quad (3.33)$$

with

$$t_D = 0 ; T_D = 0$$

$$\rho_D \rightarrow \infty ; T_D \rightarrow 0$$

$$\rho_D = 0 ; T_D = 1$$

In the limit of large t_D we can extract the steady-states

$$- v_D \frac{\partial T_D}{\partial \rho_D} \sim \frac{1}{Pe} \cdot \frac{\partial^2 T_D}{\partial \rho_D^2} \quad (3.34)$$

$$T_D \sim e^{-Pe v_D \rho_D} \quad (3.35)$$

analogous to Equation (3.28) of the linear problem. The conductive heat flux at the moving origin, in dimensional notation, becomes

$$- k_{hR} \left. \frac{\partial T}{\partial r} \right|_{r=vt} \sim (T_s - T_i) v M^{(2)} \quad (3.36)$$

which indicates that in such a case the convective heat transfer is dominated, at large times, solely by the steam front velocity [compare to (3.29)].

3.5.2 Convective Term a Function of Time

3.5.2.1 A Particular Solution. Linear Geometry.

When the net convective heat flux W_{FD} is proportional to $1/\sqrt{t_D}$, the

heat transfer problem is defined by

$$\frac{\partial T_D}{\partial t_D} - \frac{\alpha}{\sqrt{t_D}} \cdot \frac{\partial T_D}{\partial \xi_D} = \frac{\partial^2 T_D}{\partial \xi_D^2} ; \quad 0 < t_D, \quad 0 < \xi_D \quad (3.37)$$

$$t_D = 0 ; T_D = 0$$

$$\xi_D \rightarrow \infty ; T_D \rightarrow 0$$

$$\xi_D = 0 ; T_D = 1$$

This situation is often visualized in a pure heat conduction problem with a boundary moving with velocity $v_D = \frac{\alpha}{\sqrt{t_D}}$.

The solution of (3.37) is obtained via the similarity transformation

$$\eta = \xi_D / 2t_D^{1/2} + \alpha. \text{ Then,}$$

$$-\eta \frac{dT_D}{d\eta} = \frac{1}{2} \frac{d^2 T_D}{d\eta^2} \quad (3.38)$$

which, if solved together with the appropriate boundary conditions, generates the solution of (3.37) in terms of ξ_D, t_D :

$$T_D(t_D, \xi_D) = \operatorname{erfc} \left\{ \xi_D / 2t_D^{1/2} + \alpha \right\} / \operatorname{erfc} \alpha \quad (3.39)$$

Figure 17 shows typical T_D profiles for various t_D and α . The important conductive heat flux at the origin becomes

$$\left. \frac{\partial T_D}{\partial \xi_D} \right|_0 = - \frac{1}{\sqrt{\pi t_D}} \cdot \frac{\exp(-\alpha^2)}{\operatorname{erfc} \alpha} \quad (3.40)$$

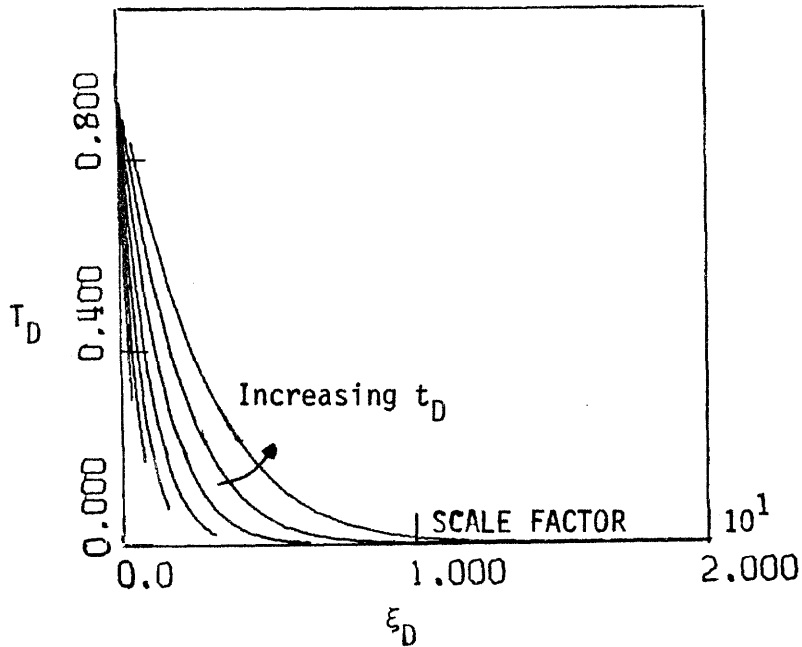


Figure 17a. Temperature Profiles of Eq. (3.39) for $\alpha = 0.5$ and $t_D = 0.4, 0.8, 1.6, 3.2, 6.4, 12.8, 25.6$.

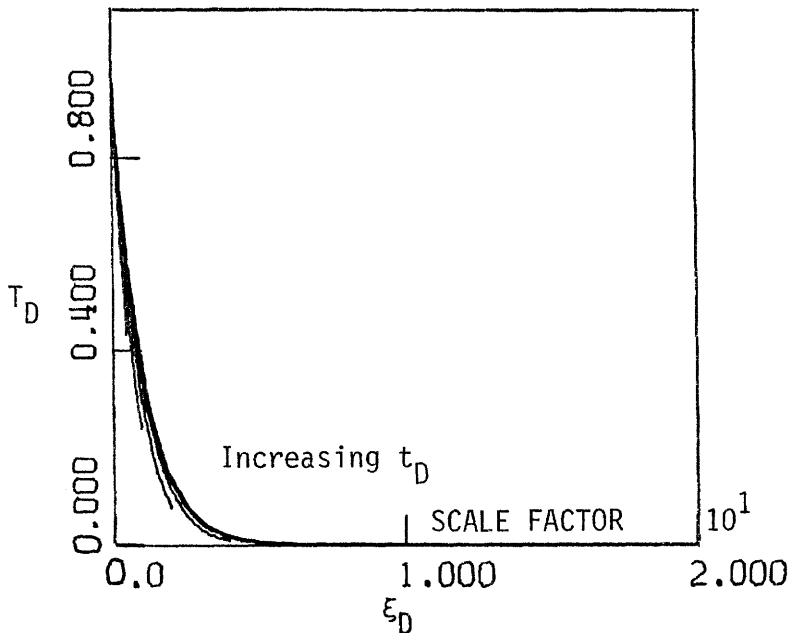


Figure 17b. Temperature Profiles of Eq. (3.39) for $\alpha = 1.5$ and $t_D = 0.4, 0.8, 1.6, 3.2, 6.4, 12.8, 25.6$.

which as expected tends asymptotically to zero.

3.5.2.2 Cylindrical Geometry

The analogous situation, in cylindrical geometry, corresponds to a front travelling with a radial velocity proportional to $\sqrt{t_D}$. In dimensionless notation, the front position r_{FD} satisfies the equation

$$\pi r_{FD}^2 = ct_D \quad (3.41)$$

which shows that the area enclosed by the front increases linearly with time. Inserting the B.C. (3.41) in (3.31) and using the similarity transformation defined in Subsection 3.5.1.2, we derive the solution

$$T_D = \frac{\left\{ 1 - P \left(\beta, \frac{Pe r_D^2}{4t_D} \right) \right\}}{\left\{ 1 - P \left(\beta, \frac{Pec}{4\pi} \right) \right\}} \quad (3.42)$$

which reduces to (3.32) when $c = 0$.

The conductive heat flux at the origin

$$\left. \frac{\partial T_D}{\partial r_D} \right|_{\pi r_D^2 = ct_D} = - \frac{2}{t^{\frac{1}{2}}} \left(\frac{c}{\pi} \right)^{\beta - \frac{1}{2}} \left(\frac{Pe}{4} \right)^{\beta} \frac{e^{-\frac{Pec}{4\pi}}}{\Gamma(\beta) \left\{ 1 - P \left(\beta, \frac{Pec}{4\pi} \right) \right\}} \quad (3.43)$$

tends to zero asymptotically with t_D , in much the same way as the conductive heat flux in the linear case, Eq. (3.40). The above results of Section 3.5 are further utilized in connection with Sections 3.6, 3.7, 3.8.

3.6 One-Dimensional Treatment of the Two-Dimensional Heat Transfer

In a two-dimensional geometry, the energy equation assumes the more complicated form (2.16):

$$\begin{aligned} & (\phi S_w \rho_w c_{pw} + \phi S_o \rho_o c_{po} + (1 - \phi) \rho_R c_{pR}) \frac{\partial T_R}{\partial t} \\ & + (\underline{u}_w \rho_w c_{pw} + \underline{u}_o \rho_o c_{po}) \cdot \nabla T_R = k_{hR} \nabla^2 T_R \quad \underline{r} \in R(t) \end{aligned}$$

The region of integration $R(t)$ is bounded by the reservoir boundaries and the advancing front and generally has an irregular shape (see Figure 18). According to its geometry, we may consider two distinct cases. In the first (Figure 18a), properties are uniform with respect to the vertical coordinate (thin reservoirs), whereas the second case involves radial symmetry and relatively large thickness (Figure 18b). The analysis to follow is primarily concerned with the second case, in which heat losses from the hot liquid zone to the over- and under-burden are not as important as in the first case. In both cases, the B.C. are:

$$t = 0; T_R = T_i$$

$$\underline{r} \rightarrow \infty; T_R \rightarrow T_i$$

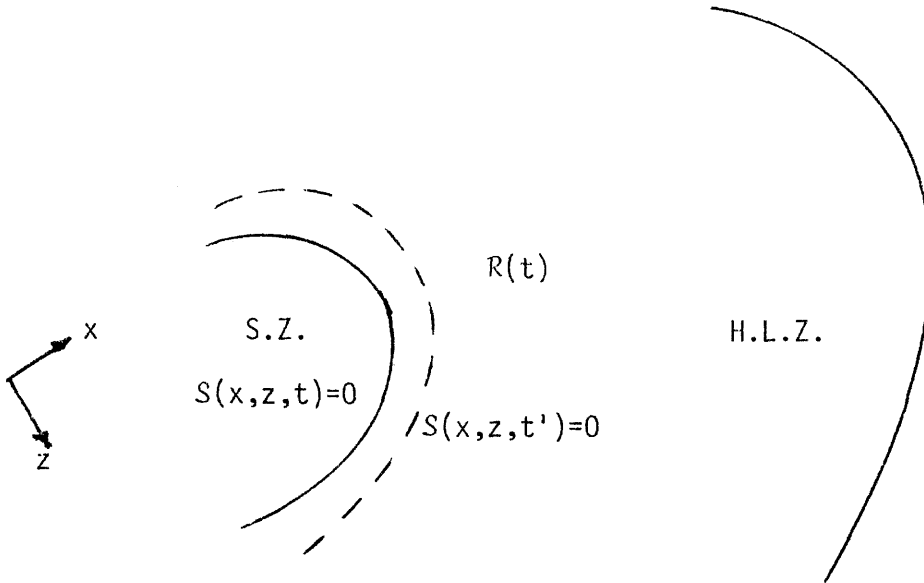


Figure 18a. Region of Integration $R(t)$. Thin Reservoirs.

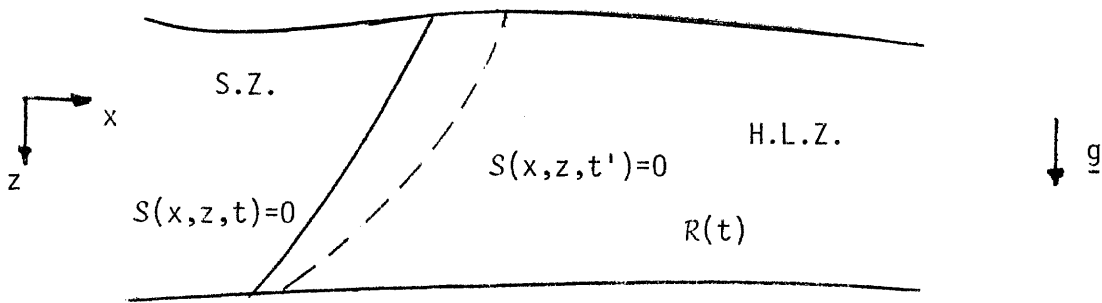


Figure 18b. Region of Integration $R(t)$. Thick Reservoirs..

$$S(x,z,t) \equiv 0 ; \quad T_R = T_s \quad (\text{B.C. at the front})$$

Introduce the system of the natural orthogonal coordinates η, σ , where $\eta(x,z) - \lambda = S(x,z,\lambda) \equiv 0$ implicitly defines the front position at time λ and $\sigma = \sigma(x,z)$ is the coordinate running along the steam front. Thus, the family of curves $\eta(x,z) = \text{const.}$ gives the successive positions of the front in the (x,z) domain whereas the curves $\sigma(x,z) = \text{const.}$ define its orthogonal trajectories (see Figure 19). In the new coordinate system, Eq. (2.16) transforms into:

$$\begin{aligned} & \left(\phi S_w \rho_w c_{pw} + \phi S_o \rho_o c_{po} + (1 - \phi) \rho_R c_{pR} \right) \frac{\partial T_R}{\partial t} \\ & + (u_{w\eta} \rho_w c_{pw} + u_{o\eta} \rho_o c_{po}) \frac{1}{h_\eta} \frac{\partial T_R}{\partial \eta} + (u_{w\sigma} \rho_w c_{pw} + u_{o\sigma} \rho_o c_{po}) \frac{1}{h_\sigma} \frac{\partial T_R}{\partial \sigma} \\ & = \frac{k_{hR}}{h_\sigma h_\eta} \left[\frac{\partial}{\partial \eta} \left(\frac{h_\sigma}{h_\eta} \frac{\partial T_R}{\partial \eta} \right) + \frac{\partial}{\partial \sigma} \left(\frac{h_\eta}{h_\sigma} \frac{\partial T_R}{\partial \sigma} \right) \right] \end{aligned} \quad (3.44)$$

where h_i ($i = \eta, \sigma$) are the scale factors, u_{ji} the components of \underline{u}_j along the coordinate i . The region $R(t)$ maps into $R'(t)$ (see Fig. 19) and the B.C.'s into:

$$\begin{aligned} t = 0 ; \quad T_R &= T_i \\ \eta \rightarrow \infty ; \quad T_R &\rightarrow T_i \\ \eta = t ; \quad T_R &= T_s \end{aligned}$$

Introducing the moving coordinates $t, \xi = \eta - t$, we immobilize the

moving origin. Now

$$\begin{aligned}
 M(2) \frac{\partial T_R}{\partial t} + W_{F\xi} \frac{\partial T_R}{\partial \xi} + W_{F\sigma} \frac{\partial T_R}{\partial \sigma} \\
 = \frac{k h_R}{h_\sigma h_\eta} \left[\frac{\partial}{\partial \xi} \left(\frac{h_\sigma}{h_\eta} \frac{\partial T_R}{\partial \xi} \right) + \frac{\partial}{\partial \sigma} \left(\frac{h_\eta}{h_\sigma} \frac{\partial T_R}{\partial \sigma} \right) \right] \quad (3.45)
 \end{aligned}$$

$(\xi, \sigma) \in R''$

where:

$$W_{F\xi} = (u_{0\eta} \rho_w c_{pw} + u_{0\eta} \rho_o c_{po}) \frac{1}{h_\eta} - M(2)$$

$$W_{F\sigma} = (u_{w\sigma} \rho_w c_{pw} + u_{o\sigma} \rho_o c_{po}) \frac{1}{h_\sigma}$$

The region R'' , shown in Fig. 19, is fixed in space. The B.C.'s become

$$t = 0 ; T_R = T_i$$

$$\xi \rightarrow \infty ; T_R \rightarrow T_i$$

$$\xi = 0 ; T_R = T_s$$

On the lateral boundaries we have the interfacial conditions that couple the heat transfer in the reservoir and the surroundings through the heat losses. In addition, the energy Equation (3.45) is coupled to momentum transfer through the convective terms. So far everything is exact.

In order to simplify the problem we are going to assume a constant convection term, as before. Then, one could apply approximate analytical techniques [such as those employed by Poots (1962), Goodman (1964)]. The boundary condition at the front, however, suggests that, at least near the front, T_R is not a function of σ , the front coordinate. The extent of the validity of this claim may be shown to increase with Peclet number.

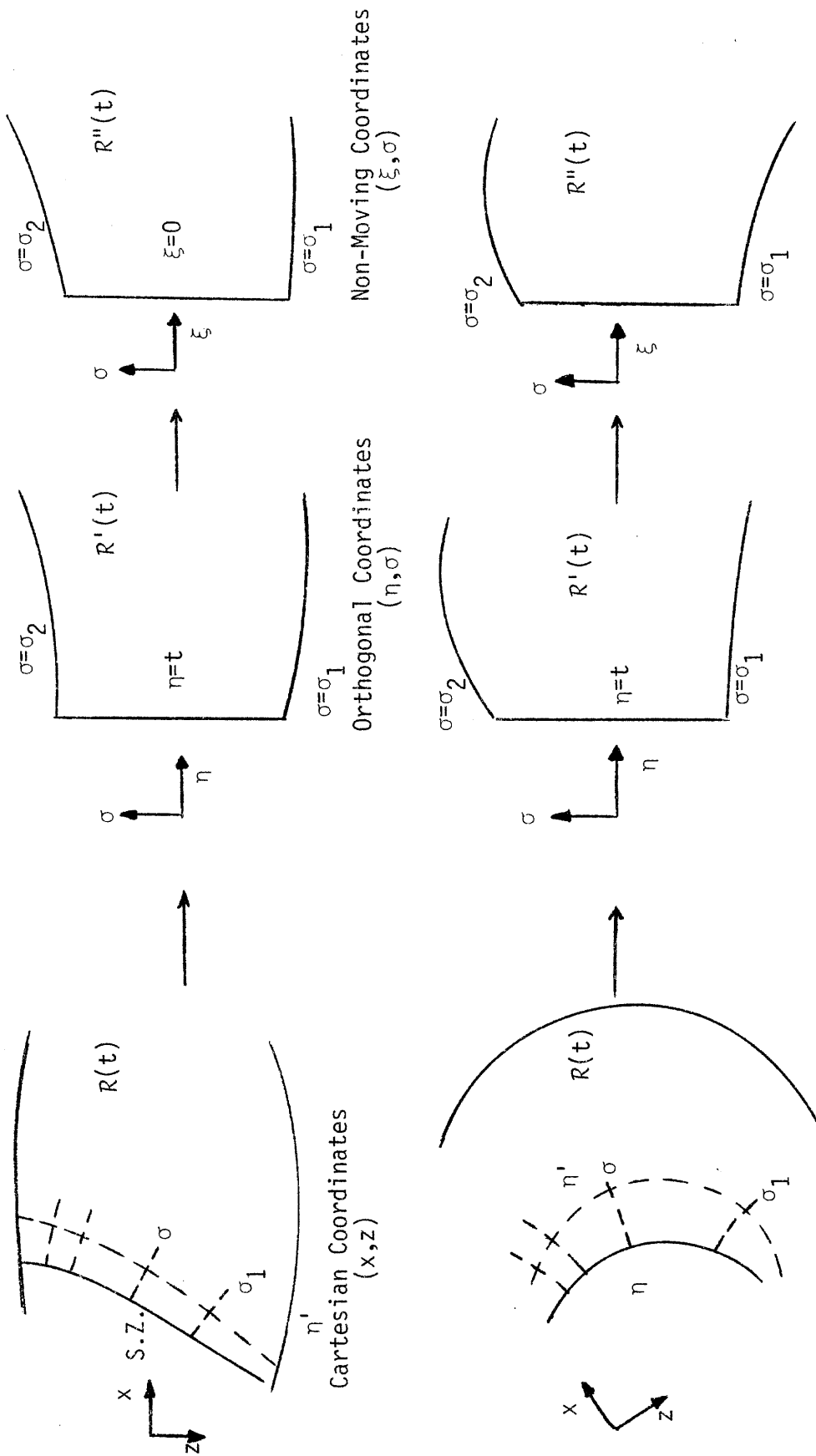


Figure 19. Systems of Coordinates and the Respective Regions of Integration.

For relatively thick reservoirs and for high convection terms, therefore, we can approximate (3.45) by the one-dimensional model:

$$M^{(2)} \frac{\partial T_R}{\partial t} + W_{F\xi} \frac{\partial T_R}{\partial \xi} = \frac{k_{hR}}{h_o h_\eta} \frac{\partial}{\partial \xi} \left(\frac{h_\sigma}{h_\eta} \cdot \frac{\partial T_R}{\partial \xi} \right) \quad (3.46)$$

and

$$t = 0 ; T_R = T_i$$

$$\xi \rightarrow \infty ; T_R \rightarrow T_i$$

$$\xi = 0 ; T_R = T_s$$

The latter has a closed form solution for particular geometries.

3.6.1 The Quasi-Steady State Approximation (No Lateral Heat Losses)

For an arbitrary geometry one can apply a version of Goodman's (1964) integral technique. However, if the temperature penetration depth, along the ξ -coordinate, is small relative to the radius of curvature of the front (or in cases of flat geometry), we can make use of the one-dimensional considerations of the previous Section 3.5. Neglecting lateral heat losses, under steady state conditions:

$$\left. \frac{\partial T_R}{\partial \xi} \right|_0 \sim \begin{cases} \frac{(T_s - T_i)}{k_{hR}} |W_{F\xi}| ; & W_{F\xi} < 0 \\ 0 & ; \quad W_{F\xi} > 0 \end{cases}$$

Now, $h_\eta = \frac{1}{|\nabla \eta|}$ [Pearson (1974)], $v_n = v_\eta = \frac{1}{|\nabla \eta|}$, from (2.21) and the definition of η . Thus, the normal component of the conductive heat flux through the moving front is approximated by

$$-k_{hR} \frac{\partial T_R}{\partial n} \Big|_F = -\frac{k_{hR}}{h_\eta} \cdot \frac{\partial T_R}{\partial \xi} \Big|_0 \sim \begin{cases} -(T_s - T_i)W_{Fn} & ; W_{Fn} < 0 \\ 0 & ; W_{Fn} > 0 \end{cases} \quad (3.47)$$

$$\text{where } W_{Fn} = u_{wn}\rho_w c_{pw} + u_{on}\rho_o c_{po} - (\phi S_w \rho_w c_{pw} + \phi S_o \rho_o c_{po} + (1 - \phi)\rho_R c_{pR}) v_n.$$

It should be stressed, that the above asymptotic expression is based upon several approximations, which become more accurate as the assumptions of high volumetric velocities (injection rates), small curvature and large thickness (smaller heat losses) are better satisfied [compare with Miller (1975)].

3.6.2 The Zero Net Convection Approximation (Includes Lateral Heat Losses)

So far, the only attempt to estimate the heat transfer in the hot liquid zone, for a two-dimensional geometry, was made by Neuman (1975). Under the assumption of flat fronts, he derived a one-dimensional version of the energy equation similar to (3.46). By further assuming that the net convective heat flux through the front is negligible, he converted the problem to one of pure heat conduction. If we insert this approximation into Eq. (3.46) we get

$$M^{(2)} \frac{\partial T_R}{\partial t} = \frac{k_{hR}}{h_\sigma h_\eta} \frac{\partial}{\partial \xi} \left(\frac{h_\sigma}{h_\eta} \frac{\partial T_R}{\partial \xi} \right) \quad (3.48a)$$

and

$$t = 0 ; T_R = T_i$$

$$\xi \rightarrow \infty ; T_R \rightarrow T_i$$

$$\xi = 0 ; T_R = T_s$$

Assuming, further, negligible front curvature we obtain for the conductive heat flux:

$$-k_{hR} \frac{\partial T_R}{\partial n} \bigg|_F = \frac{\sqrt{k_{hR} M^{(2)}}}{\sqrt{\pi}} \cdot \frac{(T_s - T_i)}{\sqrt{t}} \quad (3.48b)$$

which is the usual expression for heat conduction in a semi-infinite medium [compare to (3.15)].

Equation (3.48a) describes well the heat transfer inside the hot liquid zone, in those cases where heat conduction to the surroundings is the dominant heat transfer mechanism. This is clearly favored by low volumetric velocities (low injection rates) and small thickness (larger heat losses).

3.7 One-Dimensional Heat Transfer in the Hot Liquid Zone by Convection, a Steady or Moving Boundary and Lateral Heat Losses (No Horizontal Conduction)

3.7.1 General Formulation

Heat transfer in a hot liquid zone with lateral heat losses and moving boundaries is typical of steam injection and combustion processes, where, due to the occurring phase change, the front which separates condensed and gaseous phases, propagates through the reservoir continuously. When the boundary is fixed (no travelling front) we deal with a typical case of hot fluid injection (hot waterflood).

To decouple the heat and momentum transfer, Equations (2.13), (3.14), (2.16), we assume, as before, constant convection and volumetric heat capacity. We integrate the heat balance, Eq. (2.15), along the vertical

coordinate z (Figure 20) and use the energy boundary condition (2.31b), to obtain the following one-dimensional equation:

$$\begin{aligned} & (\phi S_w \rho_w c_{pw} + \phi S_o \rho_o c_{po} + (1 - \phi) \rho_R c_{pR}) \frac{\partial T_R}{\partial t} \\ & + (u_{wx} \rho_w c_{pw} + u_{ox} \rho_o c_{po}) \frac{\partial T_R}{\partial x} = k_{hR} \frac{\partial^2 T_R}{\partial x^2} + \frac{2k_{hf}}{h} \left(\frac{\partial T_f}{\partial z} \right)_{z=0} \end{aligned} \quad (3.49)$$

Substituting the expression for the heat losses, Eq. (3.13), we further obtain

$$\begin{aligned} M^{(2)} \frac{\partial T_R}{\partial t} + (u_{wx} \rho_w c_{pw} + u_{ox} \rho_o c_{po}) \frac{\partial T_R}{\partial x} \\ = k_{hR} \frac{\partial^2 T_R}{\partial x^2} - \frac{2k_{hf}}{h} \frac{1}{\sqrt{\pi \alpha_f}} \int_0^t \frac{\partial T_R}{\partial \tau} \frac{d\tau}{\sqrt{t - \tau}} \end{aligned} \quad (3.50a)$$

and similarly in cylindrical geometries

$$\begin{aligned} M^{(2)} \frac{\partial T_R}{\partial t} + (u_{wr} \rho_w c_{pw} + u_{or} \rho_o c_{po}) \frac{\partial T_R}{\partial r} \\ = \frac{k_{hR}}{r} \frac{\partial}{\partial r} \left(r \frac{\partial T_R}{\partial r} \right) - \frac{2k_{hf}}{h} \frac{1}{\sqrt{\pi \alpha_f}} \int_0^t \frac{\partial T_R}{\partial \tau} \frac{d\tau}{\sqrt{t - \tau}} \end{aligned} \quad (3.50b)$$

$$0 < t, \quad \int_0^t v(\tau) d\tau < x, \pi r^2$$

The B.C.'s are:

$$\begin{aligned} t = 0 & \quad ; T_R = T_i \\ x, r \rightarrow \infty & \quad ; T_R \rightarrow T_i \\ x, \pi r^2 = \int_0^t v(\tau) d\tau & \quad ; T_R = T_s \end{aligned}$$

With the additional assumption of negligible horizontal conduction, we get

$$M^{(2)} \frac{\partial T_R}{\partial t} + W_F^0 \frac{\partial T_R}{\partial x} = - \frac{2k_{hf}}{h\sqrt{\pi\alpha_f}} \int_0^t \frac{\partial T_R}{\partial \tau} \frac{d\tau}{\sqrt{t-\tau}} \quad (3.51)$$

where $W_F^0 = u_{wx}\rho_w c_{pw} + u_{ox}\rho_o c_{po}$. An identical equation is also derived for cylindrical geometries where πr^2 takes the place of x and q of W_F^0 [see also Eq. (3.30)]. With this in mind we can now introduce the dimensionless variables $T_D = \frac{T_R - T_i}{T_s - T_i}$,

$$x_D = \frac{x}{\left(\frac{|W_F^0| h^2 M^{(2)}}{4k_{hf}\rho_f c_{pf}} \right)}, \quad t_D = \frac{t}{\left(\frac{(M^{(2)})^2 h^2}{\rho_f c_{pf}} \right) \frac{1}{4\alpha_f}}$$

and rewrite (3.51) in a uniform notation for both linear and cylindrical geometries

$$\frac{\partial T_D}{\partial t_D} + \frac{W_F^0}{|W_F^0|} \cdot \frac{\partial T_D}{\partial x_D} = - \frac{1}{\sqrt{\pi}} \int_0^{t_D} \frac{\partial T_D}{\partial \tau_D} \cdot \frac{d\tau_D}{\sqrt{t_D - \tau_D}} \quad (3.52)$$

in the domain $0 < t_D, \int_0^{t_D} v_D(\tau_D) d\tau_D \leq x_D$ with B.C.:

$$t_D = 0 ; T_D = 0$$

$$x_D \rightarrow \infty ; T_D \rightarrow 0$$

$$x_D = \int_0^{t_D} v_D(\tau_D) d\tau_D ; T_D = 1$$

3.7.2 Solution of the Integro-Differential Equation (3.52)

The main difficulty associated with the solution of (3.52) arises

from the existence of the moving boundary. Fixing the boundary by a simple translation of coordinates does not help in this case, so we would rather proceed differently.

We first observe that (3.52) is composed of a hyperbolic part (LHS) and a sink term of the convolution integral type (RHS). Since the initial condition is $T_D = 0$, we expect a non-trivial solution to exist if and only if $W_F^0 > 0$. The non-trivial part of this solution lies in the domain

$0 < t_D, x_D < t_D$ (see Figure 21a) outside of which $T_D = 0$, as can be easily verified by a direct use of the Laplace Transform. On the other hand, the variable x_D , in the region of interest, satisfies

$\int_0^{t_D} v_D(\tau_D) d\tau_D \leq x_D$. Combining with $x_D < t_D$, gives rise to the following constraint on $v_D(t_D)$

$$\int_0^{t_D} v_D(\tau_D) d\tau_D < t_D \quad \forall \quad 0 < t_D \quad (3.53)$$

for a non-trivial solution to exist. The constraint simply states that, since we neglect horizontal conduction, heat transfer can only occur if the convective heat wave travels faster than the moving boundary.

Let us now introduce the new coordinate system (χ, θ) such that

$$\theta = t_D - x_D, \quad \chi = x_D \quad (3.54)$$

The region of integration in the new system becomes

$$\theta > 0, \quad \chi \geq \Gamma(\theta) \quad (\text{see Fig. 21b})$$

where $\chi = \Gamma(\theta)$ is the image of the curve $x_D = c(t_D) = \int_0^{t_D} v_D(\tau_D) d\tau_D$, under the above transformation. Thus, $\Gamma(\theta)$ is implicitly defined by

$$\chi = \int_0^{\theta+\chi} v_D(\tau_D) d\tau_D \quad (3.55)$$

and the respective boundary velocity

$$\omega(\theta) = \frac{d\chi}{d\theta} = \frac{v_D(t_D)}{1 - v_D(t_D)} \quad (3.56)$$

In the new variables, $T_D(x_D, t_D) = \Theta(\theta, \chi)$ and our integro-differential equation takes the form:

$$\frac{\partial \Theta}{\partial \chi} = - \frac{1}{\sqrt{\pi}} \int_0^\theta \frac{\partial \Theta}{\partial \tau} \cdot \frac{d\tau}{\sqrt{\theta - \tau}} \quad (3.57)$$

$$0 < \theta, \quad \Gamma(\theta) \leq \chi$$

with B.C.:

$$\theta = 0 ; \quad \Theta = 0$$

$$\chi = \int_0^\theta \omega(\tau) d\tau ; \quad \Theta = 1$$

We now claim that Eq. (3.57) admits every solution of the pure heat conduction equation and vice-versa:

$$\frac{\partial \Theta}{\partial \theta} = \frac{\partial \Theta}{\partial \chi^2} \quad (3.58)$$

with I.C. $\theta = 0 ; \quad \Theta = 0$

and B.C. $\chi \rightarrow \infty ; \quad \Theta \rightarrow 0$

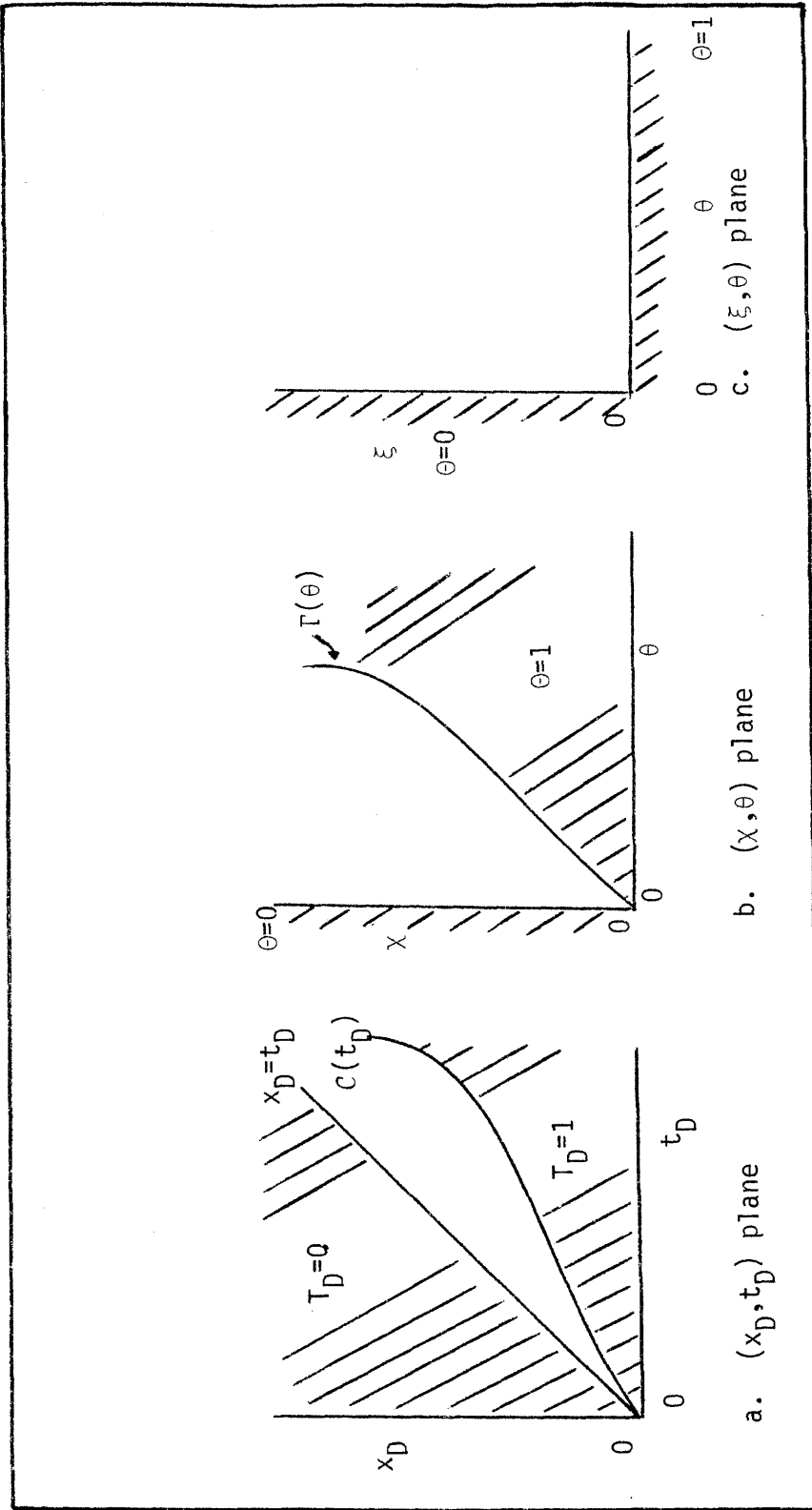


Figure 21. Regions of Integration for Eq. (3.51).

$$\chi = \int_0^\theta \omega(\tau) d\tau ; \quad \theta = 1$$

Indeed, by taking the Laplace Transform of both (3.57), (3.58) and the respective B.C., we see that, within a multiplicative factor, $A(s)$, to be determined from the moving boundary condition, both equations give rise to the same transformed expression:

$$A(s) \exp(-\chi \sqrt{s})$$

Invoking uniqueness in the inversion of Laplace Transform, one concludes that every solution of (3.58) does indeed satisfy Eq. (3.57) and its boundary conditions and vice-versa.

We, thus, showed that a solution to the problem of heat transfer by convection along the x direction of a semi-infinite thin layer and by conduction along the z direction of a semi-infinite medium, is provided by solving a pure heat conduction problem along the x -direction, in a time coordinate shifted by the space coordinate x .

The resulting moving boundary problem (3.58) can be solved in either of the two ways:

- (a) By the application of the h -transform [Widder (1975)] to (3.58) with the result

$$\Theta(\theta, \chi) = \int_0^\theta A(\tau) h(\chi, \theta - \tau) d\tau$$

where

$$h(\chi, \theta) = \frac{\chi}{2\sqrt{\pi\theta^3}} \exp\left\{-\frac{\chi^2}{4\theta}\right\} \quad \text{and } A(\theta) \text{ an unknown, yet,}$$

function to be determined as a solution of the integral equation:

$$\int_0^\theta A(\tau) h\left[\int_0^\theta \omega(\lambda) d\lambda, \theta - \tau\right] d\tau = 1 \quad (3.59)$$

- (b) By going to the moving coordinates θ , $\xi = \chi - \int_0^\theta \omega(\tau) d\tau$, thus immobilizing the moving origin (Fig. 21c).

$$\frac{\partial \theta}{\partial \theta} - \omega(\theta) \frac{\partial \theta}{\partial \xi} = \frac{\partial^2 \theta}{\partial \xi^2} \quad (3.60)$$

with B.C.

$$\theta = 0 ; \quad \theta = 0$$

$$\xi \rightarrow \infty ; \quad \theta \rightarrow 0$$

$$\xi = 0 ; \quad \theta = 1$$

From a previous discussion (Subsection 3.5.1.1) we recall that this problem admits analytical solutions for certain classes of functions $\omega(\theta)$. The following subsections examine several cases of practical interest in thermal methods.

3.7.3 Fixed Boundary

This case is typical of hot water injection (hot-waterflood) with negligible horizontal conduction. Here $v_D(t_D) \equiv 0$ and, by (3.56), $\omega(\theta) \equiv 0$. Also $\xi = \chi$ and (3.58) reads:

$$\frac{\partial \theta}{\partial \theta} = \frac{\partial^2 \theta}{\partial \xi^2} \quad (3.61)$$

with

$$\theta = 0 ; \quad \theta = 0$$

$$\xi \rightarrow \infty ; \quad \theta \rightarrow 0$$

$$\xi = 0 ; \quad \theta = 1$$

Solving [Stakgold (1968)] we get:

$$\Theta(\theta, \xi) = \operatorname{erfc} \left\{ \frac{\xi}{2\sqrt{\theta}} \right\} \cdot H(\theta)$$

and, by back transformation to the original variables,

$$T_D(t_D, x_D) = \operatorname{erfc} \left\{ \frac{x_D}{2\sqrt{t_D - x_D}} \right\} \cdot H(t_D - x_D) \quad (3.62)$$

where $H(t)$ is the Heaviside step function. Figure 22 shows temperature profiles for various times. From (3.62)

$$\frac{\partial T_D}{\partial x_D} = - \frac{1}{\sqrt{\pi t_D}} \quad (3.63)$$

which shows that the conductive heat flux at the origin approaches zero, as $t_D \rightarrow \infty$, but not as fast as in the case of zero lateral heat losses (Subsection 3.5.1.1).

An identical to (3.62) solution has been obtained by Lauwerier (1955) by more complicated means. We believe that the present method is much simpler and can be easily applied to cases with different boundary conditions. For example, in case of variable boundary temperature $g_D(t_D)$, one can easily derive by superposition:

$$T_D(t_D, x_D) = \frac{x_D}{2\sqrt{\pi}} \int_0^{t_D} \exp \left\{ - \frac{x_D^2}{4\tau_D} \right\} \frac{g_D(t_D - \tau_D)}{\tau_D^{3/2}} d\tau_D \cdot H(t_D - x_D) \quad (3.64)$$

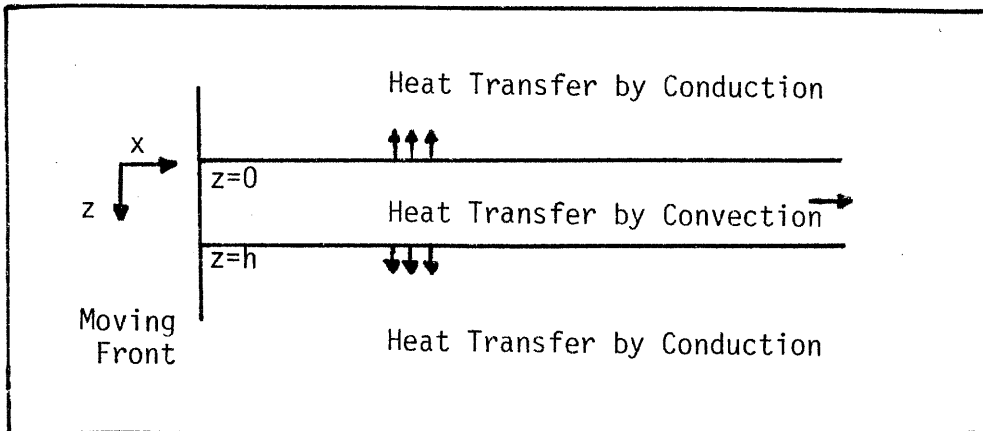


Figure 20. System Examined in Section 3.7.

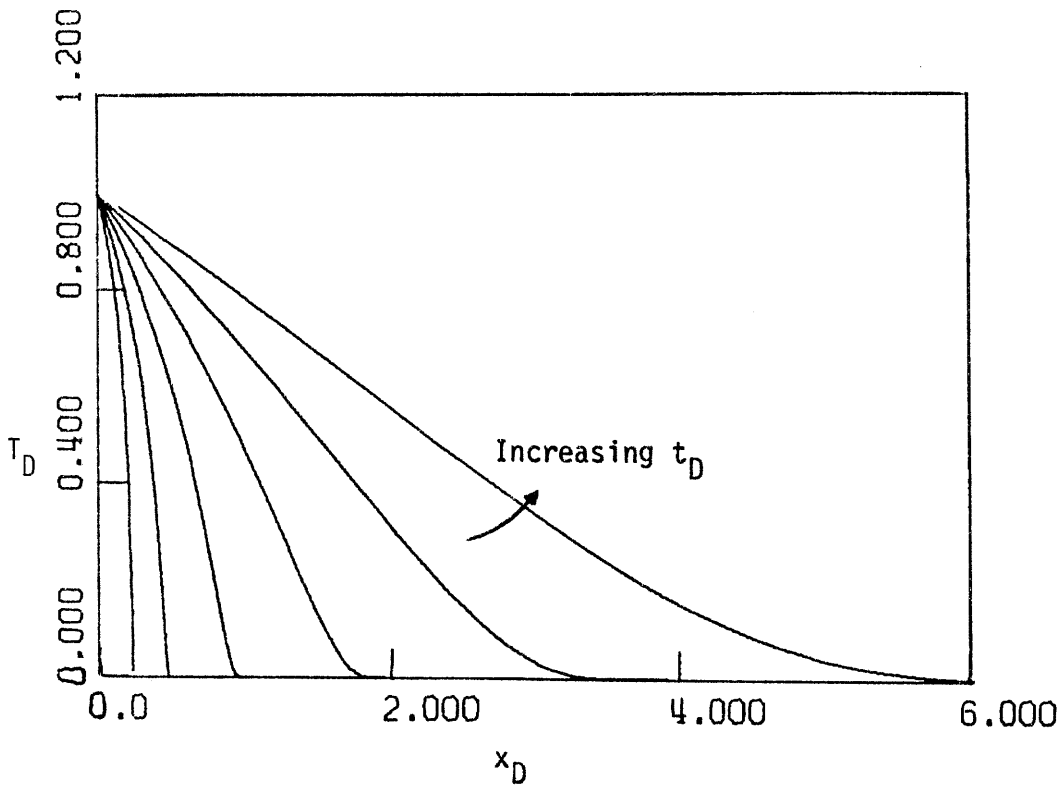


Figure 22. Temperature Profiles of Eq. (3.62) for $t_D = 0.25, 0.5, 1.0, 2.0, 4.0, 8.0$.

3.7.4 Constant Front Velocity

We consider steam injection where the front travels with constant velocity $v_D(t_D) = c$. In the absence of horizontal conduction, the constraint (3.53) dictates $c < 1$ and in dimensional variables

$$M^{(2)}_V < W_F^0 \quad (3.65)$$

From (3.56), $\omega(\theta) = \frac{c}{1-c} > 0$. The curve $C : x_D = ct_D$ maps onto $\Gamma :$

$x = \frac{c}{(1-c)} \theta$ (see Figure 23), hence $\xi = x - \frac{c}{(1-c)} \theta$ and the heat transfer equation reads:

$$\frac{\partial \theta}{\partial \theta} - \frac{c}{(1-c)} \frac{\partial \theta}{\partial \xi} = \frac{\partial^2 \theta}{\partial \xi^2} \quad 0 < \theta, \quad 0 < \xi \quad (3.66)$$

with

$$\theta = 0 ; \quad \Theta = 0$$

$$\xi \rightarrow \infty ; \quad \Theta \rightarrow 0$$

$$\xi = 0 ; \quad \Theta = 1$$

According to Section 3.5 , we get

$$\Theta(\theta, \xi) = \frac{1}{2} \left\{ \operatorname{erfc} \left\{ \frac{\xi + \frac{c}{1-c} \theta}{2\sqrt{\theta}} \right\} + \exp \left\{ -\frac{c\xi}{1-c} \right\} \cdot \operatorname{erfc} \left\{ \frac{\xi - \frac{c}{1-c} \theta}{2\sqrt{\theta}} \right\} \right\} \cdot H(\theta)$$

and, in terms of the original variables,

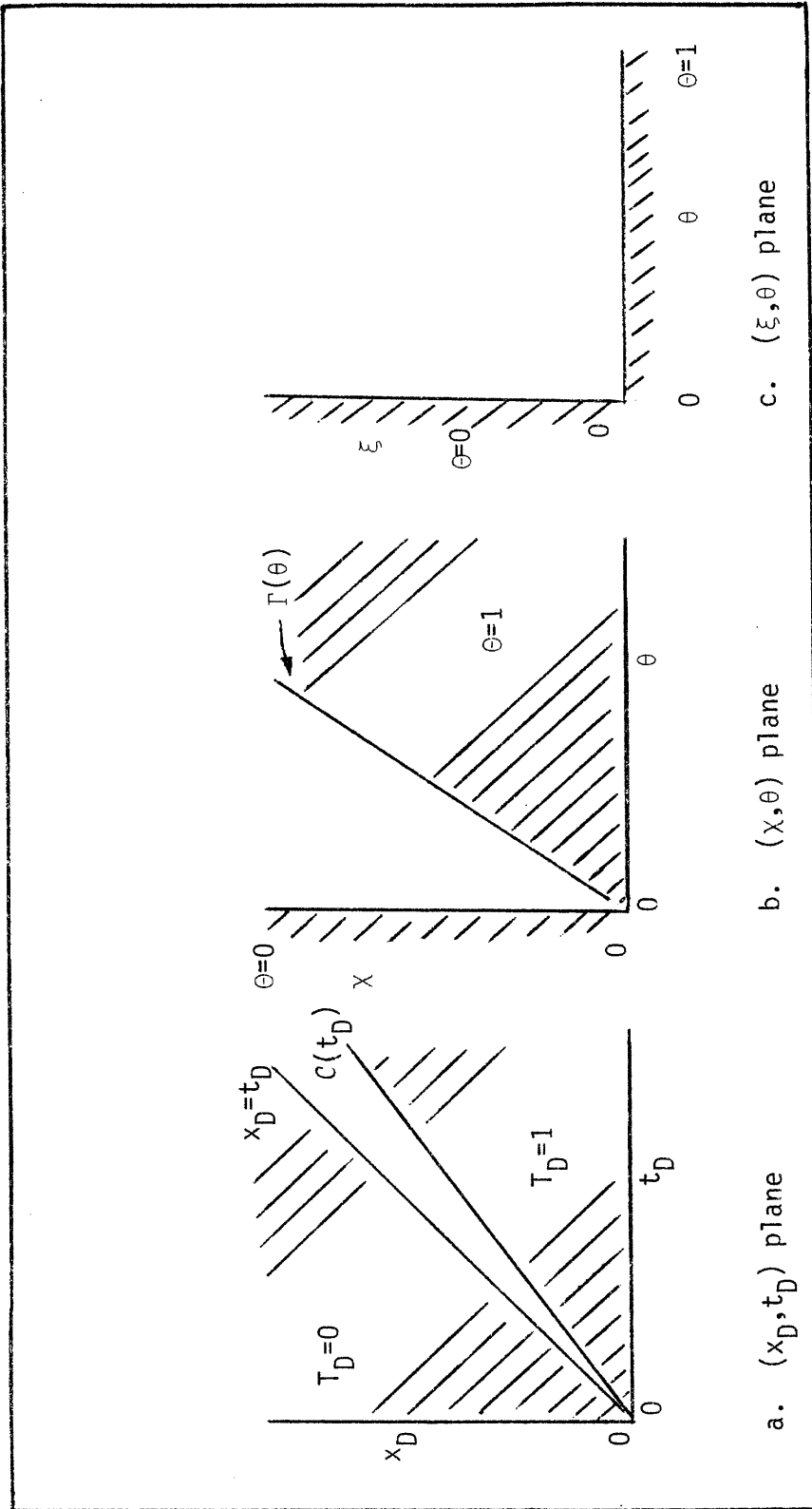


Figure 23. Regions of Integration for System 3.7.4.

$$T_D(t_D, x_D) = \frac{1}{2} \left\{ \operatorname{erfc} \left(\frac{x_D}{2\sqrt{t_D - x_D}} \right) + \exp \left\{ -\frac{c}{(1-c)^2} (x_D - ct_D) \right\} \cdot \right. \\ \left. \cdot \operatorname{erfc} \left[\frac{x_D(1+c) - 2ct_D}{2(1-c)\sqrt{t_D - x_D}} \right] \right\} H(t_D - x_D) \quad (3.67)$$

$$0 < t_D, \quad ct_D < x_D$$

Figure 24 shows various profiles of T_D versus x_D for different t_D and c . The temperature distribution is seen to approach a quasi-steady state. Indeed, from (3.67), we can verify that $T_D(t_D, x_D)$ approaches, as $t_D \rightarrow \infty$, the travelling wave solution

$$T_D(t_D, x_D) = \exp \left\{ -\frac{c}{(1-c)^2} (x_D - ct_D) \right\} H(t_D - x_D) \quad (3.68)$$

In other words, the temperature profile assumes, at large times, the form of a wave which travels with a velocity c imposed by, and equal to, the moving front velocity.

The dimensionless conductive flux through the front

$$\left. \frac{\partial T_D}{\partial x_D} \right|_{x_D=ct_D} = -\frac{c}{(1-c)^2} - \frac{1}{\sqrt{\pi}} \cdot \frac{1}{(1-c)^{3/2}\sqrt{t_D}} \exp \left\{ -\frac{c^2 t_D}{4(1-c)} \right\} + \\ + \frac{c}{2(1-c)^2} \operatorname{erfc} \left\{ \frac{c\sqrt{t_D}}{2\sqrt{1-c}} \right\} \quad (3.69a)$$

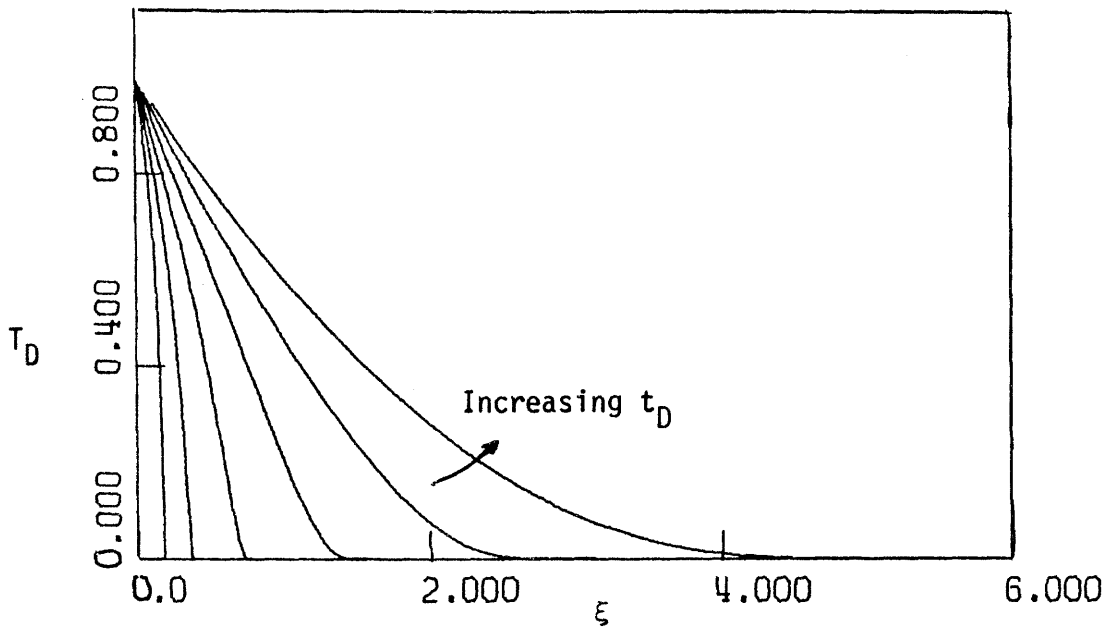


Figure 24a. Temperature Profiles of Eq. (3.67) for $c = 0.2$ and $t_D = 0.25, 0.5, 1.0, 2.0, 4.0, 8.0$.

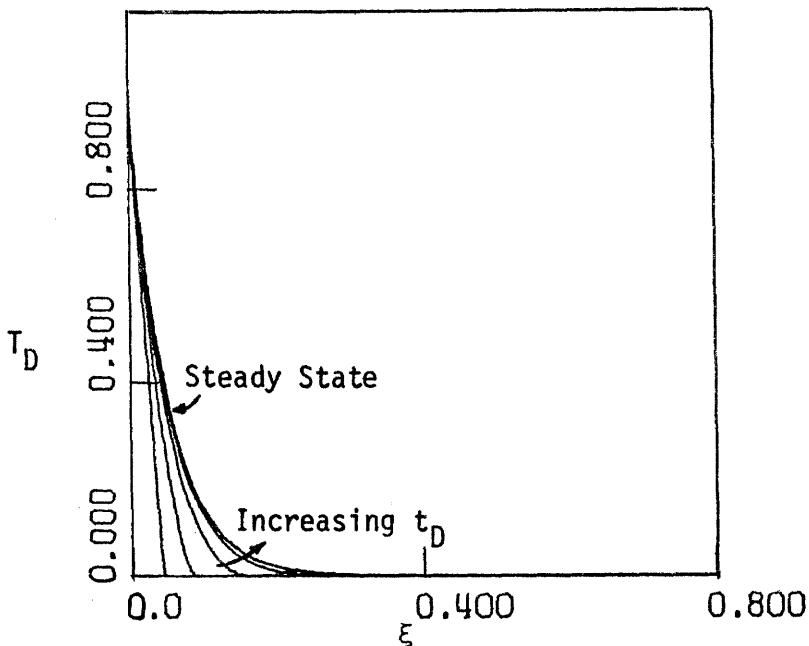


Figure 24b. Temperature Profiles of Eq. (3.67) for $c = 0.8$ and $t_D = 0.25, 0.5, 1.0, 2.0, 4.0, 8.0$.

approaches exponentially the non-zero value $-\frac{c}{(1-c)^2}$. The characteristic time for the approach to this asymptotic value is of the order of

$$\left[\frac{(1-c)}{c^2} \left(\frac{M^{(2)}}{\rho_f c_{pf}} \right)^2 \frac{h^2}{\alpha_f} \right], \text{ in dimensional variables. The larger the}$$

front velocity, the faster the convergence but also the steeper the T-distribution (Figure 24). Note that it is the front velocity alone that controls the approach to the steady state values and not the net convective heat flux as in Subsection 3.5.1.1.

For future reference we consider the behavior of (3.69) for small values of c . Then, the dimensionless conductive heat flux approaches the front velocity c

$$\left. \frac{\partial T_D}{\partial x_D} \right|_{x_D=ct_D} \sim -c - \frac{1}{\sqrt{\pi} t_D} \exp \left\{ -\frac{c^2 t_D}{4} \right\} + \frac{c}{2} \operatorname{erfc} \left\{ \frac{c\sqrt{t_D}}{2} \right\} \quad (3.70)$$

The applicability of the above results in real cases is restricted, by the constraint (3.65), to those cases where the net convective flux through the front is positive.

$$\text{3.7.5 } \underline{\text{Front Velocity of the Form}} \quad v_D(t_D) = \frac{\alpha}{\sqrt{t_D + \alpha^2}}.$$

The class of fronts characterized by the velocity expression

$$v_D = \frac{\alpha}{\sqrt{t_D + \alpha^2}}, \quad \alpha > 0, \text{ is of considerable interest to us for the following}$$

two reasons: (i) it can fairly accurately describe the steam front velocity for large times, (ii) it leads to an analytical solution.

Now, the curve C is described by: $x_D = -2\alpha^2 + 2\alpha\sqrt{t_D + \alpha^2}$, which maps onto Γ : $\chi = 2\alpha\sqrt{\theta}$ (Fig. 25). From (3.56), we obtain $\omega(\theta) = \frac{\alpha}{\sqrt{\theta}}$ and $\xi = \chi - 2\alpha\sqrt{\theta}$. Note that the constraint (3.53) is satisfied for any $\alpha > 0$. The subsidiary Equation (3.60) becomes:

$$\frac{\partial \theta}{\partial \theta} - \frac{\alpha}{\sqrt{\theta}} \cdot \frac{\partial \theta}{\partial \xi} = \frac{\partial^2 \theta}{\partial \xi^2} \quad (3.71)$$

with

$$\theta = 0 ; \theta = 0$$

$$\xi \rightarrow \infty ; \theta \rightarrow 0$$

$$\xi = 0 ; \theta = 1$$

This problem has been already discussed in Subsection 3.5.2.1, where we developed a similarity solution for θ . In terms of the original variables

$$T_D(t_D, x_D) = \operatorname{erfc} \left\{ \frac{x_D}{2\sqrt{t_D - x_D}} \right\} / \operatorname{erfc} \alpha \cdot H(t_D - x_D) \quad (3.72)$$

on $-2\alpha^2 + 2\alpha\sqrt{t_D + \alpha^2} < x_D$

Expression (3.72) is the same, within a multiplicative constant, with Lauwerier's solution, Eq. (3.62), obtained for non-moving fronts. In fact, for $\alpha = 0$, Eq. (3.72) reduces to (3.62), as expected.

In Fig. 26 we show typical T_D profiles for various times and values of α . Variations in α have a significant effect. As α increases, the temperature profiles become steeper, due to the increased front velocity. The conductive heat flux at the origin

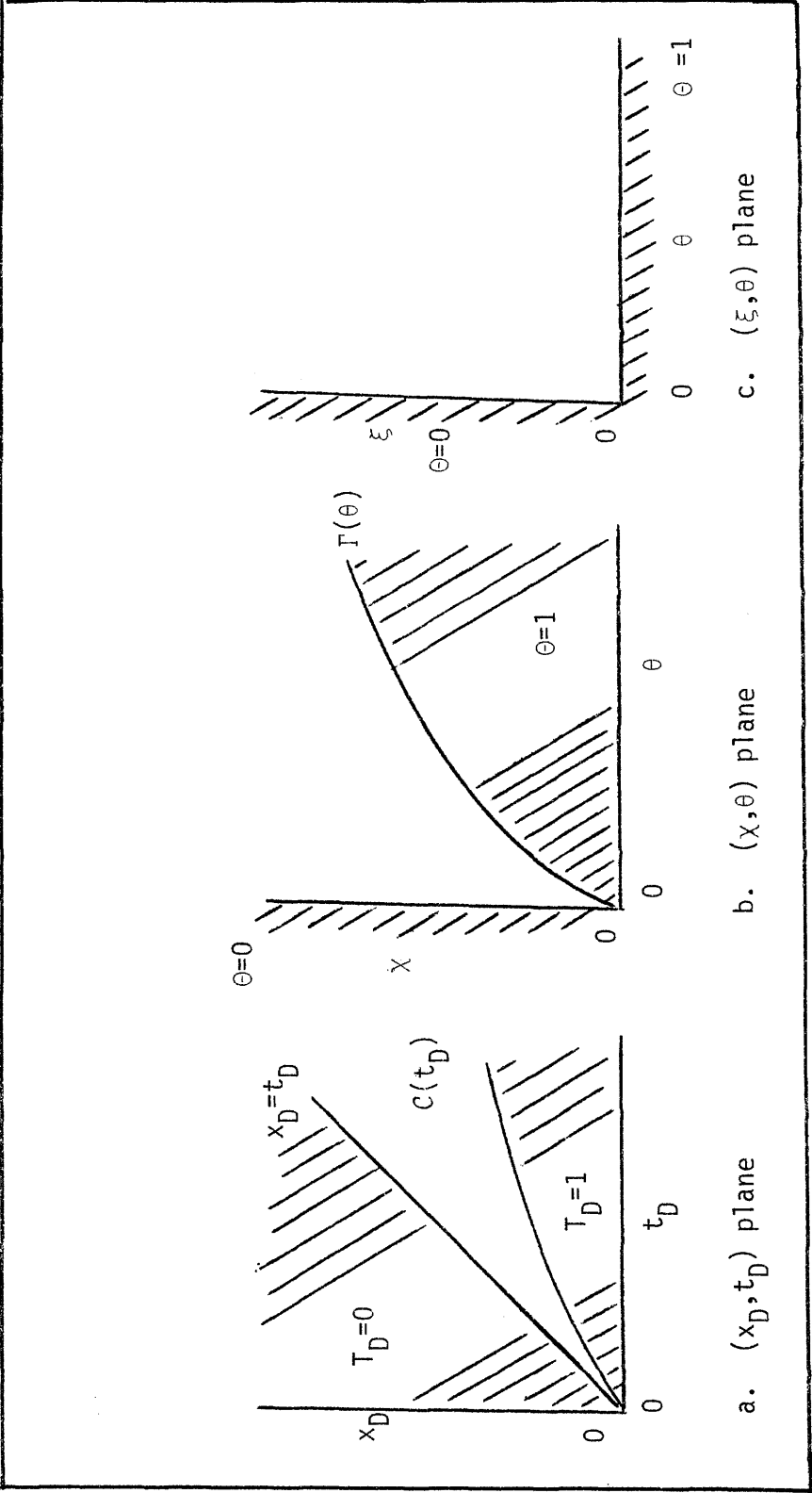


Figure 25. Regions of Integration for System 3.7.5.

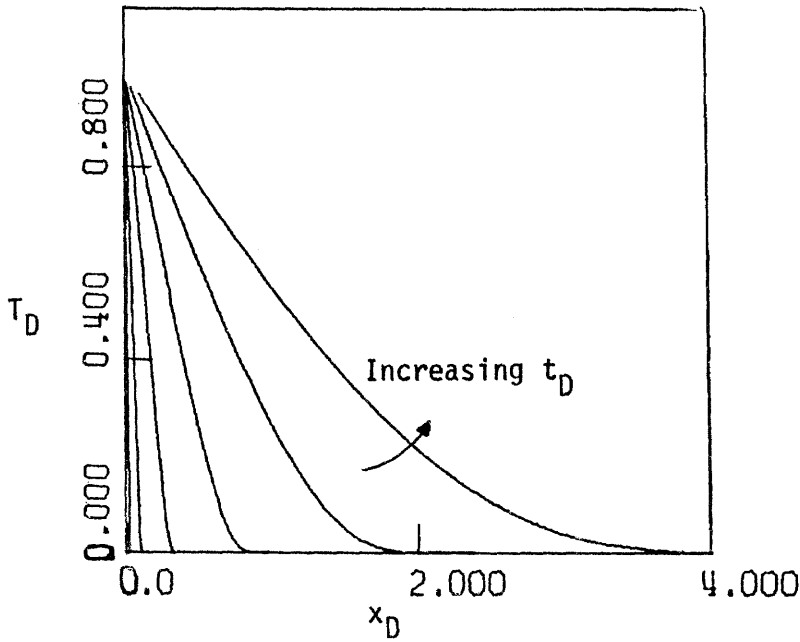


Figure 26a. Temperature Profiles of Eq. (3.72) for $\alpha = 0.5$ and $t_D = 0.25, 0.5, 1.0, 2.0, 4.0, 8.0$.

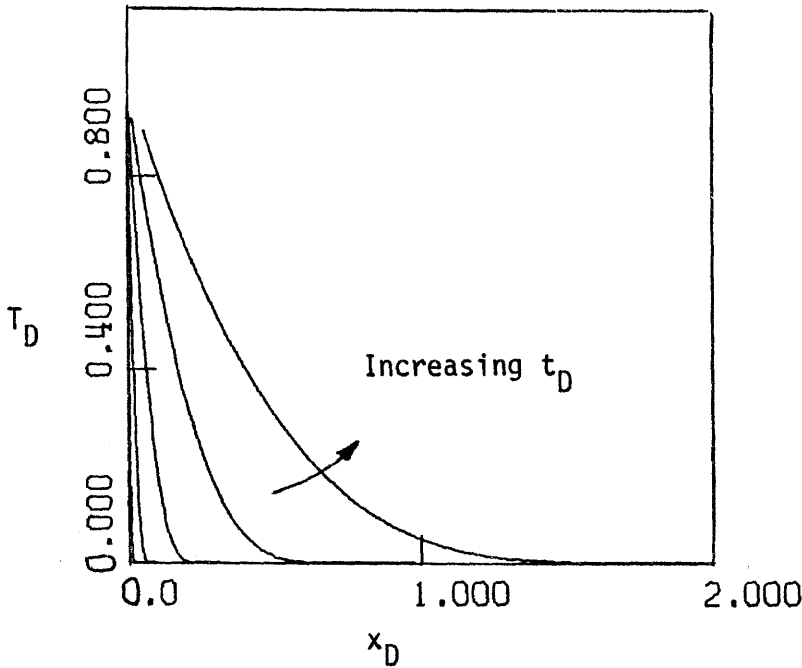


Figure 26b. Temperature profiles of Eq. (3.72) for $\alpha = 1.5$ and $t_D = 0.25, 0.5, 1.0, 2.0, 4.0, 8.0$.

$$\left. \frac{\partial T_D}{\partial x_D} \right|_{x_D \in C} = - \frac{e^{-\alpha^2}}{\sqrt{\pi} \operatorname{erfc} \alpha} \cdot \left\{ \frac{t_D - \alpha \sqrt{t_D + \alpha^2} + \alpha^2}{(t_D - 2\alpha \sqrt{t_D + \alpha^2} + 2\alpha^2)^{3/2}} \right\} \quad (3.73)$$

approaches zero like $\frac{\exp(-\alpha^2)}{\sqrt{\pi} \operatorname{erfc} \alpha} \cdot \frac{1}{\sqrt{t_D}}$, as $t_D \rightarrow \infty$. This asymptotic

behavior is identical to that of a pure heat conduction problem with a moving origin of velocity $\frac{\alpha}{\sqrt{t_D}}$ (see Subsection 3.5.2.1). The results of this Section 3.7 and in particular the asymptotic behavior at large t_D , are applied in Chapter IV to determine the steam front velocity.

3.8 One-Dimensional Heat Transfer by Convection, Conduction, Lateral Heat Losses and a Steady or Moving Boundary.

3.8.1 General Formulation

Including horizontal conduction along the x-axis, allows for more realistic results and it also removes the constraint (3.53) imposed upon the front velocity when conduction is neglected. The governing equations (3.50a,b), in dimensional notation, have been derived in Section 3.7.1. The addition of horizontal conduction does not permit a uniform representation for both linear and cylindrical geometries [in contrast to (3.51)], therefore we consider the two geometries separately.

In a linear geometry, non-dimensionalizing as in Section 3.7.1 we get:

$$\frac{\partial T_D}{\partial t_D} + \frac{w_F^0}{|w_F^0|} \cdot \frac{\partial T_D}{\partial x_D} = \frac{1}{R} \cdot \frac{\partial^2 T_D}{\partial x_D^2} - \frac{1}{\sqrt{\pi}} \int_0^{t_D} \frac{\partial T_D}{\partial \tau_D} \cdot \frac{d\tau_D}{\sqrt{t_D - \tau_D}}$$

$$0 < t_D, \int_0^{t_D} v_D(\tau_D) d\tau_D \leq x_D \quad (3.74a)$$

with

$$t_D = 0 ; T_D = 0$$

$$x_D \rightarrow \infty ; T_D \rightarrow 0$$

$$x_D = \int_0^{t_D} v_D(\tau_D) d\tau_D ; T_D = 1$$

The dimensionless group $R = \frac{w_F^{02} h^2}{4k_{hf}^2} \cdot \frac{\alpha_f}{\alpha_R}$ can be regarded as a modified

Peclet number because it expresses the product of the two ratios

$\frac{(\text{convection x-direction})}{(\text{conduction x-direction})} \cdot \frac{(\text{convection x-direction})}{(\text{conduction z-direction})}$. Usually $\alpha_f \approx \alpha_R$,

thus R is simply the square of a Peclet number equal to $\frac{w_F^0 h}{2k_{hf}}$.

In cylindrical geometries, introducing the dimensionless notation

$$T_D = \frac{T_R - T_i}{T_s - T_i}, \quad t_D = \frac{t}{\left(\left(\frac{M^{(2)}}{\rho_f c_{pf}} \right)^2 \frac{h^2}{4\alpha_f} \right)} \quad \text{and}$$

$$r_D = \frac{r}{\left(\frac{M^{(2)}}{\rho_f c_{pf}} \right) \frac{h}{2} \sqrt{\frac{q}{\alpha_f M^{(2)}}}}$$

we transform (3.50b) to:

$$\frac{\partial T_D}{\partial t_D} + \frac{1}{2\pi r_D} \cdot \frac{\partial T_D}{\partial r_D} = \frac{1}{Pe} \cdot \frac{1}{r_D} \frac{\partial}{\partial r_D} \left(r_D \frac{\partial T_D}{\partial r_D} \right) - \frac{1}{\sqrt{\pi}} \int_0^{t_D} \frac{\partial T_D}{\partial \tau_D} \cdot \frac{d\tau_D}{\sqrt{t_D - \tau_D}} \quad (3.74b)$$

$$0 < t_D, \int_0^{t_D} v_D(\tau_D) d\tau_D < \pi r_D^2$$

with

$$t_D = 0 ; T_D = 0$$

$$r_D \rightarrow \infty ; T_D \rightarrow 0$$

$$\pi r_D^2 = \int_0^{t_D} v_D(\tau_D) d\tau_D ; T_D = 1$$

Notice that now, the Peclet number, $Pe = \frac{q}{k_{hR}}$, replaces R as the important dimensionless group.

For arbitrary R , Pe and $v_D(t_D)$, the above equations are not easily amenable to analytical treatment. Particular values of R and a certain class of functions $v_D(t_D)$, however, allow analytical or asymptotic solutions. This is not equally true in cylindrical geometries except in the special case $Pe \rightarrow \infty$ which, however, has been already treated in Section 3.7. Therefore, our discussion will be limited to linear geometries only, while keeping in mind that the asymptotic results as $R, Pe \rightarrow \infty$ are identical.

3.8.2. Fixed Boundary, Arbitrary R

By removing the complexities associated with the moving boundary, we are able to solve the linear Equation (3.74a). This problem, which is a more realistic representation of a hot waterflood than Lauwerier's problem, (Section 3.7), is briefly discussed in a review paper by Spillette

(1965) who also presents the resulting temperature distribution as derived by Avdonin (1964). Since Avdonin's work is not readily available, we sketch the method of solution of the integro-differential Equation (3.74a) and comment on the results.

Using a Laplace Transformation on Eq. (3.74a) and the B.C. we get, after inversion

$$T_D(t_D, x_D) = \frac{x_D \sqrt{R}}{2\sqrt{\pi}} \int_0^{t_D} \exp \left\{ -\frac{R\tau_D}{4} \left(1 - \frac{x_D w_F^0}{\tau_D |w_F^0|} \right)^2 \right\} \cdot \operatorname{erfc} \left\{ \frac{\tau_D}{2\sqrt{t_D - \tau_D}} \right\} \frac{d\tau_D}{\tau_D^{3/2}} \quad (3.75)$$

which, within a multiplication factor, is identical to the expression presented by Spillette (1965). (The disagreement is probably due to a typing error.) Note that, now, Eq. (3.75) is valid for any w_F^0 , in contrast with Lauwerier's solution, where the condition $w_F^0 > 0$ was necessary for the existence of a non-trivial solution.

The above integral simplifies considerably when $R = 1$. Then (3.75) reduces to:

$$T_D(t_D, x_D) = \operatorname{erfc} \left(\frac{x_D}{2\sqrt{t_D}} \right) \quad w_F^0 > 0 \quad (3.76)$$

$$T_D(t_D, x_D) = e^{-x_D} \operatorname{erfc} \left(\frac{x_D}{2\sqrt{t_D}} \right) \quad w_F^0 < 0 \quad (3.77)$$

(see also Subsection 3.8.4.1). Figure 27 plots T_D profiles for different times and $R = 1$ in the two cases, $w_F^0 > 0$, $w_F^0 < 0$. When $w_F^0 > 0$, the

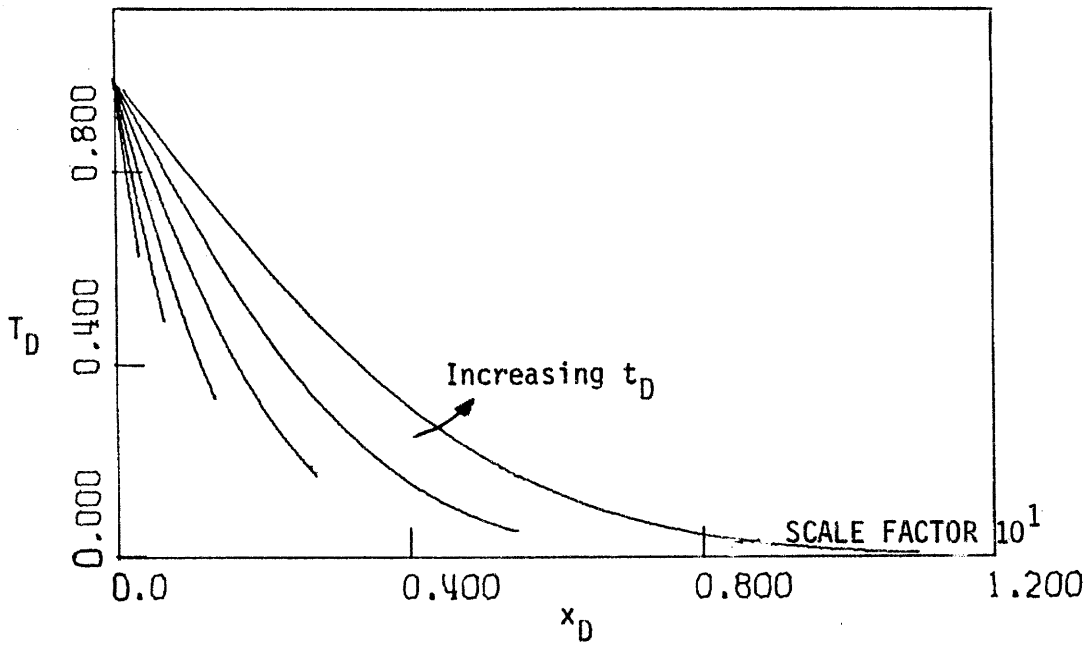


Figure 27a. Temperature Profiles of Eq. (3.75) for $W_F = 1$, $R = 1$ and $t_D = 0.25, 0.5, 1.0, 2.0, 4.0, 8.0$.

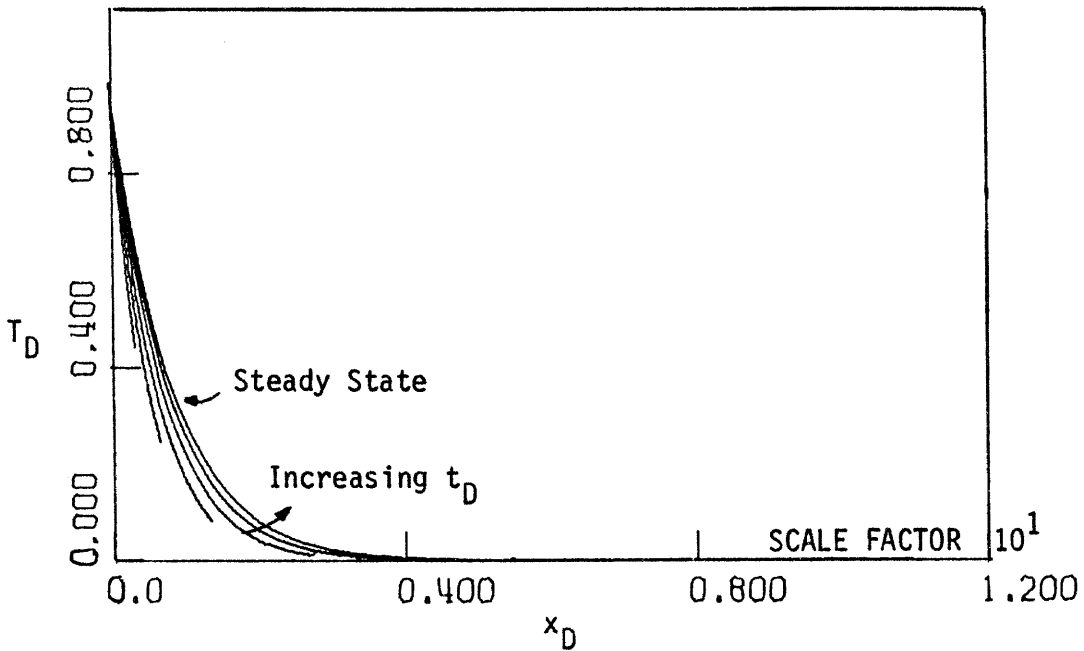


Figure 27b. Temperature Profiles of Eq. (3.75) for $W_F = -1$, $R = 1$ and $t_D = 0.25, 0.5, 1.0, 2.0, 4.0, 8.0$.

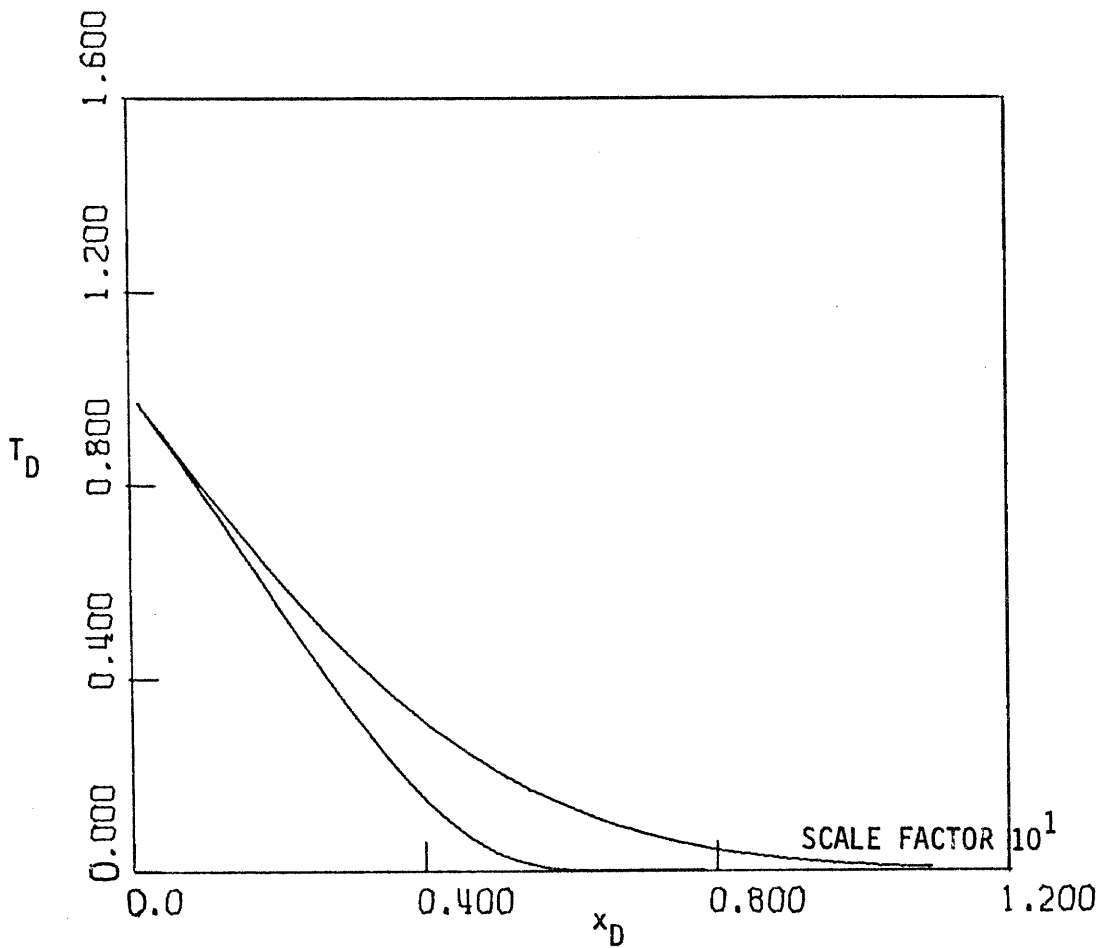


Figure 28. Temperature Profiles of Eq. (3.75) for $W_F = 1$, $R = 1$, (upper curve) and Eq. (3.62) (lower curve), at $t_D = 8.0$ (Avdonin vs. Lauwerier).

profiles are close to Lauwerier's profiles except for large x_D , when the heat wave penetrates farther into the unheated zone. When $W_F^0 < 0$, the T_D profile slowly approaches the steady-state solution

$$T_D = \exp[-x_D R] \quad (3.78)$$

As R increases, the two profiles come closer and as $R \rightarrow \infty$ they eventually coincide.

The conductive heat flux at the origin assumes the following asymptotic form as $t_D \rightarrow \infty$:

$$\left. \frac{\partial T_D}{\partial x_D} \right|_0 \sim \left(\frac{W_F^0}{|W_F^0|} - 1 \right) \frac{R}{2} - \frac{1}{\sqrt{\pi}} \frac{1}{\sqrt{t_D}} + O\left(\frac{1}{t_D^{3/2}}\right) \quad (3.79)$$

The first term in the above expansion is similar to that obtained by conduction and convection alone [Eq. (3.27)], the second is of the Lauwerier type (3.63), the third etc. are of mixed type. In the limit of large times, the results are very similar to those obtained in Section 3.5 where heat losses are neglected.

(i) When $W_F^0 < 0$, $\left. \frac{\partial T_D}{\partial x_D} \right|_0 \sim -R$ which, if translated in terms of

the scaling employed in 3.5.1.1, is equivalent to $\left. \frac{\partial T_D}{\partial x_D} \right|_0 \sim -1$, exactly as in Eq. (3.27).

(ii) When $W_F^0 > 0$, $\left. \frac{\partial T_D}{\partial x_D} \right|_0 \sim 0$, as before.

The above results imply that after sufficiently large times, the effect of lateral heat losses becomes insignificant and the process is

dominated by horizontal convection and conduction. However, the convergence to the steady state is much slower than the exponential convergence of (3.30).

3.8.3 Constant Boundary Velocity, Steady States for Arbitrary R

When the boundary has a constant (or asymptotically constant) velocity, we can easily extract the steady state solutions. Introducing the moving coordinates $t_D, \xi_D = x_D - ct_D$ we rewrite Eq. (3.74a) and the B.C.

$$\begin{aligned} \frac{\partial T_D}{\partial t_D} + \left(\frac{w_F^0}{|w_F^0|} - c \right) \frac{\partial T_D}{\partial \xi_D} &= \frac{1}{R} \cdot \frac{\partial^2 T_D}{\partial \xi_D^2} \\ &- \frac{1}{\sqrt{\pi}} \int_0^{t_D} \frac{\partial T_D}{\partial u_1} (\tau_D, \xi_D + (t_D - \tau_D)c) \frac{d\tau_D}{\sqrt{t_D - \tau_D}} \\ &+ \frac{c}{\sqrt{\pi}} \int_0^{t_D} \frac{\partial T_D}{\partial u_2} (\tau_D, \xi_D + (t_D - \tau_D)c) \frac{d\tau_D}{\sqrt{t_D - \tau_D}} \end{aligned} \quad (3.80)$$

$$t_D = 0 ; T_D = 0$$

$$\xi_D \rightarrow \infty ; T_D \rightarrow 0$$

$$\xi_D = 0 ; T_D = 1$$

where c is the velocity of the boundary and u_1, u_2 are the independent variables of the function $T_D(u_1, u_2)$. Being unable to develop exact solutions for arbitrary R , we are interested in the steady states, if any, of (3.80). In the limit $t_D \rightarrow \infty$,

$$\left(\frac{w_F^0}{|w_F^0|} - c \right) \frac{\partial T_D}{\partial \xi_D} = \frac{1}{R} \cdot \frac{\partial^2 T_D}{\partial \xi_D^2} + \frac{c}{\sqrt{\pi}} \lim_{t_D \rightarrow \infty} \int_0^{t_D} \frac{\partial T_D}{\partial u_2} (\xi_D + c(t_D - \tau_D)) \frac{d\tau_D}{\sqrt{t_D - \tau_D}} \quad (3.81)$$

which becomes

$$\left(\frac{w_F^0}{|w_F^0|} - c \right) \frac{\partial T_D}{\partial \xi_D} = \frac{1}{R} \cdot \frac{\partial^2 T_D}{\partial \xi_D^2} + \frac{\sqrt{c}}{\sqrt{\pi}} \int_0^\infty \frac{\partial T_D}{\partial \sigma} (\xi_D + \sigma) \frac{d\sigma}{\sqrt{\sigma}} \quad (3.82)$$

with B.C.

$$\xi_D \rightarrow \infty ; T_D \rightarrow 0$$

$$\xi_D = 0 ; T_D = 1$$

The solution of this simpler integro-differential equation in one independent variable provides the steady-state solutions. Notice that, now, c is not bound by the condition (3.53).

To make the presentation simpler, we introduce the notation:

$$x = \xi_D, \quad \phi(x) = \frac{\partial T_D}{\partial \xi_D}, \quad \lambda = \frac{\sqrt{c}}{\left(\frac{w_F^0}{|w_F^0|} - c \right)}, \quad \mu = \frac{1}{R \left(\frac{w_F^0}{|w_F^0|} - c \right)}$$

where we assumed $c \neq \frac{w_F^0}{|w_F^0|}$ and $c > 0$. (An identical analysis can be followed when $c < 0$). We, then, obtain

$$\phi(x) = \mu \phi'(x) + \frac{\lambda}{\sqrt{\pi}} \int_0^{\infty} \phi(\sigma + x) \frac{d\sigma}{\sqrt{\sigma}} \quad (3.83)$$

In Appendix III we show that Eq. (3.83) can be reduced to the ODE

$$\phi'''(x) - \frac{2}{\mu} \phi''(x) + \frac{1}{2} \phi'(x) + \frac{\lambda^2}{2} \phi(x) = 0 \quad (3.84)$$

which admits the general solution

$$\phi(x) = A_1 \exp(z_1 x) + A_2 \exp(z_2 x) + A_3 \exp(z_3 x) \quad (3.85)$$

where the roots z_1, z_2, z_3 satisfy the algebraic equation:

$$z(z - \frac{1}{\mu})^2 + \frac{\lambda^2}{2} = 0 \quad (3.86)$$

Depending upon the sign of $\frac{1}{27\mu} + \frac{\lambda^2}{4}$ we have one negative and a pair of complex conjugate roots (positive sign), or three real negative roots (negative sign).

Returning to the original notation and integrating, we get the physically acceptable solution

$$T_D(\xi_D) = \exp(z_1 \xi_D) \quad (3.87)$$

$$\left. \frac{\partial T_D}{\partial \xi_D} \right|_0 = z_1 \quad (3.88)$$

where z_1 is the real negative root of (3.86). Values of z_1 for various

	c = 0.1	0.2	0.3	0.4	0.5	0.6	0.7	0.8	0.9	1.00
R = 100	-0.12311	-0.31009	-0.60185	-1.0724	-1.8591	-3.2130	-5.5414	-9.3114	-14.7236	-25.5443
R = 1000	-0.12342	-0.31225	-0.61117	-1.1070	-1.9842	-3.6819	-7.4074	-16.9905	-43.627	-100.0000
R $\rightarrow \infty$	-0.12345	-0.31250	-0.61224	-1.1111	-2.0000	-3.7500	-7.7777	-20.0000	-90.000	$-\infty$

Values of z_1 for various values of R,c.

Table 3

c	R	z_1
100	100	-9,910
	10	- 993
	1	- 100
	0.1	- 10.21
10	100	- 910
	10	- 93
	1	- 10
	0.1	- 1.11
1	100	- 21.54
	10	- 4.64
	1	- 1
	0.1	- 0.21
0.1	100	- 0.1231
	10	- 0.1202
	1	- 0.1
	0.1	- 0.050
0.1	$R \rightarrow \infty$	- 0.1234

Values of z_1 for various values of R,c.

Table 4

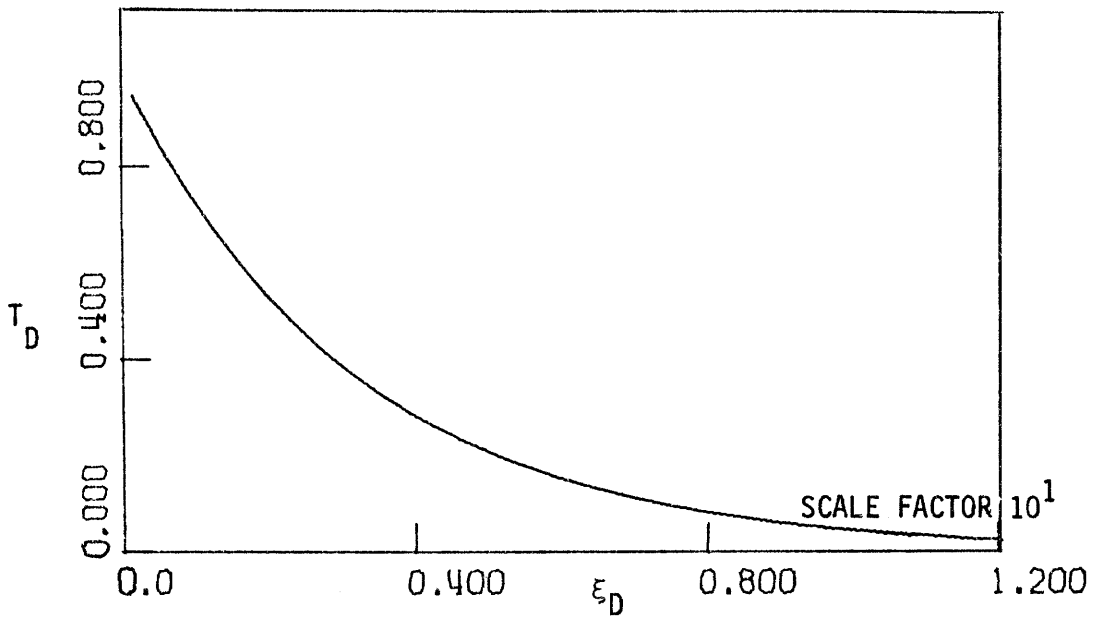


Figure 29a. Temperature Profiles of Eq. (3.87) for $R = 10^3$ and $c = 0.2$ and of Eq. (3.89) for $c = 0.2$. The two profiles coincide.

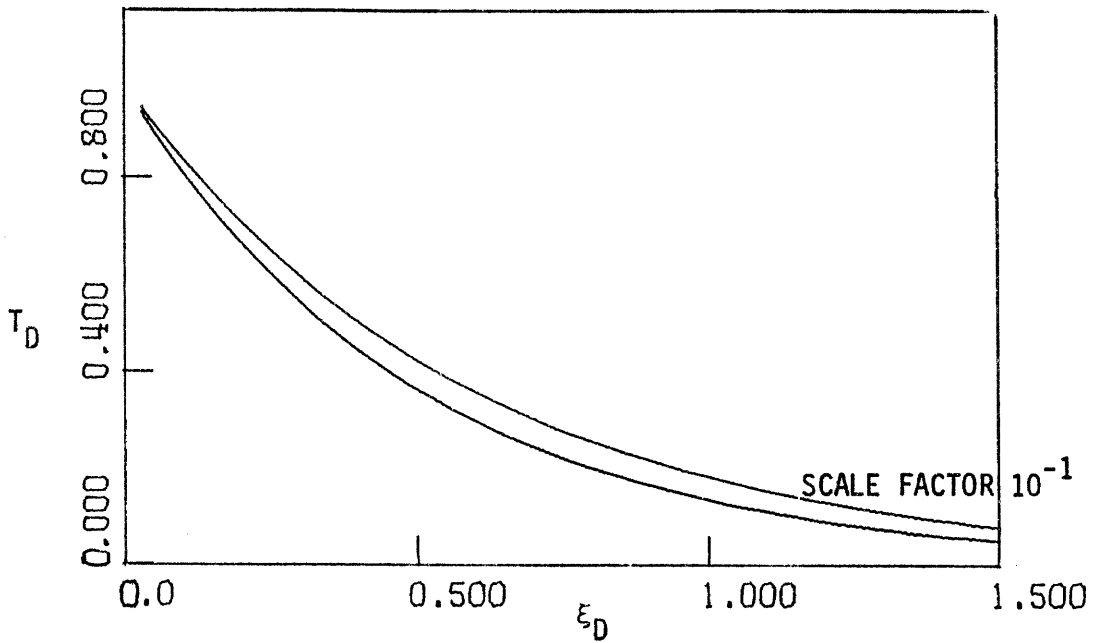


Figure 29b. Temperature Profiles of Eq. (3.87) for $R = 10^3$ and $c = 0.8$ (upper curve) and of Eq. (3.89) for $c = 0.8$ (lower curve).

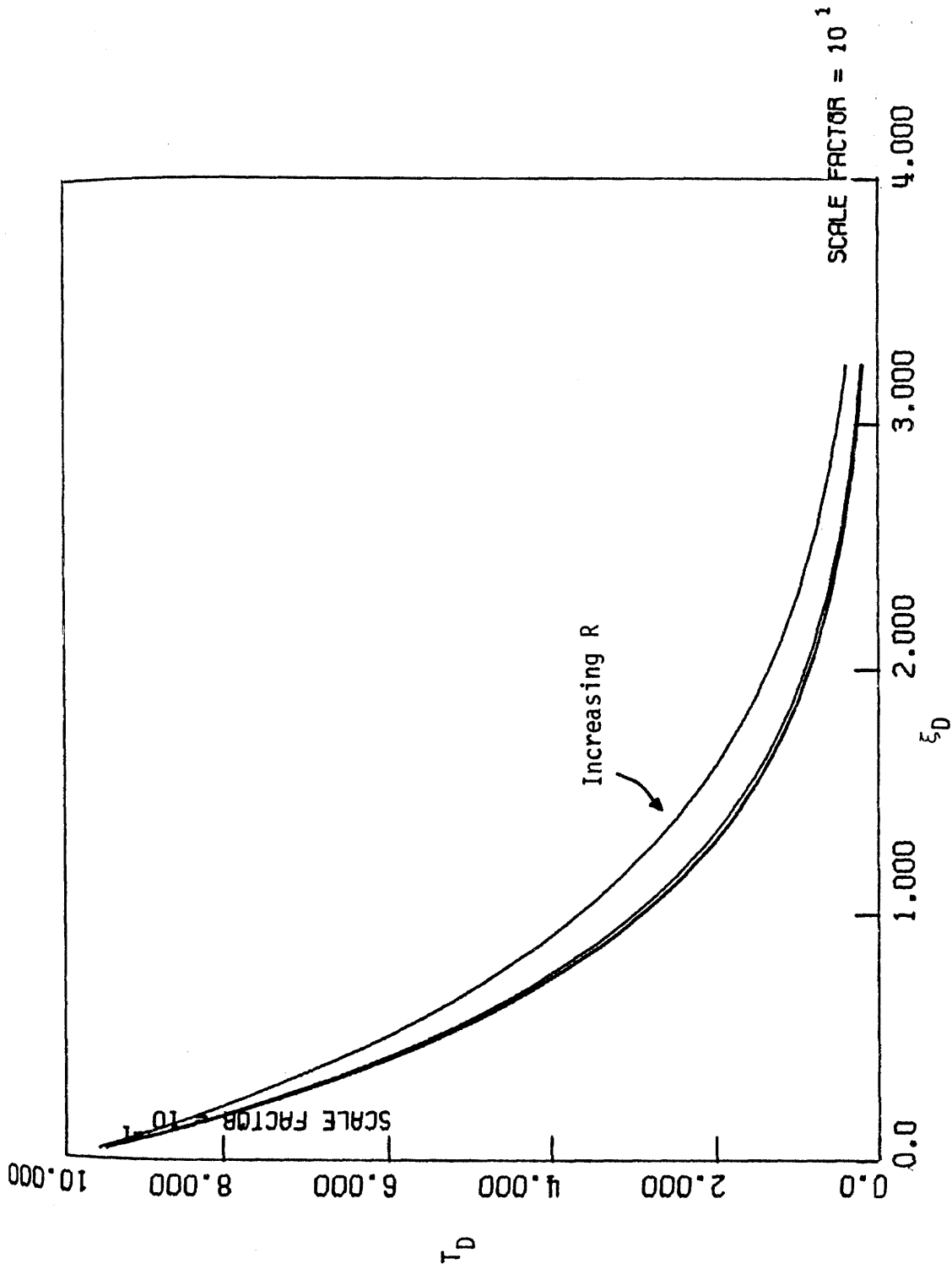


Figure 30a. Temperature Profiles of Eq. (3.87) for $c = 0.8$ and $R = 1, 10, 100, 1000$, and of Eq. (3.89) for $c = 0.8$. The last three profiles ($R = 100, 1000, \infty$) coincide.

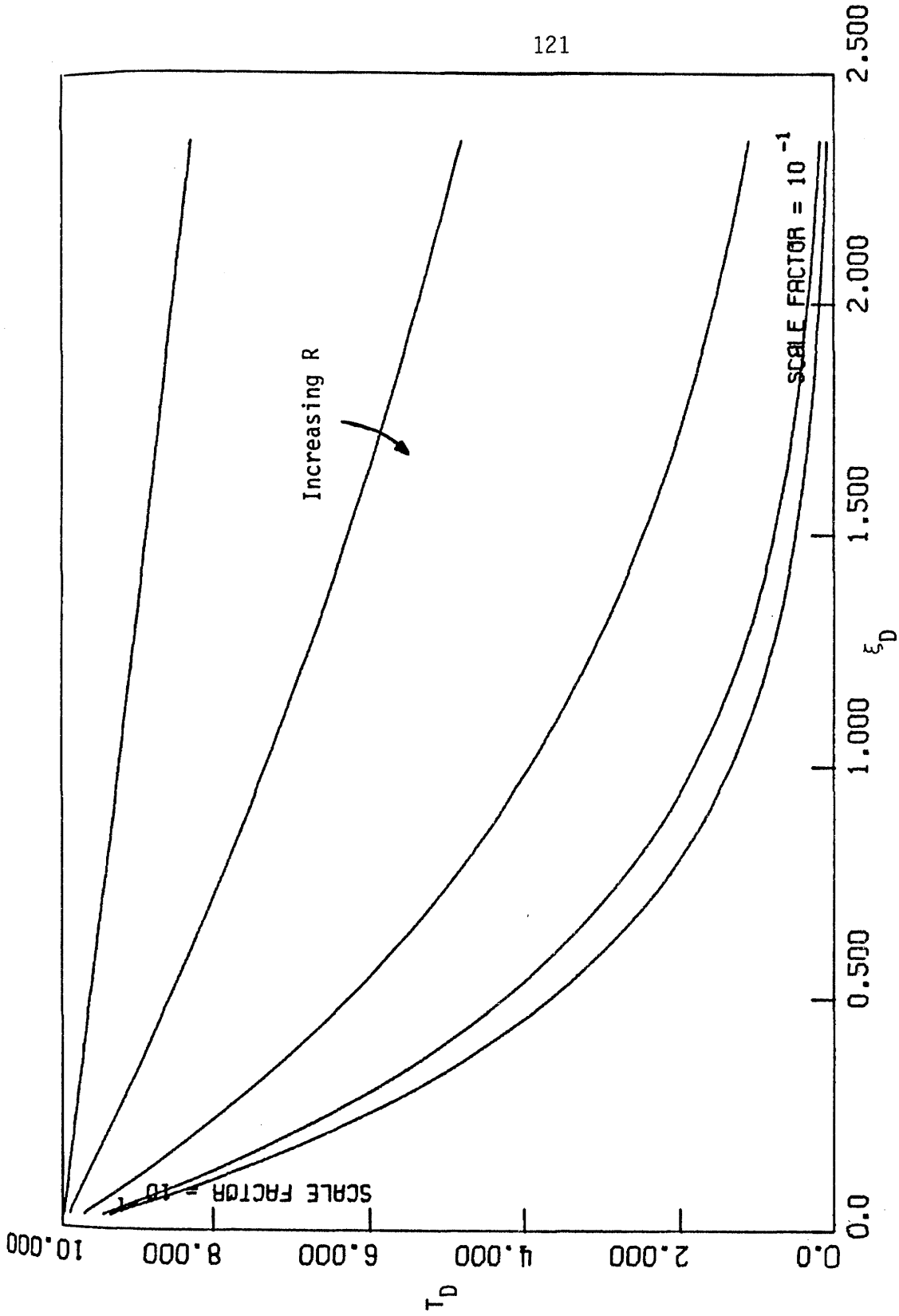


Figure 30b. Temperature Profiles of Eq. (3.87) for $c = 0.1$ and $R = 1, 10, 100, 1000$ (upper four curves), and of Eq. (3.89) for $c = 0.1$ (lower curve).

R , c are tabulated in Tables 3,4. As expected, the larger R and/or c is, the steeper the temperature gradient at the moving origin. These results should check with the steady states discussed in Section 3.7. Indeed, for $R \rightarrow \infty$, $\mu \rightarrow 0$ and Eq. (3.86) admits the unique solution $z = -\lambda^2$, hence,

$$T_D(\xi_D; R_D \rightarrow \infty) = \exp \left[-\frac{c}{(1-c)^2} \xi_D \right] \quad (3.89)$$

which agrees with expression (3.68). Figures 29, 30 show steady-state profiles for various c , R . Note that as R increases, at constant $c < 1$, the temperature profiles approach the solution (3.68), with horizontal conduction neglected. The agreement is better for large R and small c (Figure 30, Table 4) as this can be easily shown by a regular perturbation of (3.86) when $c \ll 1$.

3.8.4 $R = 1$, Arbitrary Velocity

As with 3.8.2, the integro-differential Equation (3.74a) admits a simple solution when the parameter R takes the value 1. In order to derive an analytical solution, we take the Laplace Transform of (3.74a) with respect to time. For an arbitrary R , the resulting expression is very complicated. If $R = 1$, however, we get the simple result:

$$L_t \{T_D\} = A(s) \exp \left\{ \left[\frac{\left(\frac{w_F^0}{|w_F^0|} - 1 \right)}{2} - \sqrt{s} \right] x_D \right\} \quad (3.90)$$

where $A(s)$ is an unknown function of the transformed variable to be determined from the boundary conditions.

Consider, first, $w_F^0 > 0$. Then (3.90) becomes:

$$L_t(T_D) = A(s) \exp[-x_D \sqrt{s}] \quad (3.91)$$

which shows that $T_D(t_D, x_D)$ satisfies the pure heat conduction equation in the plane (t_D, x_D) :

$$\frac{\partial T_D}{\partial t_D} = \frac{\partial^2 T_D}{\partial x_D^2} \quad (3.92)$$

In other words, in the particular case $R = 1$ the lateral heat losses are exactly counterbalanced by the convective heat flux and, as a result, heat transfer is governed by pure heat conduction. Similarly, when $w_F^0 < 0$, we deduce that $T_D(t_D, x_D)$ satisfies the PDE

$$\frac{\partial T_D}{\partial t_D} - 2 \frac{\partial T_D}{\partial x_D} = \frac{\partial^2 T_D}{\partial x_D^2} + T_D \quad (3.93)$$

Here, convection is negative which makes the temperature profiles steeper. Indeed, we can easily check that it is the function $e^{x_D} T_D(t_D, x_D)$ that satisfies the heat conduction equation and not $T_D(t_D, x_D)$ alone, as in the previous case $w_F^0 > 0$.

Before exploring various special cases of boundary motion, we restate the conditions under which the interesting case $R = 1$ arises.

Since

$$R = \frac{w_F^0 h^2}{4k_{hf}^2} \cdot \frac{\alpha_f}{\alpha_R}, \quad \text{then } R = 1 \text{ implies } w_F^0 = \frac{2k_{hf}}{h} \sqrt{\frac{\alpha_R}{\alpha_f}}, \text{ which, for}$$

$\alpha_R \approx \alpha_f$ (as it is usually the case), shows qualitatively why convection counterbalances conduction in the over- and under-burden.

3.8.4.1 Fixed Boundary

This problem is discussed in Subsection 3.8.2. In light of the above analysis, one can immediately deduce the simple results attained when $R = 1$.

3.8.4.2 Constant Front Velocity

Now, $v_D(t_D) = c$ and in moving coordinates t_D , $\xi_D = x_D - ct_D$ we encounter the familiar equation:

$$\frac{\partial T_D}{\partial t_D} - c \frac{\partial T_D}{\partial \xi_D} = \frac{\partial^2 T_D}{\partial \xi_D^2} \quad W_F^0 > 0 \quad (3.94)$$

with B.C.

$$t_D = 0 ; T_D = 0$$

$$\xi_D \rightarrow \infty ; T_D \rightarrow 0$$

$$\xi_D = 0 ; T_D = 1$$

We limit our discussion to the physically realistic case $W_F^0 > 0$. Solving (3.94) as in Section 3.5, we get

$$T_D = \frac{1}{2} \left\{ \operatorname{erfc} \left(\frac{x_D}{2\sqrt{t_D}} \right) + \exp(-c(x_D - ct_D)) \cdot \operatorname{erfc} \left(\frac{x_D - 2ct_D}{2\sqrt{t_D}} \right) \right\} \quad (3.95)$$

$ct_D \leq x_D$

which, in the limit of large times, leads to the steady state solution:

$$T_D = \exp[-c(x_D - ct_D)] \quad (3.96)$$

Figure 31 shows T_D profiles for various t_D and c equal to 1.

The conductive heat flux through the origin

$$\left. \frac{\partial T_D}{\partial x_D} \right|_{x_D=ct_D} = -c - \frac{1}{\sqrt{\pi t_D}} \exp\left[-\frac{c^2 t_D}{4}\right] + \frac{c}{2} \operatorname{erfc}\left(\frac{c\sqrt{t_D}}{2}\right) \quad (3.97)$$

tends asymptotically to $-c$. One can accordingly estimate the character-

istic time of convergence to be $0 \left[\frac{1}{c^2} \left(\frac{M^{(2)}}{\rho_f c_{pf}} \right)^2 \frac{h^2}{\alpha_f} \right]$, in dimensional

variables. Note that it is inversely proportional to the square of the boundary velocity v , while the characteristic time obtained in Subsection 3.4.1.1 for the case of no lateral heat losses is proportional to the square of the net convective heat flux. A comparison of the corresponding steady state conductive heat fluxes shows that in (3.97) an asymptotic nonzero flux applies for any value of the net convective heat flux, provided $c \neq 0$. On the other hand, when lateral heat losses are neglected, the conductive heat flux approaches a non-zero value only if the net convective heat flux is negative.

It is also interesting to compare the heat flux (3.97) to the corresponding expression when $R \rightarrow \infty$ (no horizontal conduction). As shown in Section 3.7.2, the two expressions are identical when the front velocity is small. This, in turn, suggests that, for small front velocities, including horizontal conduction has almost no effect in determining the conductive heat flux through the steam front.

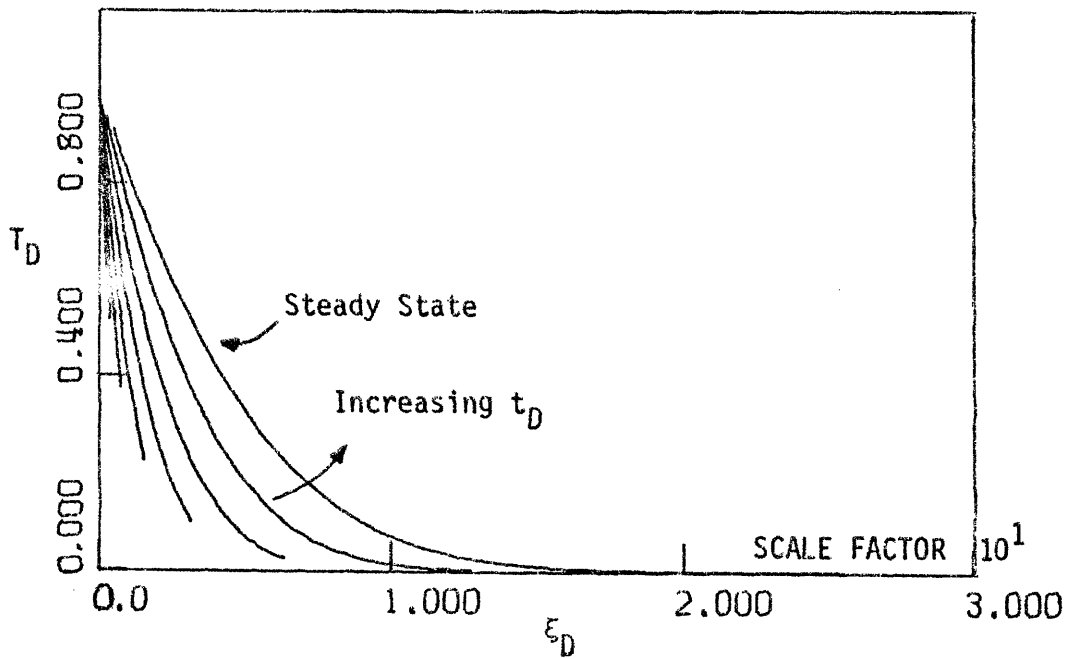


Figure 31. Temperature Profiles of Eq. (3.95) for $c = 1$ and $t_D = 0.4, 0.8, 1.6, 3.2, 6.4, 12.8, 25.6$.

In dimensional notation, we get for large times

$$-k_{hR} \left. \frac{\partial T_R}{\partial x} \right|_{x=vt} \sim \frac{\Delta T M^{(2)}}{R} v \quad (3.98)$$

which may serve as the basis for a quasi-steady state approximation including lateral heat losses, to be used in Section 4.6.

3.8.4.3 Front Velocity of the Form $\dot{v}_D(t_D) = \frac{\alpha}{\sqrt{t_D}}$

In the context of steam drive calculations, it would be also desirable to derive the temperature distribution corresponding to fronts whose velocity decreases with time. A suitable class of fronts for which an analytical solution is possible, is described by the velocity profiles $\dot{v}_D(t_D) = \frac{\alpha}{\sqrt{t_D}}$, α arbitrary. The practical importance of such fronts, in the one-dimensional modelling of steam injection, is highlighted in the next chapter.

According to Section 3.5, the resulting temperature profile is provided by

$$T_D(t_D, x_D) = \operatorname{erfc} \left\{ \frac{x_D}{2t_D^{1/2}} \right\} / \operatorname{erfc} \alpha \quad (3.99)$$

and the dimensionless conductive heat flux by

$$\left. \frac{\partial T_D}{\partial x_D} \right|_{x_D=2\alpha\sqrt{t_D}} = - \frac{1}{\sqrt{\pi t_D}} \cdot \frac{\exp(-\alpha^2)}{\operatorname{erfc} \alpha} \quad (3.100)$$

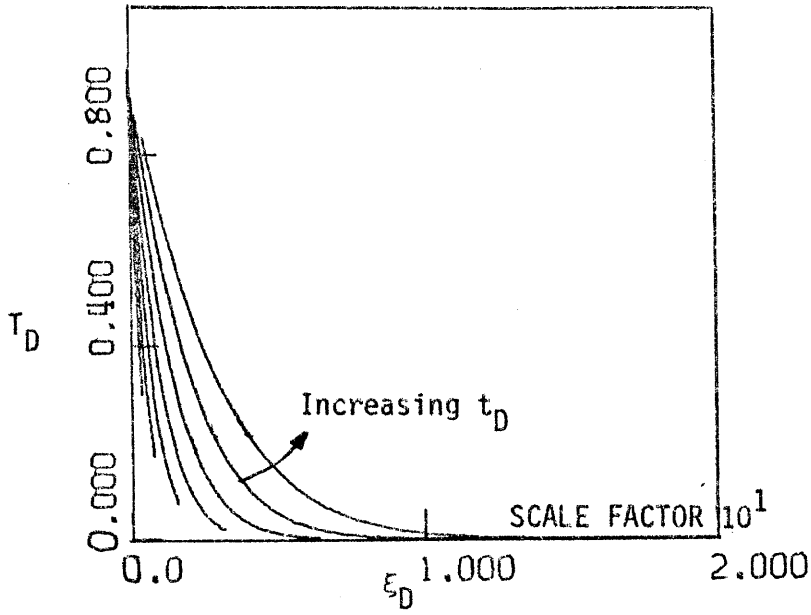


Figure 32a. Temperature Profiles of Eq. (3.99) for $\alpha = 0.5$ and $t_D = 0.4, 0.8, 1.6, 3.2, 6.4, 12.8, 25.6$.

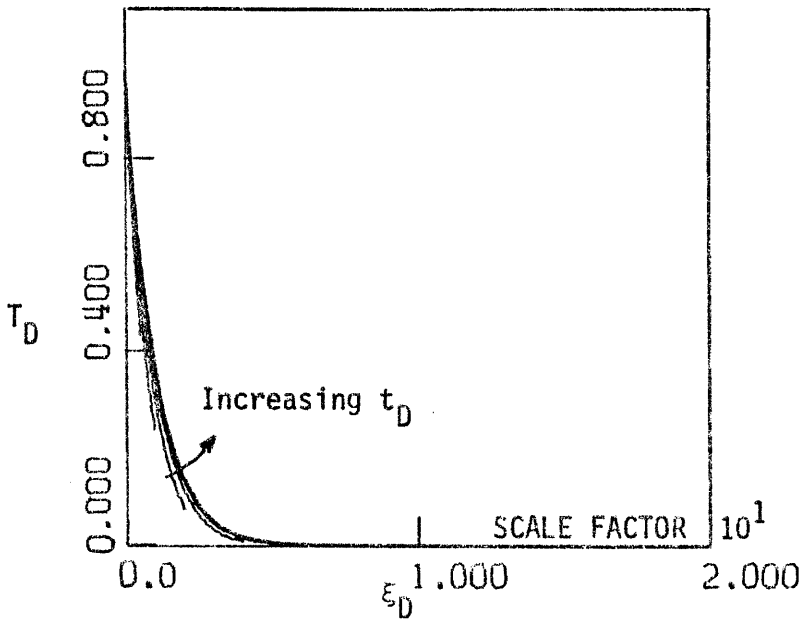


Figure 32b. Temperature Profiles of Eq. (3.99) for $\alpha = 1.5$ and $t_D = 0.4, 0.8, 1.6, 3.2, 6.4, 12.8, 25.6$.

The results are plotted in Figure 32 for various t_D and α .

There exists a remarkable similarity between expression (3.100) and that obtained when heat losses are neglected ($R \rightarrow \infty$), Eq. (3.73). As t_D increases, the front velocity in 3.6.2.3 approaches the velocity under consideration, $\frac{\alpha}{\sqrt{t_D}}$, and the dimensionless conductive heat flux, Eq. (3.73), behaves asymptotically like Eq. (3.100). In such a case, including horizontal conduction ($R = 1$) in the large time description of the heat transfer through the front does not appreciably alter the results when horizontal conduction is neglected ($R \rightarrow \infty$). This is a significant result that is further used in connection with Section 4.5.

Before we conclude this chapter, we would like to discuss in a more systematic way the solution of the class of integro-differential Equations (3.74a). In Appendix IV we comment on the transformation of the integro-differential Equation (3.74a) to a partial differential equation of higher order. The proposed technique may be useful in treating other problems that also belong to this class.

3.9 Conclusions

The results of the foregoing analysis on heat transfer can be briefly summarized as follows.

Heat transfer into the over- and under-burden is sufficiently well, within the scope of thermal recovery modelling, approximated by one-dimensional heat conduction along the vertical direction. The degree of the approximation increases with the injection rates; under normal steamflood conditions the error introduced by the approximation is

Front Velocity \ R	∞	$\neq 1$	1
Zero (3.7.3, 3.8.3, 3.8.4.1)	Yes	Yes	Yes
Constant (3.7.4, 3.8.3, 3.8.4.2)	Yes	Steady States	Yes
Parabolic (3.7.5, 3.8.4.3)	Yes	---	Yes

Studied cases that admit analytical solution.

Table 5

insignificant. On this basis, we developed analytical expressions for the heat losses at a fixed point, in terms of the temperature history of the point under consideration. By further employing known thermodynamic relationships, we were able to bound the conductive and convective heat fluxes to the hot liquid zone, with the objective of deriving bounds on the steam zone volume.

Heat transfer in the hot liquid zone has been treated according to the geometry of the system and the magnitude of the heat conduction along the horizontal direction. In one-dimensional systems, the resulting moving boundary problems have been successfully solved in a number of cases, as shown in Table 5. The results corresponding to a fixed boundary are useful in the context of hot waterflood, while the two other cases will be utilized in modelling steam injection and (eventually) in-situ combustion. In particular, the constant velocity subcase leads to the formulation of a quasi-steady approximation, while the subcase of parabolic steam front movement will be further utilized in the development of asymptotic solutions. In this last case, it is important to notice that the temperature profile, in the limit of large times, is not sensitive to the magnitude of horizontal conduction.

For the purpose of developing analytical expressions we approximated the two-dimensional heat transfer in the hot liquid zone by one-dimensional models. The approximation is seen to be reasonable near the steam front and to introduce larger errors near the reservoir boundaries. Still, it provides us with a handy expression, that will be further employed for the derivation of a first-order approximation to the steam front shape.

Chapter IV. Application to One-Dimensional Reservoirs

4.1 Introduction

With Chapter IV we start the combined application of the integral balance technique and the heat transfer considerations developed in the previous two chapters to steam injection modelling. The geometries examined here are one dimensional, linear or cylindrical, (see Figure 33) and represent processes that exhibit symmetry along two coordinate surfaces. The linear geometry model is most frequently encountered in laboratory simulations whereas the cylindrical case is a more realistic representation of actual field tests because of its two-dimensional (areal) character. It is important to notice the absence of any symmetry distortion that might be caused by the production wells. Since this is often not the case, the geometries under discussion are rather idealistic representations of an actual field pattern (compare to Figure 9). Nevertheless, modelling such processes provides a good insight on the parameters and variables that control the steam zone growth and, in any case, most of the derived results can be extended to more realistic configurations with lesser degrees of symmetry (Chapter V).

In Section 4.2 we reformulate the integral balances and outline the approach used by other investigators in modelling one-dimensional steam injection. We subsequently develop exact upper bounds (Section 4.3), lower bounds (Section 4.4), asymptotic solutions (Section 4.5) and approximate numerical solutions (Section 4.6). The interrelation of the various solutions, the physical significance of the various parameters and the importance of the derived results in actual field cases are extensively

covered. The final Section 4.7 provides solutions to the saturation distribution inside the steam zone, in the absence of steam distillation.

4.2 General Considerations

4.2.1 Reformulation of the Integral Balances

We start with the integral balances (2.47), (2.50) of Chapter II which reduce to simpler expressions due to the symmetry displayed in the present problem. Terms of the form

$$\int_{V(t)} \psi(\underline{r}, t) d\underline{r} \quad , \quad \int_{A_F(t)} \psi(\underline{r}, t) d\underline{r}$$

simplify to

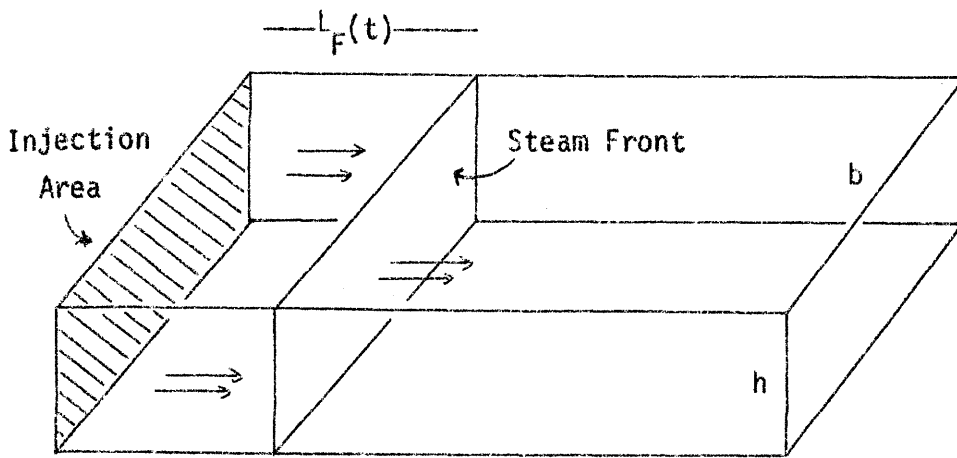
$$bh \int_0^{L_F(t)} \bar{\psi}(x, t) dx \quad , \quad b \int_0^{L_F(t)} \bar{\psi}(x, t) dx$$

in linear and to

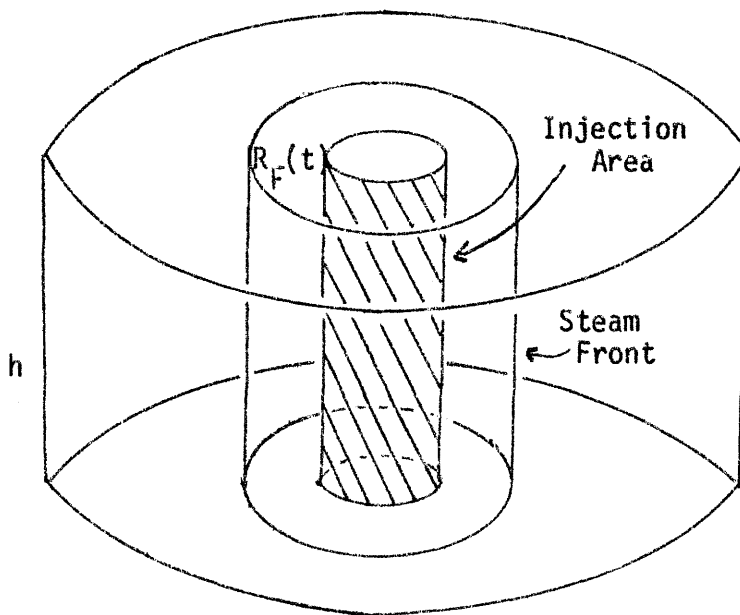
$$2\pi h \int_0^{R_F(t)} r \bar{\psi}(r, t) dr \quad , \quad 2\pi \int_0^{R_F(t)} r \bar{\psi}(r, t) dr \quad ,$$

in cylindrical geometry. Here b is the width, h the thickness of the reservoir, $L_F(t)$ the length, $R_F(t)$ the radius of the steam zone and $\bar{\psi}$ the cross sectional average of a scalar quantity ψ .

Equations (2.47), (2.50) can be written in a uniform notation:



a. Linear Geometry



b. Cylindrical Geometry

Figure 33. One-Dimensional Geometries Examined in Chapter IV.

$$\begin{aligned}
& \Delta T \frac{d}{dt} \int_0^{X_F(t)} M_1 dx + \Pi_F(t) \Delta T \{W_F(t) + Q_F(t)\} + \frac{2}{h} \int_0^{X_F(t)} \left(-k_{hf} \frac{\partial T_f}{\partial n} \right) II dx \\
& = [w_s(t) + w_w(t)] c_{pw} \Delta T + w_s(t) L_v^{(1)} \quad (4.1)
\end{aligned}$$

$$\begin{aligned}
& \Delta T \frac{d}{dt} \int_0^{X_F(t)} M_2 dx + \Pi_F(t) \Delta T Q_F(t) \\
& + \frac{2}{h} \int_0^{X_F(t)} \left(-k_{hf} \frac{\partial T_f}{\partial n} \right) II dx = w_s(t) L_v^{(1)} \quad (4.2)
\end{aligned}$$

Subtracting (4.2) from (4.1) we get the water mass balance:

$$\Delta T \frac{d}{dt} \int_0^{X_F(t)} M_3 dx + \Pi_F(t) \Delta T W_F(t) = [w_s(t) + w_w(t)] c_{pw} \Delta T \quad (4.3)$$

where $M_3 = M_1 - M_2$. Here $\Pi_F(t)$, a measure of the steam front perimeter, is equal to 1 or $2\pi R_F(t)$; $X_F(t)$ stands for steam zone length or area and the injection rates are expressed per unit injection area or unit thickness in linear and cylindrical geometries, respectively.

Throughout this chapter we are mainly concerned with the determination of the steam zone volume, $X_F(t)$, as a function of time. For this purpose we need, besides (4.1) and (4.2), information regarding the distribution of the volumetric heat capacities M_1 , M_2 and the coupling heat flux terms $W_F(t)$, $Q_F(t)$. As will be seen in Section 4.7, the average values of M_i remain approximately constant, which considerably facilitates a further development of the model. In contrast, as already indicated, the heat transfer terms are harder to handle and, since they play a dominant role in the determination of the front dynamics, particular care should be taken

in dealing with them.

While the structure of Eqs. (4.1), (4.2) is non-linear with respect to $X_F(t)$, further inspection reveals that both equations consist of the sum of an almost linear and a non-linear part

$$L_{Lj} \{X_F(t)\} + L_{Nj} \{X_F(t)\} = \Phi_j(t) \quad j = 1, 2 \quad (4.4)$$

where the subscripts 1,2 refer to energy or steam balances, respectively, and

$$\Phi_1(t) = w_s L_V^{(1)} + (w_s + w_w) c_{pw} \Delta T \quad (4.5a)$$

$$\Phi_2(t) = w_s L_V^{(1)} \quad (4.5b)$$

The almost linear operator L_{Lj} has a common structure in both equations. For continuously advancing fronts we get, invoking (3.13)

$$L_{Lj} \{X_F(t)\} = \frac{d}{dt} \int_0^{X_F(t)} f_j(x, t; X_F(t)) dx + d \int_0^{X_F(t)} \frac{dx}{\sqrt{t - \lambda(x)}} \quad j = 1, 2 \quad (4.6)$$

where $d = \frac{2k_{hf}\Delta T}{h\sqrt{\pi\alpha_f}}$. The function $f_j(x, t; X_F(t)) = \Delta T M_j$ is a slowly

varying function of $X_F(t)$, hence the term "almost linear". We will refer to L_{L1} as the Marx-Langenheim operator.

Before we proceed with the solution of (4.1), (4.2), it is interesting to discuss the methods employed by previous investigators in their attempts

to determine the one-dimensional steam zone growth.

4.2.2 The Marx-Langenheim (1959) and the Mandl-Volek (1969) Approaches

Marx and Langenheim (1959) modelled the one-dimensional, linear, steam drive with constant injection rates, by assuming constant saturations inside the steam zone and a step-temperature distribution [compare to (3.14)], which results to zero heat flux into the hot-liquid zone. Thus, they were able to arrive at an approximate energy balance which is linear with respect to $X_F(t)$.

The Marx-Langenheim equation, which is here corrected to include terms involving S_s , that did not appear in the original equation, consists, therefore, of the almost linear part alone, thus making the problem analytically tractable:

$$L_{L1} \{X_{ML}(t)\} = M_1 \Delta T \dot{X}_{ML}(t) + d \int_0^t \frac{\ddot{X}_{ML}(\lambda) d\lambda}{\sqrt{t - \lambda}} = \phi_1 \quad (4.7)$$

Here M_1 is considered constant, the subscript ML refers to Marx-Langenheim and dots denote differentiation. An identical equation can be obtained directly from the exact expression (2.45) by following the above stated assumptions ($T^{II} = T_f$).

The solution of (4.7) follows by a straightforward application of Laplace Transform, for both constant injection rates (as originally presented by Marx and Langenheim) and arbitrary injection rates [as generalized by Ramey (1959)]. Denoting the steam front velocity by $v_{ML}(t)$ we get, for constant ϕ_1

$$v_{ML}(t) = \frac{\phi_1}{M_1 \Delta T} \left[\frac{\pi d^2 t}{(M_1 \Delta T)^2} \right] \operatorname{erfc} \left[\frac{d\sqrt{\pi t}}{M_1 \Delta T} \right] \quad (4.8a)$$

the well-known Marx-Langenheim expression. When ϕ_1 varies [Ramey (1959)]

$$v_{ML}(t) = \frac{\phi_1(t)}{M_1 \Delta T} + \frac{\pi d^2}{(M_1 \Delta T)^3} \int_0^t \phi_1(\tau) \left\{ \exp \left[\frac{\pi d^2 (t - \tau)}{(M_1 \Delta T)^2} \right] \operatorname{erfc} \left[\frac{d\sqrt{\pi(t - \tau)}}{M_1 \Delta T} \right] - \frac{M_1 \Delta T}{\pi d \sqrt{t - \tau}} \right\} d\tau \quad (4.8b)$$

Incidentally, Ramey's extension, although mathematically valid, does not provide the actual rate of growth, even within the approximate Marx-Langenheim framework, in cases of receding fronts.

The Marx-Langenheim model which found considerable applications in the past, has three main drawbacks: (1) It neglects the heat flow to the hot liquid zone. (2) It is based solely on the total thermal energy balance, thus predicting a non-zero steam zone growth even if hot water only is injected. (3) It does not apply to variable injection rates that give rise to receding fronts. Therefore, use of Equations (4.8) will produce realistic results only when the front advances continuously, and for small times, when the heat penetration into the hot liquid zone is small.

Mandl and Volek (1969) were the first to object the universal validity of the Marx-Langenheim model. Based on an inequality, which in view of the considerations of Chapter III, is easily interpreted here as the constraint (3.19b) on the mass balance (4.2), they concluded that expression (4.8a) portrays indeed the actual velocity of the front, but only up to a

critical time t_c . After this time, they show qualitatively that (4.8a) serves as an upper bound on the actual front velocity.

Regarding these conclusions one can remark the following: Equation (4.8a), based on the restrictive assumption of negligible heat flow to the hot liquid zone, is certainly not an exact solution to the problem, although it may be close to it for some limited time after injection starts. (See Subsection 4.5.3.) It is also not obvious from the qualitative arguments they present, that v_{ML} is an upper bound to the actual velocity after time t_c . In fact, if translated in mathematical terms, their argument is equivalent to the following logical deduction scheme:

$$\forall x(t) > 0: L_{L1}\{x(t)\} > 0 \quad \forall t > 0 \Rightarrow \dot{x}(t) > 0 \quad \forall t > 0 \quad (4.9)$$

which can be shown not to be true for each $x(t) > 0$. On the other hand, in case of variable injection rates, in particular, one should concentrate on providing bounds for the steam zone length (area) rather than the steam front velocity. Nevertheless, their analysis is the first reported that takes into consideration important aspects of the problem other than the integral energy balance.

The possibility of a more accurate solution of (4.1), (4.2) depends mostly on our ability to relate convective and conductive heat fluxes into the hot liquid zone to the dynamics of the front. As demonstrated in Chapter III, this interrelation is furnished by two different approaches: (i) By the exact inequalities (3.18), (3.19), (3.20) which are valid for any geometrical configuration or steam front motion. (ii) By the approximate analytical treatment of the heat transfer inside the hot liquid zone

under various assumptions and geometries. The first approach will give rise to rigorous analytical bounds, whereas the second provides approximate analytical expressions for the steam zone volume. Both methods are discussed in the following sections.

4.3 Upper Bounds

The method of describing the solution of a complicated problem by placing it between upper and lower bounds has been successfully employed in several theoretical and engineering problems. In particular, Stefan and Stefan-like moving boundary problems comprise an area where, due to the complexity of the problem, this approach has attracted considerable interest [Mori and Araki (1976), Glasser and Kern (1978)] and led to successful results. From much of the foregoing discussion it is clear that steam drive is a potential candidate for the application of such an approach. We start with the derivation of upper bounds.

4.3.1 Upper Bounds Derivation

We use inequalities (3.18), (3.19), (3.20) to bound the non-linear part of (4.1), (4.2). Then, it is easy to show that

$$(L_{Lj} + L_{Nj})\{X_F(t)\} \geq \frac{d}{dt} \int_0^{X_F(t)} f_j(x, t; X_F(t)) dx + \frac{d}{\sqrt{t}} X_F(t) \quad j=1,2 \quad (4.10)$$

therefore,

$$\frac{d}{dt} \int_0^{X_F(t)} f_j(x, t; X_F(t)) dx + \frac{d}{\sqrt{t}} X_F(t) < \phi_j(t) \quad \forall 0 < t \quad j=1,2 \quad (4.11)$$

The above inequalities are a direct consequence of the physical constraints that the net heat flux through the steam front and the net steam flux reaching the front are positive. We now define $x_j^+(t)$ such that

$$\frac{d}{dt} \int_0^{x_j^+(t)} f_j(x, t; X_F(t)) dx + \frac{d}{\sqrt{t}} x_j^+(t) = \phi_j(t) \quad \forall 0 < t \quad (4.12)$$

$$x_j^+(0) = 0, \quad j = 1, 2$$

One can then prove, (Appendix V), that both $x_1^+(t)$, $x_2^+(t)$ provide two independent upper bounds on $X_F(t)$, for any rate of steam front propagation in $0 < t$.

The integro-differential equation (4.12) has an exact solution for specific functionals $f_j(x, t; X_F(t))$. Since f_j is not known we employ the relationship

$$\int_0^{x_j^+(t)} f_j(x, t; X_F(t)) dx = \bar{f}_j(t) x_j^+(t) \quad j = 1, 2 \quad (4.13)$$

where $\bar{f}_j(t)$ is the average volumetric heat capacity, a linear function of the average steam saturation. With (4.13), Equation (4.12) admits the solution

$$x_j^+(t) = \frac{1}{\bar{f}_j(t)} \int_0^t \phi_j(\tau) \exp \left\{ -d \int_{\tau}^t \frac{d\lambda}{\bar{f}_j(\lambda) \sqrt{\lambda}} \right\} d\tau \quad j = 1, 2 \quad (4.14)$$

Equation (4.14) provides a closed form expression for the calculation of

upper bounds, when $\bar{f}_j(t)$ is known. Now

$$f_1(x, t; X_F(t)) = \Delta T \cdot \left\{ \sum_{i=s, w, o} \phi S_i \rho_i c_{pi} + (1 - \phi) \rho_R c_{pR} + \frac{\phi S_s \rho_s L_v^{(1)}}{\Delta T} \right\} \quad (4.15a)$$

$$f_2(x, t; X_F(t)) = \phi S_s \rho_s L_v^{(1)} \quad (4.15b)$$

Experimental evidence [Willman et al. (1961)] indicates that the oil saturation inside the steam zone reaches a constant residual value which is independent of its initial value and can, in principle, be determined from the parameters of the system. It is also commonly assumed that the average steam and water saturations do not vary considerably. In this work, this assumption is further corroborated (Section 4.7) by showing that

$$\left| \frac{d\bar{S}_i}{dt} X_j^+(t) \right| \ll \frac{dX_j^+(t)}{dt} \bar{S}_i(t) \quad j = 1, 2 \quad i = s, w \quad (4.16)$$

as long as the injected steam has constant quality.

Therefore one can reasonably assume that the average volumetric heat capacity inside the steam zone is constant and furthermore $\bar{f}_j(t) \approx M_j \Delta T$. Instead of this approximation one can rigorously proceed by simultaneously solving for the steam saturation distribution and the steam front growth rate. However, this is a complicated procedure with little expected gain, as evidenced in Section 4.7. Substituting in (4.14), we get:

$$x_j^+(t) = \frac{\exp\left\{-\frac{2d\sqrt{t}}{M_j\Delta T}\right\}}{M_j\Delta T} \int_0^t \phi_j(\tau) \exp\left\{\frac{2d\sqrt{\tau}}{M_j\Delta T}\right\} d\tau \quad (4.17)$$

Let us now define the characteristic variables

$$B_j = \frac{d}{M_j\Delta T} (\text{time}^{-1/2}), \quad l_j = \frac{\phi_j(0)M_j\Delta T}{2d^2} (\text{length or area}) \quad (4.18)$$

and dimensionalize time with $(2B_1)^{-2}$, length with l_1 , injection rates with $\phi_1(0)$. The selection of these characteristic values for non-dimensionalization is not arbitrary but follows directly from Section 2.5. In Table 6 we present the physical variables of a steam drive and their magnitudes under normal field conditions. We note that, by using (4.18), the characteristic time turns out to be of the order of 2.65 years and the characteristic radius of the area of the steam zone of the order of 100 m.

If now subscript D symbolizes a dimensionless quantity, we get (4.12) in dimensionless form:

$$2\dot{x}_{1D}^+(t_D) + \frac{x_{1D}^+(t_D)}{\sqrt{t_D}} = \phi_{1D}(t_D) \quad (4.19)$$

$$2\frac{B_1}{B_2}\dot{x}_{2D}^+(t_D) + \frac{x_{2D}^+(t_D)}{\sqrt{t_D}} = \phi_{2D}(t_D) \quad (4.20)$$

and similarly, Eq. (4.17)

$$x_{1D}^+(t_D) = \frac{1}{2} \exp\{-\sqrt{t_D}\} \cdot \int_0^{t_D} \phi_{1D}(\tau_D) \exp[\sqrt{\tau_D}] d\tau_D \quad (4.21)$$

<u>Parameter</u>	<u>Unit</u>	<u>Linear Steam Drive</u>	<u>Radial Steam Drive</u>
L, R, length	m	508	120
b, θ , width	m or	254	2π
h, thickness	m	25.4	19
ϕ , porosity	—	0.345	0.345
k, permeability	μm^2	2.46	3.80
c_{pw} , heat capacity	KJ/kg $\cdot^\circ\text{K}$	4.186*	4.186*
c_{po} , heat capacity	KJ/kg $\cdot^\circ\text{K}$	2.093*	2.093*
$\rho_R c_{pR}$, vol. heat capacity	MJ/m $^3\cdot^\circ\text{K}$	2.345*	2.345*
$\rho_f c_{pf}$, vol. heat capacity	MJ/m $^3\cdot^\circ\text{K}$	2.345*	2.345*
k_{hR} , ther. conductivity	W/m $^\circ\text{K}$	2.768*	2.768*
k_{hf} , ther. conductivity	W/m $^\circ\text{K}$	2.768*	2.768*
ρ_o^1 , density	kg/m 3	960.00	800.00
ρ_w^1 , density	kg/m 3	823.31	802.18
ρ_s^1 , density	kg/m 3	14.77	19.29
μ_{oi} , viscosity	mPa $\cdot\text{s}$	180.00	2.6
μ_o^1 , viscosity	mPa $\cdot\text{s}$	1.50	0.41
μ_w^1 , viscosity	mPa $\cdot\text{s}$	0.10	0.1
μ_s^1 , viscosity	mPa $\cdot\text{s}$	0.01	0.01
T_i , temperature	$^\circ\text{C}$	38	40
T_s , temperature	$^\circ\text{C}$	233	248
p_s , pressure	bar	29.55	38.450
f_{st} , steam quality	—	0.88	0.88
L_v , latent heat	MJ/kg	1.79	1.72
m_s , injection rate	kg/s	5.34	6.53

Basic Data for Steam Injection
 [van Lookeren (1977),* Chu and Trimble (1975)]

Table 6

$$x_{2D}^+(t_D) = \frac{1}{2} \frac{B_2}{B_1} \exp \left\{ -\frac{B_2}{B_1} \sqrt{t_D} \right\} \int_0^{t_D} \phi_{2D}(\tau_D) \exp \left[\frac{B_2}{B_1} \sqrt{\tau_D} \right] d\tau_D \quad (4.22)$$

The corresponding dimensionless Marx-Langenheim equation becomes

$$2\dot{x}_{MLD}(t_D) + \int_0^{t_D} \frac{\dot{x}_{MLD}(\tau_D) d\tau_D}{\sqrt{t_D - \tau_D}} = \phi_{1D}(t_D) \quad (4.23)$$

with solution

$$x_{MLD}(t_D) = \frac{1}{2} \int_0^{t_D} \phi_{1D}(\tau_D) \exp \left\{ \frac{\pi}{4} (t_D - \tau_D) \right\} \operatorname{erfc} \left\{ \frac{\sqrt{\pi}}{2} \sqrt{t_D - \tau_D} \right\} d\tau_D \quad (4.24)$$

Comparing the kernels in the integrals (4.21), (4.22), (4.24) we can show that, depending on the functional form of $\phi_{jD}(t_D)$, we may have $x_{MLD}(t_D)$ smaller, larger or equal to $x_{jD}^+(t_D)$ in various t_D regions.

Interpreting the bounds in physical terms, we may view $x_{1D}^+(t_D)$ as the dimensionless length (area) of the steam zone in the fictitious process, where every point of the steam zone loses heat to the over- and underburden at the same rate and no net heat is transported through the front to the liquid zone. In this way, the unaccounted part of heat losses is partly counterbalanced by the assumed zero net heat flux to the hot liquid zone. On the other hand, $x_{2D}^+(t_D)$ may be viewed as the steam zone length (area) in the fictitious process, where every point of the zone losses heat to the surrounding formations at the same rate and the conductive heat flux to the hot liquid zone is identically zero. We, therefore, expect $x_{1D}^+(t_D)$ to be closer to the actual solution at small times, when heat has not had

enough time to penetrate deeply inside the liquid zone, whereas $x_{2D}(t_D)$ is close to the actual solution at larger times, when the temperature of the liquid zone has been significantly raised.

Depending on how $\phi_{jD}(t_D)$ varies with time, the difference between $x_{1D}^+(t_D)$ and $x_{2D}^+(t_D)$ may be negative, zero or positive in certain t_D regions, thus suggesting that the lowest upper bound may alternate between $x_{1D}^+(t_D)$ and $x_{2D}^+(t_D)$ (See Figure 34). The points where the lower upper bound shifts branch are the real solutions t_{Dm} of

$$x_{1D}^+(t_{Dm}) = x_{2D}^+(t_{Dm}) \quad m = a, b, c, \dots \quad (4.25)$$

and they can be assigned the following physical meaning. Considering $x_{1D}^+(t_D)$ [or $x_{2D}^+(t_D)$] as the solution of the actual physical process, we require that they also satisfy the constraints (4.10). The constraints for energy and steam mass are obeyed by $x_{1D}^+(t_D)$ and $x_{2D}^+(t_D)$, respectively, at any time. However, the steam mass and energy constraints are satisfied by $x_{1D}^+(t_D)$ and $x_{2D}^+(t_D)$, respectively, only in regions where

$$x_{1D}^+(t_D) - x_{2D}^+(t_D) < 0 \quad \text{and}$$

$$x_{1D}^+(t_D) - x_{2D}^+(t_D) > 0 \quad , \text{ respectively.}$$

Thus, the physical interpretation given to $x_{1D}^+(t_D)$ [or $x_{2D}^+(t_D)$] is consistent whenever $x_{1D}^+(t_D) - x_{2D}^+(t_D) < 0$ (or > 0). The constants t_{Dm} , $m = a, b, c, \dots$ delineate the time intervals where this happens. From (4.19), (4.20) we

also conclude, that at t_{Dm} , the following relationship holds:

$$\frac{dX_{1D}^+(t_{Dm})}{dt_D} = \frac{\phi_{1D}(t_{Dm}) - \phi_{2D}(t_{Dm})}{2} \quad (4.26)$$

where we made use of the inequality $B_1 \ll B_2$ (see Table 6).

We next rewrite the water mass balance, Equation (4.3), in dimensionless notation:

$$2 \left(1 - \frac{B_1}{B_2} \right) \frac{dX_{FD}}{dt_D} + W_{FD} = \phi_{1D} - \phi_{2D} \quad (4.27)$$

where W_{FD} is the dimensionless net convective heat flux through the steam front, which may be positive or negative. At the times t_{Di} , $i = 1, 2, 3, \dots$, when W_{FD} changes sign, we accordingly have:

$$\frac{dX_{FD}}{dt_D}(t_{Di}) = \frac{\phi_{1D}(t_{Di}) - \phi_{2D}(t_{Di})}{2} \quad (4.28)$$

Therefore, at t_{Di} the conduction dominated heat transfer in the hot liquid zone becomes convection dominated or vice versa, depending on whether W_{FD} turns positive or negative. Comparing (4.26) to (4.28) we can establish a relationship between t_{Dm} and t_{Di} , which depends, among others, on the injection rates $\phi_{1D}(t_D)$, $\phi_{2D}(t_D)$. In particular, for constant injection rates, it is not difficult to show that $t_{Dm,m} = a, b, c, \dots$ are upper bounds to t_{Di} , $i = 1, 2, 3, \dots$.

In the rest of Section 4.3 we examine the application of the derived bounds on steam injection with various injection rates.

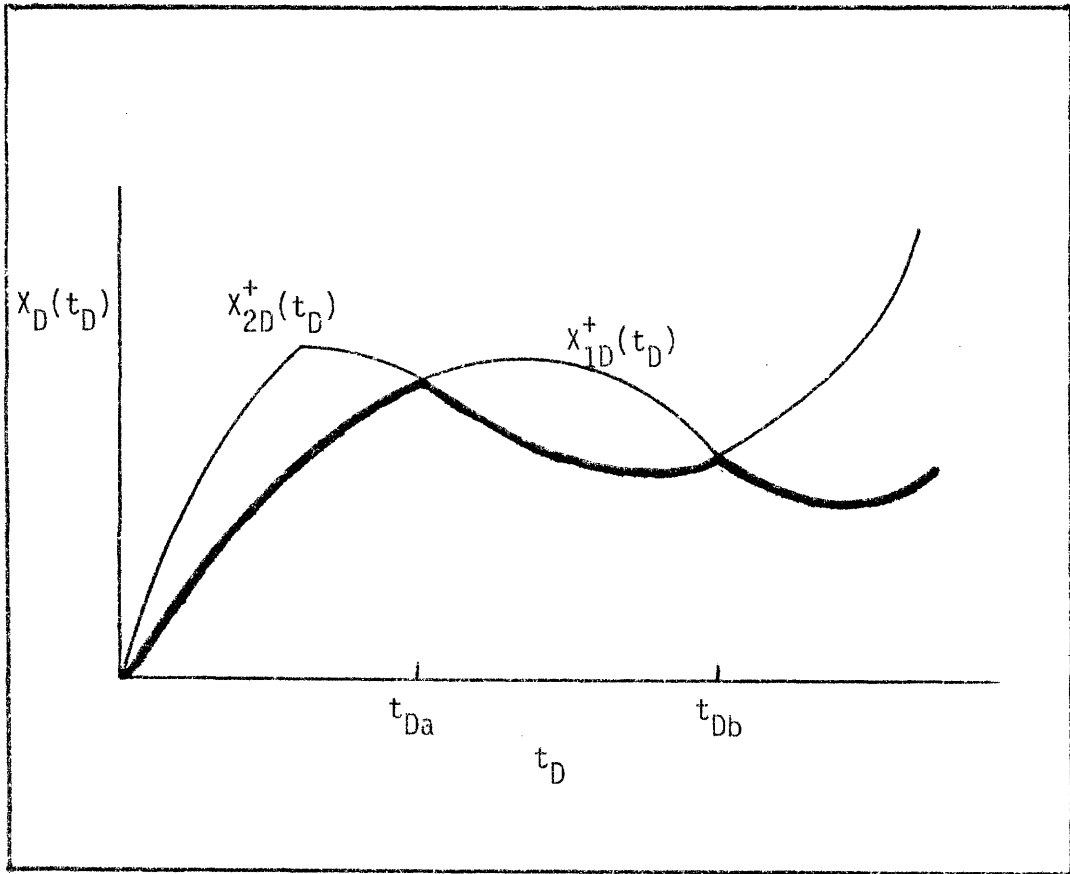


Figure 34. Schematic Diagram of Upper Bounds x_{1D}^+ , x_{2D}^+ .
 — Lower Upper Bound.

4.3.2 Variable Injection Rates

We first discuss typical cases where the injection rates are functions of time. The examples to be studied are representative of field cases where the rates are allowed to vary, but the operating conditions (steam temperature, steam quality) are held constant. Thus, the dimensionless ratio $A = \frac{\phi_{2D}(t_D)}{\phi_{1D}(t_D)}$ remains constant throughout the process.

4.3.2.1 Square Pulse Injection Rates

In the first example, steam is injected at a constant rate, ($\phi_{1D} = 1.0$), for a certain period of time at the end of which, ($t_D = 0.25$), injection ceases. Figure 35a shows ϕ_{1D} plotted vs. t_D . The injection parameters take the values $A = 0.5$, $B = B_1/B_2 = 0.02$. Such a case is typical of the first soaking cycle of steam stimulation operations [SPE Repr. Ser. (1972)].

The resulting upper bounds X_{1D}^+ , X_{2D}^+ and the Marx-Langenheim solution X_{MLD} are plotted versus t_D in Figure 35b. Shown also is the lowest upper bound that consists of successive branches of X_{1D}^+ , X_{2D}^+ . Initially and for as long as injection lasts, X_{1D}^+ is much smaller than X_{2D}^+ . As soon as injection stops, however, X_{2D}^+ declines very rapidly, crosses X_{1D}^+ and approaches zero much faster than X_{1D}^+ does. Thus, the actual steam zone length, which is bounded from above by the lowest upper bound, increases as long as injection continues and rapidly decreases to zero when injection is disrupted.

This is in sharp contrast to the results obtained by use of the Marx-Langenheim solution. The latter follows X_{1D}^+ very closely, which is

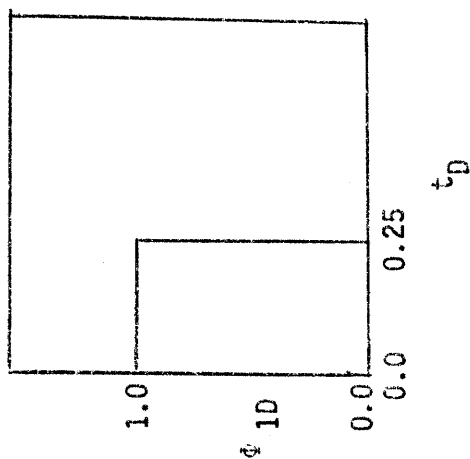


Figure 35a. Injection Rates for Case 4.3.2.1 (Square Pulse) $A = 0.5$.

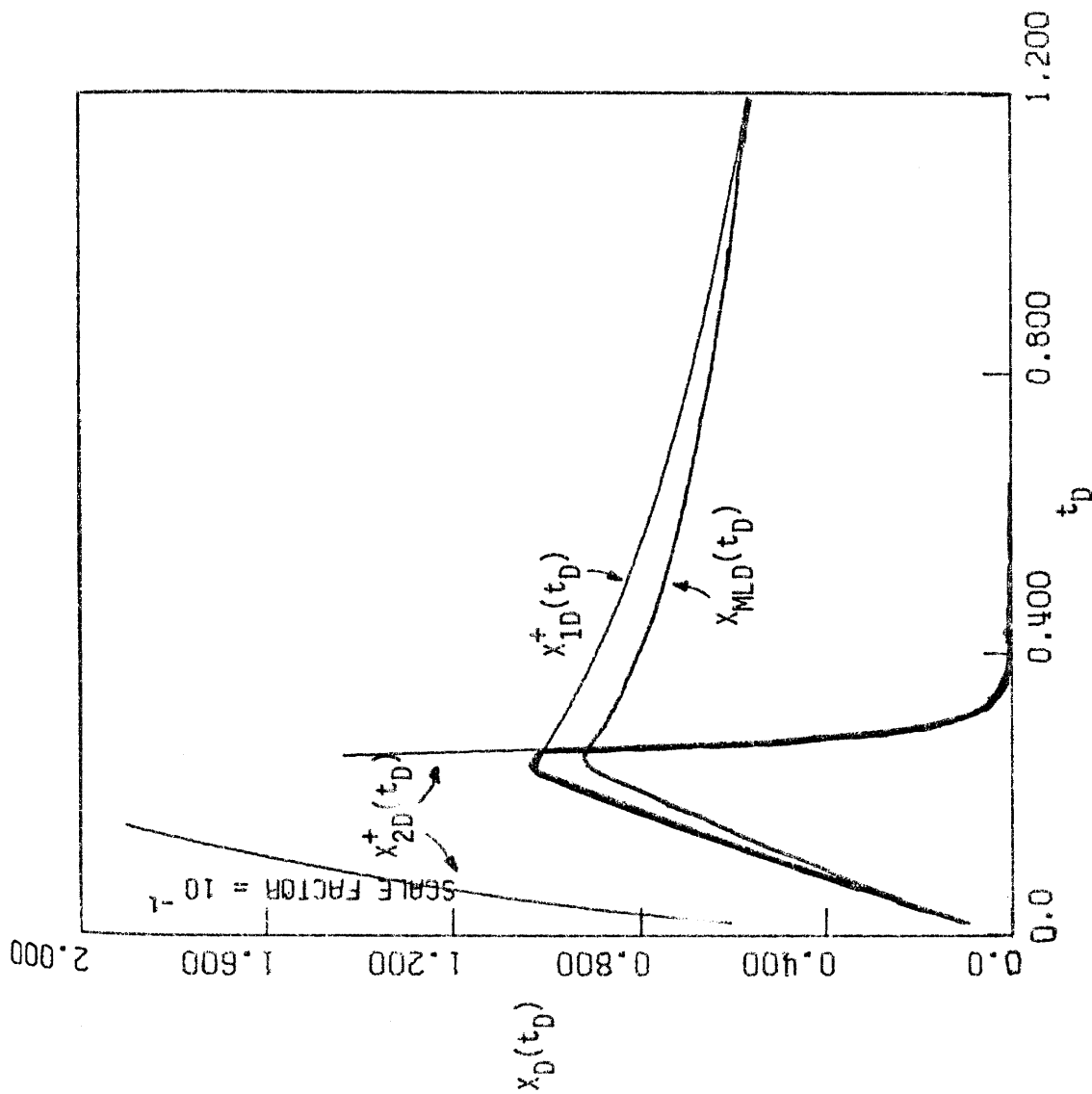


Figure 35b. Upper Bounds X_{1D}^+ , X_{2D}^+ and the Marx-Langenheim Solution X_{MLD} .

— Lower Upper Bound.

expected since both are based on the total thermal energy balance. When x_{1D}^+ is the dominant branch of the lowest upper bound, there is no significant error in using x_{MLD} as an approximate solution to the steam zone length. When, however, injection is halted, the Marx-Langenheim solution predicts a much slower decline of the steam zone volume.

We conclude that the rate at which the steam zone decreases in size is much larger than the rate predicted by Marx-Langenheim type of calculations. This is a useful result regarding the optimal design of an injection pattern for steam stimulation which, so far, is based on the Marx-Langenheim model [Boberg and Lantz (1966)]. An injection pattern usually consists of repeated square pulses of uneven duration in general. Each pulse is followed by varying periods of zero rates in order to allow for oil to flow back to the injection well (which also serves as a production well). A periodic pattern with injection rates $\phi_{1D} = 1$, $\phi_{2D} = 0.5$, equal duration intervals and period 0.5 is shown in Figure 36a. The upper bounds and the Marx-Langenheim solution that correspond to this input are plotted in Figure 36b.

The resulting behavior in the first cycle of the injection pattern is identical with the one discussed previously. Just before injection restarts ($t_D = 0.50$), the steam zone volume is negligibly small. With the onset of re-injection, the upper bound x_{1D}^+ regains control of the rate of growth and continues to do so throughout the injection interval. The upper bound x_{2D}^+ shows very drastic changes at the edges of discontinuity, shoots high above x_{1D}^+ as injection begins and assumes a dominant role after it ceases. The quick response of the function x_{2D}^+ to changes in the

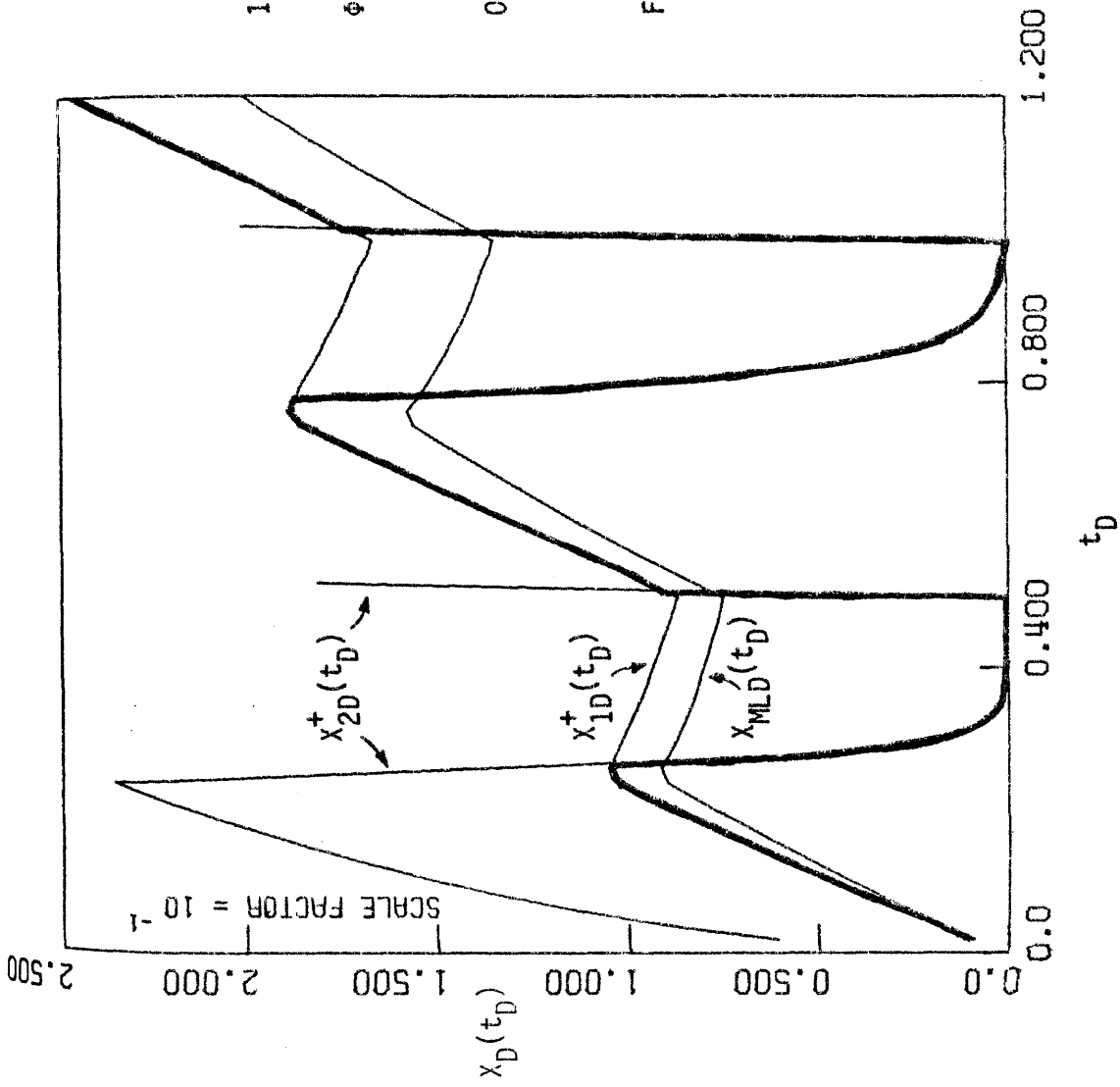


Figure 36b. Upper Bounds X_{1D}^+ , X_{2D}^+ and the Marx-Langenheim Solution X_{MLD}^- .
 — Lower Upper Bound.

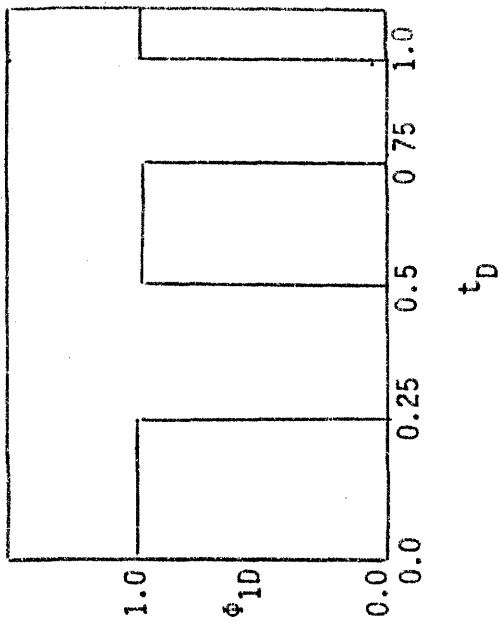


Figure 36a. Injection Rates for Case 4.3.2.1. (Periodic Injection) $A = 0.5$

input is attributed to the smallness of the parameter B which expresses the ratio of the volumetric latent heat capacity of steam to the volumetric heat capacity of the steam zone.

We further observe that the rate of decline of the steam zone volume, in periods of no injection, is very rapid, in spite of the preheating of the surrounding formations that occurred during the first cycle. This is also noticeable, although to a smaller degree, in the next cycles. In contrast, the bound X_{1D}^+ resumes control at nearly the same levels and continues to increase with a steady rate which, in turn, indicates that heating of the surrounding rocks in the previous cycles considerably lessens their thermal resistance to the steam zone growth.

As before, by comparing X_{MLD} with the derived bounds, we confirm the relative inability of the Marx-Langenheim solution to adequately describe the steam zone rate of decrease in periods of zero injection.

4.3.2.2 Two-Level Injection Rates

Another interesting case that is likely to occur in any steam injection process involves operation at two different injection levels. In the simulation shown in Figure 37a the dimensionless rate $\phi_{1D} = 1.0$ is sustained up until time $t_D = 1.0$ and subsequently reduced to $\phi_{1D} = 0.5$. Here, again, $A = 0.5$, $B = 0.02$ throughout the process.

Much as in the previous example, the lowest upper bound, which consists of a branch of X_{1D}^+ initially, experiences a rapid decline as soon as X_{2D}^+ takes over. The latter controls the steam zone dynamics from then on. The effect of preheating is rather well manifested by the quick

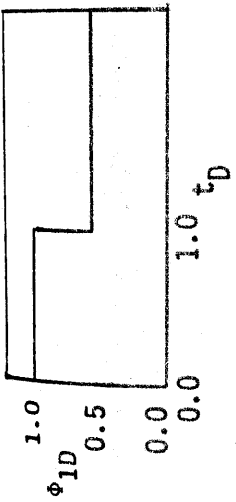


Figure 37a. Injection Rates for Case 4.3.2.2. $A = 0.5$

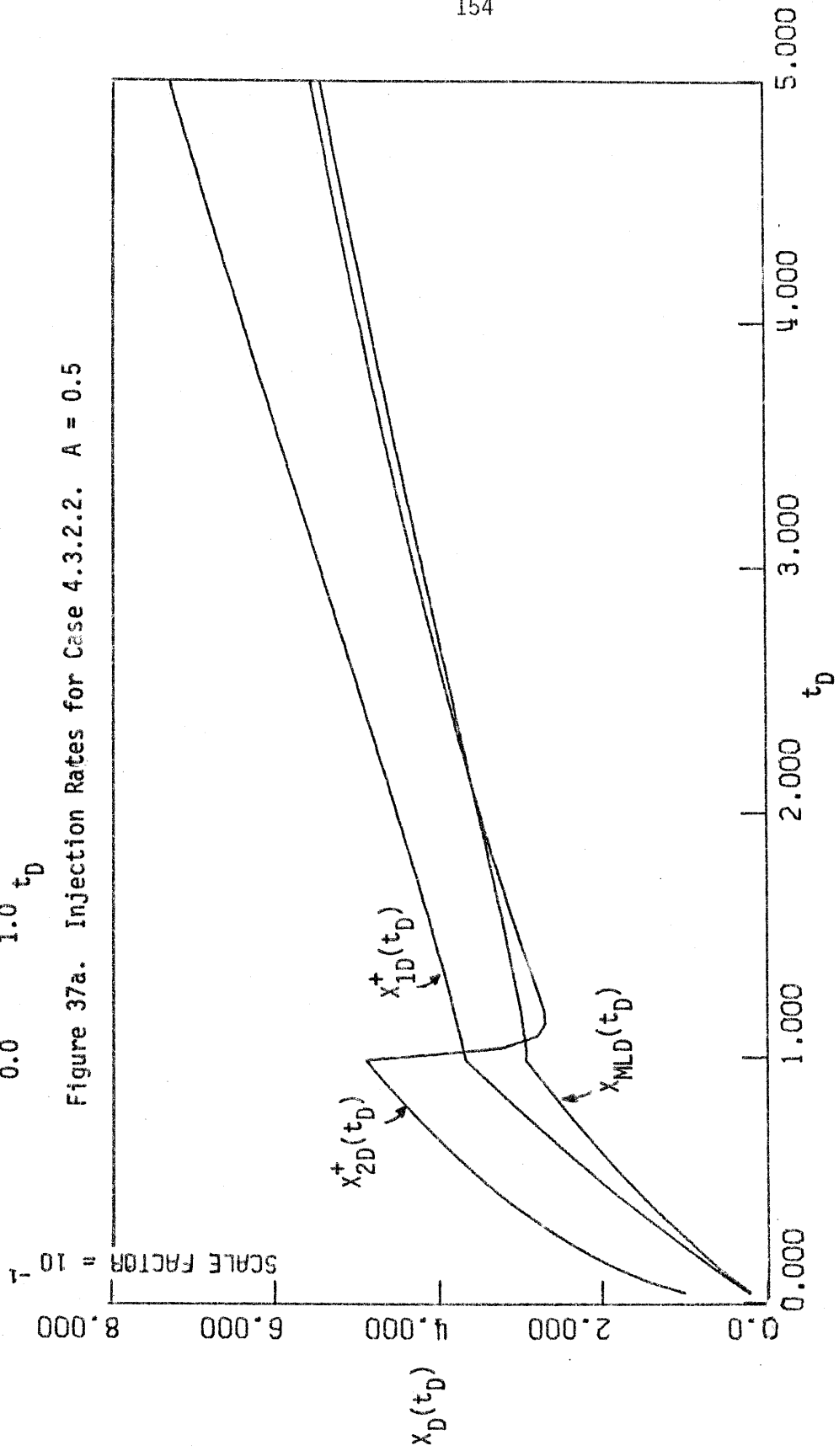


Figure 37b. Upper Bounds x_{1D}^+ , x_{2D}^+ and the Marx-Langenheim Solution x_{MLD} .

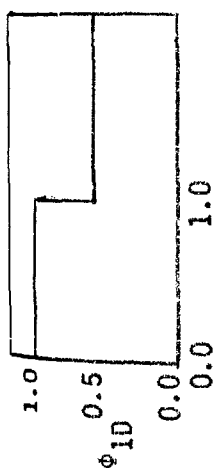


Figure 38a. Injection Rates for Case 4.3.2.2. $A = 0.3$

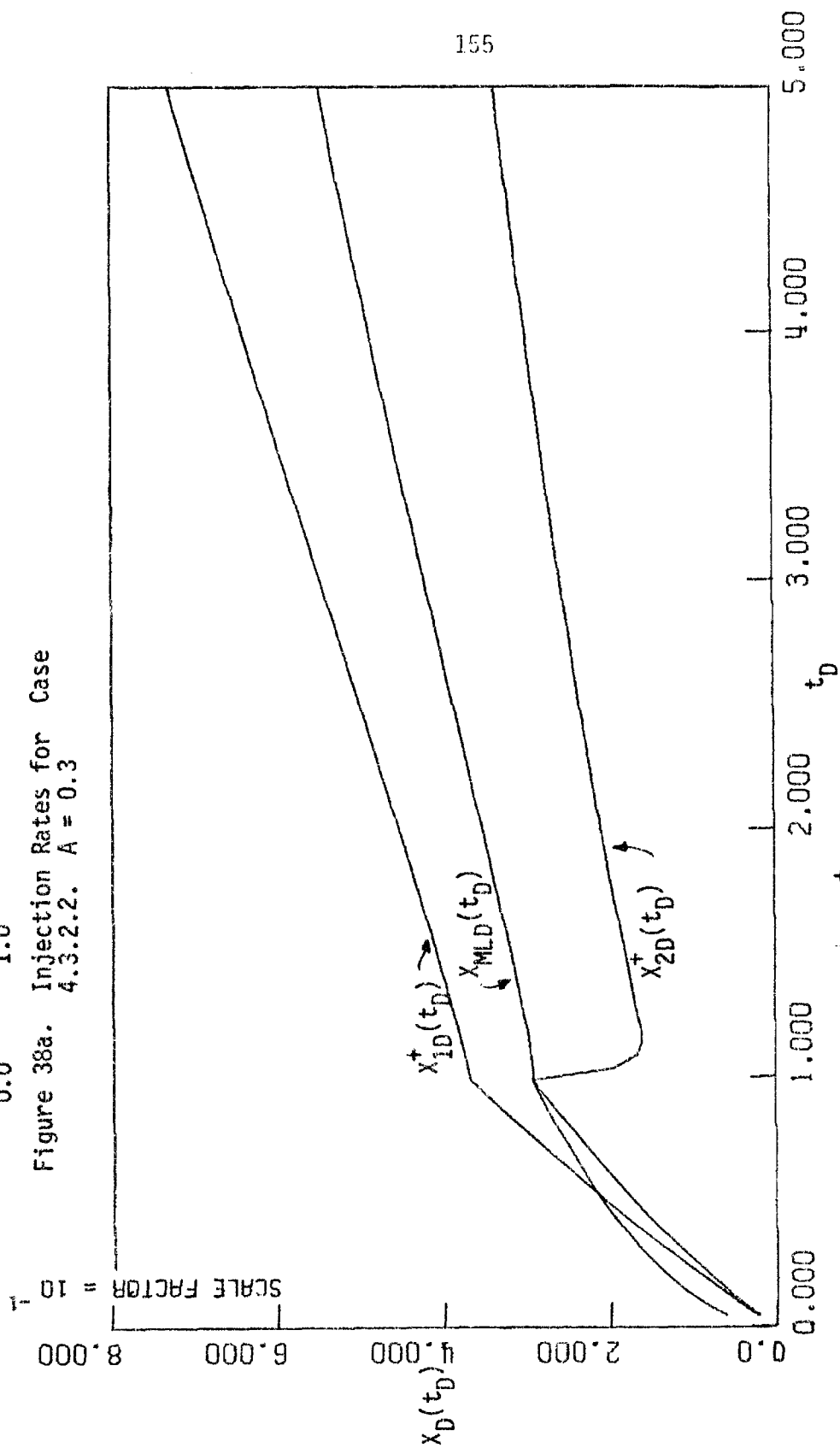


Figure 38b. Upper Bounds X_{1D}^+ , X_{2D}^+ and the Marx-Langenheim Solution X_{MLD} .

recovery of the steam zone rate of growth after the fast decrease imposed by the sudden change on the injection rates (Figure 37b).

The Marx-Langenheim solution is seen to lie above the lowest upper bound after the change takes place and to cross below it shortly thereafter. One can then conclude that it behaves reasonably well for this particular case. This is not the case, however, when the latent heat injection rate ϕ_{2D} gets smaller. The results of a simulation with $A = 0.3$ are shown in Figure 38. Now one can see that the upper bound ϕ_{2D}^+ assumes a dominant role at early times. The solution x_{MLD} is satisfactory, initially, but fails to describe the actual rate of advance after the change in injection rates. In this case the use of the Marx-Langenheim approximation would result to misleading over-optimistic predictions regarding oil recovery efficiency.

The above suggest that A plays an important role in the rate of steam zone growth and the extent of the validity of the Marx-Langenheim solution. This will become evident in the next subsection which deals with constant injection rates.

4.3.3 Constant Injection Rates

The majority of both laboratory tests and actual field operations with steam injection are carried out under constant injection rates. Under these conditions, the upper bounds expressions (4.21), (4.22) become:

$$x_{1D}^+(t_D) = \sqrt{\epsilon_D} - 1 + \exp(-\sqrt{\epsilon_D}) \quad (4.29)$$

$$x_{2D}^+(t_D) = A \left\{ \sqrt{t_D} - B + B \exp\left(-\frac{1}{B} \sqrt{t_D}\right) \right\} \quad (4.30)$$

and, similarly, the Marx-Langenheim solution, (4.24):

$$x_{MLD}(t_D) = \frac{2}{\pi} \left\{ \sqrt{t_D} - 1 + \exp\left(\frac{\pi t_D}{4}\right) \operatorname{erfc}\left(\frac{\sqrt{\pi t_D}}{2}\right) \right\} \quad (4.31)$$

where $A = \frac{\phi_{2D}}{\phi_{1D}}$, $B = \frac{B_1}{B_2}$ as before. The dimensionless parameter A expresses the ratio of the latent to the total heat injected and can also be written

$$A = \frac{f_{st}}{f_{st} + S_t} \quad (4.32)$$

where f_{st} is the steam quality at the injection point (downhole) and

$S_t = \frac{c_{pw} \Delta T}{L_v(1)}$ is the Stefan number. The latter is the ratio of the

sensible to the latent heat content of saturated steam and, as shown in Table 7, it increases with the steam temperature and decreases with the initial formation temperature. Similarly, the parameter B expresses the ratio of the latent to the total heat capacity of the steam zone and is also equal to:

$$B = \frac{1}{1 + S_t \left\{ \frac{1}{f_{st}} + \frac{\rho_o S_o c_{po}}{\rho_s S_s c_{pw}} + \frac{(1 - \phi)}{\phi} \frac{\rho_R c_{pR}}{\rho_s S_s c_{pw}} \right\}} \quad (4.33)$$

For typical values of reservoir parameters and operating conditions

Injection Temperature	Stefan Number		
$T_s(^{\circ}\text{C})$	$T_i = 20^{\circ}\text{C}$	$T_i = 30^{\circ}\text{C}$	$T_i = 40^{\circ}\text{C}$
150	0.259	0.239	0.219
160	0.284	0.263	0.243
170	0.309	0.289	0.269
180	0.337	0.316	0.296
190	0.365	0.344	0.323
200	0.396	0.374	0.352
210	0.428	0.406	0.384
220	0.462	0.440	0.419
230	0.499	0.476	0.453
240	0.540	0.516	0.492
250	0.584	0.559	0.536
260	0.632	0.607	0.581
270	0.686	0.660	0.639
280	0.747	0.720	0.691
290	0.816	0.780	0.763
300	0.897	0.868	0.838
310	0.994	0.963	0.932
320	1.113	1.080	1.054
330	1.270	1.228	1.204
340	1.470	1.430	1.387

Stefan number for various values of steam temperature, T_s ,
and initial formation temperature, T_i .

Table 7

<u>A</u>	<u>t_{Da}</u>	<u>t_{Dα}</u>	<u>t_{D1}</u>
0.70	10.2211	∞	3.4269
0.65	7.0575	∞	2.2837
0.60	4.9800	>>1	1.5605
0.55	3.5552	>>1	1.0813
0.50	2.5395	15.4716	0.7531
0.45	1.8062	7.0345	0.5230
0.40	1.2684	3.6086	0.3593
0.35	0.8717	1.9591	0.2421
0.30	0.5797	1.0882	0.1580
0.25	0.3670	0.5896	0.0983
0.20	0.2154	0.3054	0.0568
0.15	0.1117	0.1424	0.0290
0.10	0.0460	0.0535	0.0118
0.05	0.0106	0.0114	0.0027

Values of the characteristic times t_{Da} , $t_{D\alpha}$,
for various values of A.

Table 8

(Table 6) one obtains:

$$0 < A < \frac{1}{1 + S_t}, \quad 0 < B \approx 0.02 \ll 1 \quad (4.34)$$

In view of (4.34), one can easily show that

$$x_{1D}^+(t_D) \leq x_{2D}^+(t_D) \quad 0 < t_D \leq t_{Da} \quad (4.35a)$$

$$x_{2D}^+(t_D) \leq x_{1D}^+(t_D) \quad t_{Da} \leq t_D \quad (4.35b)$$

In other words, the upper bound $x_{1D}^+(t_D)$ dominates at the beginning of the process until the critical time t_{Da} , after which the upper bound $x_{2D}^+(t_D)$ assumes control. The time t_{Da} , where $x_{1D}^+(t_{Da}) = x_{2D}^+(t_{Da})$, satisfies the algebraic equation:

$$\sqrt{t_{Da}} (1 - A) = 1 - \exp(-\sqrt{t_{Da}}) \quad (4.36)$$

Table 8 shows typical values of t_{Da} as a function of A . We notice that t_{Da} is an increasing function of A , which indicates that the smaller A is, i.e. the smaller f_{st} or the larger T_s , the faster x_{2D}^+ crosses below the bound x_{1D}^+ .

Due to the exponential convergence in (4.29), (4.30) the two bounds rapidly assume their asymptotic behavior:

$$x_{1D}^+(t_D) \sim \sqrt{t_D} \quad t_D > 16 \quad (4.37a)$$

$$x_{2D}^+(t_D) \approx A\sqrt{t_D} \quad t_D > 0.006 \quad (4.37b)$$

The above characteristics are very well exhibited in the following Figures which show plots of x_{1D}^+ , x_{2D}^+ , x_{MLD} vs. t_D for various values of A .

Regarding the location of x_{MLD} with respect to the bounds, one can draw the following conclusions: We first observe that x_{MLD} is smaller than x_{1D}^+ for any t_D . Indeed, from (4.29), (4.31) one can show (Appendix VI) that

$$x_{MLD}(t_D) < x_{1D}^+(t_D) \quad \forall 0 < t_D \quad (4.38)$$

Inequality (4.38) is valid in any time domain and, for this reason, has a specific importance from a strictly mathematical viewpoint since it gives rise to an upper bound on the function erfcz (Appendix VI).

Returning to Figures 39 - 42, we notice that x_{MLD} is well below the lowest upper bound for high values of A . As A decreases, however, there exists a critical time $t_{D\alpha}$ when the Marx-Langenheim solution crosses above the upper bound x_{2D}^+ and keeps deviating thereafter. Thus, from (4.30), (4.31) one can prove that, if $A > \frac{2}{\pi}$

$$x_{MLD}(t_D) < x_{2D}^+(t_D) \quad \forall 0 < t_D < t_{D\alpha} \quad (4.39)$$

whereas, if $A < \frac{2}{\pi}$

$$x_{MLD}(t_D) < x_{2D}^+(t_D) \quad 0 < t_D < t_{D\alpha} \quad (4.40a)$$

$$x_{2D}^+(t_D) < x_{MLD}(t_D) \quad t_{D\alpha} < t_D \quad (4.40b)$$

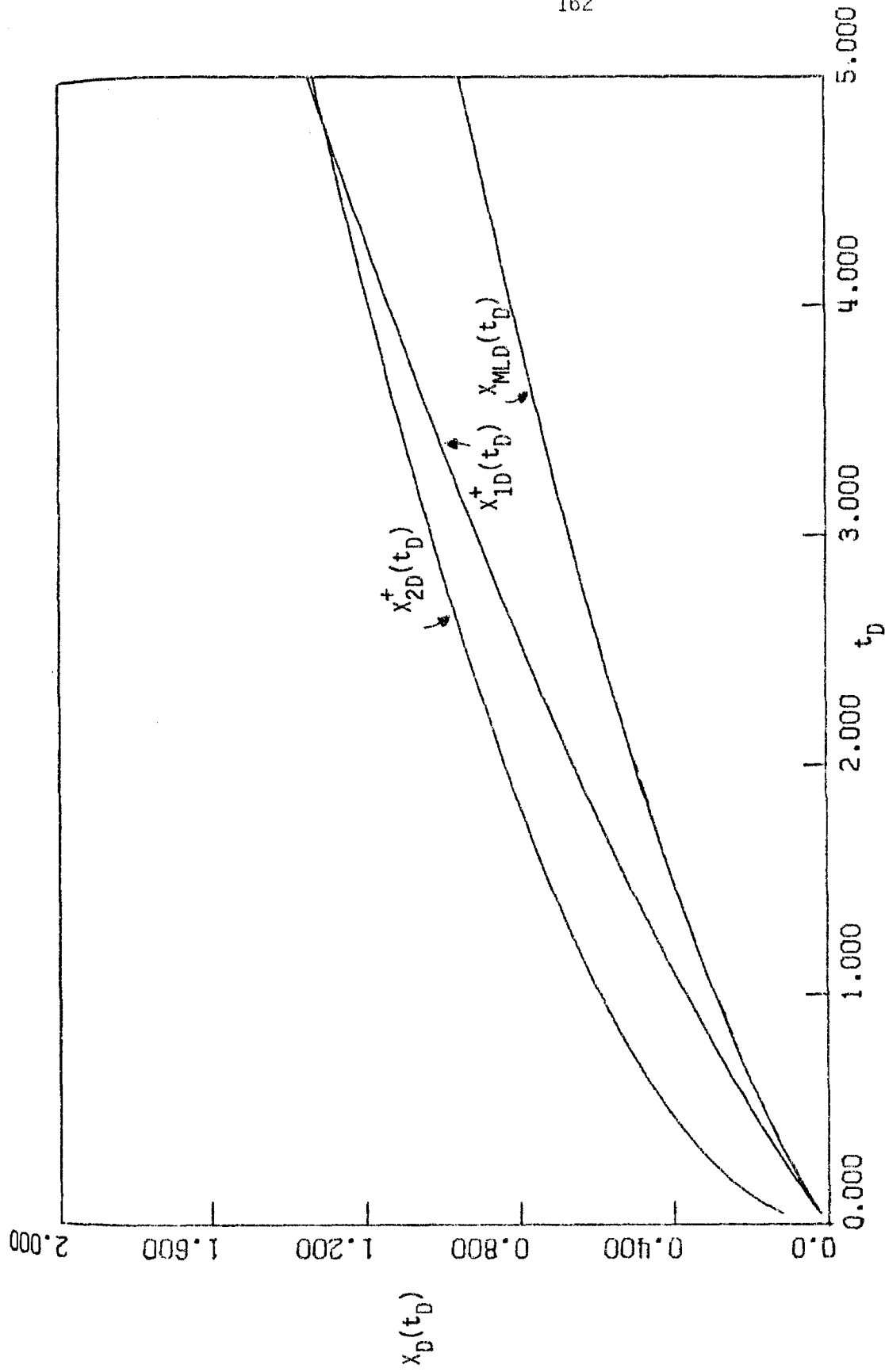


Figure 39. Upper Bounds and the Marx-Langenheim Solution X_{MLD} for Constant Injection Rates. $A = 0.6$.

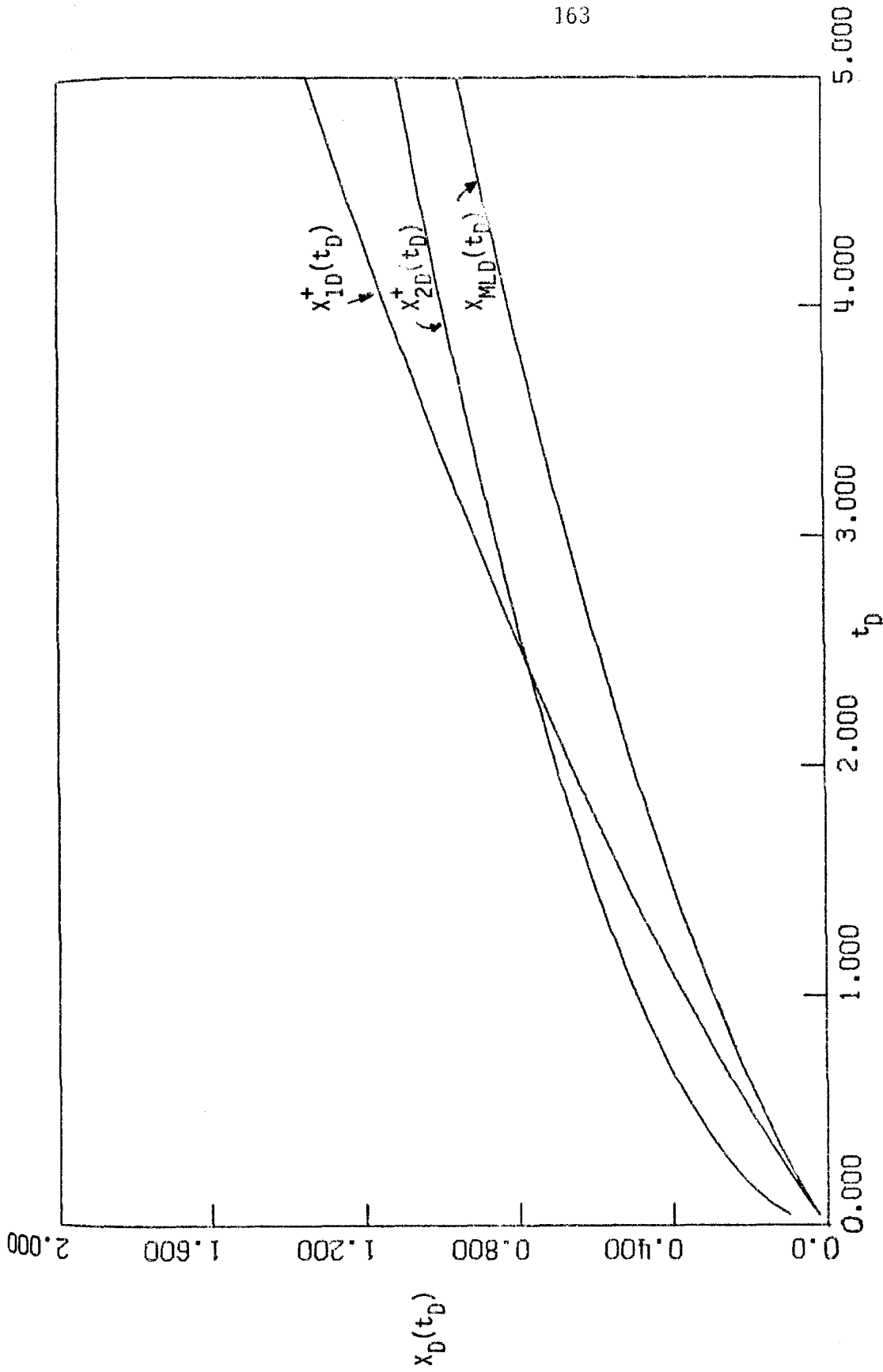


Figure 40. Upper Bounds x_{1D}^+ , x_{2D}^+ and the Marx-Langenheim Solution for Constant Injection

Rates. $A = 0.5$.

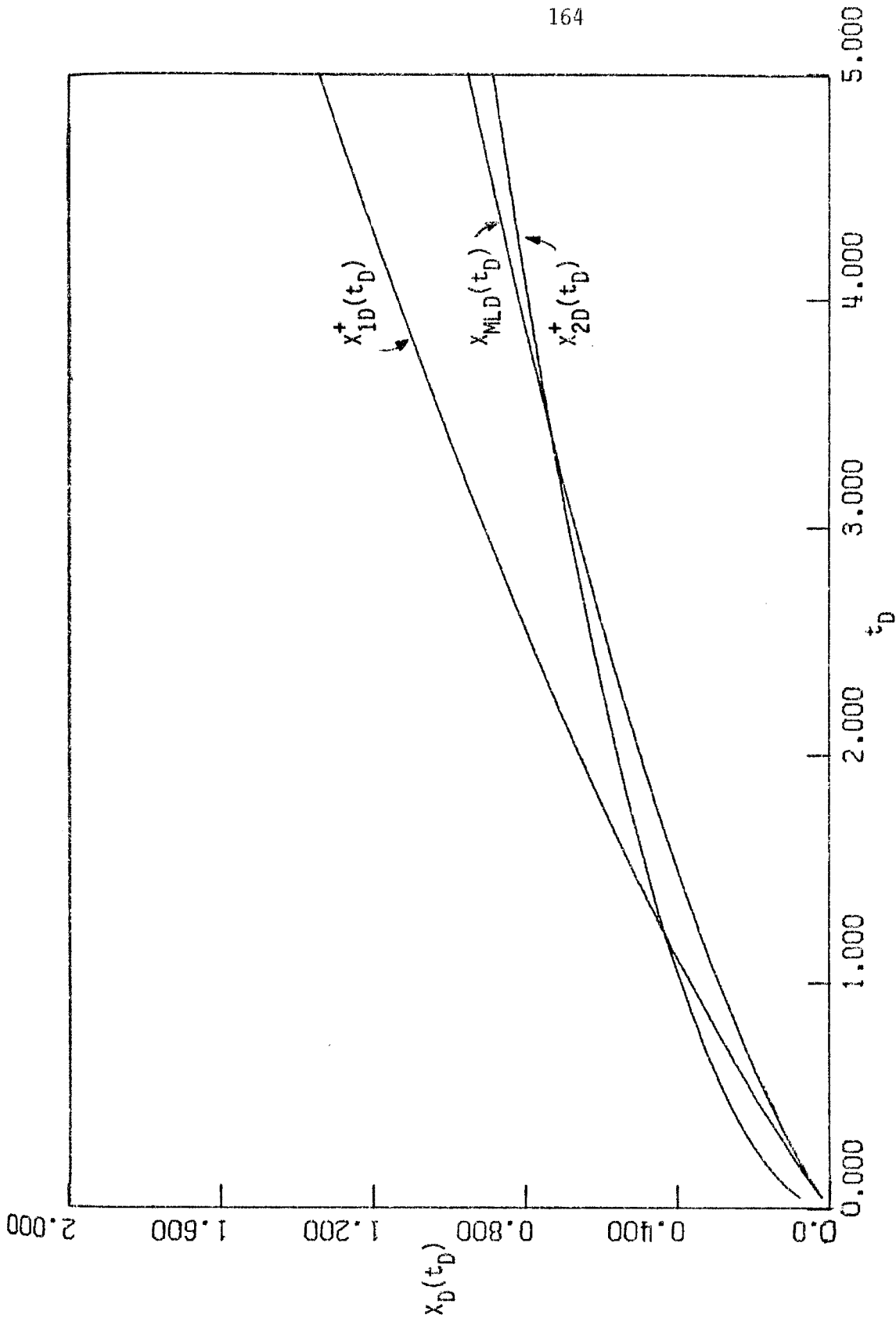


Figure 41. Upper Bounds x_{1D}^+ , x_{2D}^+ and the Marx-Langenheim Solution for Constant Injection Rates. $A = 0.4$.

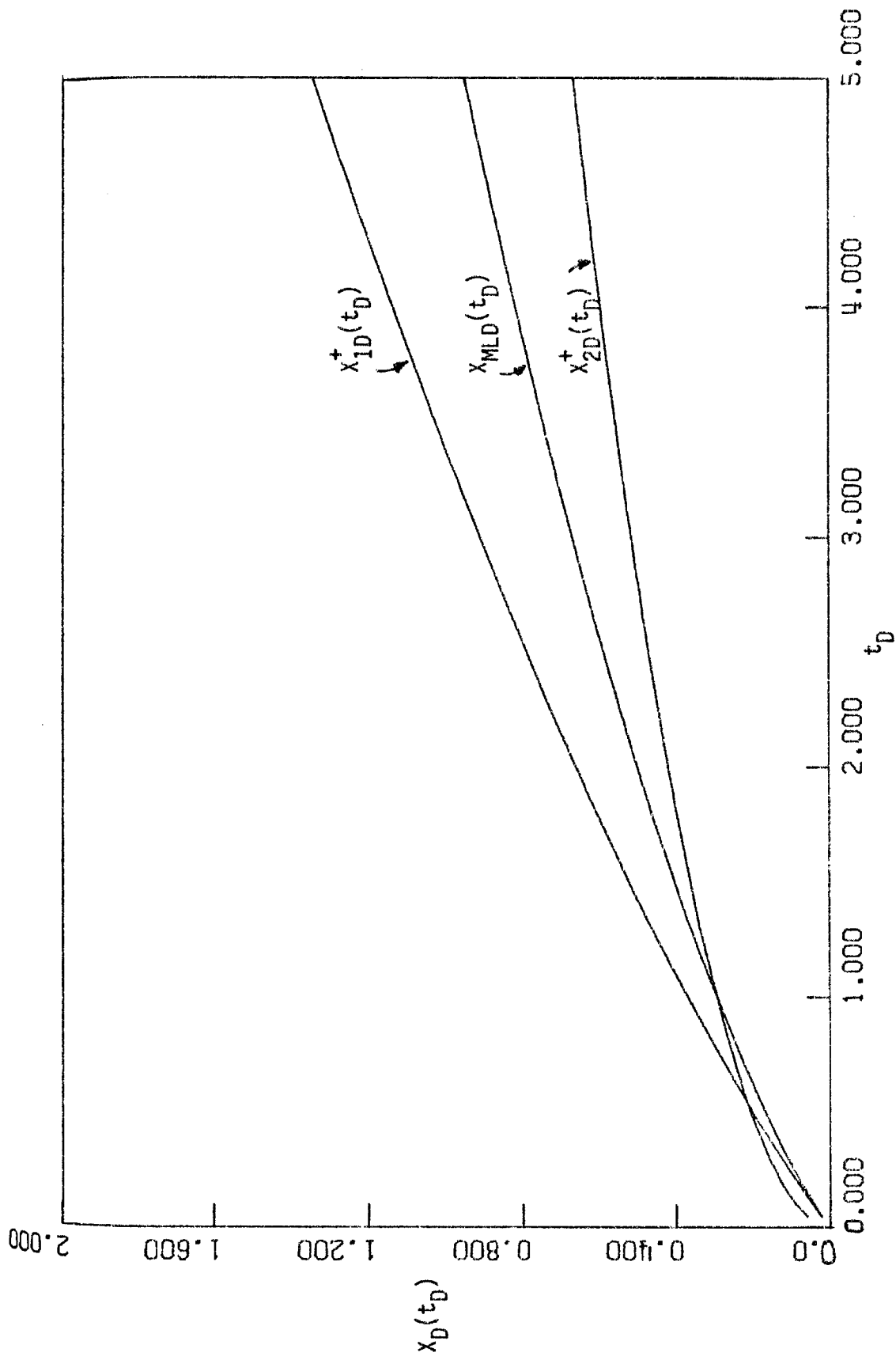


Figure 42. Upper Bounds X_{1D}^+ , X_{2D}^+ and the Marx-Langenheim Solution X_{MLD} for Constant Injection Rates. $A = 0.3$.

The time $t_{D\alpha}$, where $X_{MLD}(t_D) = X_{2D}^+(t_D)$, satisfies the algebraic equation

$$\sqrt{t_{D\alpha}} \left(1 - \frac{\pi A}{2} \right) = 1 - \exp \left(\frac{\pi t_{D\alpha}}{4} \right) \operatorname{erfc} \left(\frac{\sqrt{\pi}}{2} \sqrt{t_{D\alpha}} \right) \quad (4.41)$$

and it is an increasing function of A as shown in Table 8.

We, thus, conclude that, if $A < \frac{2}{\pi}$, the Marx-Langenheim solution will eventually intersect the lowest upper bound X_{2D}^+ and will start to deviate increasingly from the actual solution. This discrepancy is much more pronounced for small A , i.e., for low injection downhole quality and high injection temperature. In such cases, use of X_{MLD} for the description of the process will inevitably lead to over-optimistic results regarding the progress of the steam zone, with an error that may reach 30% at large times ($A = 0.3$, Figure 42). In fact, for the extreme situation of hot water injection, ($A = 0$), the Marx-Langenheim solution will erroneously predict a steam front propagation, even though no steam is injected.

Due to wellbore heat losses, low injection steam qualities at the downhole site are not uncommon. Table 9 presents the operational variables of various field projects, as reported by Myhill and Stegemeier (1978). Based on this table, we can locate their operational points on a T_s vs. f_{st} diagram (Figure 43), assuming one-dimensional (linear or radially symmetric) propagation. Concerning this diagram one should note that due to the different initial temperatures of the various formations, the temperature of each point in the diagram has to be slightly readjusted to conform with the formation temperature of 30°C used as a basis for the construction of Figure 43.

<u>Field</u>	<u>Reservoir Properties</u>			<u>Steam Properties</u>		
	<u>T_i</u>	<u>h</u>	<u>w_s</u>	<u>Quality</u>		<u>Temp.</u>
	<u>°C</u>	<u>m</u>	<u>kg/s</u>	<u>inj.</u>	<u>down-hole</u> <u>(psig)</u>	<u>°C</u>
Brea ("B" Sand)	79.4	57.45	0.880	0.75	0.54	335.4
Coalinga (Section 27, Zone 1)	35.5	10.66	0.880	0.70	0.55	229.2
El Dorado (NW Pattern)	21.1	5.18	0.352	0.75	0.45	241.6
Inglewood	37.7	13.10	1.936	0.75	0.70	229.2
Kern River	32.2	16.76	0.633	0.70	0.50	164.0
Schoonebeek	37.7	25.29	2.200	0.85	0.70	252.3
Slocum (Phase 1)	23.8	12.19	1.760	0.80	0.70	194.3
Smackover	43.3	7.62	4.425	1.00	0.80	227.8
Tatums (Hefner Steam Drive)	21.1	11.26	1.205	0.70	0.60	303.0
Tia Juana	45.0	60.96	2.464	1.00	0.80	213.8
Yorba Linda ("F" Sand)	43.3	9.75	1.496	0.80	0.70	194.33

Reservoir and Operational Data for Steam Injection in
Actual Field Cases [Myhill and Stegemeier (1978)].

Table 9

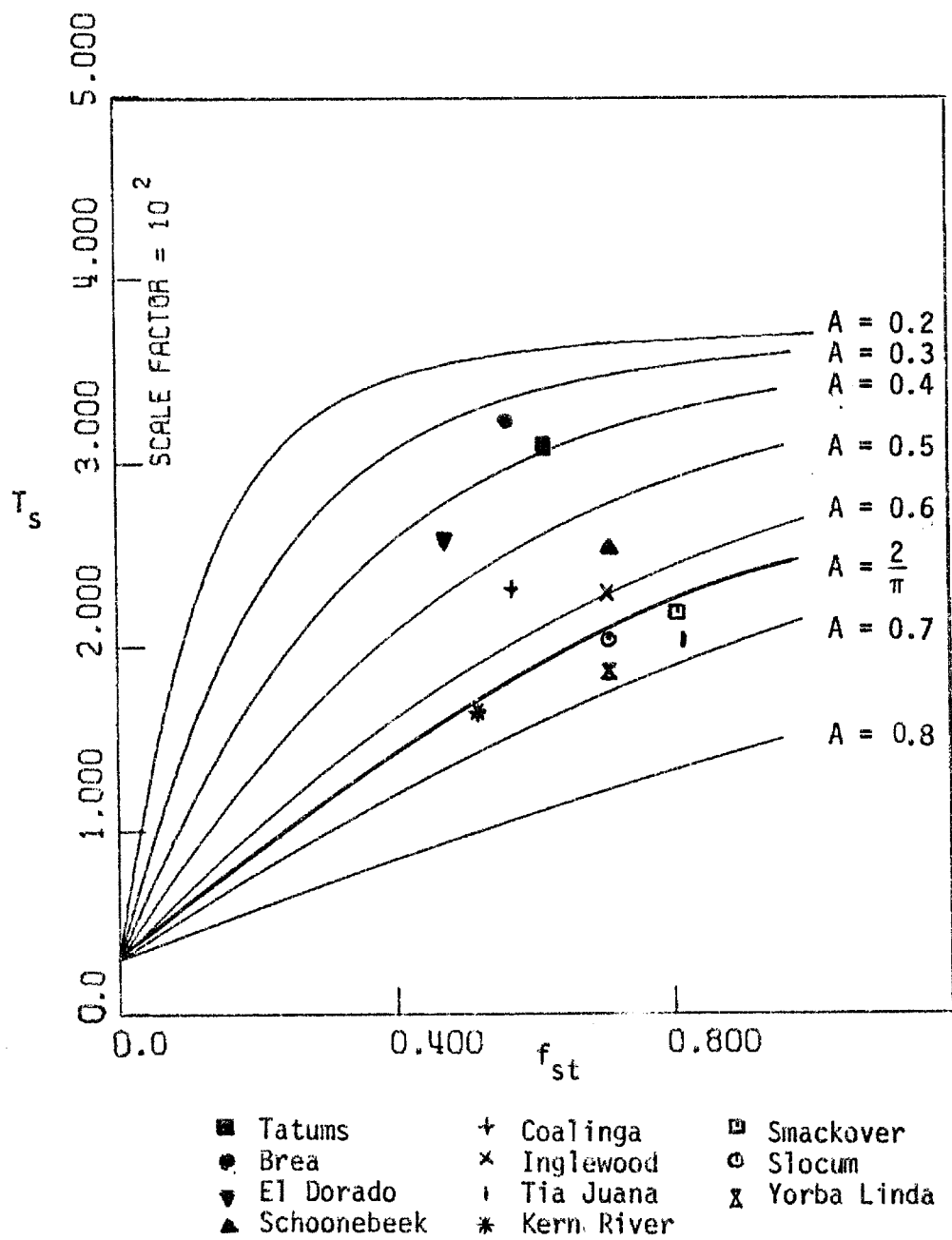


Figure 43. Operational Points of the Field Cases in Table 9.

From the Figure 43 it is clear that, although several operational points lie below or close to the critical curve $A = \frac{2}{\pi}$, another significant number of reservoirs operate at conditions prohibiting the use of the approximate Marx-Langenheim solution after a certain time has elapsed. Instead, one should rely on the rigorous upper bound x_{2D}^+ for a better estimation of the steam zone growth.

We complete this section by discussing a little more explicitly, in light of the previous analysis for constant injection rates, the Mandl and Volek (1969) approach. As outlined in 4.2.2, the approach regards the Marx-Langenheim solution as an exact solution, up until a critical time when the net convective heat flux, w_{MLD} , turns positive. According to (4.28), this occurs when

$$\frac{dx_{MLD}}{dt_D}(t_{D1}) = \frac{\phi_{1D}(t_{D1}) - \phi_{2D}(t_{D1})}{2} \quad (4.42)$$

or, after rearranging and using (4.31), when

$$1 - A = \exp\left[\frac{\pi t_{D1}}{4}\right] \operatorname{erfc}\left[\frac{\sqrt{\pi}}{2} \sqrt{t_{D1}}\right] \quad (4.43)$$

Table 8 shows that $t_{D1} < t_{D\alpha}$ for every A . Mandl and Volek subsequently claim that x_{MLD} is an upper bound to the actual solution thereafter. In light of the previous discussion, this is true whenever $A < \frac{2}{\pi}$, in which case, however, $x_{2D}^+(t_D)$ provides a better upper bound. On the other hand, the claim that x_{MLD} is an upper bound cannot be justified, if $A > \frac{2}{\pi}$.

4.4 Lower Bounds

To derive lower bounds on the steam zone rate of growth, we must provide upper bounds on the heat fluxes to the surroundings and the hot liquid zone. For the heat losses to the over- and under-burden, we use inequalities (3.18a) and (3.18b). However, in contrast to (3.19b) and (3.20b), which bound the heat fluxes to the hot liquid zone from below, upper bounds for these quantities are not readily available from direct physical arguments. In principle, such upper bounds can be developed by further studying the heat transfer mechanism inside the hot liquid zone for an arbitrary front velocity (Chapter III). It is very likely, however, that the bounds derived in this way will be coupled to the history of the front velocity, just like the bounds on the heat losses, (3.18a). This coupling would be a serious obstacle in finally deriving explicit lower bounds for the volume of the steam zone. This topic requires further study.

On the other hand, under constant injection rates, we can readily develop the asymptotic behavior of a lower bound to the steam zone volume.

4.4.1 Asymptotic Behavior of a Lower Bound at Constant Injection Rates

We consider the steam mass balance, Eq. (4.2). Using inequality (3.18b) it is easy to show that

$$\begin{aligned}
 (L_{L2} + L_{N2}) \{X_F(t)\} < \frac{d}{dt} \int_0^{X_F(t)} f_2(x, t; X_F(t)) dx \\
 + d \int_0^{X_F(t)} \frac{dx}{\sqrt{t - \lambda(x)}} + \Pi_F(t) \Delta T Q_F(t)
 \end{aligned} \tag{4.44}$$

therefore,

$$\begin{aligned} \phi_2(t) < \frac{d}{dt} \int_0^{X_F(t)} f_2(x, t; X_F(t)) dx + d \int_0^{X_F(t)} \frac{dx}{\sqrt{t - \lambda(x)}} \\ + \Pi_F(t) \Delta T Q_F(t) \end{aligned} \quad (4.45)$$

In Subsection 4.3.3 we established that $X_{FD}(t)$ grows, asymptotically, no stronger than $\sim A\sqrt{t_D}$. In Sections 3.7, 3.8, we concluded that, for any R , the conductive heat flux through the origin tends to zero, as $t \rightarrow \infty$, when the front velocity behaves asymptotically as $\frac{c}{\sqrt{t}}$ where c is a constant.

One can, thus, deduce that $Q_F(t) \rightarrow 0$ as $t \rightarrow \infty$, and accordingly inequality (4.45) reads:

$$\phi_2(t) < \frac{d}{dt} \int_0^{X_F(t)} f_2(x, t; X_F(t)) dx + d \int_0^{X_F(t)} \frac{dx}{\sqrt{t - \lambda(x)}} \quad (4.46)$$

as $t \rightarrow \infty$.

Let us now define $X_2^-(t)$ such that

$$\frac{d}{dt} \int_0^{X_2^-(t)} f_2(x, t; X_F(t)) dx + d \int_0^{X_2^-(t)} \frac{dx}{\sqrt{t - \lambda(x)}} = \phi_2(t) \quad \forall 0 < t \quad (4.47)$$

$$X_2^-(0) = 0$$

One can then prove (Appendix VII), that $X_2^-(t)$ is a lower bound on $X_F(t)$, in the limit as $t \rightarrow \infty$.

In solving (4.47) we invoke the assumption (4.16) and rewrite (4.47)

in the dimensionless notation of Section 4.3.1

$$2 \frac{B_1}{B_2} \dot{x}_{2D}^-(t_D) + \int_0^{t_D} \frac{\dot{x}_{2D}^-(\tau_D) d\tau_D}{\sqrt{t_D - \tau_D}} = A \quad (4.48)$$

with solution

$$x_{2D}^-(t_D) = \frac{2}{\pi} A \left\{ \sqrt{t_D} - B + \exp \left[\frac{\pi t_D}{4B^2} \right] \operatorname{erfc} \left[\frac{\sqrt{\pi} \sqrt{t_D}}{2B} \right] \right\} \quad (4.49)$$

which, in view of (4.34), becomes for $t_D > 0.002$

$$x_{2D}^-(t_D) \approx \frac{2}{\pi} A \sqrt{t_D} \quad (4.50)$$

This behavior is consistent with the upper bound $x_{2D}^+(t_D)$, Eq. (4.37b).

The actual steam zone volume would then be located, in the limit of large t_D , between $x_{2D}^+(t_D)$, $x_{2D}^-(t_D)$:

$$x_{FD} \sim \eta A \sqrt{t_D} \quad \frac{2}{\pi} < \eta < 1 \quad (4.51)$$

$$t_D \rightarrow \infty.$$

Obviously, the region of validity of the asymptotic expression (4.51) largely depends on how fast the conductive heat flux, $Q_F(t)$, converges to zero, which in turn implicitly depends on η . The problem of determining η brings about a new topic, which involves studying the limiting behavior of the exact solution in both large and small times.

4.5 Asymptotic Solutions

4.5.1 Introductory Remarks

Just as in the derivation of bounds, we again make use of the one-dimensional integral balance formulation (Section 4.2). In developing approximate solutions, however, we need, in addition, a detailed description of the heat transfer inside the hot liquid zone, such as the one outlined in Chapter III. The important dimensionless groups related to one-dimensional heat transfer are

$$R = \frac{w_F^{02} h^2}{4k_{hf}^2} \cdot \frac{\alpha_f}{\alpha_R}, \quad Pe = \frac{q}{k_{hf}} \quad (4.52)$$

in linear and cylindrical geometries, respectively. From Table 6 and the water mass balance (4.3), we can estimate the magnitudes of R , Pe for a typical steam drive.

To evaluate R , we first note that

$$w_F^0 = u_{wx} \rho_w c_{pw} + u_{ox} \rho_o c_{po} \quad (4.53a)$$

and due to (3.23b)

$$w_F^0 = w_F + M^{(2)} \dot{\chi}_F(t) \quad (4.53b)$$

For a linear steam drive, the water mass balance, Eq. (4.3), together with the assumption (4.16) leads to:

$$\Delta T w_F^0 = \phi_1(t) - \phi_2(t) - \Delta T (M_3 - M^{(2)}) \dot{\chi}_F(t) \quad (4.53c)$$

$$\text{Now } M_3 = \phi \bar{S}_s \rho_s c_{pw} + \phi \bar{S}_w \rho_w c_{pw} + \phi \bar{S}_o \rho_o c_{po} + (1 - \phi) \rho_R c_{pR}$$

$$M^{(2)} = \phi \bar{S}_w^{(2)} \rho_w c_{pw} + \phi \bar{S}_o^{(2)} \rho_o c_{po} + (1 - \phi) \rho_R c_{pR}$$

and, within the approximations made, $M_3 \approx M^{(2)}$. Therefore, from (4.53c),

$$\Delta T W_F^0 \approx \Phi_1(t) - \Phi_2(t) \quad (4.54)$$

Substituting in (4.52) and reading the values of the parameters from Table 6, we get $R = 640$ for a typical linear steam drive.

A higher order of magnitude estimate is obtained for $Pe = \frac{q}{k_{hf}}$ in cylindrical geometries. By definition

$$q = 2\pi R_F(t)(u_{wr}\rho_w c_{pw} + u_{or}\rho_o c_{po}) \quad (4.55a)$$

and rearranging the water mass balance, Eq. (4.3),

$$\Delta T q = \Phi_1(t) - \Phi_2(t) - \Delta T(M_3 - M^{(2)})\dot{\chi}_F(t) \quad (4.55b)$$

which leads to

$$\Delta T q \approx \Phi_1(t) - \Phi_2(t) \quad (4.56)$$

as before. Substituting back in and using the cylindrical reference field case of Table 6 we find $Pe = 10,320$, for a typical cylindrical steam drive.

One can accordingly conclude that the heat transfer in the hot liquid zone of a one-dimensional steam drive is convection dominated. This, firstly, verifies the assumption of negligible horizontal conduction, introduced in Section 3.2 for the calculation of the heat losses in the surrounding formations. In addition, it provides sound evidence that one may use the results of Section 3.7, ($R \rightarrow \infty$), with confidence in steam injection calculations for both linear and cylindrical geometries.

Before we proceed any further we recall that the dimensionless notations in Sections 3.7 and 4.3 are different. To convert to a uniform notation, we consider the ratios of the characteristic variables in the two cases:

$$\frac{x_{III}^*}{x_{IV}^*} = \frac{2(1-A)}{\pi} \cdot \frac{M^{(2)}}{M_1} \quad (4.57a)$$

$$\frac{t_{III}^*}{t_{IV}^*} = \frac{4}{\pi} \left(\frac{M^{(2)}}{M_1} \right)^2 \quad (4.57b)$$

and, therefore, the two dimensionless velocities are related to each other by

$$v_D(t_D) = \frac{2}{(1-A)} \left(\frac{M^{(2)}}{M_1} \right) \dot{x}_{FD}(t_D) \quad (4.58)$$

We choose first to discuss the asymptotic forms of the exact solution for large times, under sustained injection at constant rates.

4.5.2 Large Times Behavior at Constant Injection Rates

In Section 4.4 we concluded that, in the limit of large t_D , the actual solution x_{FD} increases monotonically in the manner indicated by Eq. (4.51). Consequently,

$$\dot{x}_{FD} \sim \frac{a}{\sqrt{t_D}} \quad \frac{A}{\pi} < a < \frac{A}{2} \quad (4.59)$$

where a has to be determined. Due to the different formalism in linear and cylindrical geometries, we examine the two cases separately.

4.5.2.1 Linear Geometries

The heat transfer problem associated with such a front velocity has been studied in Chapter III for both $R \rightarrow \infty$ (Subsection 3.7.5) and $R = 1$ (Subsection 3.8.4.3). It was shown that, for large t_D , we obtain identical results in both cases, which further implies that this is true for any R in the region $(1, \infty)$ and, therefore, for our $R = 640$, as well. We can, thus, use the solution of either problem in evaluating the asymptotic behavior of the steam zone volume. Because of the large R , we choose to follow the case $R \rightarrow \infty$. (In Appendix VIII we also present the derivation for $R = 1$, which leads to identical results.)

Consider the steam mass balance, Eq. (4.2). In the dimensionless notation of Section 4.3, the linear geometry version of (4.2) reads:

$$2B\dot{X}_{FD}(t_D) - \frac{2(1-A)^2}{\pi R} \left(\frac{M^{(2)}}{M_1} \right) \frac{\partial T_D}{\partial x_D} + \int_0^{t_D} \left(-\frac{\partial T_f}{\partial n} \right)_D \dot{X}_{FD}(\lambda_D) d\lambda_D = A \quad (4.60)$$

where $R = 640 \gg 1$. Assuming that the front behaves as portrayed in (4.59), the temperature of the hot liquid zone is, according to (3.72), (4.57a,b), (4.58):

$$T_D(t_D, x_D) = \operatorname{erfc} \left\{ \frac{\sqrt{\pi}}{2(1-A)} \cdot \frac{x_D}{\sqrt{t_D - \frac{2}{(1-A)} \left(\frac{M^{(2)}}{M_1} \right) x_D}} \right\} \cdot \frac{H \left(t_D - \frac{2}{(1-A)} \left(\frac{M^{(2)}}{M_1} \right) x_D \right)}{\operatorname{erfc} b} \quad (4.61)$$

where $b = \sqrt{\pi}a/(1-A)$. Similarly, the conductive heat flux at the origin, Eq. (3.73), gives

$$\left. \frac{\partial T_D}{\partial x_D} \right|_{x_D=2a\sqrt{t_D}} \sim - \frac{1}{(1-A)\sqrt{t_D}} \exp(-b^2)/\operatorname{erfc}b \quad (4.62)$$

in the dimensionless notation of Chapter IV.

To evaluate the heat losses term in Eq. (4.60) we make use of Eq.

(3.13):

$$\left(- \frac{\partial T_f}{\partial n} \right)_D = \int_0^{\lambda_D} \frac{\partial T_D}{\partial \tau_D} \cdot \frac{d\tau_D}{\sqrt{t_D - \tau_D}} = I_1(t_D, \lambda_D) \quad (4.63)$$

The last integral $I_1(t_D, \lambda_D)$ is calculated in Appendix IX:

$$\begin{aligned} I_1(t_D, \lambda_D) = & \frac{1}{\sqrt{t_D - \frac{2}{(1-A)} \left(\frac{M^{(2)}}{M_1} \right) x_D}} \cdot \exp \left\{ - \frac{\pi}{4(1-A)^2} \cdot \right. \\ & \cdot \left. \frac{x_D^2}{\left(t_D - \frac{2}{(1-A)} \left(\frac{M^{(2)}}{M_1} \right) x_D \right)} \right\} \cdot \\ & \cdot \operatorname{erfc} \left\{ \frac{\sqrt{\pi} x_D}{2(1-A)} \cdot \right. \\ & \cdot \left. \frac{(t_D - \lambda_D)^{\frac{1}{2}}}{\left[t_D - \frac{2}{(1-A)} \left(\frac{M^{(2)}}{M_1} \right) x_D \right]^{\frac{1}{2}} \left[\lambda_D - \frac{2}{(1-A)} \left(\frac{M^{(2)}}{M_1} \right) x_D \right]^{\frac{1}{2}}} \right\} \end{aligned} \quad (4.64)$$

We now substitute (4.64), (4.63), (4.62) in (4.60) and get the integral equation:

$$2B\dot{\chi}_{FD}(t_D) + \frac{2(1-A)}{\pi R} \left(\frac{M^{(2)}}{M_1} \right) \frac{\exp(-b^2)}{\text{erfc}b} \frac{1}{\sqrt{t_D}} + \int_0^{t_D} \dot{\chi}_{FD}(\lambda_D) I_1(t_D, \lambda_D) d\lambda_D \sim A \quad (4.65)$$

the solution of which determines the asymptotic behavior of the exact solution.

Since we have already assumed $\dot{\chi}_{FD}(t_D) = \frac{a}{\sqrt{t_D + a^2}}$, (4.65) becomes

$$2B \frac{a}{\sqrt{t_D}} + \frac{2(1-A)}{\pi R} \left(\frac{M^{(2)}}{M_1} \right) \frac{\exp(-b^2)}{\text{erfc}b} \frac{1}{\sqrt{t_D}} + a \int_0^{t_D} \frac{I_1(t_D, \lambda_D) d\lambda_D}{\sqrt{\lambda_D + a^2}} \sim A \quad (4.66)$$

An asymptotic analysis of the integral

$$I_2(t_D) = \int_0^{t_D} \frac{I_1(t_D, \lambda_D) d\lambda_D}{\sqrt{\lambda_D + a^2}} \quad (4.67)$$

indicates that (Appendix IX)

$$I_2(t_D) \sim \frac{\sqrt{\pi} a \exp(-b^2)}{b \text{erfc}b} [1 - \exp(b^2) \text{erfc}b] \quad 10b^2 < t_D \quad (4.68)$$

Substituting in (4.66) and collecting terms of the same order we find that a satisfies the algebraic equation

$$a = \frac{bA}{\sqrt{\pi}} \left[\frac{\exp(b^2) \cdot \text{erfc}b}{1 - \exp(b^2) \cdot \text{erfc}b} \right] \quad (4.69)$$

Finally, substituting for b , we find the unknown parameter a as the solution of the algebraic equation:

<u>A</u>	<u>a</u>	<u>b</u>	<u>$t_D = 10b^2$</u>
0.90	0.3135	5.5566	308.76
0.86	0.3059	3.8728	149.98
0.80	0.2993	2.6524	70.35
0.76	0.2915	2.1527	46.34
0.70	0.2777	1.6407	26.91
0.66	0.2672	1.3929	19.40
0.60	0.2498	1.1068	12.25
0.56	0.2372	0.9555	9.13
0.50	0.2169	0.7688	5.91
0.46	0.2025	0.6646	4.41
0.40	0.1798	0.5311	2.82
0.36	0.1639	0.4539	2.06
0.30	0.1391	0.3522	1.24
0.26	0.1219	0.2919	0.85
0.20	0.0953	0.2111	0.44
0.16	0.0770	0.1624	0.26
0.10	0.0488	0.0961	0.09

Values of the parameters a , b , $t_D = 10b^2$
for various values of A .

Table 10

$$\exp \left\{ \frac{\pi a^2}{(1-A)} \right\} \operatorname{erfc} \left\{ \frac{\sqrt{\pi} a}{(1-A)} \right\} = 1 - A \quad (4.70)$$

An identical equation is derived in Appendix VIII for $R = 1$.

The solution of (4.70) is plotted vs. A in Figure 44. Plotted also are the respective proportionality constants of the upper and lower bounds, $\frac{A}{2}$ and $\frac{A}{\pi}$, respectively. We verify that, as anticipated, $\frac{A}{\pi} < a < \frac{A}{2}$. (See also Figure 49.) From (4.66), (4.68) follows that the large times behavior of the exact solution is solely determined by a balance between the cumulative heat losses and the injection rates. When A is small, the actual steam zone volume is close to the upper bound expression, $x_{2D}^+(t_D)$, whereas for A near 1, it approaches the lower bound, $x_{2D}^-(t_D)$. (See also Figure 49.)

Due to $R \gg 1$, $B \ll 1$, the convergence of the front velocity to the form (4.59) is solely dependent on the asymptotic properties of $I_2(t_D)$. Choosing the time $10b^2$ as a characteristic time for convergence, we see that conversion is faster when A is smaller, for b is an increasing function of A . For $A = 0.33$, for example, $b = 0.419$ and the front assumes its asymptotic behavior when $t_D > 1.76$. On the other hand, for $A = 0.66$, $b = 1.39$ and the asymptotic form is never reached, within practical limits, (Table 10). The magnitude of R plays a significant role in determining how fast the solution approaches its asymptotic form. The larger R the faster the convergence (See Appendix VIII).

4.5.2.2 Cylindrical Geometries

The above results carry over unchanged to the case of cylindrical geometry. There the relevant dimensionless parameter is the Peclet number.

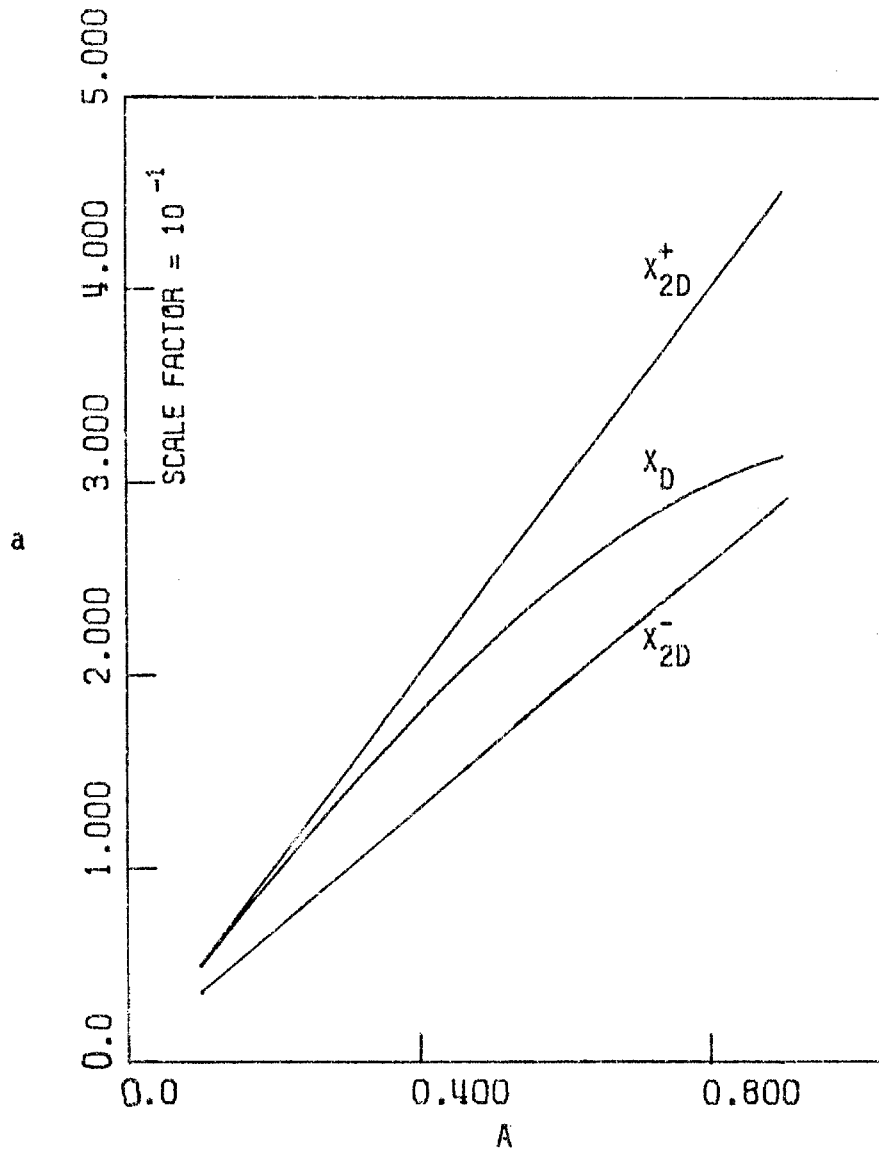


Figure 44. The Asymptotic Coefficient a of the Upper Bound X_{2D}^+ , the Lower Bound X_{2D}^- and the Exact Solution X_D , Plotted vs. A .

Since $Pe \gg 1$, the associated heat transfer problem, Eq. (3.74b), reduces to its limiting case ($Pe \rightarrow \infty$), the solution of which has been studied in Subsection 3.7.2. Accordingly, the heat transfer considerations are the same as the ones discussed in the previous section. The only difference is in the steam mass balance, Eq. (4.2), the cylindrical version of which becomes:

$$2B\dot{X}_{FD}(t_D) - \frac{4\pi(1-A)X_{FD}(t_D)}{Pe} \cdot \frac{\partial T_D}{\partial x_D} + \int_0^{t_D} \left(-\frac{\partial T_f}{\partial n} \right)_D \dot{X}_{FD}(\lambda_D) d\lambda_D = A \quad (4.71)$$

where $Pe = 10,320 \gg 1$. (Notice the difference in the second term.)

Because of the assumed behavior of X_{FD} , Eq. (4.59), and the resulting conductive heat flux, Eq. (4.62), the second term on the LHS approaches a constant value, as t_D becomes large. Due to the large Pe , however, its contribution to an equation like (4.66) is negligible and, as a result, there is no change in the value of a , as defined by Eq. (4.70). One can thus conclude that the previous results on asymptotic solutions for linear geometry carry over to the cylindrical geometries by a simple substitution of R by Pe .

4.5.3 Small Times Behavior at Constant Injection Rates

When $R, Pe \gg 1$, the constraint (3.53) is in effect. Because of this constraint and the relative high initial front velocity, the heat wave cannot significantly penetrate in the hot liquid zone, for some time after injection starts. Thus, the total heat flux in Eq. (4.1) is very small and the temperature of the hot liquid zone assumes a distribution similar

to Marx-Langenheim's, Eq. (3.14)

In the dimensionless notation of Section 4.3, we then have

$$2\dot{x}_{FD}(t_D) + \int_0^{t_D} \frac{\dot{x}_{FD}(\tau_D) d\tau_D}{\sqrt{t_D - \tau_D}} = \phi_{1D}, \quad 0 < t_D < t_{D0} \quad (4.72)$$

$$x_{FD}(0) = 0$$

which is the Marx-Langenheim equation and has the solution

$$x_{FD}(t_D) = \frac{2}{\pi} \left\{ \sqrt{t_D} - 1 + \exp\left(\frac{\pi t_D}{4}\right) \operatorname{erfc}\left(\frac{\sqrt{\pi t_D}}{2}\right) \right\}, \quad 0 < t_D < t_{D0} \quad (4.73)$$

At t_{D0} , the front velocity has been reduced to the critical value $v_D(t_{D0}) = 1$, beyond which heat starts propagating inside the hot liquid zone. By (4.58)

$$\dot{x}_{FD}(t_{D0}) = \left(\frac{1-A}{2} \right) \left(\frac{M_1}{M^{(2)}} \right) \quad (4.74)$$

and substituting in (4.73), one finds that t_{D0} satisfies the algebraic equation:

$$(1-A) \left(\frac{M_1}{M^{(2)}} \right) = \exp\left[\frac{\pi t_{D0}}{4}\right] \operatorname{erfc}\left[\frac{\sqrt{\pi}}{2} \sqrt{t_{D0}}\right] \quad (4.75)$$

Finally, in view of $M_1 \approx M^{(2)}$, t_{D0} turns out to be the same time constant, t_{D1} , derived by Mandl-Volek (1969) and tabulated in Table 8. We, thus, reach the conclusion that for injection rates such that $R, Pe \gg 1$, the results of Mandl-Volek regarding the small times behaviors of the steam

front are correct. For some initial time period, the actual solution follows closely the Marx-Langenheim expression.

Consulting Tables 3,4, we can develop a criterion on R , and consequently the injection rates, that outlines the conditions under which the above behavior is exhibited. The reasonable estimate

$$R > 100$$

sets safe lower bounds on both R and the injection rates for this to occur. As already noticed, in a typical steam drive R is quite large and the above description of the process is sufficiently accurate for small times. When low injection rates are used, however, $R = O(1)$ and there is significant penetration of heat in the hot liquid zone, as soon as injection begins. The resulting preheating of the rock cannot be neglected anymore and the more reliable upper bounds must be used to describe the growth of the steam zone.

4.5.3.1 Modified Upper Bounds. $R, Pe \gg 1$.

When the operating conditions justify the initial behavior described by Eq. (4.73), the upper bounds derived in Section 4.3 can be slightly modified. It can be easily shown that the two functions X_{jMD}^+ ($j = 1, 2$), defined by the ODE's (4.19), (4.20), but with different initial conditions

$$2 \frac{B_j}{B_1} \dot{X}_{jMD}^+(t_D) + \frac{X_{jMD}^+(t_D)}{\sqrt{t_D}} = 1 \quad \forall \quad t_{D0} < t_D \quad (4.76)$$

$$X_{jMD}^+(t_{D0}) = X_{MLD}(t_{D0})$$

are upper bounds to $X_{FD}(t_D)$, $\forall \quad t_{D0} < t_D$.

Solving (4.76) in conjunction with (4.74), (4.75) one finds

$$x_{1MD}^+(t_D) = \sqrt{t_D} - 1 + \left\{ \frac{2}{\pi} \sqrt{t_D} - \frac{2}{\pi} A - \sqrt{t_{D0}} + 1 \right\} \exp \left[-\sqrt{t_D} + \sqrt{t_{D0}} \right] \quad (4.77)$$

$$x_{2MD}^+(t_D) = A \left\{ \sqrt{t_D} - B \right\} + \left\{ \frac{2}{\pi} \sqrt{t_D} - \frac{2A}{\pi} - A\sqrt{t_{D0}} + AB \right\} \exp \left[\frac{-\sqrt{t_D} + \sqrt{t_{D0}}}{B} \right] \quad (4.78)$$

Figures 45, 46 plot $x_{1MD}^+(t_D)$, $x_{2MD}^+(t_D)$ for various values of A . As it can also be seen from (4.77), (4.78), they both approach the original bounds $x_{1D}^+(t_D)$, $x_{2D}^+(t_D)$ although at varying rates. The upper bound $x_{1MD}^+(t_D)$ rapidly crosses above the bound $x_{1D}^+(t_D)$ and approaches it asymptotically at large times. In the initial short time interval, $x_{1MD}^+(t_D)$ provides a better upper bound than $x_{1D}^+(t_D)$. On the other hand, $x_{2MD}^+(t_D)$ approaches very rapidly the upper bound $x_{2D}^+(t_D)$, due to the smallness of B . In the regions where $x_{2D}^+(t_D)$ dominates, the two bounds $x_{2MD}^+(t_D)$, $x_{2D}^+(t_D)$ practically coincide. One can, thus, conclude that there is no significant improvement in the description of the process by making use of the above derived modified bounds.

4.6 Approximate Solutions

4.6.1 The Quasi-Steady State Assumption

To complete the subject of determining the front velocity of a one-dimensional steam drive, we would like to have a representation for the solution at intermediate times. As before, to develop such a solution we will make use of the integral balances of Chapter II and the heat transfer results of Chapter III.

We start with the steam mass balance, Eq. (4.2), in its dimensionless

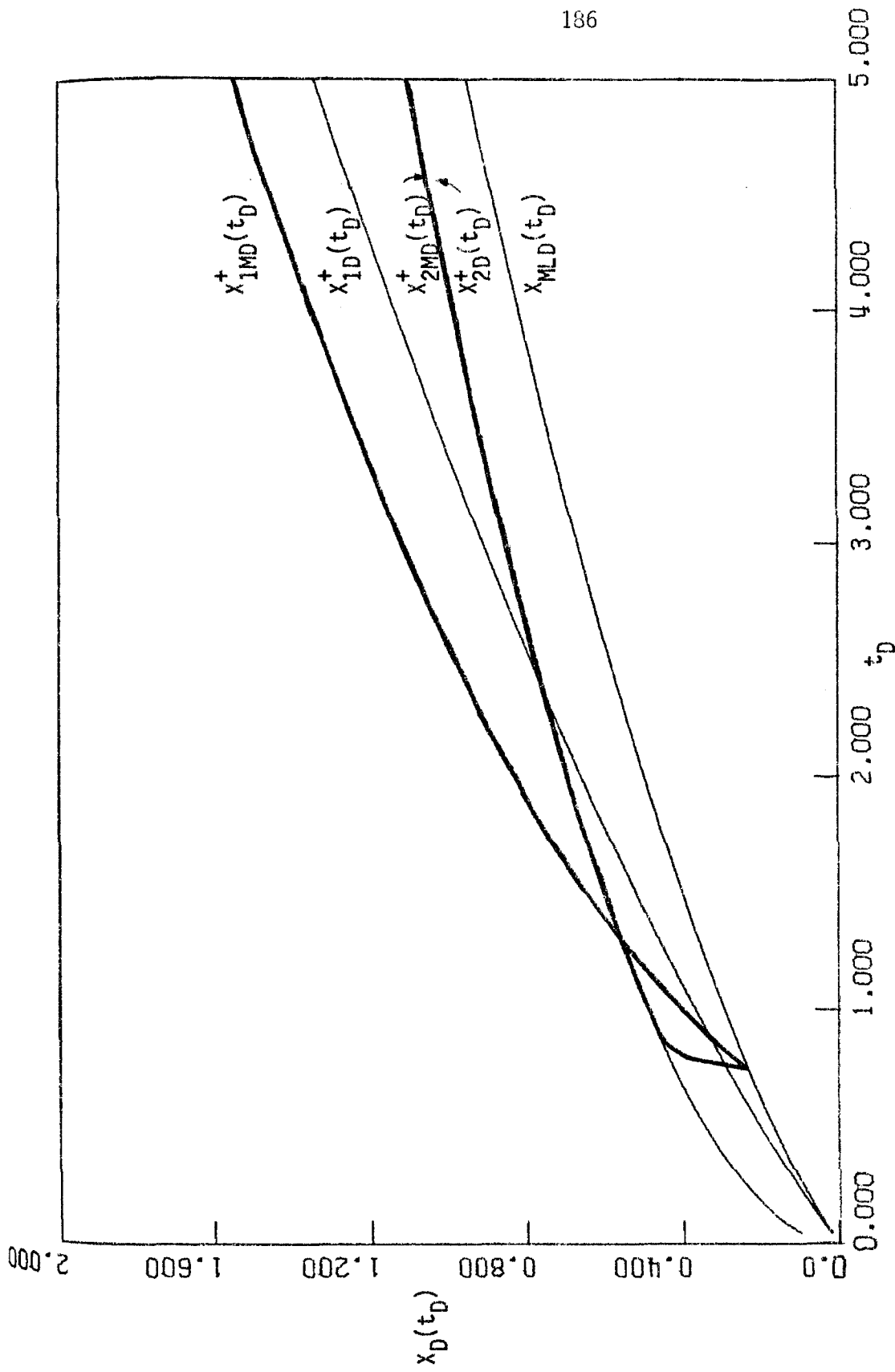


Figure 45. Modified Upper Bounds X_{1MD}^+ , X_{2MD}^+ , Upper Bounds X_{1D}^+ , X_{2D}^+ and the Marx-Langenheim Solution X_{MLD} . $A = 0.5$.

— Modified Upper Bounds.

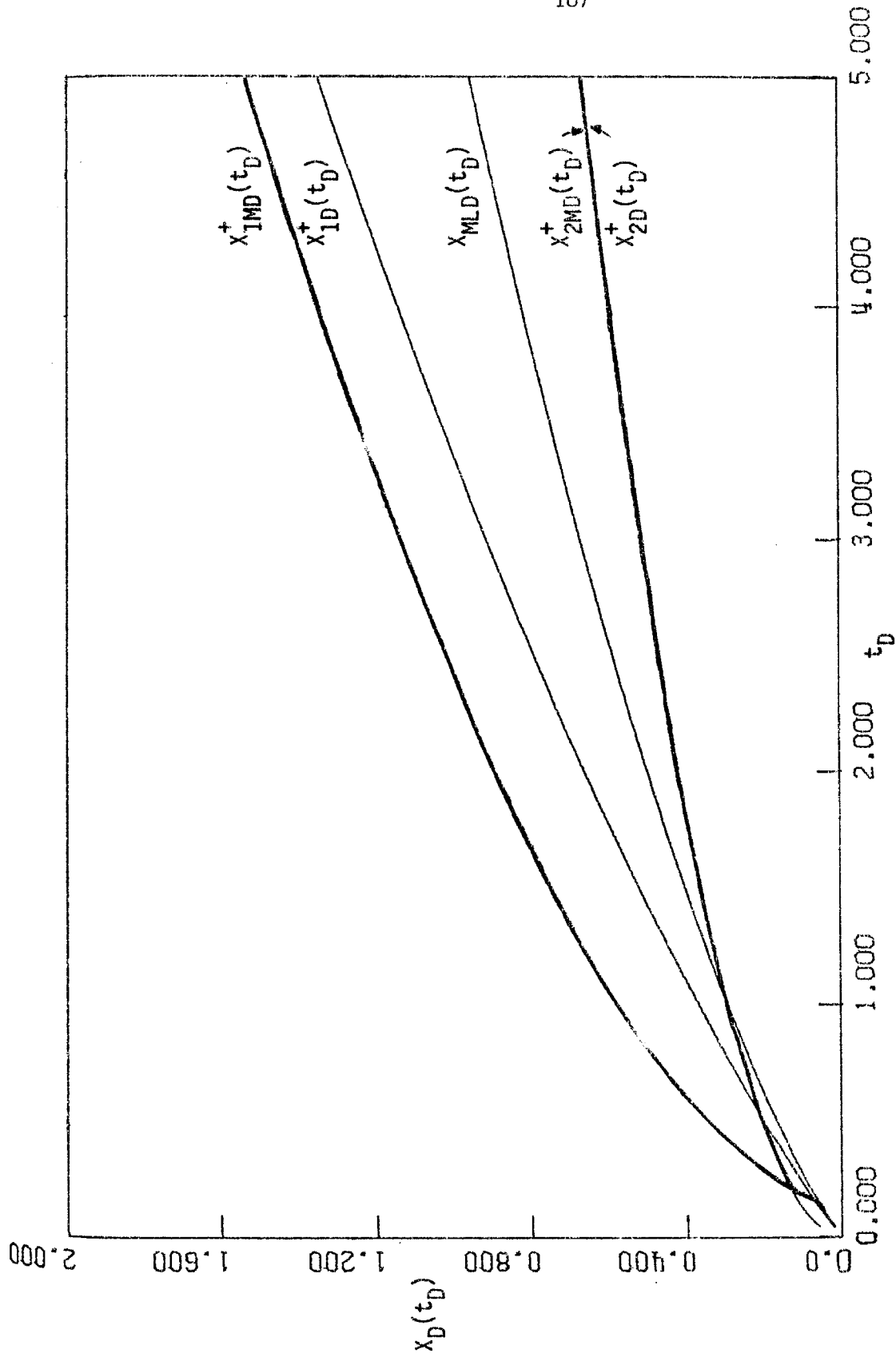


Figure 46. Modified Upper Bounds X_{1MD}^+ , X_{2MD}^+ , Upper Bounds X_{1D}^+ , X_{2D}^+ and the Marx-Langenheim Solution X_{MLD} . $A = 0.3$

— Modified Upper Bounds.

form for linear and cylindrical geometries, Eqs. (4.60) and (4.71), respectively. In dealing with the heat flux terms we encounter the problem of a suitable heat transfer model. In contrast to the limiting cases discussed in the previous sections, the solution of a heat transfer problem involving an arbitrarily moving boundary is not readily available. To resolve this difficulty we introduce a quasi-steady state approximation which postulates that the temperature distribution of the hot liquid zone quickly reaches a quasi-steady state with respect to the moving front. If this is the case, one can use the steady state expressions developed in 3.7.4 and 3.8.3 in calculating the heat fluxes. Clearly, the use of the assumption is restricted to those regions where the characteristic time of convergence to quasi-steady state values is very small compared to the characteristic time of the front motion. From Eqs. (3.69) and (3.97) one can easily deduce that this occurs at regions of relatively high velocity, where

$$\frac{4(1 - v_D(t_D))}{v_D(t_D)} \ll \frac{4}{\pi} \left(\frac{M(2)}{M_1} \right)^2 \quad (4.79)$$

[compare to (3.69), (4.57b)]. Thus, we expect the assumption to produce reasonable results at small and intermediate times under conditions of high injection rates ($R, Pe \gg 1$).

Employing the quasi-steady state approximation we obtain for the temperature of the hot liquid zone in linear geometries

$$T_D(t_D, x_D) = \exp \left\{ \frac{\pi}{2(1-A)} \left(\frac{M_1}{M(2)} \right) z_1 [x_D - x_{FD}(t_D)] \right\} \quad (4.80)$$

The corresponding heat flux is given by

$$\left. \frac{\partial T_D}{\partial x_D} \right|_{x_D = x_{FD}(t_D)} = \frac{\pi}{2(1-A)} \left(\frac{M_1}{M(2)} \right) z_1 \quad (4.81)$$

where z_1 is the negative root of Eq. (3.86) and depends on \dot{x}_{FD} , R among others. To evaluate the heat losses term in Eq. (4.60) one makes use of Eq. (3.13), as before:

$$\left(- \frac{\partial T_f}{\partial n} \right)_D = \int_0^{\lambda_D} \frac{\partial T_D}{\partial \tau_D} \frac{d\tau_D}{\sqrt{t_D - \tau_D}} \quad (4.82)$$

We can now substitute (4.81), (4.82) in the steam mass balance, Eq. (4.60), and derive the integral equation:

$$2B\dot{x}_{FD}(t_D) - \frac{(1-A)}{R} z_1(\dot{x}_{FD}; R) + \int_0^{t_D} \dot{x}_{FD}(\lambda_D) \int_0^{\lambda_D} \frac{\partial T_D}{\partial \tau_D} \frac{d\tau_D}{\sqrt{t_D - \tau_D}} d\lambda_D = A \quad (4.83)$$

the solution of which provides the front velocity and, consequently, the steam zone volume as a function of time, for linear geometry. Since for large R , the temperature distribution is almost identical in both linear and cylindrical geometries (Sections 3.7, 3.8), we expect Eq. (4.83) to be equally valid in cylindrical geometries as well, when R is large.

4.6.2 Numerical Solution at Constant Injection Rates

Due to the exhibited strong non-linearities in (4.83), an analytical solution is not possible and therefore we will follow a numerical procedure. The numerical technique used involves approximating the integrals by a simple quadrature (trapezoidal rule) and solving the resulting

algebraic equation by use of standard routines. The initial value of the front velocity, $X_{FD}(0)$, is obtained by solving the algebraic equation that results when the integral term is set equal to zero. To test the accuracy of the numerical scheme, we solved Eq. (4.83) in the special case $R = 1$ and where the heat losses were evaluated by means of the Marx-Langenheim expression. This modified version of Eq. (4.83) also admits an analytic solution which is shown to be in very good agreement with the respective numerical one, particularly at small times.

The numerical solution of Eq. (4.83) for the values $A = 0.5$ and $R = 1, 100$ and 640 , is shown in Figures 47, 48, 49, respectively. Plotted also are the two upper bounds X_{1D}^+ , X_{2D}^+ , the Marx-Langenheim solution X_{MLD} and the asymptotic expressions of the lower bound X_{2D}^- , and the exact solution X_{FD} , as evaluated in Section 4.5. The curves corresponding to $R = 100, 640$ are close to X_{MLD} , initially, and tend to X_{FD} at large times, as expected from Sections 4.5 and 4.6. Notice that the convergence of the exact solution to its asymptotic form is obtained at times larger than 5.91 (see Table 10 for $A = 0.5$) which explains the not so good agreement of the numerical with the asymptotic results. On the other hand, the solution for $R = 1$ is quite smaller than X_{MLD} and approaches the asymptotic expansion very slowly. Again this behavior is justified due to the slow convergence when $R = 1$ (see Appendix VIII).

The above results seem to indicate that the quasi-steady state approximation 4.6.1 is quite reliable in the calculation of the steam zone volume rate of growth and can be used with confidence. This should be further tested by using a more accurate numerical model (such as Simpson's rule or another higher accuracy quadrature) and a wider range

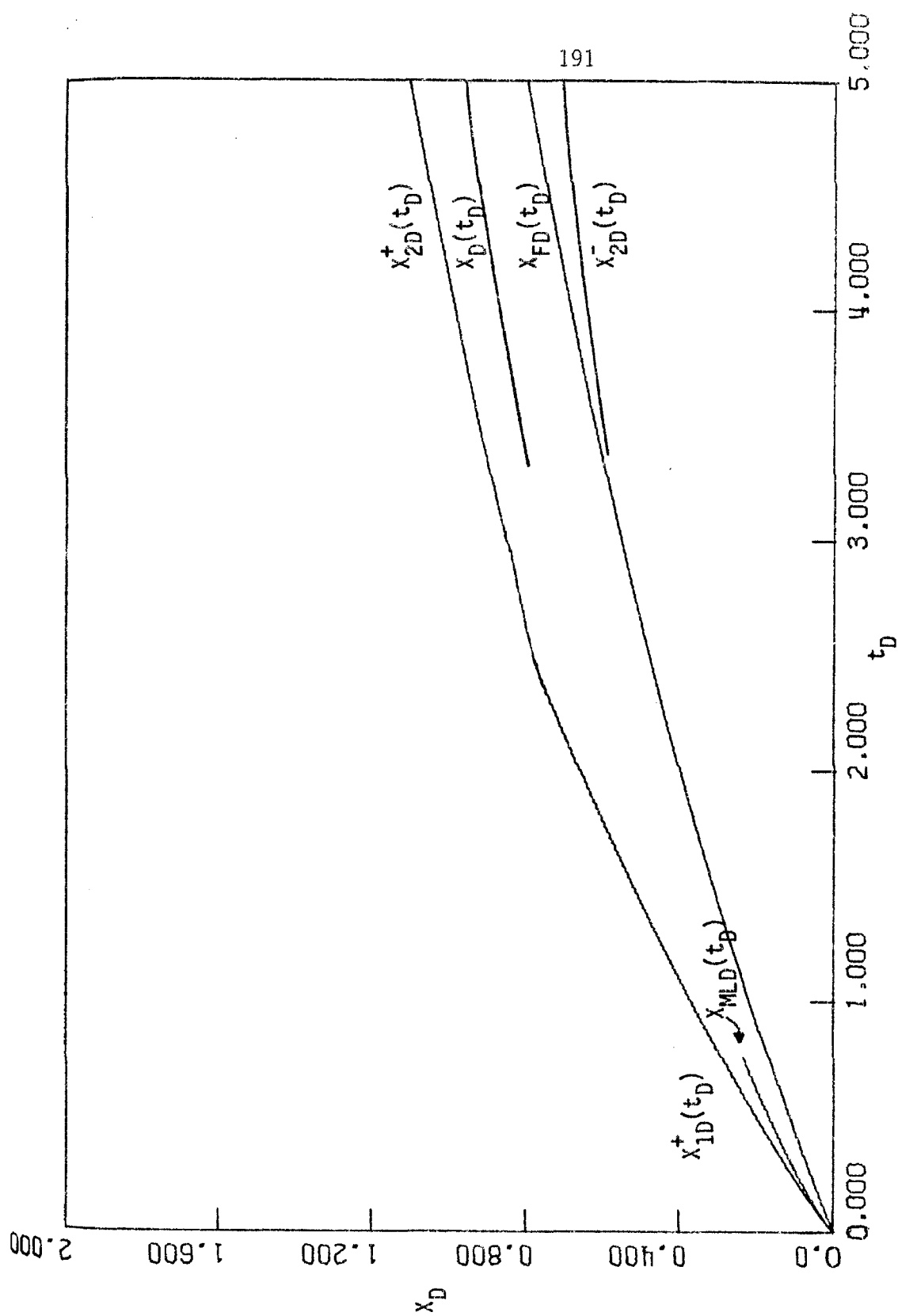


Figure 47. Numerical Solution of Eq. (4.83), x_{FD} , Upper Bounds x_{1D}^+ , x_{2D}^+ , the Marx-Langenheim Solution x_{MLD} . — Asymptotic Behavior of the Exact Solution, $x_D(t_D)$, and of the Lower Bound, $x_{2D}^-(t_D)$. $A = 0.5$, $R = 1$.

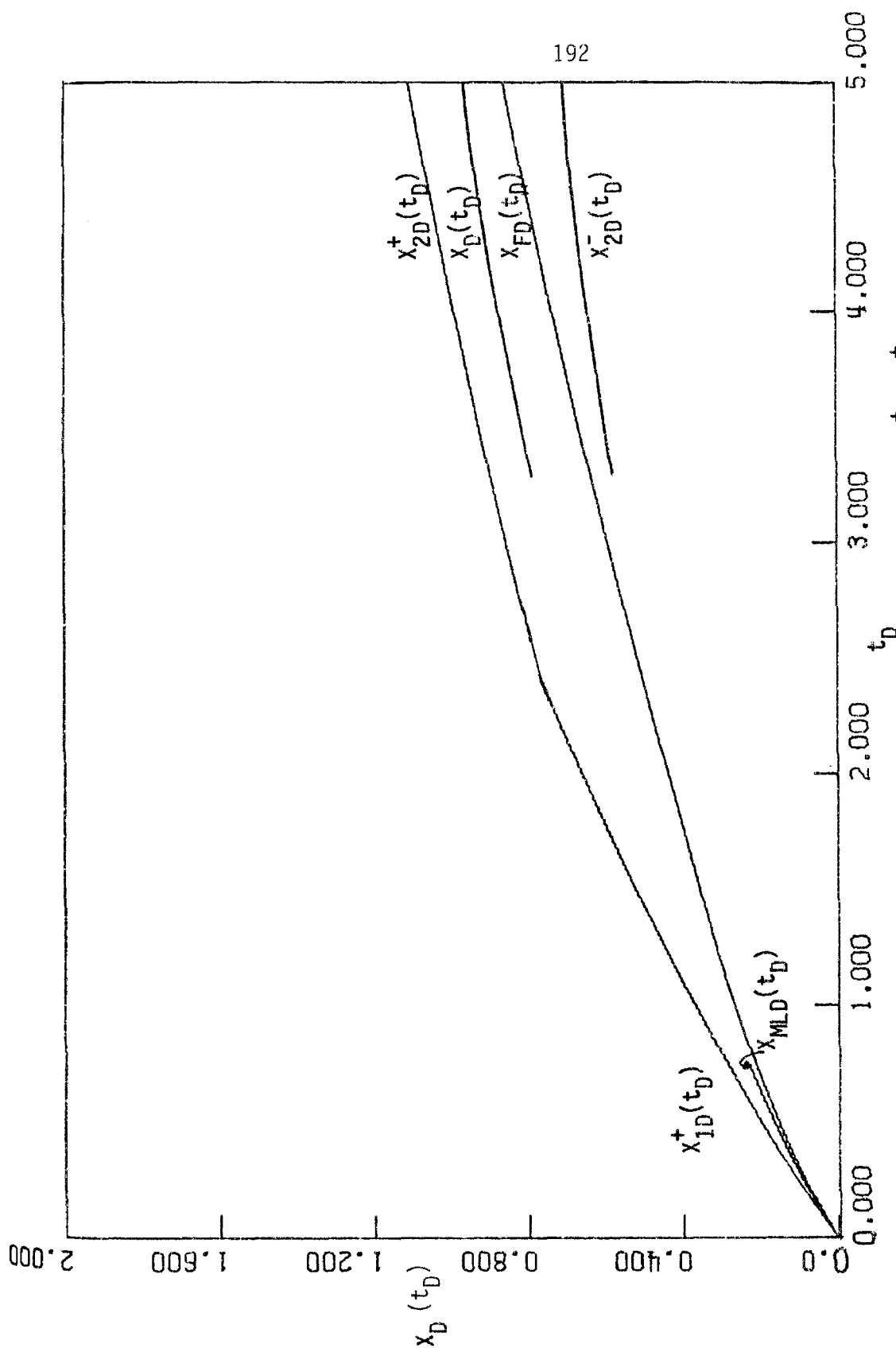


Figure 48. Numerical Solution of Eq. (4.83), x_{FD} , Upper Bounds x_{1D}^+ , x_{2D}^+ , the Marx-Langenheim Solution x_{MLD} . — Asymptotic Behavior of the Exact Solution, $x_D(t_D)$, and of the Lower Bound, $x_{2D}^-(t_D)$. $A = 0.5$, $R = 100$.

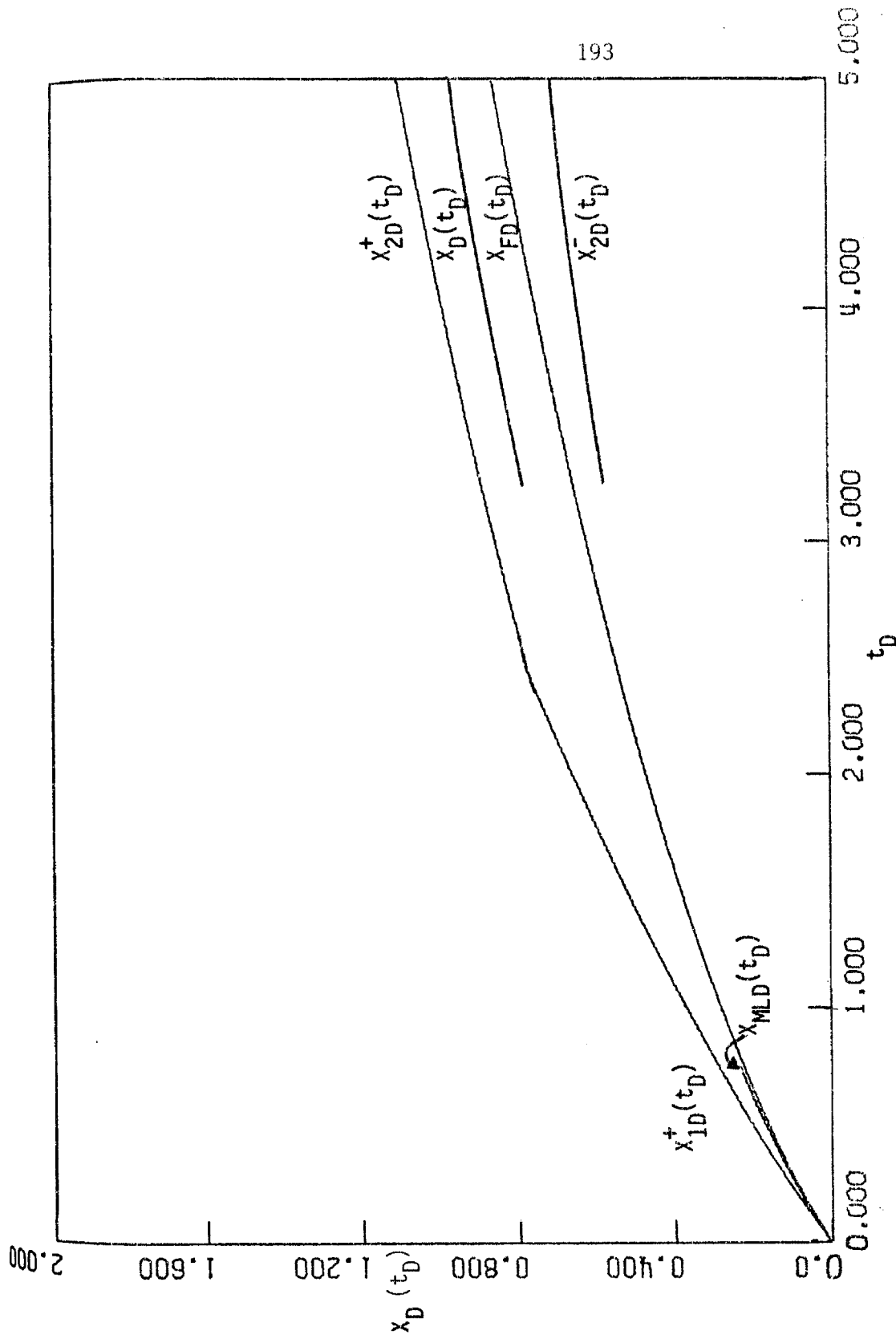


Figure 49. Numerical Solution of Eq. (4.83) X_{FD} , Upper Bounds X_{1D}^+ , X_{2D}^+ , the Marx-Langenheim Solution X_{MLD} . — Asymptotic Behavior of the Exact Solution, $X_D(t_D)$, and of the Lower Bound, $X_{2D}^-(t_D)$. $A = 0.5$, $R = 640$.

of values of the parameter A . It is very reasonable to expect that this much simpler numerical procedure could be used as an alternative to the much more sophisticated numerical simulators that are currently employed for the prediction of the steam zone growth in one-dimensional systems.

4.7 The Saturation Distribution Inside the Hot Liquid Zone

4.7.1 Introduction

In the previous sections of this chapter we were able to obtain explicit bounds and approximate solutions for the position of the steam front based, among others, on the assumption that the average saturations inside the steam zone are constant. This assumption which has been frequently employed in past theoretical investigations [Marx and Langenheim (1959), Mandl and Volek (1969)] draws its main support from reported experimental data. In this section we develop a theoretical model of the fluid flow and heat transfer phenomena of the steam zone with the objective to determine the saturation distribution and test the validity of the above approximation. Thus far, the only reported theoretical analysis on this subject was presented by Boberg and Shutler (1972) who discuss the fluid flow inside the steam zone by using an approximate analytical technique which neglects the local steam condensation due to heat losses.

4.7.2 Theoretical Considerations

In a one-dimensional, linear or cylindrical, geometry the respective mass balances for steam, liquid water and oil in the steam zone [Equations (2.1), (2.2), (2.3)] read:

$$\phi \frac{\partial S_s}{\partial t} + \frac{\partial \hat{u}_s}{\partial x} = -\gamma G(x,t) \quad (4.84)$$

$$\phi \frac{\partial S_w}{\partial t} + \frac{\partial \hat{u}_w}{\partial x} = G(x,t) \quad (4.85)$$

$$\phi \frac{\partial S_o}{\partial t} + \frac{\partial \hat{u}_o}{\partial x} = 0 \quad (4.86)$$

where \hat{u}_i stands for volumetric velocity per unit cross-sectional area or unit thickness, dx is the length or area element, in linear or cylindrical geometry, respectively.

The development of (4.84) to (4.86) is based upon the assumption of constant steam zone temperature, negligible steam distillation and uniform properties along the vertical coordinate of the basic Equations (2.1) to (2.3). We denote by γ the density ratio $\frac{\rho_w}{\rho_s}$ and by $G(x,t)$ the volume of liquid water, generated by steam condensation at x,t , per unit reservoir volume and time. The quantity G can be expressed in terms of the local heat losses

$$G(x,t) = \frac{2k_{hf} \left(\frac{\partial T_f}{\partial z} \right)_{z=0}}{hL_v (1) \rho_w} \quad (4.87)$$

Adding (4.84), (4.85), (4.86) and recalling (2.4), we get

$$\hat{u} = \hat{u}_s + \hat{u}_w + \hat{u}_o = (\hat{u}_s + \hat{u}_w + \hat{u}_o)_{inj} - (\gamma - 1) \int_0^x G(x',t) dx' \quad (4.88)$$

which defines u , the total volumetric flux at any point, as an explicit function of x,t .

We, next, introduce

$$f_s = \frac{\hat{u}_s}{\hat{u}_s + \hat{u}_w + \hat{u}_o}, \quad f_o = \frac{\hat{u}_o}{\hat{u}_s + \hat{u}_w + \hat{u}_o} \quad (4.89)$$

the fractional volumetric flow of steam and oil, respectively. For simplicity we confine our attention to horizontal reservoirs. The subsequent analysis can be easily extended to include gravity terms. Assuming negligible capillary effects, we can easily deduce, through Darcy's law, that f_s, f_o are functions of the saturations S_s, S_o alone (for the case of constant temperature). In fact,

$$f_s = \frac{k_{rs}/\mu_s}{k_{rs}/\mu_s + k_{rw}/\mu_w + k_{ro}/\mu_o}, \quad f_o = \frac{k_{ro}/\mu_o}{k_{rs}/\mu_s + k_{rw}/\mu_w + k_{ro}/\mu_o} \quad (4.90)$$

The unknown volumetric velocities can thus be eliminated from (4.84), (4.85), (4.86):

$$\phi \left(1 - \frac{1}{\gamma}\right) \frac{\partial S_s}{\partial t} + \phi \frac{\partial S_o}{\partial t} + \frac{\partial}{\partial x} \left\{ \left[\left(1 - \frac{1}{\gamma}\right) f_s(S_s, S_o) + f_o(S_s, S_o) - 1 \right] u(x, t) \right\} = 0 \quad (4.91)$$

$$\phi \frac{\partial S_s}{\partial t} + \frac{\partial}{\partial x} [f_s(S_s, S_o) \hat{u}(x, t)] = -\gamma G(x, t) \quad (4.92)$$

Equations (4.91), (4.92) form a system of two quasi-linear, first order, hyperbolic, partial differential equations which along with appropriate initial and boundary conditions can be solved numerically by the method

of characteristics [Whitham (1974)]. On the other hand, in certain circumstances, the functions f_s , f_o assume a certain convenient form which allows an analytical solution.

4.7.3 Oil Saturation at its Residual Value

Inspection of Eqs. (4.91), (4.92) reveals that the system becomes uncoupled when f_s is a function only of the variable S_s . Such a case can be realized, in principle, when an exceptional combination of the proper oil and reservoir characteristics exists. A more likely situation occurs under conditions of a typical steam drive. It has been experimentally proven [Willman et al. (1961)] that the oil left behind in the steam zone is practically unrecoverable, in other words, near its residual value. Then $k_{ro} \ll 1$, $\hat{u}_o \ll \hat{u}_s$ so that $f_s \approx f_s(S_s)$. Thus, both Eqs. (4.91), (4.92) reduce to:

$$\phi \frac{\partial S_s}{\partial t} + \frac{\partial}{\partial x} \left\{ \left(f_s(S_s) - \frac{\gamma}{\gamma - 1} \right) \hat{u}(x, t) \right\} = 0 \quad (4.93)$$

where, now, $f_s(S_s) = \frac{1}{1 + \frac{k_{rw}^{\mu_s}}{k_{rs}^{\mu_w}}}$, i.e., the usual fractional flow function

one encounters in isothermal, two-phase, immiscible displacement [Bear (1972)] (see Figure 50).

Equation (4.93) is a typical conservation equation with a sink term to account for steam condensation. If $\hat{u}(x, t)$ was position independent, (4.93) would be identical to the Buckley-Leverett equation, which governs isothermal, two-phase, immiscible displacement [Buckley and Leverett (1942)]. To solve Eq. (4.93), we use Eq. (4.88) and denote

$\hat{u}_0(t) = u(0,t) = \frac{w_s}{\rho_s} + \frac{w_w}{\rho_w}$. Then,

$$\phi \frac{\partial S_s}{\partial t} + \frac{\partial}{\partial x} \left\{ \left(f_s(S_s) - \frac{\gamma}{\gamma - 1} \right) \left(\hat{u}_0(t) - (\gamma - 1) \int_0^x G(x',t) dx' \right) \right\} = 0 \quad (4.94)$$

Note that if capillary and gravity terms are included, we get the more general form:

$$\begin{aligned} \phi \frac{\partial S_s}{\partial t} + \frac{\partial}{\partial x} \left\{ \left(f_s(S_s) - \frac{\gamma}{\gamma - 1} \right) \left(\hat{u}_0(t) - (\gamma - 1) \int_0^x G(x',t) dx' \right) \right. \\ \left. - g_s(\rho_w - \rho_s) \frac{k_{rw}}{\mu_w} f_s(S_s) - \frac{\partial P_c}{\partial S_s} \cdot \frac{k_{rw}}{\mu_w} f_s(S_s) \frac{\partial S_s}{\partial x} \right\} = 0 \end{aligned} \quad (4.95)$$

where g_s is the component of the gravity vector along the direction of flow.

The domain of integration of (4.94) is the steam zone (Figure 51). Since the equation is of hyperbolic nature, we need one boundary (or initial) condition, which is supplied by

$$S_s(0,t) = S_{s,inj}(t) \quad \forall 0 < t \quad (4.96)$$

a function of the steam quality at the injection point, f_{st} . Provided that f_{st} is constant with time, the above condition allows for a smooth, no-shocks solution.

Borrowing the dimensionless notation of Chapter 4.3.1, we can rearrange (4.96) to the form:

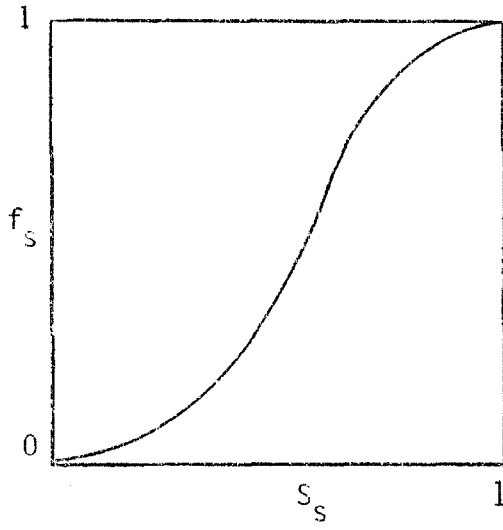


Figure 50. Typical Two-Phase Fractional Flow Curve.

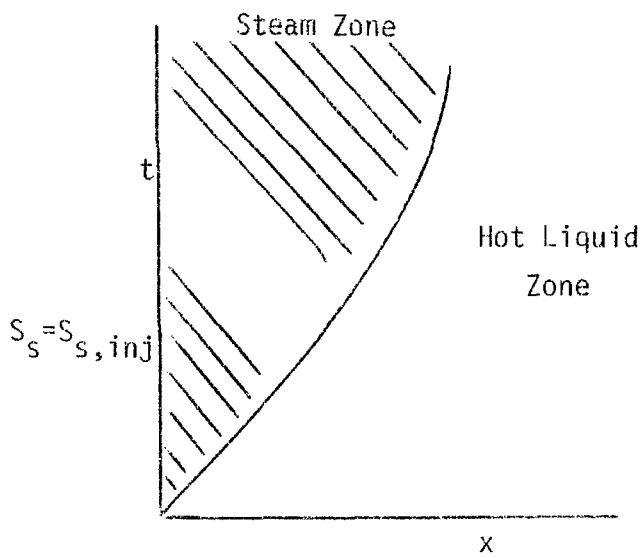


Figure 51. Domain of Integration of Eq. (4.89)

$$\begin{aligned}
\frac{\partial S_D}{\partial t_D} + \left\{ \frac{D}{2} U_{OD}(t_D) - \frac{E}{2} (CHL)_D \right\} f'_{SD}(S_D) \frac{\partial S_D}{\partial x_D} \\
= - \left\{ - f_{SD}(S_D) + \frac{\gamma}{\gamma - 1} \right\} \frac{E}{2} (HL)_D \quad (4.97)
\end{aligned}$$

$$S_D(0, t_D) = 1.0$$

where

$$D = \frac{M_1 \Delta T (f_{st} \gamma - f_{st} + 1)}{\phi \rho_w S_{s, inj} L_v^{(1)} (f_{st} + S_t)}, \quad E = \frac{(\gamma - 1) M_1 \Delta T}{\phi \rho_w S_{s, inj} L_v^{(1)}} \quad \text{are dimensionless}$$

groups, $(CHL)_D$ the dimensionless expression for the cumulative condensation

$$(\gamma - 1) \int_0^x G(x', t) dx', \quad (HL)_D \text{ the dimensionless expression for the instan-}$$

taneous condensation $(\gamma - 1)G(x, t)$, and S_s is normalized by $S_{s, inj}$. Both $(CHL)_D$, $(HL)_D$ are $O(1)$.

For typical values of reservoir parameters, the dimensionless groups D, E are of the order of 10^2 , i.e. $D, E \gg 1$. (See also Table 6) Therefore, (4.97) can be approximated by the simpler equation:

$$\begin{aligned}
\left\{ \frac{D}{E} U_{OD}(t_D) - (CHL)_D \right\} f'_{SD}(S_D) \frac{\partial S_D}{\partial x_D} = - \left\{ - f_{SD}(S_D) + \frac{\gamma}{\gamma - 1} \right\} (HL)_D \\
S_D(0, t_D) = 1.0 \quad (4.98)
\end{aligned}$$

or

$$\begin{aligned}
\frac{\partial}{\partial x_D} \left\{ \left[\frac{D}{E} U_{OD}(t_D) - (CHL)_D \right] \left[\frac{\gamma}{\gamma - 1} - f_{SD}(S_D) \right] \right\} = 0 \quad (4.99) \\
S_D(0, t_D) = 1.0
\end{aligned}$$

Equation (4.99) is the quasi-steady state form of (4.97) and applies when

the characteristic time for saturation changes is much smaller than the characteristic time for the steam zone growth.

We can now solve (4.99) to get:

$$f_{SD}(S_D) = \frac{\gamma}{\gamma - 1} - \frac{\left(\frac{\gamma}{\gamma - 1} - f_{SD}(1)\right)}{\left\{1 - \frac{E}{D} \cdot \frac{(CHL)_D}{U_{OD}(t_D)}\right\}} \quad (4.100)$$

in terms of x_D, t_D and the cumulative heat losses $(CHL)_D$. Given a distribution for the reservoir temperature, we can employ expression (3.13) in the definitions of G , $(CHL)_D$ to explicitly determine $f_{SD}(S_D)$ and S_D as a function of x_D, t_D .

It is of interest to examine the saturation at the front, S_D^I , which is expected to decrease with time. At large t_D , the cumulative heat losses consume all injected heat (see Subsection 4.5.2.1), and the total heat losses at the edge of the front $(CHL)_D \rightarrow AU_{OD}(t_D)$. Thus, Eq. (4.100) gives, after lengthy calculations,

$$f_{SD}(S_D^I) \rightarrow 0 \quad \text{as} \quad t_D \rightarrow \infty \quad (4.101)$$

which is equivalent to

$$S_D^I \rightarrow 0 \quad \text{as} \quad t_D \rightarrow \infty \quad (4.102)$$

Note that the derivation of (4.96) made use of the relationship

$$f_{SD}(1) = \frac{\gamma f_{st}}{\gamma f_{st} - f_{st} + 1} \quad (4.103)$$

Analogous considerations apply to the average steam saturation

$$\bar{S}_D(t_D) = \frac{\int_0^{x_{FD}(t_D)} S_D dx_D}{x_{FD}(t_D)}$$

which is the most important quantity with respect to the growth of the steam zone. After integrating by parts, we can rewrite

$$\bar{S}_D(t_D) = S_D^I + \frac{\int_{S_D^I}^1 x_D(S_D, t_D) dS_D}{x_{FD}(t_D)} \quad (4.104)$$

which indicates that the average steam saturation slowly decreases with time. Indeed, since as $t_D \rightarrow \infty$, $S_D^I \rightarrow 0$, we deduce that $\bar{S}_D(t_D)$ tends to a limiting value $\bar{S}_D(\infty)$:

$$\bar{S}_D(\infty) = \lim_{t_D \rightarrow \infty} \left(\frac{\int_0^1 x_D(S_D, t_D) dS_D}{x_{FD}(t_D)} \right) \quad (4.105)$$

The utilization of the above results in checking the validity of the simplifying approximations (4.16) requires that we choose a specific temperature distribution in order to evaluate the heat losses term (see Chapter 3.2). Here we shall examine two limiting cases, one in which the heat losses are approximated by the lower bound, Eq. (3.18a), and another one in which they are approximated by the upper bound, Eq. (3.18b).

4.7.4 Heat Losses Bounded from Below

Now

$$G(x, t) = \frac{2k_{hf} \cdot \Delta T}{h\rho_w L_V (1) \sqrt{\pi\alpha_f t}} \quad , \quad (HL)_D = \frac{1}{\sqrt{t_D}} \quad ,$$

$(\text{CHL})_D = \frac{x_D}{\sqrt{\tau_D}}$ and Eq. (4.97) assumes the form:

$$\begin{aligned} \frac{\partial S_D}{\partial t_D} + \left\{ \frac{D}{2} u_{0D}(t_D) - \frac{E}{2} \cdot \frac{x_D}{\sqrt{\tau_D}} \right\} f'_{SD}(S_D) \frac{\partial S_D}{\partial x_D} \\ = - \left\{ - f_{SD}(S_D) + \frac{\gamma}{\gamma - 1} \right\} \frac{E}{2 \sqrt{\tau_D}} \end{aligned} \quad (4.106)$$

$$S_D(0, t_D) = 1.0$$

The solution of (4.106) can be obtained analytically by a transformation of variables and a subsequent hodograph transformation without recourse to any approximation. Let $\tau_D = \sqrt{\tau_D}$ be the dependent variable, a function of x_D, S_D . Then, Eq. (4.106) becomes:

$$\left[D \tau_D u_{0D}(\tau_D) - E x_D \right] f'_{SD}(S_D) \frac{\partial \tau_D}{\partial x_D} - E \left[\frac{\gamma}{\gamma - 1} - f_{SD}(S_D) \right] \frac{\partial \tau_D}{\partial S_D} = 1 \quad (4.107)$$

which is solved by the method of characteristics:

$$\begin{aligned} \frac{d\tau_D}{dS_D} &= - \frac{1}{E \left(\frac{\gamma}{\gamma - 1} - f_{SD}(S_D) \right)} \\ \frac{dx_D}{dS_D} &= - \left[\frac{D}{E} \tau_D u_{0D}(\tau_D) - x_D \right] \frac{f'_{SD}(S_D)}{\left(\frac{\gamma}{\gamma - 1} - f_{SD}(S_D) \right)} \end{aligned} \quad (4.108)$$

The pair of Equations (4.108) with the boundary condition

$S_D(0, \tau_D) = 1$, admits the solution:

$$x_D = -\frac{D}{E} \cdot \frac{1}{\left[\frac{\gamma}{\gamma-1} - f_{SD}(S_D)\right]} \cdot \left\{ \int_1^{S_D} f'_{SD}(\zeta) \cdot u_{0D} \left(\tau_D - \frac{1}{E} K(S_D) + \frac{1}{E} K(\zeta) \right) \tau_D d\zeta \right. \\ \left. + \frac{1}{E} \int_1^{S_D} f'_{SD}(\zeta) u_{0D} \left(\tau_D - \frac{1}{D} K(S_D) + \frac{1}{E} K(\zeta) \right) \cdot (K(\zeta) - K(S_D)) d\zeta \right\} \quad (4.109)$$

where

$$K(\zeta) = - \int_1^{\zeta} \frac{d\zeta'}{\left[\frac{\gamma}{\gamma-1} - f_{SD}(\zeta')\right]} \quad (4.110)$$

Recalling that $E \gg 1$, we recover the quasi-steady solution by neglecting the term of order $\left(\frac{1}{E}\right)$:

$$x_D \approx \frac{D}{E} \cdot \frac{1}{\left[\frac{\gamma}{\gamma-1} - f_{SD}(S_D)\right]} u_{0D}(\tau_D) \tau_D (f_{SD}(1) - f_{SD}(S_D)) \quad (4.111)$$

which is the particular form of Eq. (4.96) when the heat losses term is proportional to $\frac{1}{\sqrt{E}}$.

For constant injection rates, (4.109) simplifies to:

$$x_D = \frac{D}{E} \cdot \frac{1}{\left[\frac{\gamma}{\gamma-1} - f_{SD}(S_D)\right]} \sqrt{E}_D [f_{SD}(1) - f_{SD}(S_D)] + \frac{D}{E^2} \frac{I(S_D)}{\left[\frac{\gamma}{\gamma-1} - f_{SD}(S_D)\right]} \quad (4.112)$$

where

$$I(S_D) = \int_1^{S_D} \frac{[f_{SD}(1) - f_{SD}(\zeta)] d\zeta}{\left[\frac{\gamma}{\gamma-1} - f_{SD}(\zeta)\right]} \quad (4.113)$$

Equation (4.113) indicates that the steam saturation is constant along the curves $x_D = a_1 \sqrt{E}_D + a_2$, with a_1, a_2 constant for fixed saturation. In

Figures 52 - 54 we plot the characteristic curves $X_D(S_D)$ for various values of t_D and f_{st} (or A). We observe that the steam condensation near the front increases with time. The rate of condensation is also seen to depend on the injection quality. The higher r_{st} (or A), the less steam is condensed for fixed x_D, t_D .

In Figures 55, 56 we plot the saturation at the edge of the front, S_D^I , and the average saturation, \bar{S}_D , for various values of f_{st} . The variable S_D^I is a decreasing function of time, approaching zero slowly as $t_D \rightarrow \infty$ in accordance with (4.102). By contrast, the average steam saturation approaches quickly its limiting value

$$\bar{S}_D(\infty) = -\frac{D}{EA} I(0) \quad (4.114)$$

Table 11 shows that the final value $\bar{S}_D(\infty)$ is not very sensitive to the injected steam quality, except at very small values of f_{st} .

To test the hypothesis (4.16),

$$\left| \frac{d\bar{S}_D}{dt_D} x_{jD}^+(t_D) \right| \ll \left| \frac{d}{dt_D} (\bar{S}_D x_{jD}^+(t_D)) \right|, \text{ we calculate the error}$$

$$1 - \frac{\left| \bar{S}_D \dot{x}_{jD}^+(t_D) \right|}{\left| \frac{d}{dt_D} (\bar{S}_D x_{jD}^+(t_D)) \right|} \quad \text{as a function of time for various values of}$$

f_{st} (Figure 57). We verify that the approximation (4.16) is good for small and particularly for large times when bound $x_{2D}^+(t_D)$ dominates the growth rate. The calculated error is of the order $O(10^{-2})$. The approximation is not as good in an intermediate time interval when the bound $x_{1D}^+(t_D)$ predominates and the error may be significant for a short time

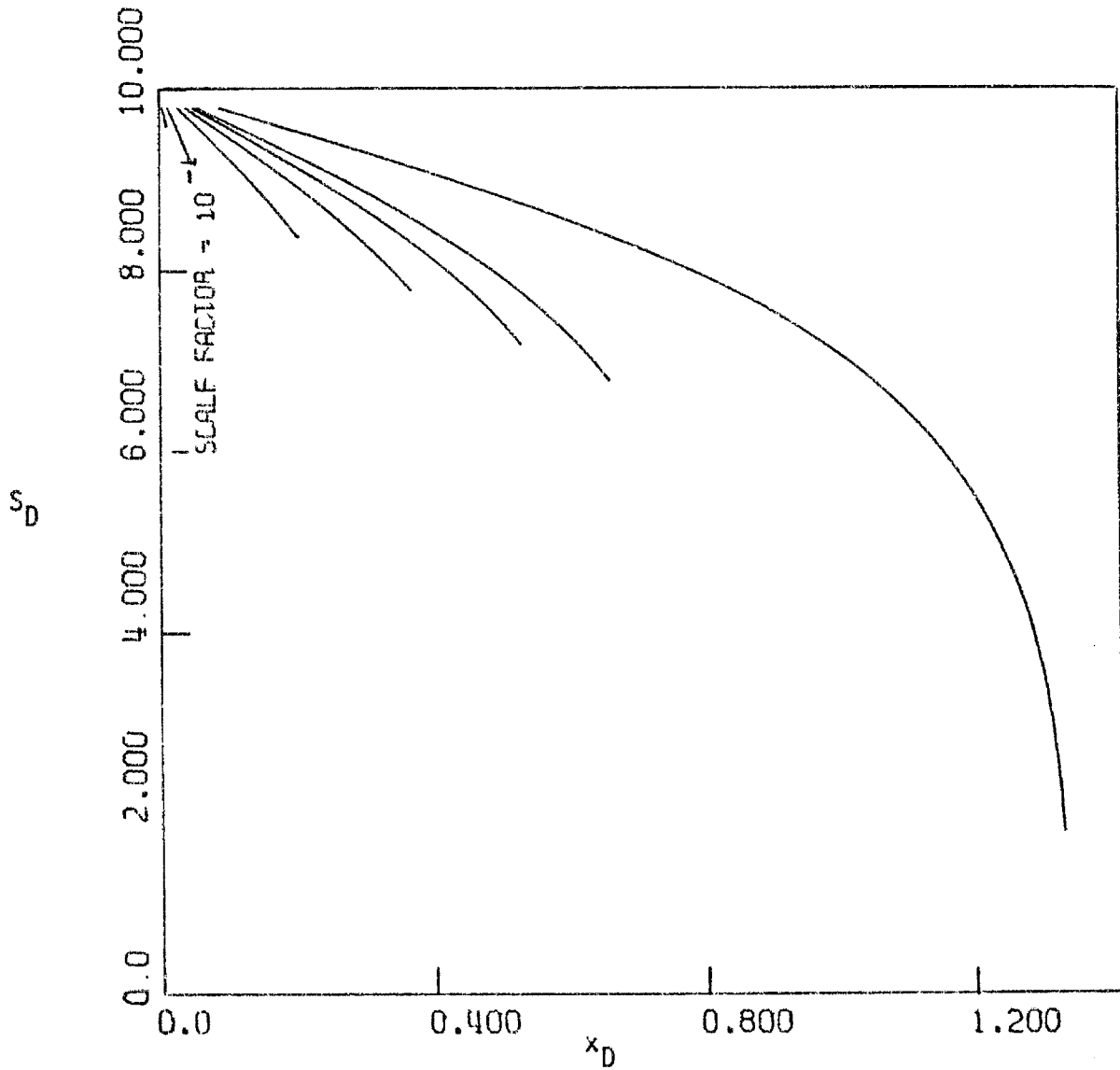


Figure 52. Steam Saturation Distribution for Case 4.7.4
 $t_D = 0.02, 0.1, 0.5, 1.0, 1.5, 2.0, 5.0$.
 $T_s = 250^\circ\text{C}$, $f_{st} = 0.84$.

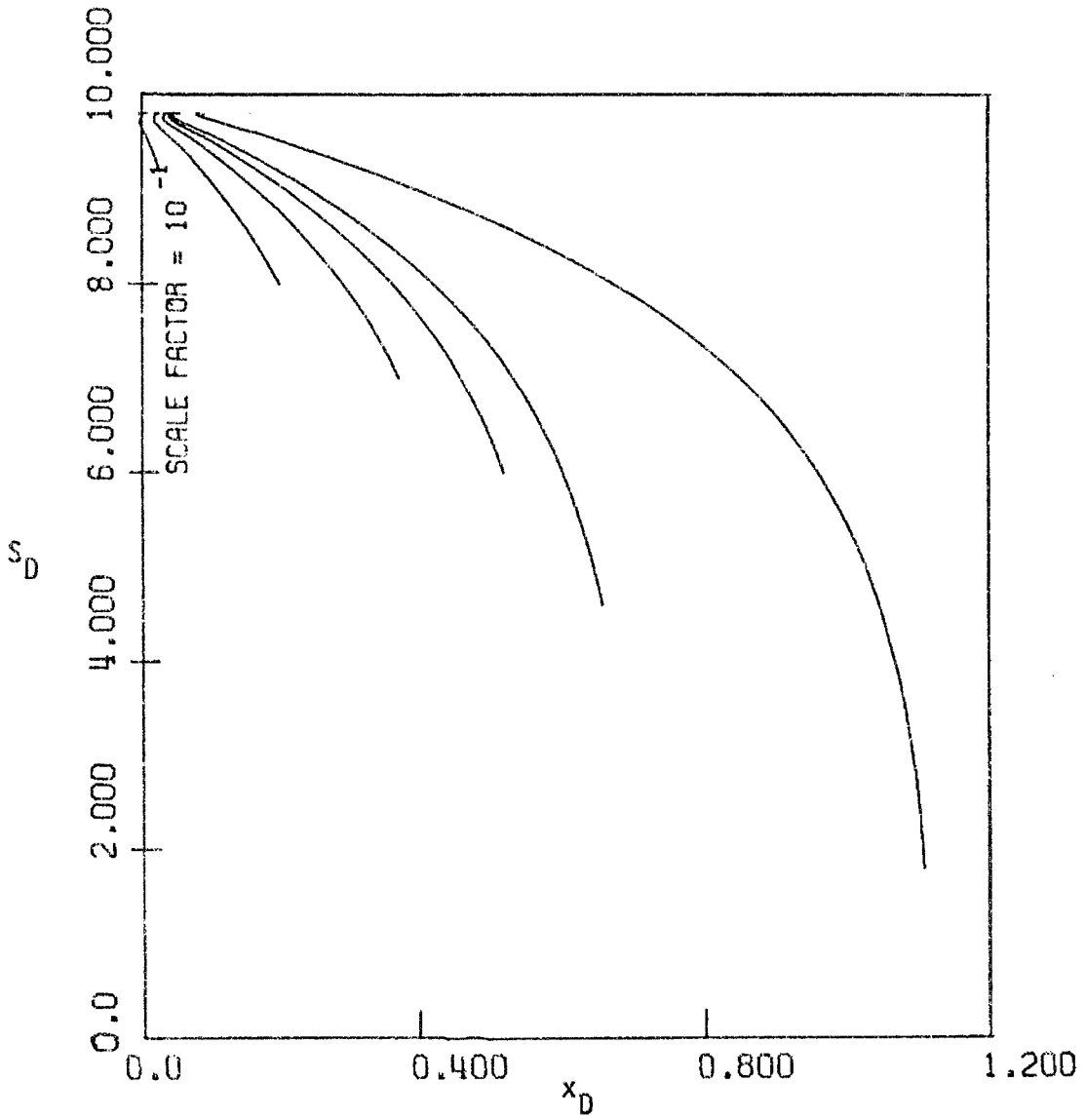


Figure 53. Steam Saturation Distribution for Case
 4.7.4. $t_D = 0.02, 0.1, 0.5, 1.0, 1.5, 2.0, 5.0$.
 $T_s = 250^\circ\text{C}$, $f_{st} = 0.56$.

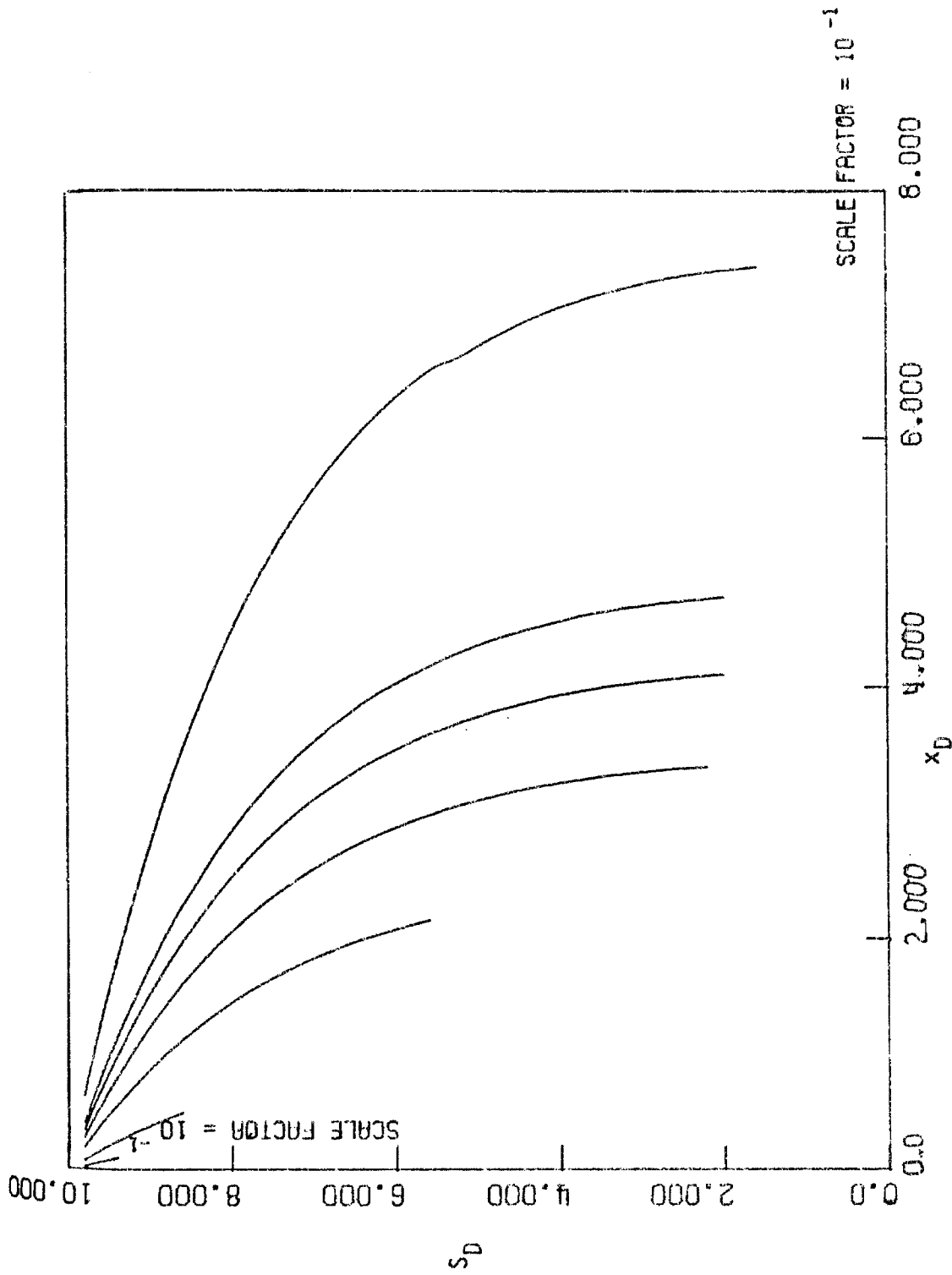


Figure 54. Steam Saturation Distribution for Case 4.7.4. $t_D = 0.02$, $0.1, 0.5, 1.0, 1.5, 2.0, 5.0$. $T_s = 2500C$, $f_{st} = 0.29$.

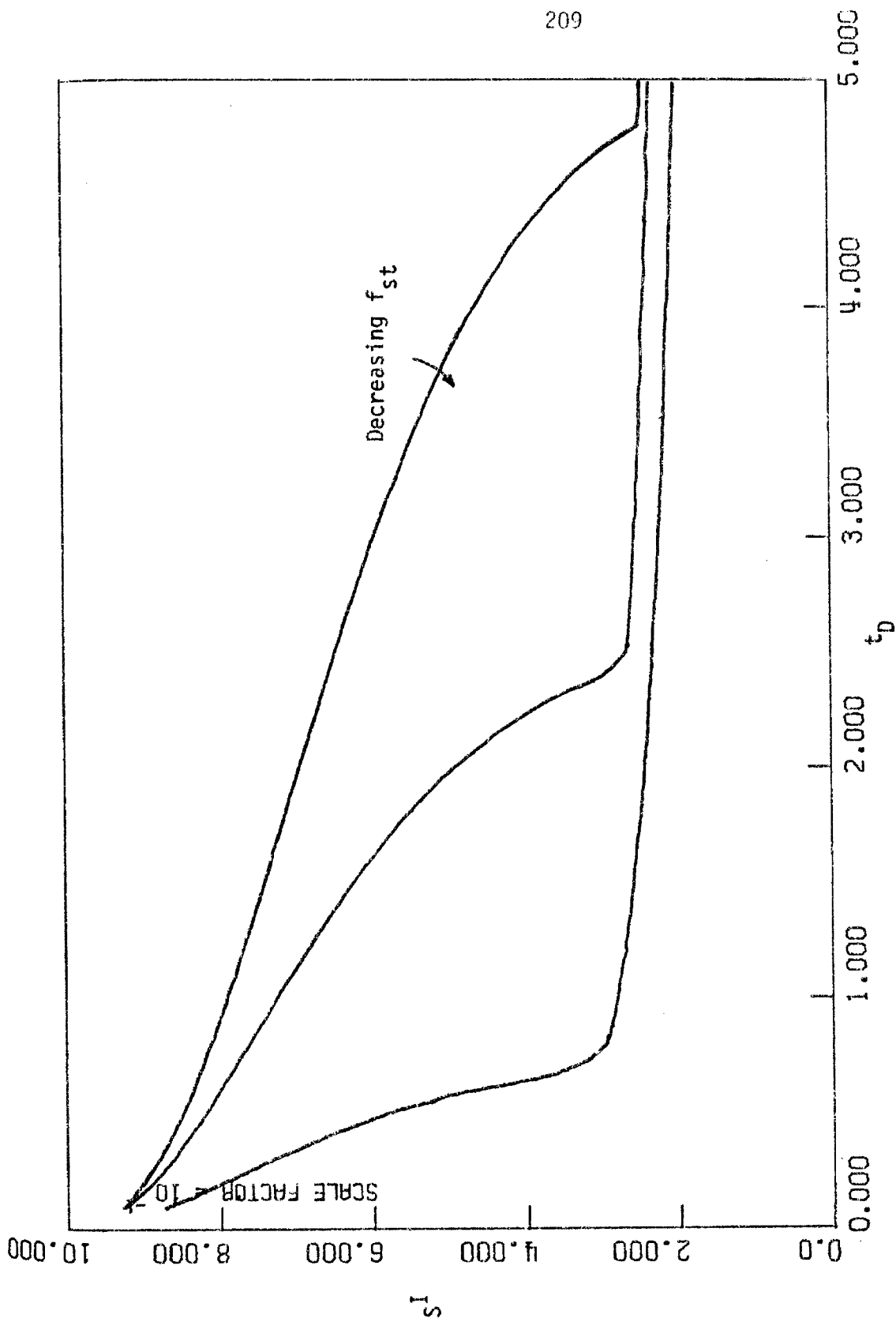


Figure 55. Steam Saturation at the Edge of the Steam Front, s^I , for Case 4.7.4.

$T_s = 250^\circ\text{C}$, $f_{st} = 0.84, 0.56, 0.29$.

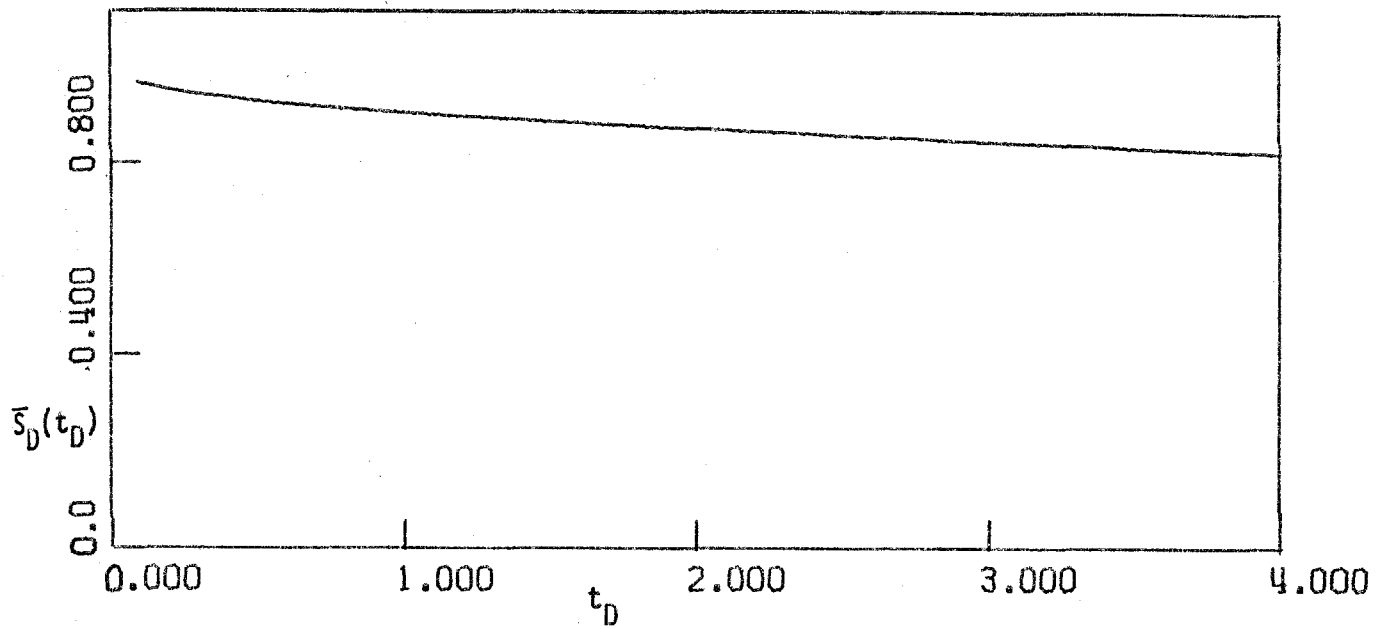


Figure 56a. Average Steam Saturation, \bar{s}_D , for Case 4.7.4. $T_s = 250^\circ\text{C}$, $f_{st} = 0.84$.

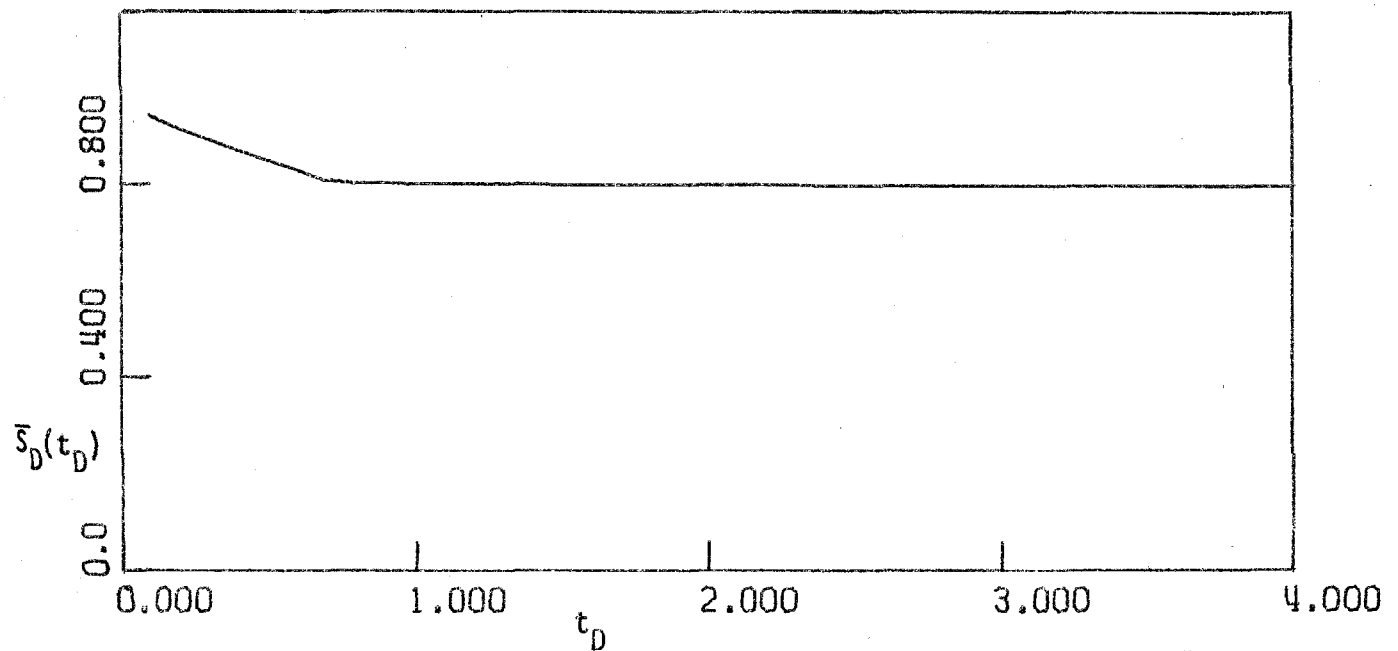


Figure 56b. Average Steam Saturation, \bar{s}_D , for Case 4.7.4. $T_s = 250^\circ\text{C}$, $f_{st} = 0.29$.

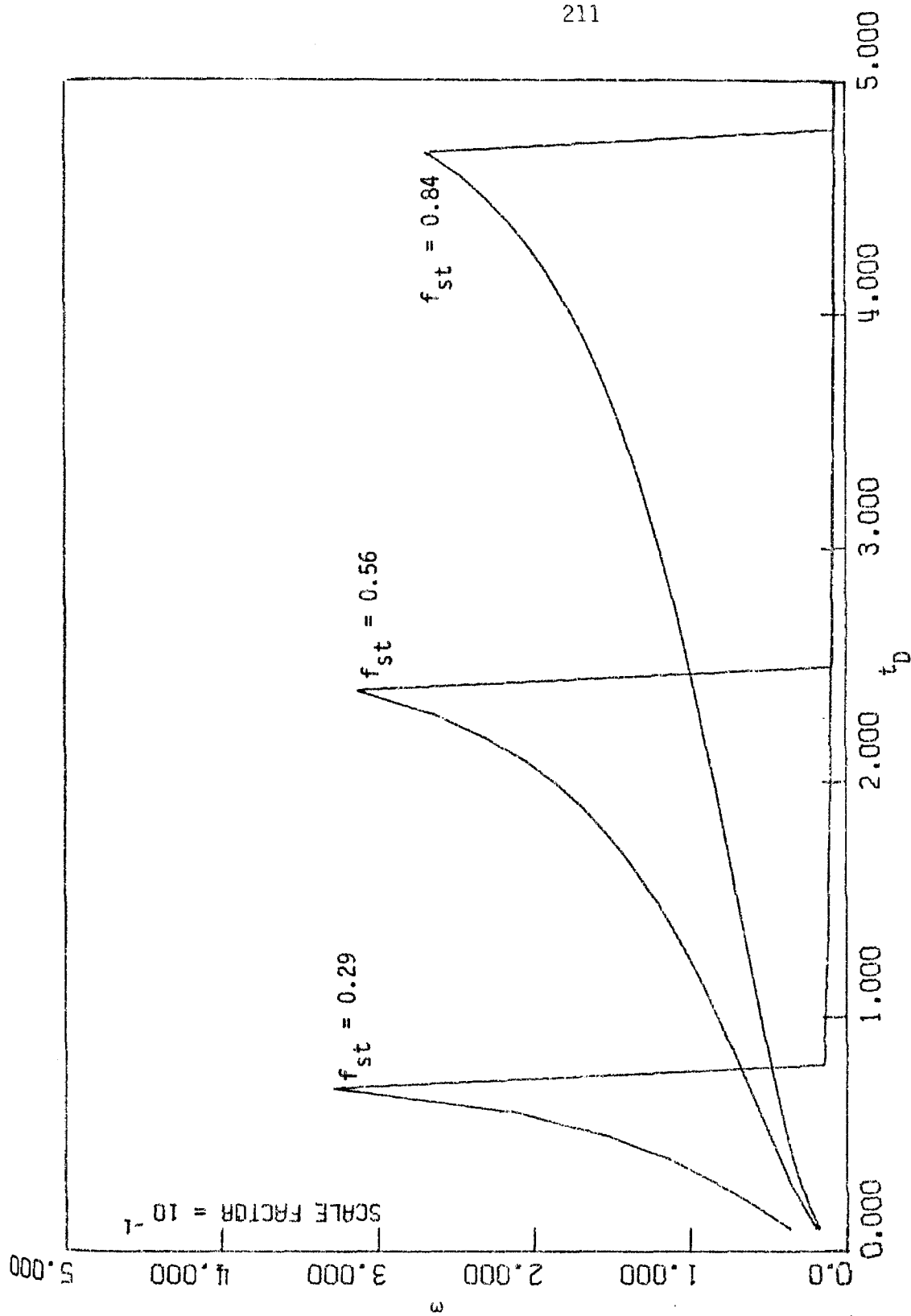


Figure 57. Error, ϵ , Introduced by Assumption (4.16), for Case 4.7.4. $T_S = 250^\circ\text{C}$, $f_{st} = 0.84, 0.56, 0.29$.

f_{st}	$\bar{S}_D(\infty)$
1.00	0.7300
0.90	0.7815
0.80	0.7933
0.70	0.7990
0.60	0.8015
0.50	0.8016
0.40	0.7992
0.30	0.7938
0.20	0.7841
0.10	0.7651

Limiting values of the average steam saturation for various values of the injected steam quality.

Table 11

interval. This may be attributed to the fact that, locally, we over-estimate the actual solution significantly by using the upper bound $X_{1D}^+(t_D)$. The approximation (4.16) also depends on the value of the parameter A , and becomes better for small values of A . The resulting conclusion is that use of (4.16) is reasonable, in calculating the upper bound $X_{1D}^+(t_D)$, and very good in calculating the upper bound $X_{2D}^+(t_D)$.

In carrying out the above calculations, the function $f_{SD}(S_D)$ was approximated by the expression

$$f_{SD}(S_D) = \frac{1}{1 + \frac{\mu_S}{\mu_W} \left(\frac{1 + \sqrt{\frac{(1 - f_{st})\mu_W}{\gamma f_{st}\mu_S} - S_D}}{S_D} \right)^2} \quad (4.115)$$

which fits well the steam-water relative permeability data curve presented by Martin (1975) (see Figure 58).

4.7.5 Heat Losses Bounded from Above

When the heat losses are evaluated by the upper bound of Eq. (3.18a)

$$G(x,t) = \frac{2k_{hf}\Delta T}{h\rho_w L_V^{(1)} \sqrt{\pi\alpha_f} \sqrt{t - \lambda(x)}} , \quad (HL)_D = \frac{1}{\sqrt{t_D - \lambda_D(x_D)}} ,$$

$$(CHL)_D = \int_0^{x_D} \frac{dx'}{\sqrt{t_D - \lambda_D(x')}} ,$$

thus the governing equation reads

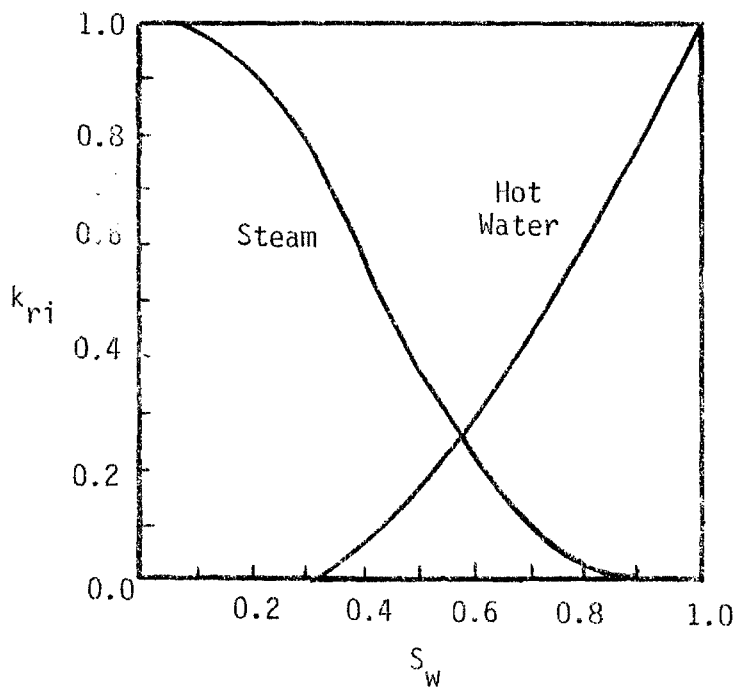


Figure 58. Relative Permeability Curves for Steam-Hot Water [Martin (1975)].

$$\begin{aligned} \frac{\partial S_D}{\partial t_D} + \left\{ \frac{D}{2} u_{0D}(t_D) - \frac{E}{2} \int_0^{x_D} \frac{dx'}{\sqrt{t_D - \lambda_D(x')}} \right\} f'_{SD}(S_D) \frac{\partial S_D}{\partial x_D} = \\ - \left\{ - f_{SD}(S_D) + \frac{\gamma}{\gamma - 1} \right\} \frac{E}{2\sqrt{t_D - \lambda_D(x_D)}} \end{aligned} \quad (4.116)$$

$$S_D(0, t_D) = 1$$

The corresponding expressions for the steam front position are given by the Marx-Langenheim solution and the lower bound $x_{2D}^-(t_D)$ derived in Section 4.4.

In contrast to Equation (4.106), there is no easy way to solve (4.116) analytically. Although a numerical solution is feasible, the determination of S_D as a function of x_D and t_D can be obtained from the quasi-steady state approximation (4.95)

$$f_{SD}(S_D) = \frac{\gamma}{\gamma - 1} - \frac{\left[\frac{\gamma}{\gamma - 1} - f_{SD}(1) \right]}{\left\{ 1 - \frac{E}{D} \cdot \frac{1}{u_{0D}(t_D)} \int_0^{x_D} \frac{dx'}{\sqrt{t_D - \lambda_D(x')}} \right\}} \quad (4.117)$$

Iso-saturation curves, for constant injection rates, are implicitly determined by $\int_0^{x_D} \frac{dx'}{\sqrt{t_D - \lambda_D(x')}} = a_3$, where a_3 is constant for fixed

S_D . Plotted in Figs. 59, 60 are the characteristic curves $x_D(S_D)$ for various t_D . The saturations S_D and S_D^I are shown to vary faster than in the previous case due to the higher heat losses. The relative error introduced by the assumption (4.16) when calculating the Marx-Langenheim expression and the lower bound is smaller than in 4.7.4 since, here, the steam front velocity is smaller. Overall, one concludes that the approximation (4.16) is good for small times, reasonable at intermediate times and very

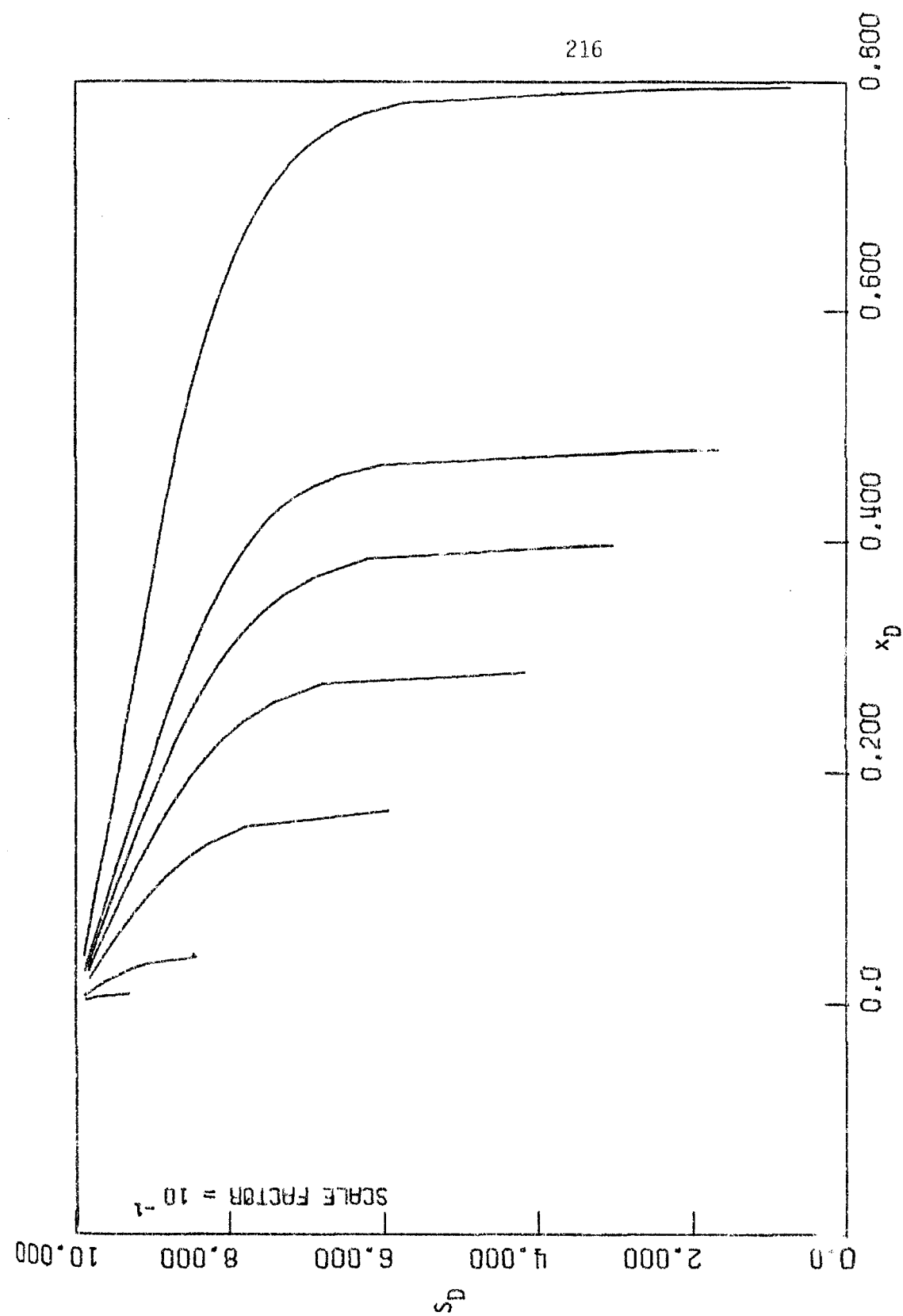


Figure 59. Steam Saturation Distribution for Case 4.7.5. $t_D = 0.02, 0.1, 0.5, 1.5, 2.0, 5.0$. $T_s = 250^\circ\text{C}$, $f_{st} = 0.84$.

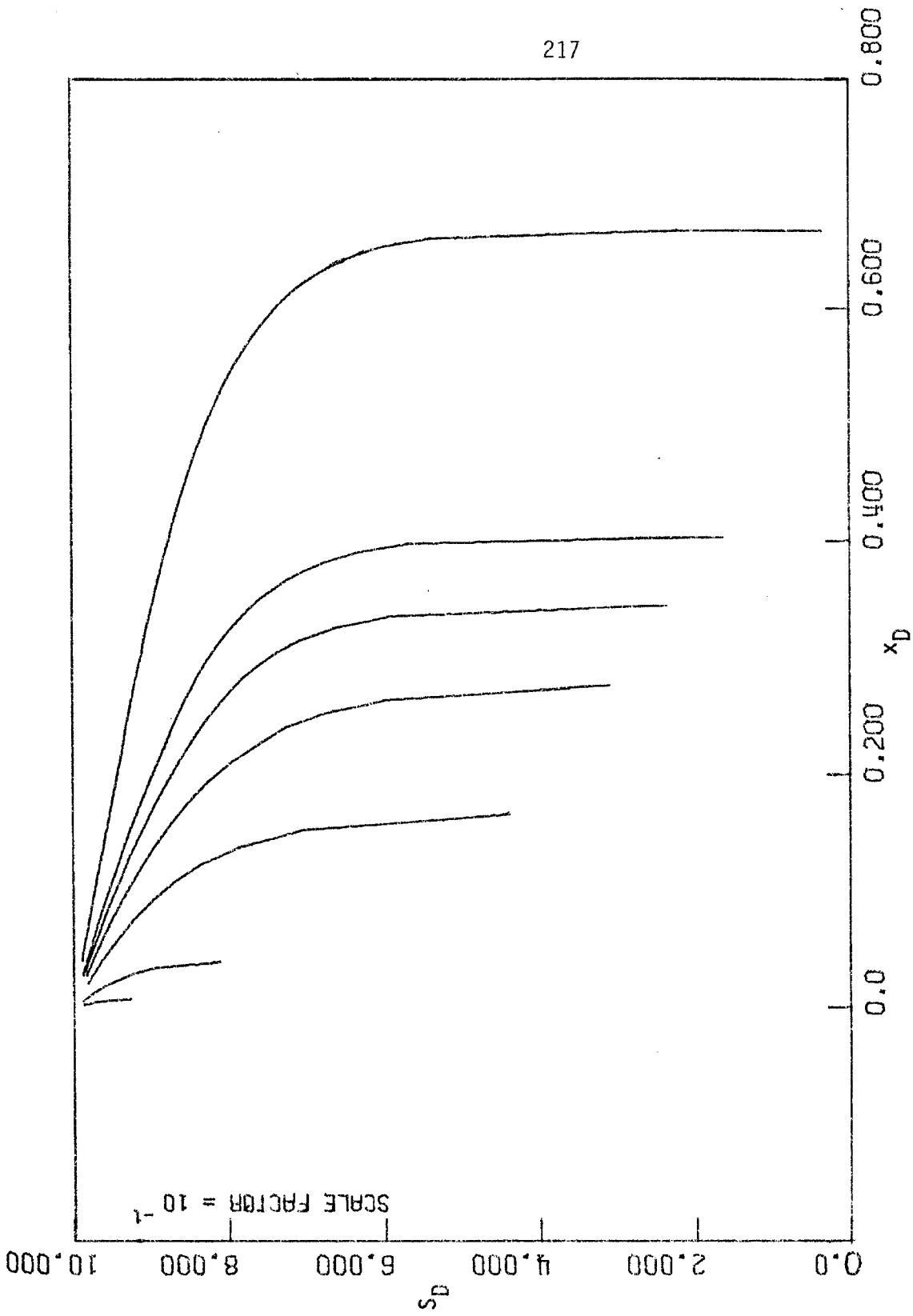


Figure 60. Steam Saturation Distribution for Case 4.7.5. $t_D = 0.02, 0.1, 0.5, 1.5, 2.0, 5.0$. $T_s = 250^\circ\text{C}$, $f_{st} = 0.56$.

good at large times .

4.7.6 Some Additional Remarks

The foregoing analysis provides a pretty good description of the saturation distribution inside the steam zone and defines the regions of validity of the assumption of the constant average saturation, under the conditions of residual oil saturation. As already emphasized, identical results hold under any other assumption, as long as the fractional volumetric flow of steam, f_{SD} , is a function of the steam saturation alone. This is tantamount to replacing the three-phase flow problem by a two-phase flow problem with steam as one of the two flowing phases. These lines can be extended to other problems, for example, the steam-oil flow system described by Shutler and Boberg (1972), where now we take into account local steam condensation.

Another approach can be followed in systems where $f_o = f_o(S_o)$, i.e. a function of the oil saturation alone. We can then define the new variables $S_t = S_w + S_s$, $\hat{u}_t = \hat{u}_w + \hat{u}_s$, $f_t = \frac{\hat{u}_s + \hat{u}_w}{\hat{u}_s + \hat{u}_w + \hat{u}_o}$ and rearrange

Eqs. (4.91), (4.92) to obtain:

$$\begin{aligned} \phi \frac{\partial S_t}{\partial t} + \left\{ \hat{u}_o(t) - (\gamma - 1) \int_0^x G(x', t) dx' \right\} f'_t(S_t) \frac{\partial S_t}{\partial x} \\ = - \left[\gamma (1 - f_t(S_t)) + f_t(S_t) \right] G(x, t) \end{aligned} \quad (4.118)$$

This is equivalent to (4.93) with S_t replacing S_s , thus the previous analysis holds throughout. Proceeding in this way we may get a fairly good estimate of the oil saturation distribution in the steam zone. Since,

however, $f_t(S_t)$ is expected to be fairly close to a step-distribution due to the high oil viscosity, the resulting average oil saturation should not lie significantly above its residual value. This should provide additional evidence that the oil left behind in the steam zone is at an irreducible saturation that cannot be further reduced by steam drive.

4.8 Conclusions

Summarizing the above we are led to the conclusion that the integral balance technique of Chapter II, combined with the proper heat transfer models of Chapter III, can be successfully applied to describe the one-dimensional steamflooding. In addition, a reliable, although approximate, account of the steam saturation distribution revealed that variations in the average saturations inside the steam zone do not significantly affect the performance of a steam drive. Since an exact representation of the steam zone volume as a function of time is not feasible, we concentrated on deriving bounds, asymptotic and approximate solutions instead.

An upper limit on the steam zone rate of growth and the expected recovery efficiency is provided by two upper bounds that are derived from the total thermal energy and the latent heat balances, respectively. Each of the two bounds assumes control of the rate of growth in certain time intervals depending on the heat transfer characteristics. In particular, under constant injection rates the bound based on the steam mass balance controls the rate of growth after some initial time has elapsed.

The asymptotic behavior of the solution at large times is obtained by a balance between the heat losses and the injection rates. It is shown

that the steam zone volume behaves as a parabolic function of time, at large times. This expansion is consistent with the upper and lower bounds description and is insensitive to variations in the horizontal conduction term and the injection rates, as long as R varies between 1 and ∞ , although the time of convergence does depend on R . The solution behaves more like an upper bound for small A and more like a lower bound for large A .

By formulating a quasi-steady state approximation for the heat transfer in the hot liquid zone, we were able to obtain an integral equation the numerical solution of which provides the steam zone volume as a function of time, under constant injection rates. The approximation seems to work pretty well in the cases studied which provides us with a fairly good tool for a uniform description of the solution.

The validity of the Marx-Langenheim solution has been carefully re-examined. It is shown that for large values of R (high injection rates) it describes the solution pretty well up until some critical time beyond which it increasingly deviates. This deviation becomes more significant as A decreases and for small A it may lead to high over-optimistic predictions. It is established that when $A < \frac{2}{\pi}$ the description based on the upper bounds gives a more realistic picture of the actual process. These conclusions have a significant importance on the design of a large class of actual field cases which operate at high injection temperatures and low downhole qualities.

Chapter V. Application to Two-Dimensional Reservoirs

5.1 Introduction

This final chapter consists of two parts. In Part A we generalize the discussion of Section 4.3 regarding upper bounds, to three-dimensional geometries where the steam zone assumes an arbitrary shape. Section 5.2 deals with reservoirs of small thickness where one can reasonably expect vertical fronts. The results obtained extend the validity of the results of Section 4.3 to reservoirs where the steam zone areal extent is non-symmetric due to areal inhomogeneities or the particular production pattern. In Section 5.3 and in Part B we consider three-dimensional systems that exhibit another kind of symmetry, along the lateral ($-y$) direction, in the so-called rectangular geometries, or along the angular ($-\theta$) coordinate, in the so-called radially symmetric geometries (see Figure 62). To facilitate the discussion, we isolate two particular modes of displacement, separable fronts (Subsection 5.3.3) and parabolic displacement (Subsection 5.3.5). In Part B we attempt to develop a model for the determination of the steam front shape for the above referred geometries (Section 5.5). The resulting partial differential equations are derived in Section 5.6, and their structure and methods of solution are further discussed in Section 5.7.

Part A. Integral Characterization of the Steam Zone Growth

5.2 Three-Dimensional Reservoirs with Vertical Fronts (Thin Reservoirs)

In thin reservoirs the steam front is vertical and the character of the displacement is essentially two dimensional (Figure 61). Due to the symmetry along the vertical ($-z$) direction, the integral balances (2.47),

(2.50) transform to:

$$\begin{aligned} \Delta T \frac{d}{dt} \int_{A_{fo}(t)} M_1 dA + \Pi_F(t) \Delta T \{W_F(t) + Q_F(t)\} + \frac{2}{h} \int_{A_{fo}(t)} \left(-k_{hf} \frac{\partial T_f}{\partial n} \right)_{II} dA \\ = [w_s(t) + w_w(t)] c_{pw} \Delta T + w_s(t) L_V^{(1)} \end{aligned} \quad (5.1)$$

$$\begin{aligned} \Delta T \frac{d}{dt} \int_{A_{fo}(t)} M_2 dA + \Pi_F(t) \Delta T Q_F(t) + \frac{2}{h} \int_{A_{fo}(t)} \left(-k_{hf} \frac{\partial T_f}{\partial n} \right)_{II} dA \\ = w_s(t) L_V^{(1)} \end{aligned} \quad (5.2)$$

where $A_{fo}(t)$ is the reservoir-overburden (or underburden) boundary surface, $\Pi_F(t)$ the perimeter of $A_{fo}(t)$, and $w_s(t)$, $w_w(t)$ are expressed per unit reservoir thickness. To derive upper bounds for the steam zone volume, we recall inequalities (3.20a), (3.20b), (3.20c), which are good for any geometry, and proceed along the lines of Subsection 4.3.1. Then, the following inequalities result:

$$\frac{d}{dt} \int_{A_{fo}(t)} f_j(x, y, t; A_{fo}(t)) dA + \frac{d}{dt} A_{fo}(t) < \phi_j(t) \quad \forall 0 < t \quad (5.3)$$

$$j = 1, 2$$

The similarity between (5.3) and (4.11) indicates that the analysis of Section 4.3 concerning one-dimensional upper bounds can be easily carried over to the present geometry, by simply substituting $\chi_F(t)$ by $A_{fo}(t)$, and $\chi_j^+(t)$ by $A_j^+(t)$. As a result, the properly non-dimensionalized quantities,

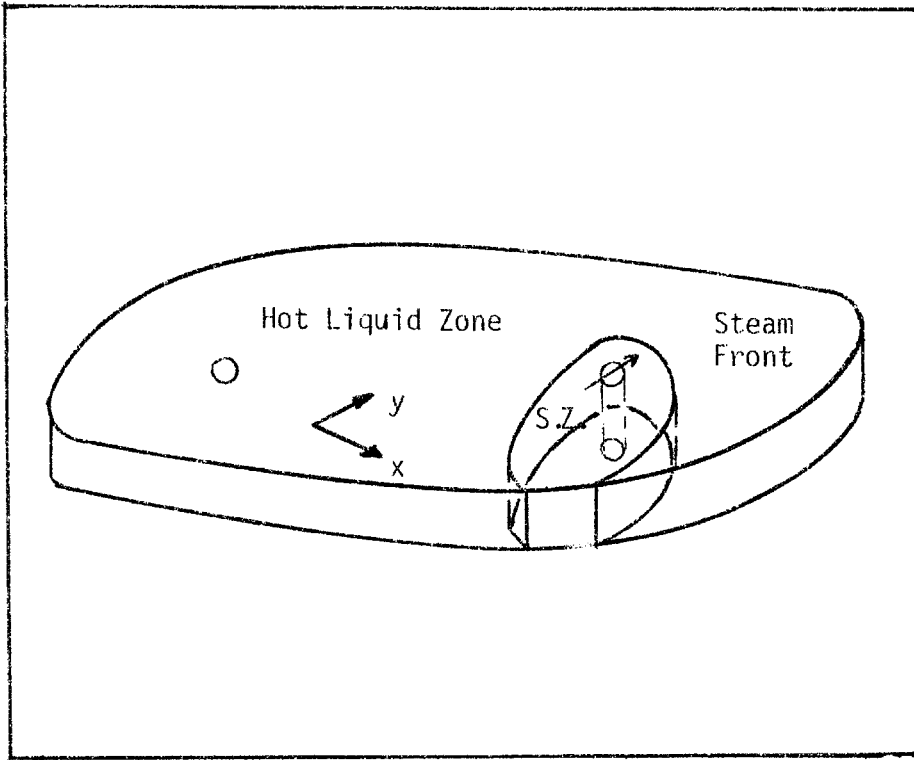


Figure 61. Two-Dimensional (Thin) Reservoirs
Examined in Section 5.2.

$A_{jD}^+(t)$ ($j = 1, 2$), defined by

$$2\dot{A}_{1D}^+(t_D) + \frac{A_{1D}^+(t_D)}{\sqrt{t_D}} = \phi_{1D}(t_D) \quad (5.4)$$

$$2\frac{B_1}{B_2}\dot{A}_{2D}^+(t_D) + \frac{A_{2D}^+(t_D)}{\sqrt{t_D}} = \phi_{2D}(t_D) \quad (5.5)$$

$$A_{jD}^+(0) = 0$$

are upper bounds to the dimensionless steam zone area of an arbitrary two-dimensional steam drive involving vertical fronts, for arbitrary injection rates. Similarly, the dimensionless Marx-Langenheim expression for such a geometry is simply given by:

$$2\dot{A}_{MLD}(t_D) + \int_0^{t_D} \frac{\dot{A}_{MLD}(\tau_D)d\tau_D}{\sqrt{t_D - \tau_D}} = \phi_{1D}(t_D) \quad (5.6)$$

[compare with Eq. (4.23)].

Clearly, the discussion in Section 4.3 regarding varying or constant injection rates and the lower bounds of Section 4.4 follow in a straightforward manner. In short, we are able to bound the steam zone area of a two-dimensional steam drive, regardless of the steam front shape, production pattern or areal inhomogeneities, as long as the front remains vertical. Obviously, this extends the region of validity of the results of the previous Sections 4.3, 4.4, to more realistic cases. On the other hand, all the approximate solutions to the steam zone growth that are based on the assumption of one-dimensional heat transfer (Sections 4.5, 4.6), cannot carry over to this geometry, in general. Similarly, a separate

analysis should be carried out for the determination of the saturation distribution inside a two-dimensional steam zone.

5.3 Three-Dimensional Fronts with One Degree of Symmetry (Rectangular or Radially Symmetric Geometry)

A more realistic case involves geometries that do not display vertical fronts. For simplicity of the discussion, we confine our attention to systems that exhibit one degree of symmetry along the lateral (-y) or the angular (- θ) direction (rectangular or radially symmetric) as shown in Figure 62.

5.3.1 Reformulation of the Integral Balances

In such a case the integral balances (2.47), (2.50) assume slightly simpler expressions. Terms of the form

$$\int_{V(t)} \psi(\underline{r}, t) d\underline{r}, \quad \int_{A_f(t)} \psi(\underline{r}, t) d\underline{r}$$

transform to

$$b \int_{A(t)} \bar{\psi}(r, t) dr, \quad b \left\{ \int_0^{L_{Fo}(t)} \bar{\psi}(x, t) dx + \int_0^{L_{Fu}(t)} \bar{\psi}(x, t) dx \right\}$$

and to

$$\int_{V(t)} \psi(r, t) dr, \quad \left\{ 2\pi \int_0^{R_{Fo}(t)} r\psi(r, t) dr + 2\pi \int_0^{R_{Fu}(t)} r\psi(r, t) dr \right\}$$

in the respective geometries. Here subscripts Fo, Fu stand for overburden

and underburden, respectively, $A(t)$ is the cross section of the steam zone along the plane of symmetry in rectangular geometries (Figure 62a).

In a uniform notation, we rewrite (2.47), (2.50) as follows:

$$\begin{aligned} \Delta T \frac{d}{dt} \int_{R(t)} M_1(r, t) dr + \Pi_F(t) \Delta T \{W_F(t) + Q_F(t)\} \\ + \left\{ \int_0^{X_{Fo}(t)} \left(-k_{hf} \frac{\partial T_f}{\partial n} \right) II \, dx + \int_0^{X_{Fu}(t)} \left(-k_{hf} \frac{\partial T_f}{\partial n} \right) II \, dx \right\} \\ = \phi_1(t) \end{aligned} \quad (5.7)$$

$$\begin{aligned} \Delta T \frac{d}{dt} \int_{R(t)} M_2(r, t) dr + \Pi_F(t) \Delta T Q_F(t) + \left\{ \int_0^{X_{Fo}(t)} \left(-k_{hf} \frac{\partial T_f}{\partial n} \right) II \, dx \right. \\ \left. + \int_0^{X_{Fu}(t)} \left(-k_{hf} \frac{\partial T_f}{\partial n} \right) II \, dx \right\} = \phi_2(t) \end{aligned} \quad (5.8)$$

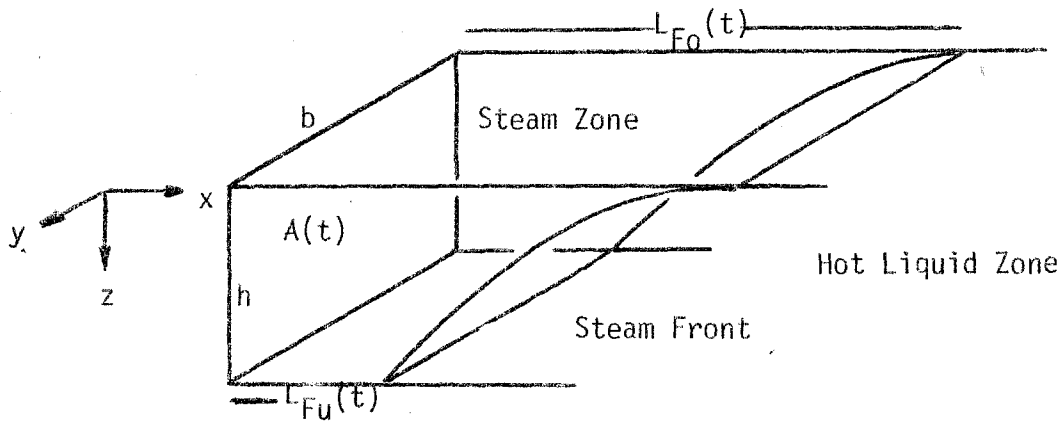
where $R(t)$ stands for $A(t)$ or $V(t)$, $X_{Fo}(t)$ and $X_{Fu}(t)$ represent boundary length or area, and $\Pi_F(t)$ refers to steam front perimeter or steam front area, in rectangular or radially symmetric geometries, respectively.

In deriving rigorous upper bounds, we employ inequalities (3.20a), (3.20b), (3.20c), as before, to obtain

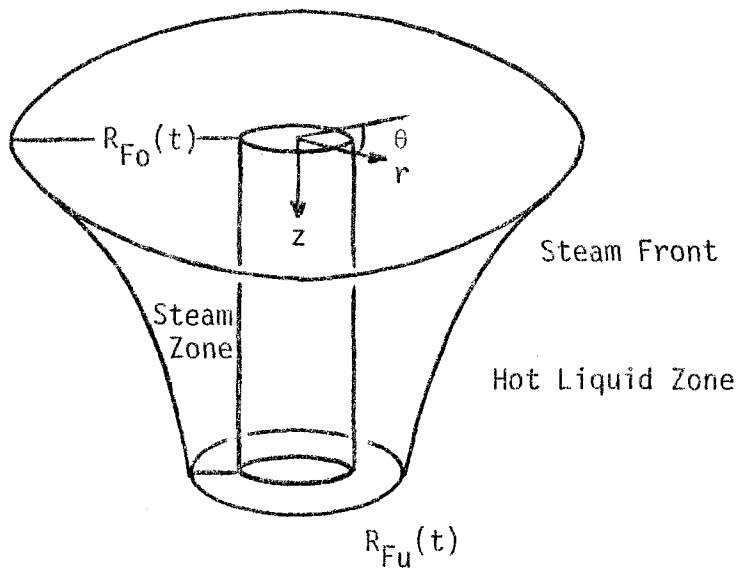
$$\begin{aligned} \frac{d}{dt} \int_{R(t)} i_j(x, z, t) dx dz + \frac{d}{\sqrt{t}} \cdot \left\{ h \frac{(X_{Fo}(t) + X_{Fu}(t))}{2} \right\} < \phi_j(t) \quad \forall 0 < t \\ j=1,2 \end{aligned} \quad (5.9)$$

which is a generalized version of the one-dimensional constraints, (4.11).

In particular, the heat losses term has a spatial dependence given by the



a. Rectangular



b. Radially Symmetric

Figure 62. Three-Dimensional Geometries Examined in Chapter V.

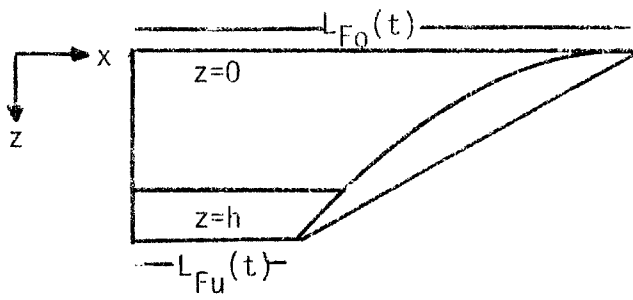
expression $\frac{h(X_{Fo}(t) + X_{Fu}(t))}{2}$ [compared to $hX(t)$] which represents the area of a trapezoidal with sides $L_{Fo}(t)$, $L_{Fu}(t)$ (Figure 63a), or the volume of the frustum of a paraboloid of revolution with sides of area $A_{Fo}(t)$, $A_{Fu}(t)$ (Figure 63b), in rectangular or radial geometries, respectively. Since the area (volume) $A(t)$ of $R(t)$ is a function of time alone, we can define F , a function of $A(t)$, such that

$$F(A) = \frac{h(X_{Fo}(t) + X_{Fu}(t))}{2} \quad (5.10)$$

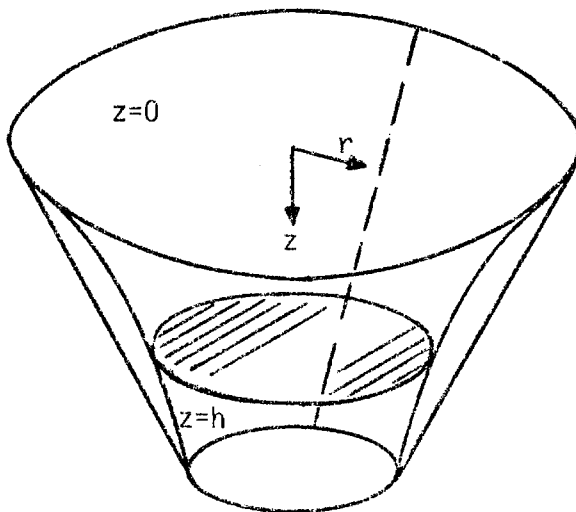
The function F characterizes the steam front shape in an integral sense and varies with the assumed kind of displacement. For example, for vertical fronts (Section 5.2), $F(A) = A$. Once the steam front shape is known, one is able to calculate F explicitly as a function of A .

5.3.2 The Assumption of Uniform Propagation

Because of the many complexities associated with the determination of the steam front shape of a three-dimensional steam drive, (Section 5.6), we elect instead to proceed by introducing certain assumptions regarding the properties of the displacement. In so doing, we will get information regarding the zone volume rate of growth without recourse to the exact solution of the steam front shape. We first introduce the assumption of uniform propagation, which postulates that the function $F(A)$, defined by Eq. (5.10), is an increasing function of the steam zone extent, A . In other words, we assume that the arithmetic mean area (volume) increases with the steam zone area (volume). The assumption is expected to be valid as long as the heat losses to the surroundings are the controlling factor in the propagation of the



a.



b.

Figure 63. Trapezoidal (a) and frustum of a cone (b) referred to in Subsection 3.5.2.

steam zone, and there are no acute inhomogeneities inside the oil reservoir, such as a highly permeable streak. It is also expected that the assumption is not valid in cases of unstable propagation that favor growth of "fingers".

We can now define $A_j^+(t)$ such that

$$\frac{d}{dt} \int_{A_j^+(t)} f_j(\underline{r}, t) dx dz + \frac{d}{\sqrt{t}} F(A_j^+(t)) = \phi_j(t) \quad (5.11)$$

$$A_j^+(0) = 0 \quad j = 1, 2$$

Using the dimensionless notation of Chapter IV and invoking the constant average saturation assumption, we recast (5.11) in the form:

$$2 \frac{B_j}{B_1} \dot{A}_{jD}^+(t_D) + \frac{1}{\sqrt{t_D}} F_D(A_{jD}^+(t_D)) = \phi_{jD}(t_D) \quad (5.12)$$

$$A_{jD}^+(0) = 0 \quad j = 1, 2$$

In view of the above assumption, one can then prove (Appendix X) that $A_{jD}^+(t_D)$ ($j = 1, 2$) are two independent upper bounds of $A_D(t)$, for any injection rates, just as in the one-dimensional case. In an analogous manner, we can develop the three-dimensional analog of the Marx-Langenheim solution

$$2 \dot{A}_{MLD}(t_D) + \int_0^{t_D} \frac{F_D(A_{MLD}(\tau_D))}{\sqrt{t_D - \tau_D}} d\tau_D = \phi_{1D}(t_D) \quad (5.13)$$

$$A_{MLD}(0) = 0$$

Equation (5.12) is a first order, non-linear ODE, the solution of which largely depends on the functional form of the unknown function $F_D(A_D)$. The determination of the front shape (and F_D) is fully discussed in Sections 5.5, 5.6. Here, we shall only develop the solution of (5.12) when F_D assumes simple functional forms. Such an approach, although approximate in nature, will significantly clarify the effect of the steam front shape in the performance of a steam drive.

5.3.3 Vertical Fronts

When the front remains vertical to the bedding plane, $F_D(A_D) = A_D$ and the uniform propagation assumption is satisfied. Then, Eq. (5.12) reduces to the well studied Eqs. (4.19), (4.20) (Sections 4.3, 5.2).

5.3.4 Separable Fronts

A more general linear dependence is provided by the relationship $F_D(A_D) = \kappa A_D$, where κ is a positive constant. Such fronts have the property that the area of any cross section of the steam zone parallel to the reservoir bedding plane is a separable function of time and the vertical coordinate. In dimensionless notation

$$X_D(z_D, t_D) = T_D(t_D)Z_D(z_D) \quad \forall \quad 0 < t_D, \quad 0 < z_D < 1 \quad (5.14)$$

where T_D , Z_D are arbitrary functions (see Figure 63). We refer to fronts with this property as separable fronts. From (5.14) one deduces that the ratio of the areas of any two cross sections of the steam zone is constant

with time. In particular, the ratio of the leading to the trailing edges

$\frac{x_D(0,t_D)}{x_D(1,t_D)} = \frac{Z_D(0)}{Z_D(1)}$ remains constant and so does the vertical sweep efficiency of the steam drive, E_v , defined as the ratio of the steam zone area (volume) to the area (volume) under the steam zone's leading edge [Baker (1973)]

$$E_v = \frac{\int_0^1 Z_D(z_D) dz_D}{Z_D(0)} \quad (5.15)$$

In view of the above, the parameter κ assumes the form

$$\kappa = \frac{Z_D(0) + Z_D(1)}{2 \int_0^1 Z_D(z_D) dz_D} \quad (5.16)$$

which is the ratio of the area (volume) of a trapezoidal (paraboloid of revolution) with sides $Z_D(0)$ and $Z_D(1)$, to the area (volume) of the steam zone.

Experimental evidence [Baker (1973), van Lookeren (1977)] suggests that fronts of this type are actually realized under both laboratory and field conditions. van Lookeren (1977) developed a simplified model for the determination of the front shape in a three-dimensional, radially symmetric steam drive, which enables us to express κ in terms of the physical parameters of the system. In our notation, his model is equivalent to:

$$x_D(z_D, t_D) = \tau_D(t_D) \exp \left\{ -\frac{2z_D^2}{A_R^2} \right\} \quad (5.17)$$

$$A_R = \left\{ \frac{\mu_s m_s}{\pi(\rho_0 - \rho_s) g h^2 k \rho_s} \right\}^{1/2} \quad (5.18)$$

then

$$\kappa = \frac{\sqrt{2}}{\sqrt{\pi}} \frac{[1 + \exp(-2/A_R^2)]}{A_R \operatorname{erf}[\sqrt{2}/A_R]} \quad (5.19a)$$

which, when $A_R < \frac{1}{\sqrt{2}}$, simplifies to

$$\kappa \approx \frac{\sqrt{2}}{A_R \sqrt{\pi}} = \left[\frac{2(\rho_0 - \rho_s) g h^2 k \rho_s}{\mu_s m_s} \right]^{1/2} \quad (5.19b)$$

Expression (5.19b) shows that in this case κ varies inversely proportional to the dimensionless group A_R . For a typical radial steam drive (Table 6 of Section 4.3) we estimate $\kappa = 2.65$.

In Section 5.7, we derive an analogous model for a stable radial steam drive. Now the z_D dependence and the group A_R are slightly different

$$x_D(z_D, t_D) = T_D(t_D) \exp \left\{ \frac{2(1 - z_D)}{A_R^2} \right\} \quad (5.20)$$

$$A_R = \left\{ \frac{(1 - N) \left[(m_s + m_w) c_{pw} \Delta T + m_s L_v^{(1)} \right] \left[\sum_{i=w,0} \frac{\rho_i^{(2)} c_{pi}}{N_i^{II}} \right]}{\pi h^2 k g \Delta T \left[\sum_{i=s,w,0} \frac{\rho_i^{(1)} c_{pi}}{N_i^I} + \rho_s \frac{L_v^{(1)}}{\Delta T} \right] \left[\sum_{i=w,0} \rho_i^{(2)} c_{pi} \left(\frac{k_{ri}}{\mu_i} \right)^{II} (\rho_i - \rho_s) \right]} \right\}^{1/2} \quad (5.21)$$

where, N_i^I , N_i^{II} are defined in Subsection 5.5.1.2. Based on this model the parameter κ becomes:

$$\kappa = \frac{1}{2A_R^2} \cdot \frac{[1 + \exp(-2/A_R^2)]}{[1 - \exp(-2/A_R^2)]} \quad (5.22)$$

which varies inversely proportional to the square of A_R , for small A_R .

Both models above demonstrate the usefulness of the concept of separable fronts in simulating a three-dimensional steam drive. Table 12 shows values of the parameter κ calculated from (5.19b), for the various field projects reported by Myhill and Stegemeier (1978).

Returning to Eq. (5.12), we now define the upper bounds $A_{jD}^+(t_D)$:

$$2 \frac{B_j}{B_1} \dot{A}_{jD}^+(t_D) + \frac{\kappa A_{jD}^+(t_D)}{\sqrt{t_D}} = \phi_{jD}(t_D) \quad (5.23)$$

$$A_{jD}^+(0) = 0 \quad j = 1, 2$$

which admit the following solution, in case of constant injection:

$$A_{1D}^+(t_D) = \frac{1}{\kappa^2} \left\{ \kappa \sqrt{t_D} - 1 + \exp[-\kappa \sqrt{t_D}] \right\} \quad (5.24)$$

$$A_{2D}^+(t_D) = \frac{A}{\kappa^2} \left\{ \kappa \sqrt{t_D} - B + B \exp \left[-\frac{\kappa \sqrt{t_D}}{B} \right] \right\} \quad (5.25)$$

Notice that expressions (5.24), (5.25) can be obtained from the respective one-dimensional ones, Eqs. (4.29), (4.30) by simply rescaling the dimensionless rates by $1/\kappa$ and the dimensionless time by κ^2 . Therefore, the equivalent Marx-Langenheim model in three dimensions would simply be:

$$A_{MLD}(t_D) = \frac{2}{\pi \kappa} \left\{ \kappa \sqrt{t_D} - 1 + \exp \left[\frac{\pi \kappa^2 t_D}{4} \right] \operatorname{erfc} \left[\frac{\kappa \sqrt{\pi t_D}}{2} \right] \right\} \quad (5.26)$$

<u>Field</u> *	<u>κ</u>
Brea ("B" Sand)	15.34
Coalinga (Section 27, Zone 1)	2.83
El Dorado (NW pattern)	2.17
Inglewood	2.34
Kern River	5.25
Schoonebeek	4.25
Slocum (Phase 1)	2.28
Smackover	0.90
Tatums (Hefner steam drive)	2.65
Tia Juana	9.70
Yorba Linda ("F" Sand)	1.98

* Calculations based on a reservoir permeability of $2 \mu\text{m}^2$.

Values of the parameter κ for field cases reported
by Myhill and Stegemeier (1978)

Table 12

The above equations reduce to their one-dimensional analogues when $\kappa = 1$, as expected. Figures 64, 65, 66 plot $A_{1D}^+(t_D)$, $A_{2D}^+(t_D)$, $A_{MLD}(t_D)$ for various characteristic values of κ and $A = 0.5$. Comparison with the one-dimensional case reveals that the relative magnitude of κ plays an important role in the growth rate of the steam zone area (volume). When $\kappa < 1$, i.e. when the steam zone area (volume) is larger than the corresponding trapezoidal (or paraboloid of revolution) of Figure 63, the two upper bounds and the M-L expression are larger than the ones corresponding to $\kappa = 1$. On the other hand, when $\kappa > 1$, i.e. when the steam zone area (volume) is smaller than in the corresponding trapezoidal (or paraboloid by revolution), the upper bounds and the Marx-Langenheim expression are smaller than in the case $\kappa = 1$ (see Figures 65, 66). These effects are more pronounced as κ becomes smaller or larger, respectively. (Figures 64, 66). For example, when $\kappa = 2$ the calculated upper bounds and the M-L expression are smaller than half the values of the expressions corresponding to $\kappa = 1$. Even lower values are obtained when $\kappa = 5$ (Figure 66).

The effects of the relative magnitude of κ can be physically interpreted as follows: When $\kappa > 1$, the steam zone tends to propagate along the top of the reservoir more rapidly, due to (5.16), thus creating a finger (tongue) which grows with time faster than the remaining part of the steam zone (Figure 67a). This effect, usually called gravity override, is largely due to the large density difference between the displacing (steam) and displaced (water and oil) phases and is very frequently occurring in three-dimensional steam drives. As one can see from (5.19b), the override is favored by a large density difference, steam mobility and reservoir thickness but decreases with the increasing injection rate. On the other hand, when $\kappa < 1$,

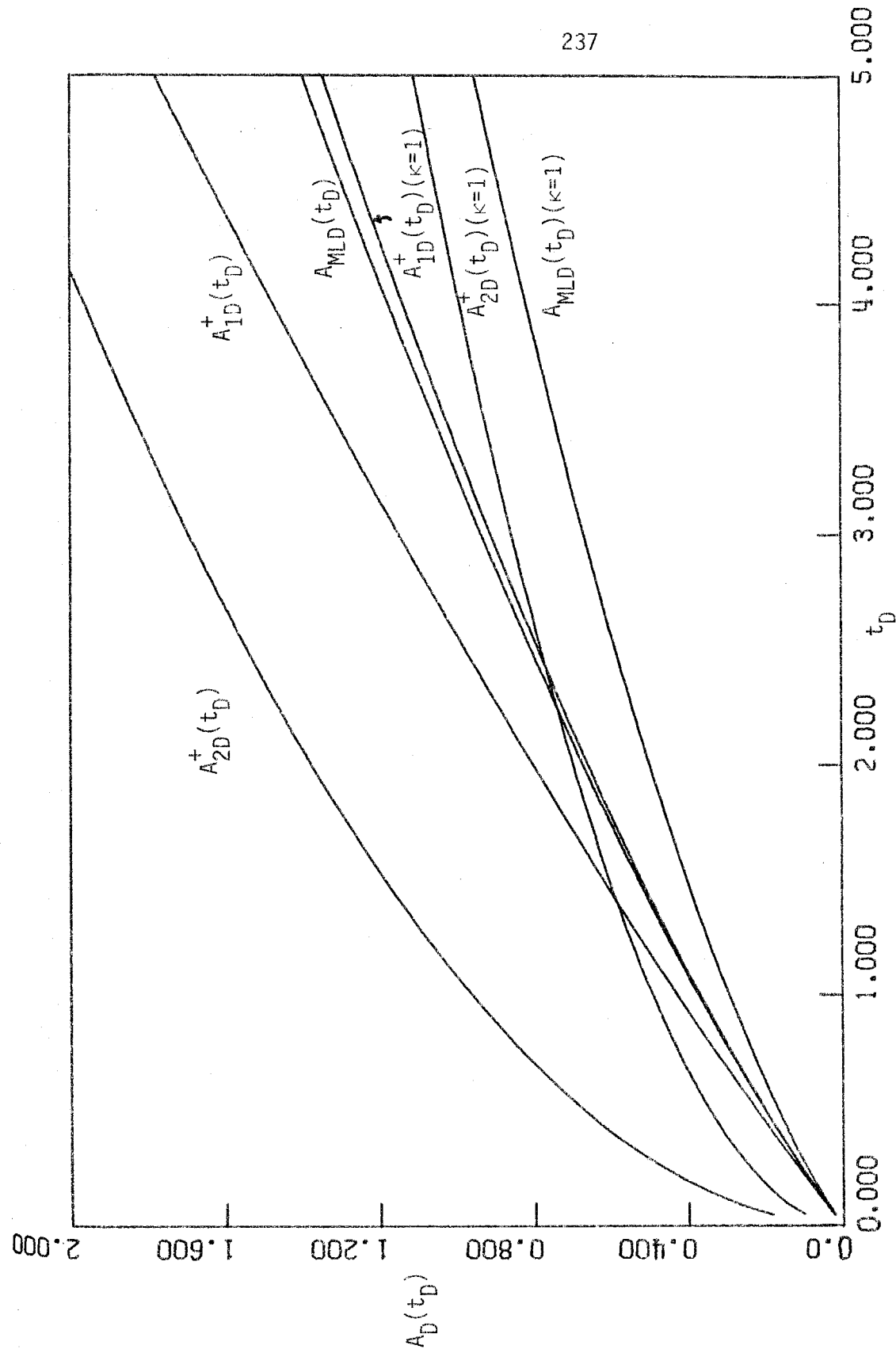


Figure 64. Upper Bounds A_{1D}^+ , A_{2D}^+ and the Marx-Langenheim Solution A_{MLD} for $\kappa = 0.5$, $T_s = 250^\circ\text{C}$, $f_{st} = 0.56$. (Separable Displacement) Also Plotted A_{1D}^+ , A_{2D}^+ , A_{MLD} for $\kappa = 1.0$.

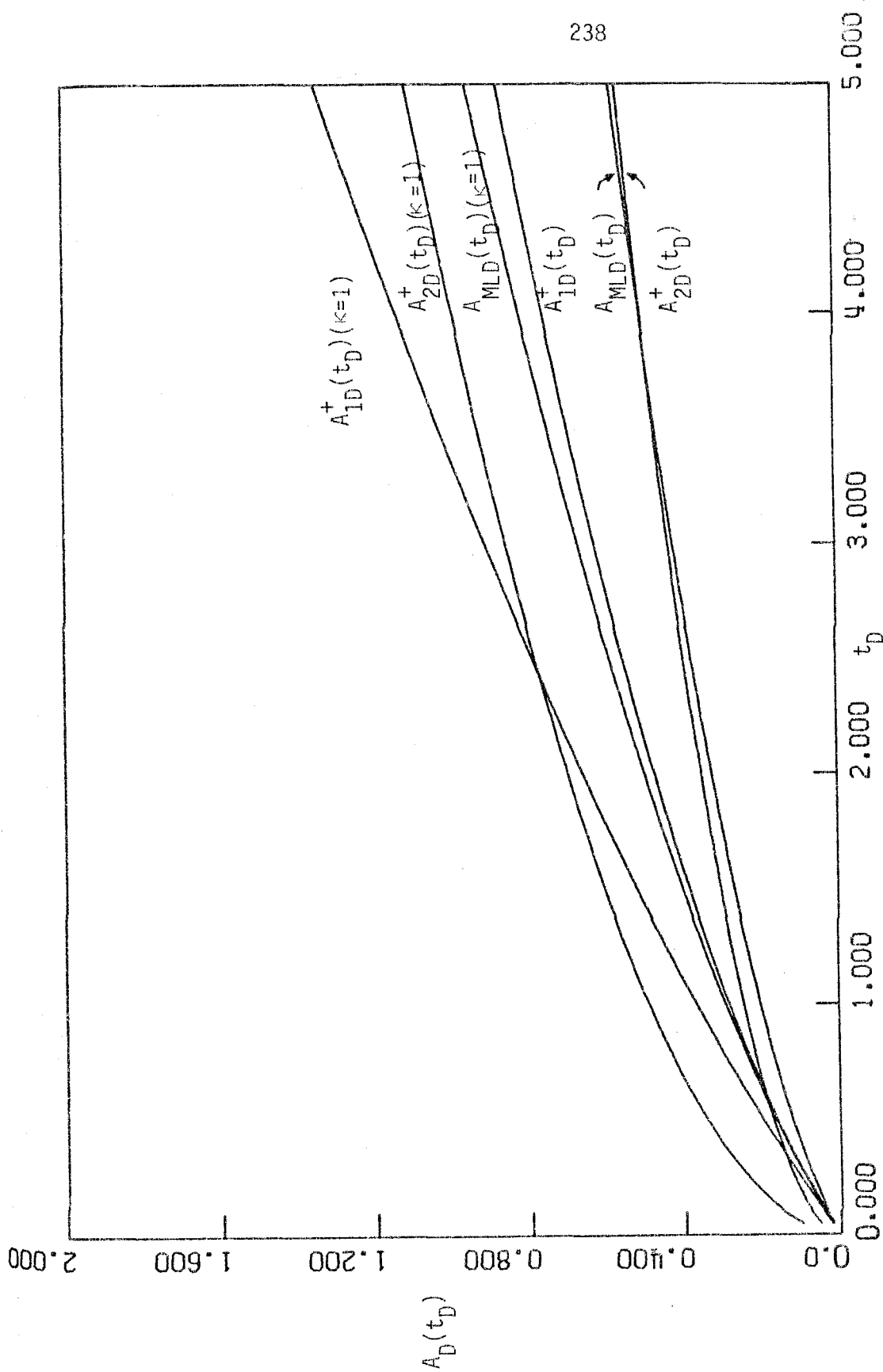


Figure 65. Upper Bounds A_{1D}^+ , A_{2D}^+ and the Marx-Langenheim Solution A_{MLD} for $\kappa = 2.0$,

$T_s = 250^\circ\text{C}$, $f_{st} = 0.56$. (Separable Displacement) Also Plotted A_{1D}^+ , A_{2D}^+ ,

A_{MLD} for $\kappa = 1.0$.

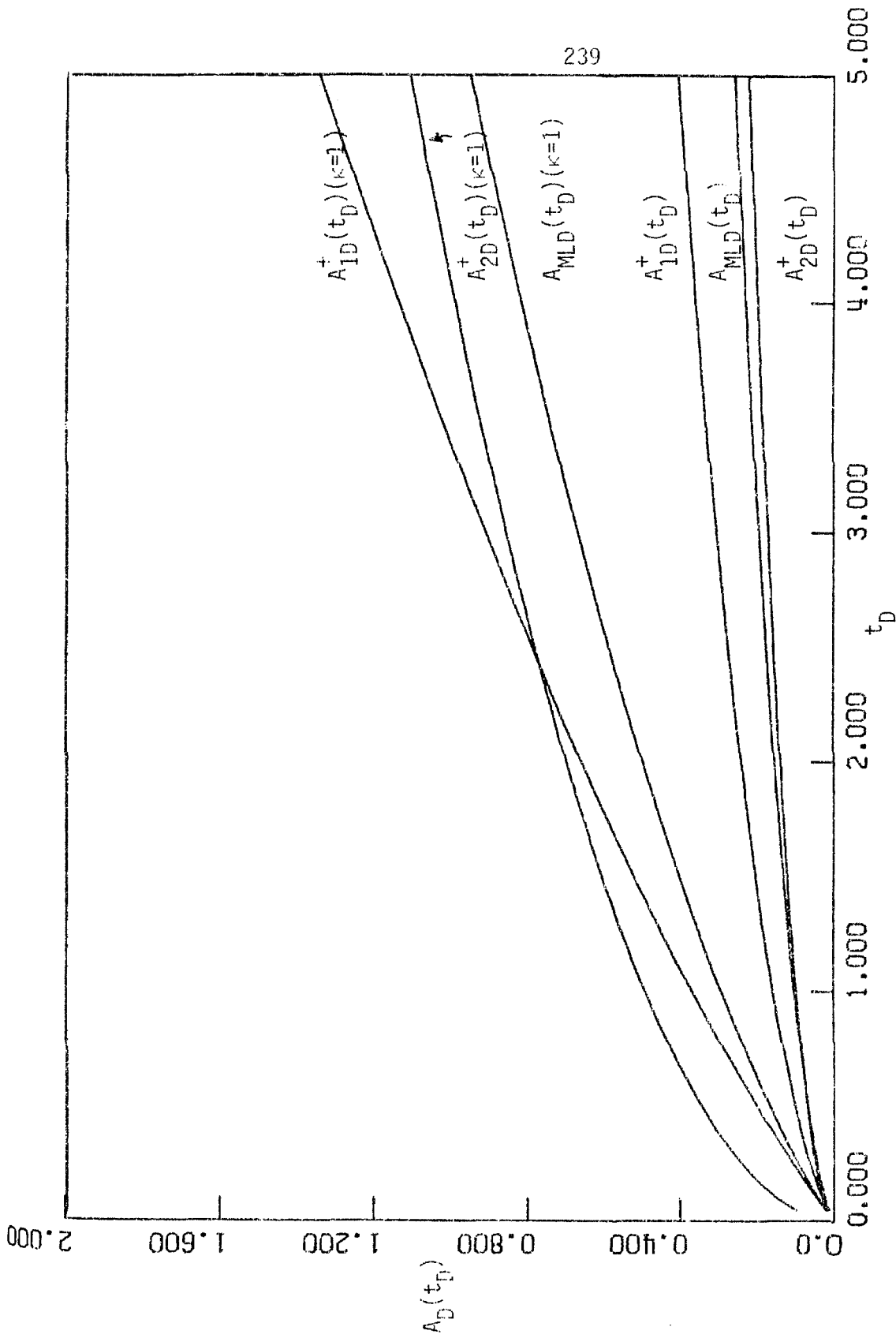


Figure 66. Upper Bounds A_{1D}^+ , A_{2D}^+ and the Marx-Langenheim Solution A_{MLD} for $\kappa = 5.0$, $T_s = 250^\circ\text{C}$, $f_{st} = 0.56$. (Separable Displacement) Also Plotted A_{1D}^+ , A_{2D}^+ , A_{MLD} for $\kappa = 1.0$.

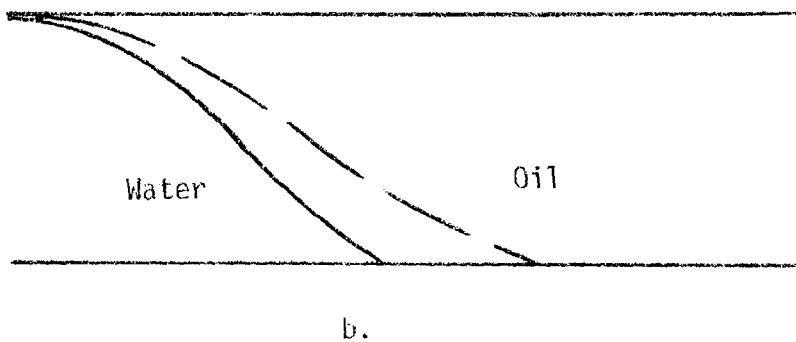
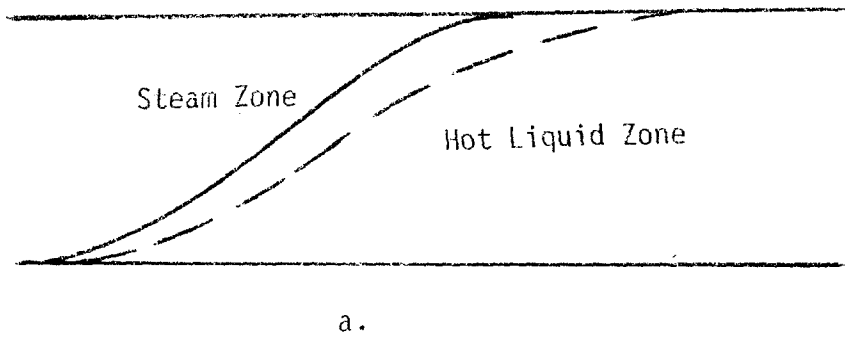


Figure 67. Tongue(Finger) Formation Due to Gravity Segregation.
(a) Override.
(b) Underrun. (Not Realized in Steam Drive)

the steam zone tends to propagate along the middle of the reservoir (Figure 67b) resulting in less heat loss. Such situation, although common practice when the displacing phase is more dense than the displaced one [Chuoque et al. (1959)], is not realized under steam injection conditions and, therefore, we will not carry the discussion any further.

We can, thus, conclude that if we ignore any geometrical or gravity considerations, and estimate the steam zone area (volume) by employing the usual one-dimensional methods ($\kappa = 1$), we introduce an error which may be very significant [compare with Blevins and Billingsley (1975)]. In fact, if the three-dimensional character of the process is not properly recognized, the oil recovery is overestimated by about 100% in a typical case ($\kappa = 2.65$) and by about 400% when $\kappa = 5$.

Another interesting observation can be made regarding the region of applicability of the upper bound A_{1D}^+ and the Marx-Langenheim solution, A_{MLD} , in its modified form. As evidenced from Figures 65, 66, both curves cross over the upper bound A_{2D}^+ much earlier when $\kappa > 1$ than when $\kappa = 1$ and this is shown to become pronounced as κ becomes larger. Table 13 shows the values of the time instants t_{Da} , $t_{D\alpha}$ when this occurs, for various values of κ and for $A = 0.5$. Notice that, as in Section 4.3, a necessary condition for A_{2D}^+ and A_{MLD} to intersect is $A < \frac{2}{\pi}$. Consequently, the upper bound A_{2D}^+ assumes control of the growth of the steam zone much earlier when $\kappa > 1$ and, for this reason, describes the steam zone rate of growth more accurately than the upper bound A_{1D}^+ and the modified Marx-Langenheim solution, for a larger time domain.

κ	$t_{D\alpha}$	$t_{D\alpha}$
1.0	2.5395	15.4716
1.5	1.1286	6.8762
2.0	0.6348	3.8679
2.5	0.4063	2.4754
3.0	0.2821	1.7190
3.5	0.2073	1.2629
4.0	0.1587	0.9669
4.5	0.1254	0.7640
5.0	0.1015	0.6188

Values of t_{Da} , t_D for various values
of κ and $A = 0.5$.

Table 13

5.3.5 Parabolic Displacement

In the last subsection we dealt with steam drives characterized by the linear expression $F_D(A_{FD}) = \kappa A_{FD}$. It is interesting to see how other functional forms influence the steam zone propagation. In this context, we will examine the parabolic form $F_D(A_{FD}) = \lambda A_{FD}^2$, λ a positive constant. To the author's knowledge, fronts of this type have not been reported in either theoretical or experimental investigations. Still, we are interested in studying the solutions they give rise to, in order to shed some light in displacements governed by a stronger-than-linear dependence of F_D on A_{FD} . Our upper bounds are now defined by

$$2 \frac{B_j}{B_1} \dot{A}_{jD}^+(t_D) + \lambda \frac{[A_{jD}^+(t_D)]^2}{\sqrt{t_D}} = \Phi_{jD}(t_D) \quad (5.27)$$

$$A_{jD}^+(0) = 0 \quad j = 1, 2$$

which admits an exact solution, in the case of constant injection rates.

To show this, we introduce the variables $\tau_{1D} = \sqrt{t_D}$ and $\tau_{2D} = \sqrt{\frac{A}{B}} \cdot \sqrt{t_D}$ and rewrite (5.27):

$$\frac{dA_{1D}^+(\tau_{1D})}{d\tau_{1D}} + \lambda [A_{1D}^+(\tau_{1D})]^2 = \tau_{1D} \quad (5.28a)$$

$$A_{1D}^+(0) = 0$$

$$\frac{dA_{2D}^+(\tau_{2D})}{d\tau_{2D}} + \left(\frac{\lambda}{\sqrt{AB}} \right) [A_{2D}^+(\tau_{2D})]^2 = \tau_{2D} \quad (5.28b)$$

$$A_{2D}^+(0) = 0$$

Equations (5.28a), (5.28b) are of a particular Ricatti type that gives rise to analytical solutions [Davis (1962)]. In terms of the original time variables, the solutions read

$$A_{1D}^+(t_D) = \frac{t_D^{1/4} I_{2/3} \left(\frac{2}{3} t_D^{3/4} \lambda^{1/2} \right)}{\lambda^{1/2} I_{-1/3} \left(\frac{2}{3} t_D^{3/4} \lambda^{1/2} \right)} \quad (5.29)$$

$$A_{2D}^+(t_D) = \frac{A^{1/2} t_D^{1/4}}{\lambda^{1/2}} \cdot \frac{I_{2/3} \left(\frac{2}{3} \frac{A^{1/2}}{B} t_D^{3/4} \lambda^{1/2} \right)}{I_{-1/3} \left(\frac{2}{3} \frac{A^{1/2}}{B} t_D^{3/4} \lambda^{1/2} \right)} \quad (5.30)$$

where $I_\nu(z)$ the modified Bessel function of the first kind of order ν .

The parameter λ is again a function of the physical variables of the system. Figures 68, 69, 70 plot the two bounds $A_{1D}^+(t_D)$, $A_{2D}^+(t_D)$ as a function of time for $\lambda = 0.1, 1, 10.0$. The upper bound $A_{2D}^+(t_D)$ is initially larger than $A_{1D}^+(t_D)$, but later crosses below $A_{1D}^+(t_D)$, just as in the linear case. As it is expected, the larger λ the slower the rate of steam zone growth. An asymptotic analysis reveals that as $t_D \rightarrow \infty$

$$A_{1D}^+(t_D) \sim t_D^{1/4} / \lambda^{1/2} \quad (5.31a)$$

$$A_{2D}^+(t_D) \sim A^{1/2} t_D^{1/4} / \lambda^{1/2} \quad (5.31b)$$

which indicates that the growth of the steam zone is much slower ($\sim t_D^{1/4}$) than in the previous case ($\sim t_D^{1/2}$). It is also easily shown that when the dependence of F_D in A_{FD} is given by the general non-linear relationship $F_D = A_{FD}^n$, where n positive, the rate of growth behaves asymptotically $\sim t_D^{1/2n}$. One can, thus, conclude that when the steam front obeys a higher order relationship the estimated oil recovery is smaller

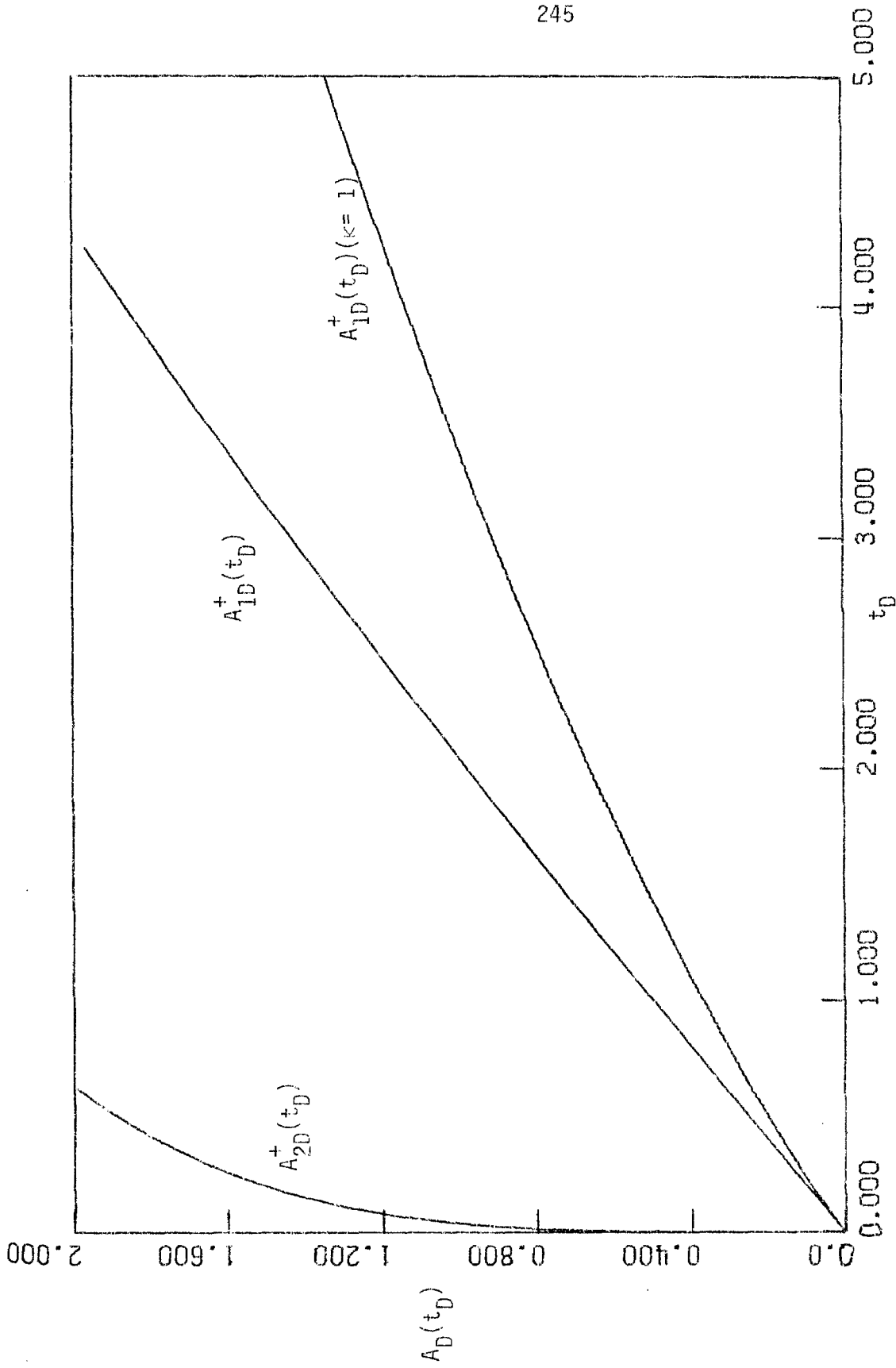


Figure 68. Upper Bounds A_{1D}^+ , A_{2D}^+ for $\lambda = 0.1$, $T_s = 250^\circ\text{C}$, $f_{st} = 0.56$.
(Parabolic Displacement). Also Plotted $A_{1D}^+(t_D)$ for $\kappa = 1.0$.

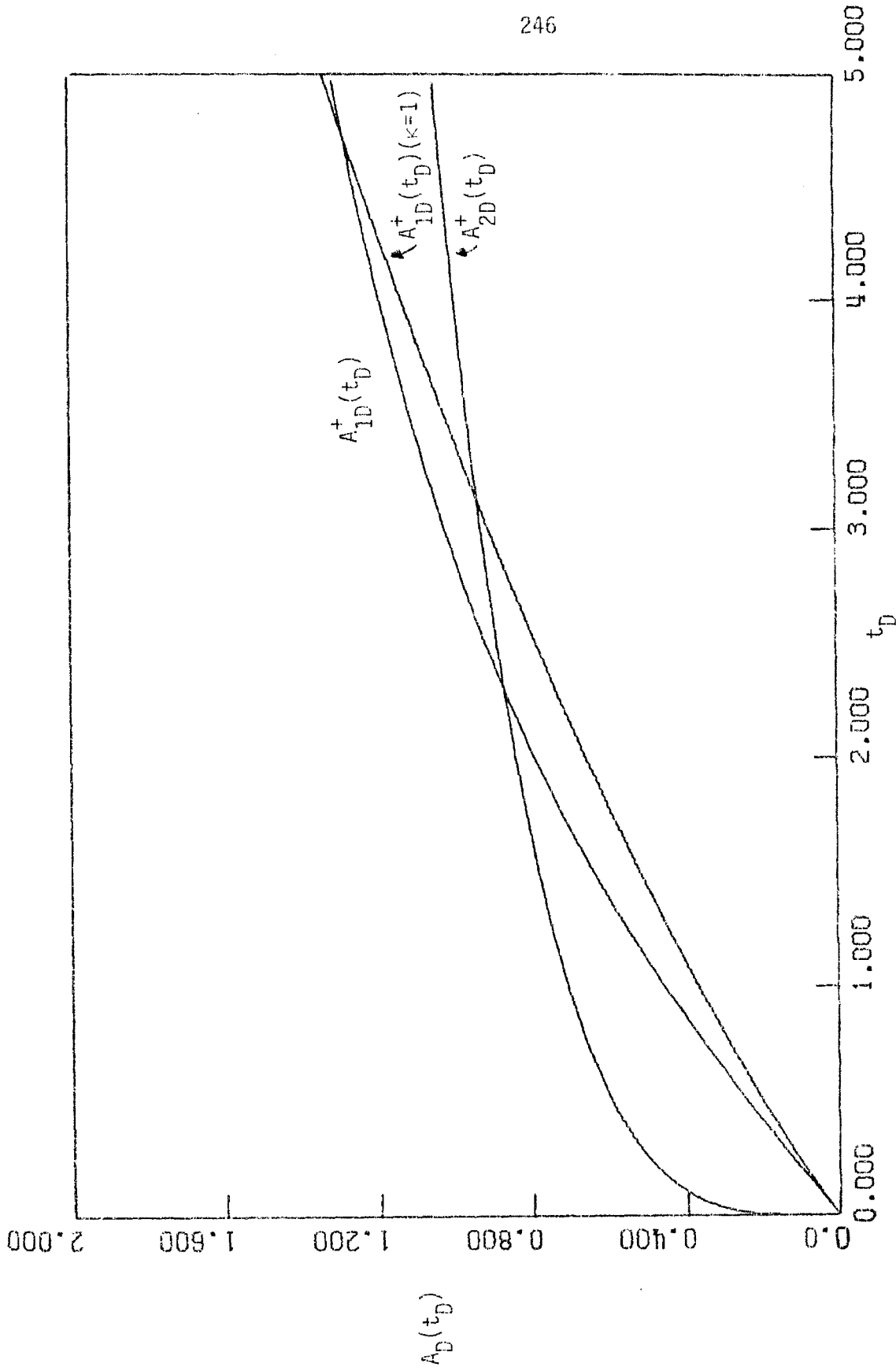


Figure 69. Upper Bounds A_{1D}^+ , A_{2D}^+ for $\lambda = 1.0$, $T_s = 250^\circ\text{C}$, $f_{st} = 0.56$.
(Parabolic Displacement.) Also Plotted $A_{1D}^+(t_D)$ for $\kappa = 1.0$.

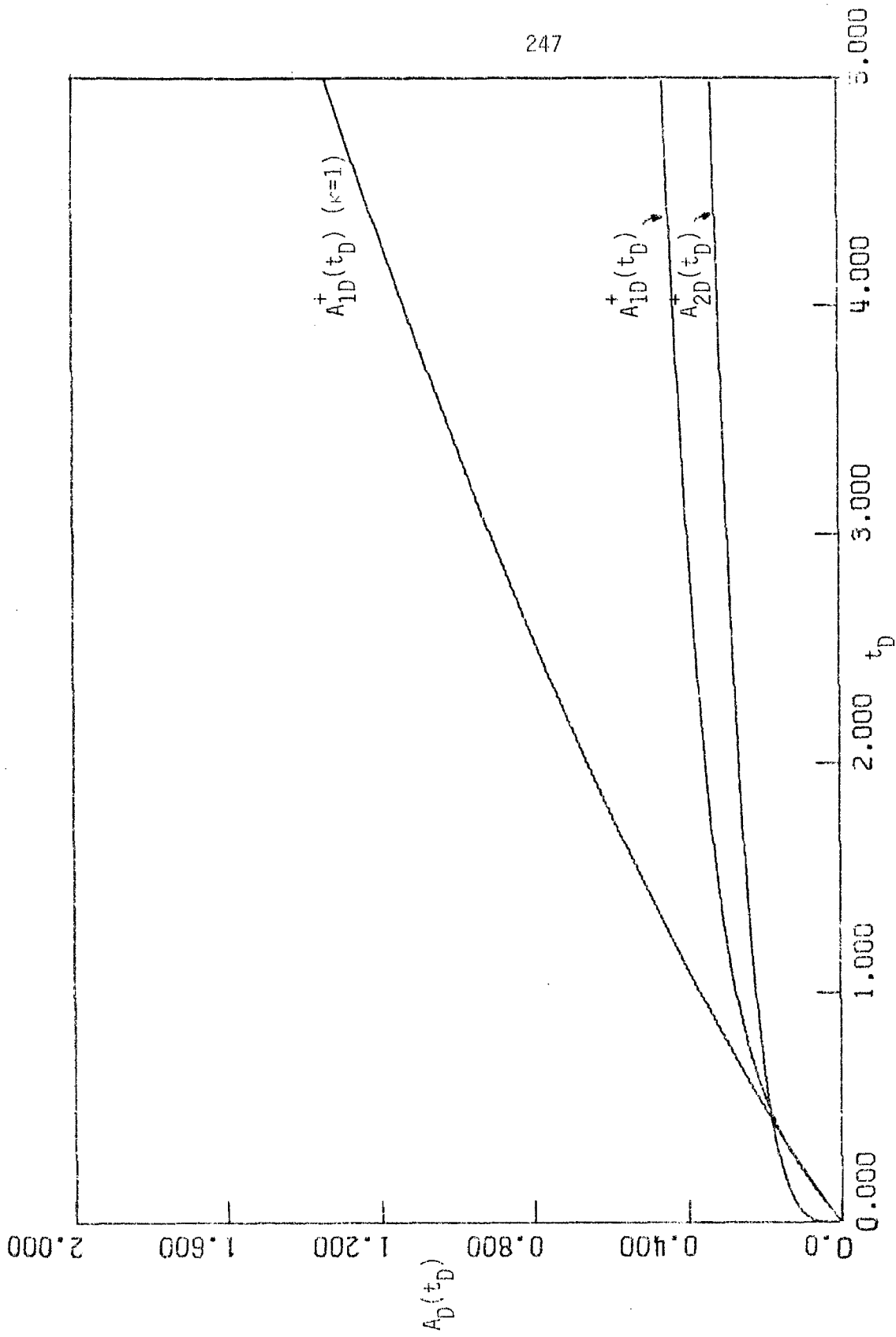


Figure 70. Upper Bounds A_{1D}^+ , A_{2D}^+ for $\lambda = 10.0$, $T_s = 250^\circ\text{C}$, $f_{st} = 0.56$ (Parabolic Displacement). Also Plotted $A_{1D}^+(t_D)$ for $\kappa = 1.0$.

than the recovery predicted when the function F_D is linear.

Part B. Determination of the Steam Front Shape

5.4 Introductory Remarks

In Sections 5.2, 5.3 we stressed the importance attached to integral characteristics of the steam front shape in estimating the steam zone volume growth rate and the vertical efficiency of the process. As already indicated, gravity plays a most important role in the front shape evolution by forcing the steam zone to spread along the top of the reservoir much faster than at the bottom (see Fig. 67). As a result, at the time when steam breaks through the producing well, which for all practical purposes spells the termination of the process, a significant portion of the original oil in place has been bypassed by the leading edge of the steam front and cannot be recovered. It is imperative that the mechanism of this displacement be well understood, so that appropriate control policies can be developed to improve the vertical efficiency and increase oil recovery. The first reported attempt to tackle this complex problem analytically was undertaken by Neuman (1975), who obtained results of rather limiting validity. Recently, van Lookeren (1977) constructed simple models for stable displacement, which however, neglect the important effect of heat losses to the surroundings. The absence of a reliable model for the important effect of gravity override calls for additional research in this area.

In this section we will devote our efforts to the description of the dynamics of the steam front shape by using the line (area) averaging method outlined in Section 2.4. The method borrows concepts and assumptions frequently employed in the modelling of two-dimensional, isothermal,

immiscible displacement . In addition, we will incorporate the two-dimensional heat transfer considerations developed in Section 3.6, in order to account for the complicated mechanism of heat transfer to the surroundings and the hot liquid zone. For simplicity, we will limit, as before, our discussion to symmetric (rectangular and radially symmetric) geometries.

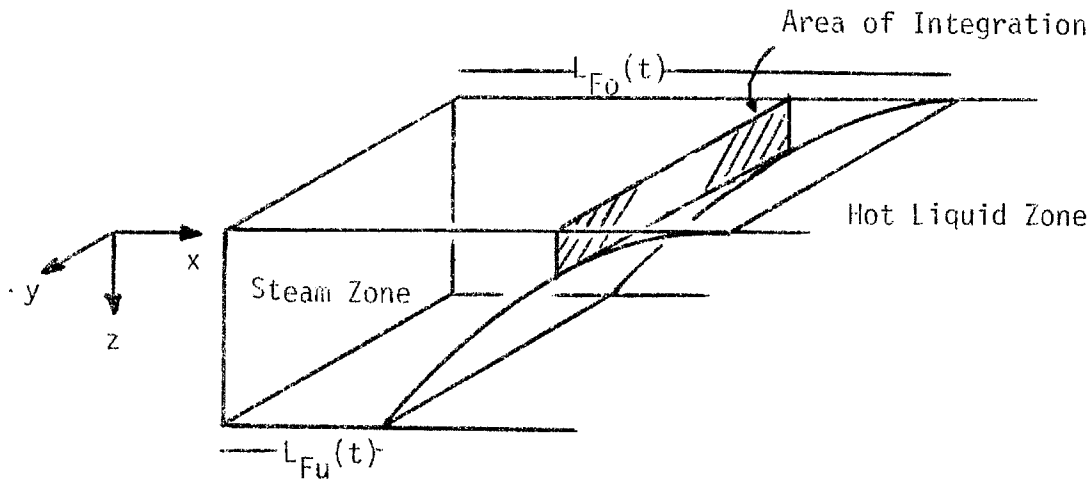
5.5 Mathematical Formulation

In the notation of Section 2.4, the energy balance at (x,t) averaged over the thickness of the steam zone, (Fig. 71), reads [Eq. (2.54)]:

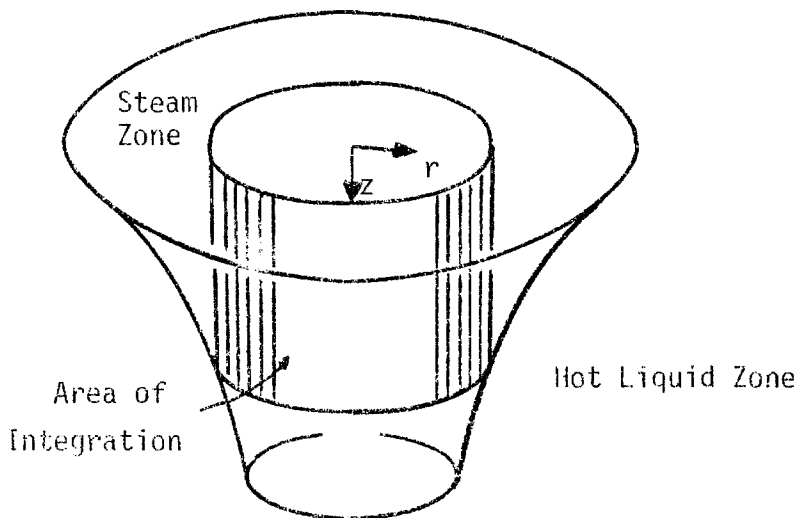
$$\begin{aligned} \Delta T \frac{d}{dt} \int_0^{z(x,t)} M_1 dz + \Delta T \left\{ \sum_{i=w,0} \rho_i^{II} c_{pi}^{II} (u_{in}^{II} - \phi S_i^{II} v_n) \right. \\ \left. - (1 - \phi) \rho_R^{II} c_{pR}^{II} v_n \right\} |\nabla F| + \left(-k_{hR} \frac{\partial T_R}{\partial n} \right)^{II} |\nabla F| + \left(-k_{hf} \frac{\partial T_f}{\partial n} \right)^{II} \\ = - \Delta T \frac{\partial}{\partial x} \left\{ \int_0^{z(x,t)} \left[\sum_{i=s,w,0} \rho_i^{(1)} c_{pi} \hat{u}_{ix}^{(1)} + \rho_s \frac{L_v^{(1)}}{\Delta T} \hat{u}_{sx}^{(1)} \right] dz \right\} \quad (5.32) \end{aligned}$$

By adding Eqs. (2.55) and (2.58), we get the total water mass balance, at any point of the front (x,t) , averaged over the thickness of the reservoir

$$\begin{aligned} \frac{d}{dt} \int_0^{z(x,t)} (\phi \rho_s S_s^{(1)} + \phi \rho_w^{(1)} S_w^{(1)}) dz + \frac{d}{dt} \int_{z(x,t)}^h \phi \rho_w^{(2)} S_w^{(2)} dz \\ = - \frac{\partial}{\partial x} \left\{ \int_0^{z(x,t)} (\rho_s \hat{u}_{sx}^{(1)} + \rho_w^{(1)} \hat{u}_{wx}^{(1)}) dz \right\} - \frac{\partial}{\partial x} \left\{ \int_{z(x,t)}^h \rho_w^{(2)} \hat{u}_{wx}^{(2)} dz \right\} \quad (5.33) \end{aligned}$$



a. Rectangular



b. Radial

Figure 71. Geometries Examined in Section 5.5.
 Notation for Area (Line) Integration.

where superscripts (1), (2) refer to the steam or hot liquid zones, respectively. Similarly, adding Eqs. (2.56) and (2.59) we recover the total oil mass balance

$$\begin{aligned} \frac{d}{dt} \int_0^{z(x,t)} \phi \rho_o^{(1)} S_o^{(1)} dz + \frac{d}{dt} \int_{z(x,t)}^h \phi \rho_o^{(2)} S_o^{(2)} dz = & - \frac{\partial}{\partial x} \int_0^{z(x,t)} \rho_o^{(1)} \hat{u}_{ox}^{(1)} dz \\ & - \frac{\partial}{\partial x} \int_{z(x,t)}^h \rho_o^{(2)} \hat{u}_{ox}^{(2)} dz \end{aligned} \quad (5.34)$$

Multiplying Eqs. (5.33), (5.34) by $c_{pw} \Delta T$, $c_{po} \Delta T$, respectively and subtracting their sum from (5.32), we obtain

$$\begin{aligned} \Delta T \frac{d}{dt} \int_0^{z(x,t)} \left(\phi \rho_s S_s^{(1)} \frac{L_v^{(1)}}{\Delta T} + (1 - \phi) \rho_R c_{pR} \right) dz \\ - \Delta T \frac{d}{dt} \int_{z(x,t)}^h \left[\phi \rho_w^{(2)} c_{pw} S_w^{(2)} + \phi \rho_o^{(2)} c_{po} S_o^{(2)} \right] dz \\ + \Delta T \{ W_F(x,t) + Q_F(x,t) \} |\nabla F| + \left(-k_{hf} \frac{\partial T_f}{\partial n} \right) II \\ = - \frac{\partial}{\partial x} \int_0^{z(x,t)} \rho_s L_v^{(1)} \hat{u}_{sx}^{(1)} dz + \Delta T \frac{\partial}{\partial x} \\ \cdot \left[\int_{z(x,t)}^h \left[\rho_w^{(2)} c_{pw} \hat{u}_{wx}^{(2)} + \rho_o^{(2)} c_{po} \hat{u}_{ox}^{(2)} \right] dz \right] \end{aligned} \quad (5.35)$$

which is a linear combination of the thermal energy and the latent heat (steam mass) balances. The two conservation relations (5.32), (5.35) are

the basic equations, just as in the one-dimensional case, upon which we will develop our model.

Before we proceed any further, we once more introduce the assumption of constant volumetric heat capacities in both the steam and the hot liquid zone [compare with (4.16), Section 3.4]. Then M_1 and M_4 , which is defined by

$$M_4 = \phi \rho_s S_s \frac{L_v^{(1)}}{\Delta T} + (1 - \phi) \rho_R c_{pR} + \phi \rho_w^{(2)} c_{pw} S_w^{(2)} + \phi \rho_o^{(2)} c_{po} S_o^{(2)} \quad (5.36)$$

are considered constant (or slowly varying) relative to the steam zone rate of growth. Under this assumption, we can suitably approximate the first term on the LHS of both (5.32), (5.35) by

$$\Delta T \frac{d}{dt} \int_0^{z(x,t)} M_i dz \approx M_i \Delta T \frac{\partial z}{\partial t} \quad (5.37)$$

and subsequently eliminate $\frac{\partial z}{\partial t}$ between (5.32) and (5.35) with the result:

$$\begin{aligned} \Delta T \frac{\partial}{\partial x} \left\{ \int_0^{z(x,t)} \left[\sum_{i=s,w,o} \rho_i^{(1)} c_{pi} \hat{u}_{ix}^{(1)} + \rho_s \frac{L_v^{(1)}}{\Delta T} (1 - \alpha) \hat{u}_{sx}^{(1)} \right] dz \right. \\ \left. + \alpha \int_{z(x,t)}^h \left[\rho_w^{(2)} c_{pw} \hat{u}_{wx}^{(2)} + \rho_o^{(2)} c_{po} \hat{u}_{ox}^{(2)} \right] dz \right\} \\ + (1 - \alpha) \Delta T \{ W_F(x,t) + Q_F(x,t) \} |\nabla F| + (1 - \alpha) \left(-k_{hf} \frac{\partial T_f}{\partial n} \right)_{II} = 0 \end{aligned} \quad (5.38)$$

where α stands for the dimensionless parameter $\frac{M_1}{M_4} < 1$. Equation (5.38) can then be integrated with respect to x , over the interval $L_{Fu}(t)$ to x :

$$\begin{aligned} \Delta T \int_0^{z(x,t)} & \left[\sum_{i=s,w,o} \rho_i^{(1)} c_{pi} \hat{u}_{ix}^{(1)} + \rho_s \frac{L_v^{(1)}}{\Delta T} (1 - \alpha) \hat{u}_{sx}^{(1)} \right] dz \\ & + \alpha \Delta T \int_{z(x,t)}^h \left[\rho_w^{(2)} c_{pw} \hat{u}_{wx}^{(2)} + \rho_o^{(2)} c_{po} \hat{u}_{ox}^{(2)} \right] dz \\ & + (1 - \alpha) \Delta T \int_{L_{Fu}(t)}^x \left[W_F(x',t) + Q_F(x',t) \right] |\nabla F| dx' \\ & + (1 - \alpha) \int_{L_{Fu}(t)}^x \left(-k_{hf} \frac{\partial T_f}{\partial n} \right)^{II} dx' = h \Phi_\alpha(t) \end{aligned} \quad (5.39)$$

Here $L_{Fu}(t)$ is the position of the trailing edge of the front and $\Phi_\alpha(t)$ represents a heat input term at the site of the trailing edge:

$$\begin{aligned} \Phi_\alpha(t) = & \frac{\Delta T}{h} \int_0^h \left[\sum_{i=s,w,o} \rho_i^{(1)} c_{pi} \hat{u}_{ix}^{(1)} \right]_{x=L_{Fu}(t)} \\ & + \rho_s \frac{L_v^{(1)}}{\Delta T} (1 - \alpha) \hat{u}_{sx}^{(1)} \Big|_{x=L_{Fu}(t)} dz \end{aligned} \quad (5.40)$$

The conservation Equation (5.39) is important in relating in a quasi-steady state manner the volumetric flow rates

$$\int_0^{z(x,t)} \hat{u}_{ix}^{(1)} dz, \quad \int_{z(x,t)}^h \hat{u}_{ix}^{(2)} dz \quad \text{to the net total heat flow rate to}$$

the hot liquid zone, $\Delta T \int_{L_{Fu}(t)}^x \left[W_F(x',t) + Q_F(x',t) \right] |\nabla F| dx'$, and

to the heat losses to the overburden, $\int_{L_{Fu}(t)}^x \left(-k_{hf} \frac{\partial T_f}{\partial n} \right) II \, dx'$. Its physical significance is much more clear in isothermal, immiscible displacement of oil by water. Then, the heat transfer terms drop out and we get the conservation equation

$$\int_0^{z(x,t)} \hat{u}_{wx}^{(1)} dz + \int_{z(x,t)}^h \hat{u}_{ox}^{(2)} dz = \int_0^h \hat{u}_{wx}^{(1)} \Big|_{x=L_{Fu}(t)} dz \quad (5.41)$$

which is the total mass balance for incompressible phases. Eq. (5.39) also acquires a simple physical meaning when $\alpha = 1$, i.e. $M_1 \approx M_4$. Then, after proper rearrangement, the sensible heat balance emerges

$$\begin{aligned} \Delta T \int_0^{z(x,t)} \sum_{i=s,w,o} \rho_i^{(1)} c_{pi} \hat{u}_{ix}^{(1)} dz + \Delta T \int_{z(x,t)}^h \sum_{i=w,o} \rho_i^{(2)} c_{pi} \hat{u}_{ix}^{(2)} dz \\ = \Delta T \int_0^h \sum_{i=s,w,o} \rho_i^{(1)} c_{pi} \hat{u}_{ix}^{(1)} \Big|_{x=L_{Fu}(t)} dz \end{aligned} \quad (5.42a)$$

Finally, if we neglect heat losses from the steam zone, we get a simplified balance, by means of which we can relate the parameter α to the rates of injection, $w_i^{(1)}$, and the rates of production, $w_i^{(2)}$:

$$\alpha = \frac{w_s^{(1)} h_s^{(1)} + w_w^{(1)} h_w^{(1)} + w_o^{(1)} h_o^{(1)}}{w_w^{(2)} h_w^{(1)} + w_o^{(2)} h_o^{(1)} + w_s^{(1)} L_v^{(1)}} \quad (5.42b)$$

The next step involves the determination of the unspecified volumetric flow rates $\int_0^{z(x,t)} \hat{u}_{ix}^{(1)} dz$, $\int_{z(x,t)}^h \hat{u}_{ix}^{(2)} dz$ from Eq. (5.34). For this

purpose, we need to develop additional expressions that relate these terms to each other. Clearly, the integral thermal energy and mass balances alone cannot furnish such relationships. As a consequence, one has to employ the linear momentum balance in its differential form, Darcy's Law, Eqs. (2.5), (2.6), (2.7), and follow an integral balance approach after the adoption of suitable approximations.

5.5.1 A Momentum Integral Balance

5.5.1.1 The Dupuit Approximation

A most powerful tool for treating a large class of problems of flow through porous media (unconfined flows in ground water hydrology, gravity segregation in isothermal immiscible displacement in oil recovery), is the Dupuit approximation [Bear (1972)]. The underlying assumption, as formalized in its final form by Dietz (1953), states that, at any point of the interface, the volumetric velocity components parallel to the reservoir boundaries are equal to the mean volumetric components. In mathematical terms, this is shown to be equivalent with retaining only the first term, in a Taylor series expansion about a point at the front (see Figure 72a):

$$\int_0^{z(x,t)} \hat{u}_{ix}^{(1)} dz = z(x,t) \hat{u}_{ix}^I(x, z(x,t), t) + O(z^2(x,t)) \quad (5.43a)$$

$$\int_{z(x,t)}^h \hat{u}_{ix}^{(2)} dz = [h - z(x,t)] \hat{u}_{ix}^{II}(x, z(x,t), t) + O\left((h - z(x,t))^2\right) \quad (5.43b)$$

The assumption is more closely satisfied as the vertical variations in \hat{u}_{ix} are smaller, which is favored by high injection rates and relatively small

reservoir thickness. Although the assumption is not of general validity, we will make use of it in deriving a first order approximate solution to the steam front shape of an arbitrary steam drive. By introducing the Dupuit approximation, we can now substitute the integral volumetric velocities in (5.39) by their local values at the steam front. The latter are related to each other by means of the following dynamic boundary condition.

5.5.1.2 The Dynamic Boundary Condition

Let us consider a fixed point along the steam front $(x, z(x, t))$ (Fig. 72). Neglecting capillary terms and using Darcy's law, we obtain for the local volumetric velocities at the inner side of the steam front,

$\hat{u}_{ix}^I(x, z(x, t), t)$:

$$\hat{u}_{wx}^I = \left(\frac{k_{rw} \mu_s}{k_{rs} \mu_w} \right)^I \hat{u}_{sx}^I \quad (5.44a)$$

$$\hat{u}_{ox}^I = \left(\frac{k_{ro} \mu_s}{k_{rs} \mu_o} \right)^I \hat{u}_{sx}^I \quad (5.44b)$$

[compare with Eqns. (2.5), (2.6), (2.7), (2.9a), (2.9b)]. From geometrical considerations at the inner side of the front

$$\hat{u}_{sn}^I = \hat{u}_{sx}^I \cos \theta - |\hat{u}_{sz}^I| \sin \theta \quad (5.45a)$$

$$\hat{u}_{ss}^I = \hat{u}_{sx}^I \sin \theta + |\hat{u}_{sz}^I| \cos \theta \quad (5.45b)$$

and similarly at the outer side:

$$\hat{u}_{in}^{II} = \hat{u}_{ix}^{II} \cos \theta + |\hat{u}_{iz}^{II}| \sin \theta \quad i=w, o \quad (5.46a)$$

$$\hat{u}_{is}^{II} = \hat{u}_{ix}^{II} \sin \theta - |\hat{u}_{iz}^{II}| \cos \theta \quad i=w, o \quad (5.46b)$$

where θ is the angle between the horizontal and the outwards pointing normal to the front (Fig. 72b). Employing the pressure dynamic condition, Eq. (2.33b), and Darcy's law, we also have:

$$\left(\frac{\mu_s}{k_{rs}}\right)^I \hat{u}_{ss}^I + k(\rho_i - \rho_s) \hat{g}_s = \left(\frac{\mu_i}{k_{ri}}\right)^{II} \hat{u}_{is}^{II} \quad i=w,0 \quad (5.47)$$

As before, the superscript \wedge renders the notation uniform for both rectangular and radially symmetric geometries, thus $\hat{g}_s = g_s$ or $2\pi r g_s$ in the respective geometries, whereas the subscript s refers to the direction parallel to the steam front (Fig. 72). We can now eliminate \hat{u}_{ss}^I , \hat{u}_{is}^{II} from (5.45a,b), (5.46a,b), (5.47) with the result:

$$\begin{aligned} \hat{u}_{ix}^{II} = & \hat{u}_{sx}^I \left(\frac{k_{ri}}{\mu_i}\right)^{II} \left(\frac{\mu_s}{k_{rs}}\right)^I - k \left(\frac{k_{ri}}{\mu_i}\right)^{II} (\rho_i - \rho_s) \hat{g} \frac{1}{\tan\theta} \\ & + \left\{ |\hat{u}_{sz}^I| \left(\frac{k_{ri}}{\mu_i}\right)^{II} \left(\frac{\mu_s}{k_{rs}}\right)^I + |\hat{u}_{iz}^{II}| \right\} \frac{1}{\tan\theta} \quad i=w,0 \end{aligned} \quad (5.48)$$

For simplicity of notation, we let $J_i = \left\{ |\hat{u}_{sz}^I| \left(\frac{k_{ri}}{\mu_i}\right)^{II} \left(\frac{\mu_s}{k_{rs}}\right)^I + |\hat{u}_{iz}^{II}| \right\} \rho_i^{(2)} c_{pi}$, $N_i^I = \left(\frac{k_{rs} \mu_i}{k_{ri} \mu_s}\right)^I$, $N_i^{II} = \left(\frac{\mu_i}{k_{ri}}\right)^{II} \cdot \left(\frac{k_{rs}}{\mu_s}\right)^I \quad i=w,0$. The

quantity J_i represents a convective heat flux term along the vertical ($-z$) direction, while the dimensionless groups N_i^I , N_i^{II} express the ratio of mobilities between steam and phase i , in the inner and outer side of the front, respectively [mobility ratios, see Bear (1972)]. Using the above equations we can express the local volumetric velocities at the steam front in terms of the single unknown quantity \hat{u}_{sx}^I . We are now in a position to

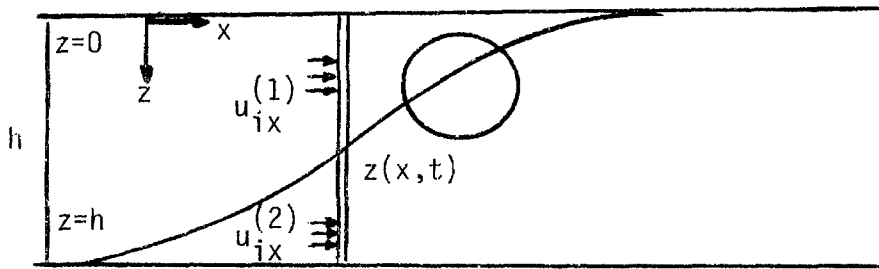


Figure 72a. Notation for Subsection 5.5.1.1 (The Dupuit Approximation).

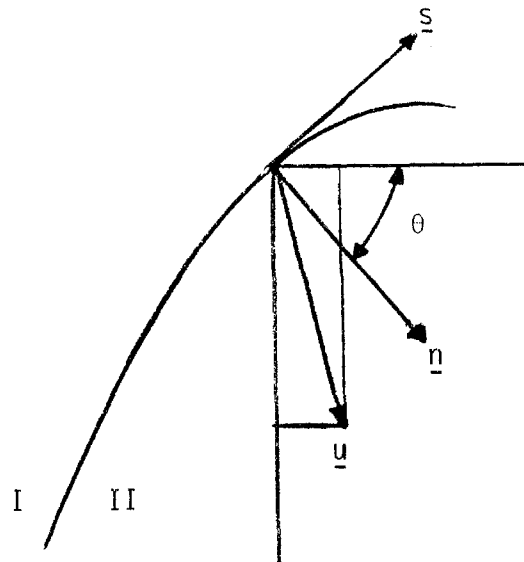


Figure 72b. Notation for Subsection 5.5.1.2 (The Dynamic Boundary Condition) Encircled portion of Fig. 72a.

develop the governing equations of the steam front.

5.6 Derivation of the Governing Partial Differential Equations

5.6.1 The Thermal Energy Equation

Employing the Dupuit approximation (5.43) and introducing expressions (5.44a,b), (5.48) in the basic Equation (5.39), we get, after lengthy calculations:

$$\begin{aligned} \hat{u}_{sx}^I = & \frac{h\phi_{\alpha}(t) - (1 - \alpha)\{CNHF + CHL\}}{z \left\{ \sum_{i=s,w,0} \frac{\rho_i^{(1)} c_{pi}}{N_i^I} + \rho_s \frac{L_v^{(1)}}{\Delta T} (1 - \alpha) \right\} \Delta T + (h - z) \alpha \sum_{i=w,0} \frac{\rho_i^{(2)} c_{pi}}{N_i^{II}} \Delta T} \\ & + \frac{\alpha \Delta T \left\{ \sum_{i=w,0} \rho_i^{(2)} c_{pi} k \left(\frac{k_{ri}}{\mu_i} \right)^{II} \frac{(\rho_i - \rho_s) \hat{g}}{\tan \theta} - \sum_{i=w,0} \frac{J_i}{\tan \theta} \right\} (h - z)}{z \left\{ \sum_{i=s,w,0} \frac{\rho_i^{(1)} c_{pi}}{N_i^I} + \rho_s \frac{L_v^{(1)}}{\Delta T} (1 - \alpha) \right\} \Delta T + (h - z) \alpha \sum_{i=w,0} \frac{\rho_i^{(2)} c_{pi}}{N_i^{II}} \Delta T} \end{aligned} \quad (5.49)$$

$$\text{with } CNHF = \Delta T \int_{L_{Fu}(t)}^x [W_F(x', t) + Q_F(x', t)] |\nabla F| dx',$$

$$CHL = \int_{L_{Fu}}^x (t) \left(-k_{hf} \frac{\partial T_f}{\partial n} \right)^{II} dx'$$

denoting respectively the cumulative net heat flux to the hot liquid zone and the cumulative heat losses to the overburden. Expression (5.49) combined with Eq. (5.44a,b) and inserted into the thermal energy balance, Eq. (5.32), gives rise to a partial differential equation that the steam front satisfies. To simplify notation, let the local net heat flux to the hot liquid zone be denoted by

$$NHF = \Delta T \{W_F(x, t) + Q_F(x, t)\} |\nabla F| \quad (5.50a)$$

the local heat losses to the overburden by

$$HL = \left(-k_{hf} \frac{\partial T_f}{\partial n} \right) II \quad (5.50b)$$

and the total (sensible + latent) heat input at the trailing edge of the front by

$$\Phi_1'(t) = \frac{\Delta T}{h} \int_0^h \left[\sum_{i=S,W,0} \rho_i^{(1)} c_{pi} \hat{u}_{ix}^{(1)} \Big|_{x=L_{Fu}(t)} + \rho_s \frac{L_v^{(1)}}{\Delta T} \hat{u}_{sx}^{(1)} \Big|_{x=L_{Fu}(t)} \right] dz \quad (5.50c)$$

[Note that $L_{Fu}(t) = 0$ implies $\Phi_1'(t) = \Phi_1(t)$]. Also, consider the dimension-

less groups

$$\beta_1 = (1 - \alpha) \frac{\left\{ \sum_{i=S,W,0} \frac{\rho_i^{(1)} c_{pi}}{N_i^I} + \rho_s \frac{L_v^{(1)}}{\Delta T} \right\}}{\left\{ \sum_{i=S,W,0} \frac{\rho_i^{(1)} c_{pi}}{N_i^I} + \frac{\rho_s L_v^{(1)}}{\Delta T} (1 - \alpha) \right\}} \quad (5.51a)$$

a multiplicative factor of $O(1)$, and

$$N = \frac{\left\{ \sum_{i=S,W,0} \frac{\rho_i^{(1)} c_{pi}}{N_i^I} + \frac{\rho_s L_v^{(1)}}{\Delta T} (1 - \alpha) \right\}}{\alpha \left\{ \sum_{i=W,0} \frac{\rho_i^{(2)} c_{pi}}{N_i^{II}} \right\}} \quad (5.51b)$$

N is a most important parameter expressing the ratio of the mobilities of the steam and the hot liquid zones; it can be considered as a generalized mobility ratio. Its physical meaning is more clear in isothermal,

immiscible displacement. There, the displacing agent is water alone, the displaced phase oil, and N reduces to

$$N = \frac{\rho_w c_{pw}}{\rho_o c_{po}} \cdot \frac{M_o}{M_w} \cdot \frac{1}{\alpha} = \frac{k_{rw}}{k_{ro}} \cdot \frac{\mu_o}{\mu_w}, \text{ in accordance with the theory of}$$

isothermal, immiscible displacement [Sheldon and Fayers (1962)].

Finally, let

$$L_1 = \frac{\left\{ \sum_{i=S,W,O} \frac{\rho_i^{(1)} c_{pi}}{N_i^I} + \rho_s \frac{L_v^{(1)}}{\Delta T} \right\} \left\{ \sum_{i=W,O} \rho_i^{(2)} c_{pi} \left(\frac{k_{ri}}{\mu_i} \right)^{II} (\rho_i - \rho_s) \right\} \text{kg}}{\left(\sum_{i=W,O} \frac{\rho_i^{(2)} c_{pi}}{N_i^{II}} \right)} \quad (5.52a)$$

denote a parameter that includes the gravity terms and

$$J_1 = \frac{\left\{ \sum_{i=S,W,O} \frac{\rho_i^{(1)} c_{pi}}{N_i^I} + \rho_s \frac{L_v^{(1)}}{\Delta T} \right\} \left\{ \sum_{i=W,O} J_i \right\}}{\sum_{i=W,O} \frac{\rho_i^{(2)} c_{pi}}{N_i^{II}}} \quad (5.52b)$$

be a correction term that accounts for vertical heat transfer by convection. Using the above notation, the thermal energy balance, (5.32), reads after proper rearrangement

$$M_1 \Delta T \frac{\partial z}{\partial t} + \frac{\partial}{\partial x} \left\{ \left[\frac{zN}{zN + h - z} - \frac{1}{\beta_1} \right] \left[h\Phi_1'(t) - \beta_1 \{ \text{CNHF} + \text{CHL} \} \right] \right. \\ \left. + \frac{z(h - \quad)}{zN + h - z} \frac{\Delta T [L_1 - J_1]}{\tan \theta} \right\} = 0 \quad (5.53)$$

Eq. (5.53) is the desired partial differential equation, the solution of which determines z , the steam front vertical position, as a function of x , the horizontal coordinate, and time. To simplify further, we non-dimensionalize $x, t, \Phi_1'(t), \{ \text{CNHF} \}, \{ \text{CHL} \}$ by the dimensional variables of

Chapter IV, and z by h . From geometrical considerations at the front,

$$\tan \theta = \begin{cases} -\frac{\partial x}{\partial z} & , \quad \text{rectangular geometry} \\ -\frac{\partial r}{\partial z} & , \quad \text{radial geometry} \end{cases} \quad (5.54a)$$

$$(5.54b)$$

so that one finally obtains

$$\begin{aligned} \frac{\partial z_D}{\partial t_D} + \frac{\partial}{\partial x_D} \left\{ \left[\frac{z_D^N}{z_D^N + 1 - z_D} - \frac{1}{\beta_1} \right] \left[\frac{\Phi'_{1D}(t_D)}{2} - \frac{\beta_1}{2} \{ \text{CNHF} + \text{CHL} \}_D \right] \right. \\ \left. - \frac{z_D(1 - z_D)}{z_D^N + 1 - z_D} G_{L1} [1 - C_{1D}] \frac{\partial z_D}{\partial x_D} \right\} = 0 \end{aligned} \quad (5.55a)$$

and

$$\begin{aligned} \frac{\partial z_D}{\partial t_D} + \frac{1}{2\pi r_D} \cdot \frac{\partial}{\partial r_D} \left\{ \left[\frac{z_D^N}{z_D^N + 1 - z_D} - \frac{1}{\beta_1} \right] \left[\frac{\Phi'_{1D}(t_D)}{2} - \frac{\beta_1}{2} \{ \text{CNHF} + \text{CHL} \}_D \right] \right. \\ \left. - \frac{z_D(1 - z_D)}{z_D^N + 1 - z_D} G_{r1} [1 - C_{1D}] \frac{2\pi r_D}{\partial r_D} \frac{\partial z_D}{\partial r_D} \right\} = 0 \end{aligned} \quad (5.55b)$$

in the respective geometries. In the above equations, the first term is a transient capacity (storage) term, the second expresses the steam zone growth due to a combination of viscous and heat transfer effects, whereas the third term incorporates the effect of gravity on the steam front shape. Out of the process of non-dimensionalization, the following dimensionless groups emerge:

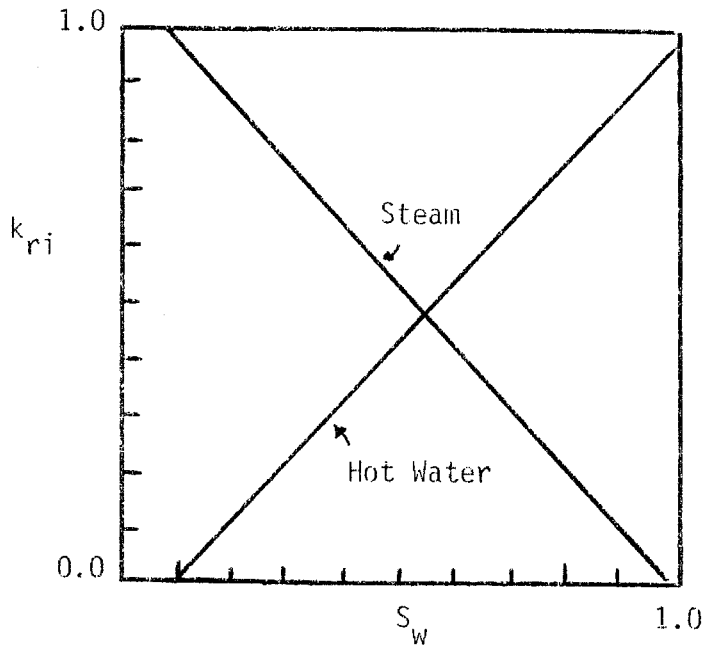
$$G_{L1} = \frac{hd^2 kg}{\Phi_1^2 M_1} \frac{\left\{ \sum_{i=S,w,o} \frac{\rho_i^{(1)} c_{pi}}{N_i^{II}} + \rho_s \frac{L_v^{(1)}}{\Delta T} \right\} \left\{ \sum_{i=w,o} \varepsilon_i^{(2)} c_{pi} \left(\frac{k_{ri}}{u_i} \right)^{II} (\rho_i - \rho_s) \right\}}{\left(\sum_{i=w,o} \frac{\rho_i^{(2)} c_{pi}}{N_i^{II}} \right)} \quad (5.56a)$$

$$G_{r1} = \frac{hkg\Delta T}{2\phi_1} \frac{\left\{ \sum_{i=s,w,0} \frac{\rho_i^{(1)} c_{pi}}{N_i^I} + \rho_s \frac{L_v^{(1)}}{\Delta T} \right\} \left\{ \sum_{i=w,0} \rho_i^{(2)} c_{pi} \left(\frac{k_{ri}}{\mu_i} \right)^{II} (\rho_i - \rho_s) \right\}}{\left(\sum_{i=w,0} \frac{\rho_i^{(2)} c_{pi}}{N_i^{II}} \right)} \quad (5.56b)$$

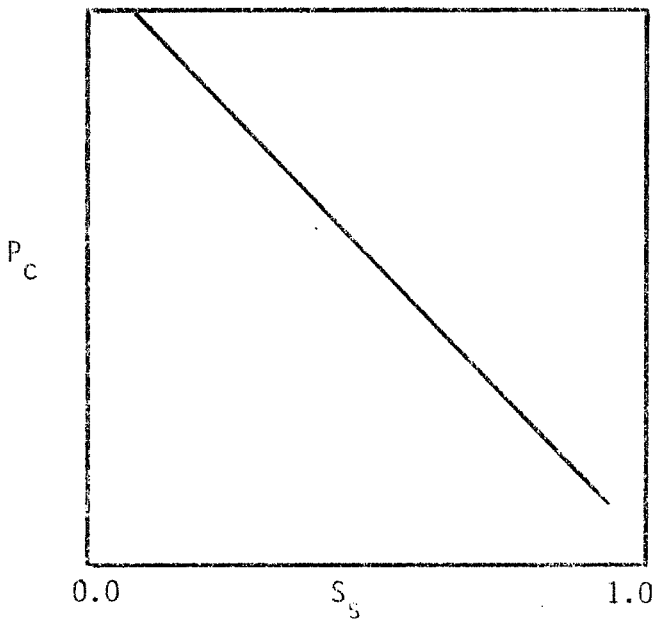
$$C_1 = \frac{\rho_w^{(2)} c_{pw}}{\sum_{i=w,0} \rho_i^{(2)} c_{pi} \left(\frac{k_{ri}}{\mu_i} \right)^{II} (\rho_i - \rho_s)} \left(\frac{4hd^2}{kgM_1^2 \Delta T^2} \right) \quad (5.56c)$$

The two groups G_{L1} , G_{r1} express the relative magnitude of a term representing a convective heat flux along the vertical direction, induced by Darcy's flow, to the total injected heat flow rate, in the respective geometries. On the other hand, C_1 is the ratio of the heat capacity of the hot liquid zone to the above convective heat flux term. For typical values of reservoir parameters, $C_1 \approx 0(10^{-2})$ (Table 6).

Equations (5.55a,b) are based on the total thermal energy balance. Their functional form is very similar to that of the one-dimensional saturation distribution, Eq. (4.97), if G_{L1} , G_{r1} are small, and to that of Eq. (4.95) if G_{L1} , G_{r1} are of $O(1)$. Therefore, one can envisage Eqns. (5.55a,b) as the equations that govern the distribution of the steam saturation in a one-dimensional steam drive, where the steam saturation is z_D , the fractional flow curve is given by $f_{sD} = \frac{z_D^N}{z_D^N + 1 - z_D}$ and the capillary terms equal $\frac{(1 - z_D)G_{L1}[1 - C_1 J_D]}{N}$ (and similarly in radially symmetric geometries). In view of the above interpretation of f_{sD} and the capillary terms, we deduce that in such a case the relative permeability curves and the capillary pressure vs. steam saturation curves are straight lines. (See Figure 73.) The above analogy is identical to the analogy



a.



b.

Figure 73. Fictitious Relative-Permeability (a) and Capillary Pressure (b) Curves Corresponding to the One-Dimensional Analog of Eq. (5.55) ($C_1 \ll 1$).

between two-dimensional and one-dimensional isothermal, immiscible, two-phase displacement [LeFur and Sourieau (1963)]. This similarity further justifies the approach followed and validates Equation (5.53).

5.6.2 The Steam Mass Equation

In deriving (5.53) we used conservation Equation (5.39) which provides explicit representation, by means of the Dupuit assumption, for the volumetric flow rates, followed by a substitution of the expressions obtained in the energy Equation (5.32). The resulting differential Equation (5.53) contains heat transfer terms that will be treated approximately along the lines of the approximations 3.6.1 and 3.6.2. If, instead of the energy equation, we make use of the linearly independent steam mass balance, Eq. (2.57), we obtain another partial differential equation, the solution of which must be identical to the solution of Eq. (5.53), barring any differences in approximating heat transfer. The two solutions should complement each other in regions where the approximations fail to properly account for the heat transfer, in much the same way the two upper bounds of Chapter IV do.

To derive the steam mass equation we substitute Eq. (5.49) in (2.57) and get, after lengthy calculations

$$\begin{aligned}
 B \frac{\partial z_D}{\partial t_D} + \frac{\partial}{\partial x_D} \left\{ \frac{z_D^N}{z_D^N + 1 - z_D} \left[\frac{\phi_{2D}'(t_D)}{2} - \frac{\beta_2}{2} \{ \text{CNHF} + \text{CHL} \}_D \right] \right. \\
 \left. - \frac{z_D(1 - z_D)}{z_D^N + 1 - z_D} G_{L2} [1 - C_{2J}] \frac{\partial z_D}{\partial x_D} \right\} + \frac{1}{2} \{ \text{CHF} + \text{HL} \}_D = 0 \quad (5.57a)
 \end{aligned}$$

for rectangular geometries and

$$B \frac{\partial z_D}{\partial t_D} + \frac{1}{2\pi r_D} \cdot \frac{\partial}{\partial r_D} \left\{ \frac{z_D^N}{z_D^N + 1 - z_D} \left[\frac{\Phi'_{2D}(t_D)}{2} - \frac{\beta_2}{2} \{ \text{CNHF} + \text{CHL} \}_D \right] \right. \\ \left. - \frac{z_D(1 - z_D)}{z_D^N + 1 - z_D} \cdot G_{r2} [1 - C_{2J_D}] 2\pi r_D \frac{\partial z_D}{\partial r_D} \right\} + \frac{1}{2} \{ \text{CHF} + \text{HL} \}_D = 0 \quad (5.57b)$$

for radially symmetric geometries. The notation is the same one used previously and, in addition,

$$\text{CHF} = \Delta T Q_f(x, t) |\nabla F| \quad (5.58a)$$

denotes the local conductive heat flux to the hot liquid zone and

$$\Phi'_2(t) = \frac{\Delta T}{h} \int_0^h \frac{\rho_s L_v^{(1)}}{\Delta T} \hat{u}_{sx}^{(1)} \Big|_{x=L_{Fu}(t)} dz \quad (5.58b)$$

denotes the latent heat input at the trailing edge of the front. The dimensionless groups β_2 , G_{L2} , G_{r2} , C_2 are simply modified versions of β_1 , G_{L1} , G_{r1} , C_1 :

$$\beta_2 = \frac{\rho_s \frac{L_v^{(1)}}{\Delta T}}{\left\{ \sum_{i=s,w,o} \frac{\rho_i^{(1)} c_{pi}}{N_i} + \frac{\rho_s L_v^{(1)}}{\Delta T} \right\}} \beta_1 \quad (5.59a)$$

$$G_{L2} = \frac{\frac{\rho_s L_v^{(1)}}{\Delta T}}{\left\{ \sum_{i=s,w,o} \frac{\rho_i^{(1)} c_{pi}}{N_i} + \frac{\rho_s L_v^{(1)}}{\Delta T} \right\}} G_{L1} \quad (5.59b)$$

and similarly for G_{r2} , C_2 as indicated in Table 14b. Noticing the similarity in form between the two sets of PDE's (5.55a,b) and (5.57a,b), one needs to consider the solution of only one of the two.

$$\alpha = \frac{\left[\phi \rho_s \bar{s}_s \frac{L_v^{(1)}}{\Delta T} + \phi \rho_w c_{pw} \bar{s}_w + \phi \rho_o c_{po} \bar{s}_o + (1 - \phi) \rho_R c_{pR} \right]}{\left[\phi \rho_s \bar{s}_s \frac{L_v^{(1)}}{\Delta T} + \phi \rho_w^{(2)} c_{pw} S_w^{(2)} + \phi \rho_o^{(2)} c_{po} S_o^{(2)} + (1 - \phi) \rho_R c_{pR} \right]}$$

$$N_i^I = \left(\frac{k_{rs}}{\mu_s} \frac{\mu_i}{k_{ri}} \right)^I, \quad N_i^{II} = \left(\frac{k_{rs}}{\mu_s} \right)^I \left(\frac{\mu_i}{k_{ri}} \right)^{II}$$

$$N = \frac{\left\{ \sum_{i=s,w,o} \frac{\rho_i^{(1)} c_{pi}}{N_i^I} + (1 - \alpha) \frac{\rho_s L_v^{(1)}}{\Delta T} \right\}}{\alpha \left\{ \sum_{i=w,o} \frac{\rho_i^{(2)} c_{pi}}{N_i^{II}} \right\}}$$

Basic Dimensionless Groups for a 3-D Steam Drive

Table 14a

$$\beta_1 = (1 - \alpha) \frac{\left\{ \sum_{i=s,w,0} \frac{\rho_i^{(1)} c_{pi}}{N_i} + \frac{\rho_s L_v^{(1)}}{\Delta T} \right\}}{\left\{ \sum_{i=s,w,0} \frac{\rho_i^{(1)} c_{pi}}{N_i} + \frac{\rho_s L_v^{(1)}}{\Delta T} (1 - \alpha) \right\}}$$

$$\beta_2 = (1 - \alpha) \frac{\rho_s \frac{L_v^{(1)}}{\Delta T}}{\left\{ \sum_{i=s,w,0} \frac{\rho_i^{(1)} c_{pi}}{N_i} + \rho_s \frac{L_v^{(1)}}{\Delta T} (1 - \alpha) \right\}}$$

$$G_{Lj} = \frac{hd^2 kg}{\phi_1^2 M_1} \cdot \left\{ \sum_{i=w,0} \rho_i^{(2)} c_{pi} \left(\frac{k_{ri}}{\mu_i} \right)^{II} (\rho_i - \rho_s) \right\} \beta_j N \left(\frac{\alpha}{1 - \alpha} \right) \quad j=1,2$$

$$G_{rj} = \frac{hkg\Delta T}{2\phi_1} \left\{ \sum_{i=w,0} \rho_i^{(2)} c_{pi} \left(\frac{k_{ri}}{\mu_i} \right)^{II} (\rho_i - \rho_s) \right\} \beta_j N \left(\frac{\alpha}{1 - \alpha} \right) \quad j=1,2$$

$$C_1 = \frac{4hd^2}{kgM_1^2 \Delta T^2} \frac{\rho_w^{(2)} c_{pw}}{\sum_{i=w,0} \rho_i^{(2)} c_{pi} \left(\frac{k_{ri}}{\mu_i} \right)^{II} (\rho_i - \rho_s)}$$

$$C_2 = C_1 \cdot \frac{\beta_2}{\beta_1}$$

Dimensionless Groups of a 3-D Steam Drive

Table 14b

5.7 Methods of Solution of the PDE for the Steam Front

Solving the pair of Eqs. (5.55a,b) or (5.57a,b) is not an easy task due to the strong non-linearities and the need to model the unknown heat transfer terms. To make some progress by analytical means we introduce additional approximations.

5.7.1 Predominantly Horizontal Flows

Let us first simplify the problem by neglecting the net vertical flow term, $C_i = 0 (i=1,2)$. For typical reservoir parameters $C_i = O(10^{-2})$, ($i=1,2$), as already noted, therefore the assumption is often realistic. Conditions that favor this approximation include larger reservoir thickness and more permeable media, as can be seen from (5.56c). With this approximation, Eq. (5.55a) for rectangular geometry, becomes:

$$\frac{\partial z_D}{\partial t_D} + \frac{\partial}{\partial x_D} \left\{ \left[\frac{z_D^N}{z_D^N + 1 - z_D} - \frac{1}{\beta_1} \right] \Phi_D(t_D, x_D) - \frac{z_D(1 - z_D)}{z_D^N + 1 - z_D} G_{L1} \frac{\partial z_D}{\partial x_D} \right\} = 0 \quad (5.60)$$

where we denote $\Phi_D(t_D, x_D) = \frac{\Phi_{1D}'(t_D)}{2} - \frac{\beta_1}{2} [CNHF + CHL]_D$, to simplify the notation. This equation belongs to the general class of non-linear Fokker-Planck equations:

$$\frac{\partial z}{\partial t} + \frac{\partial}{\partial x} \left[\phi(z)Q(x,t) - g(z) \frac{\partial z}{\partial x} \right] = 0 \quad (5.61)$$

Various versions of (5.61) have been studied in different fields. For example, if $Q(x,t)$ is very small, we recover the non-linear diffusion

equation, the structure and exact solution of which have been well established [Philip (1969), Ames (1972)]. For constant Q , we get Richards' equation that describes infiltration in porous media and is extensively discussed by hydrologists [see Moré1-Seytoux (1973)]. When ϕ_D , in (5.60), is a function of time only, the resulting equation is identical in dimensionless form, to the one derived by both Sheldon and Fayers (1962) and Beckers (1965) for two-dimensional, isothermal, immiscible displacement. Unfortunately, the above authors were not able to provide an exact solution.

By adopting the approximation of predominantly horizontal flows, we shift our interest into the solution of the basic equation (5.60), for both rectangular or radially symmetric geometry, and the solution of the respective equation that arises from the steam mass PDE's, Eqs. (5.57a,b). As indicated, we encounter two main difficulties. One, just as in the one-dimensional case, is associated with the representation of the heat flux term $\phi_D(t_D, x_D)$, i.e. the heat flux to the surroundings and the hot liquid zone. The second is strictly mathematical and concerns the solution of (5.60) after the heat losses have been properly taken into account. Finally, proper attention has to be directed towards the various dimensionless quantities $N, \beta_1, \beta_2, G_{L1}, G_{r1}, G_{L2}, G_{r2}$ which in general are functions of the independent variables. Due to lack of information regarding the above dependence, however, and in the spirit of the approximations that have been already inserted in our model, we elect to consider these quantities as constant (or slowly varying). We start the study of Eq. (5.60) by considering the stability characteristics of the solution.

5.7.2 Stability Criteria. Stable Displacement

By a hodograph transformation and after proper rearrangement, we rewrite Eq. (5.60) in the more suitable form:

$$\frac{\partial x_D}{\partial t_D} = \frac{\partial}{\partial z_D} \left\{ \left(z_D - \frac{1}{\beta_1} \right) \Phi_D(t_D, x_D) + \Phi_D(t_D, x_D)(N - 1) \left[1 - \frac{G_{L1}}{\Phi_D(t_D, x_D)(N - 1)} \cdot \frac{\partial z_D}{\partial x_D} \right] \frac{z_D(1 - z_D)}{z_D^N + 1 - z_D} \right\} \quad (5.62)$$

In rectangular geometries a stable front, once formed, would travel parallel to itself. As time increases, the relative difference between the leading and the trailing edges would have to decrease, thus one can reasonably assume that $\Phi_D(t_D, x_D)$ becomes essentially a function of t_D alone. In such a case,

$$\frac{\partial x_D}{\partial t_D} = \Phi_D(t_D) + \Phi_D(t_D)(N - 1) \frac{\partial}{\partial z_D} \left\{ \left[1 - \frac{G_{L1}}{\Phi_D(t_D)(N - 1)} \cdot \frac{\partial z_D}{\partial x_D} \right] \frac{z_D(1 - z_D)}{z_D^N + 1 - z_D} \right\} \quad (5.63)$$

From this point on, one can directly follow Beckers' stability analysis: From (5.63) it is seen that if the gravity term is equal to 1, at every point of the steam front, the front shape is a straight line and each point propagates with the same velocity. In such a case the slope is:

$$\frac{\partial z_D}{\partial x_D} = \frac{\Phi_D(t_D)(N - 1)}{G_{L1}} \quad (5.64)$$

and the front obeys the relationship

$$x_D = L_{Fu}(t) + \frac{G_{L1}}{\phi_D(t_D)(N-1)} (z_D - 1) \quad (5.65)$$

The above conditions correspond to stable parallel displacement in rectangular geometries, which can be physically realized only if $\frac{\partial z_D}{\partial x_D}$ is negative, i.e. if

$$\frac{\phi_D(t_D)(N-1)}{G_{L1}} < 0 \quad (5.66)$$

Since $\phi_D(t_D) > 0$, from physical considerations, a stable front is reached if and only if the following inequality is satisfied

$$N < 1 \quad (5.67)$$

[Compare to immiscible displacement, Saffman and Taylor (1958).] Substituting for N , this stability criterion translates into

$$\frac{\left\{ \frac{\rho_s^{(1)} c_{pw}^I k_{rs}}{\mu_s^I} + \frac{\rho_w^{(1)} c_{pw}^I k_{rw}}{\mu_w^I} + \frac{\rho_o^{(1)} c_{po}^I k_{ro}}{\mu_o^I} + \frac{\rho_s^{(1)} L_v^{(1)} k_{rs}}{\Delta T \mu_s^I} \left(1 - \frac{M_1}{M_4} \right) \right\}}{\frac{M_1}{M_4} \left\{ \frac{\rho_w^{(2)} c_{pw}^{II} k_{rw}}{\mu_w^{II}} + \frac{\rho_o^{(2)} c_{po}^{II} k_{ro}}{\mu_o^{II}} \right\}} < 1 \quad (5.68)$$

When the reservoir is inclined by an angle α above the horizontal, this stability condition is easily extended to include the different geometry

$$\frac{\phi_D(t_D)(N-1)}{G_{L1}} < \sin \alpha \quad (5.69)$$

The above criterion is a generalization to three-phase flow, in a steam drive, of a previous condition derived by Miller (1975) and van Lookeren (1977), for simpler systems. Both Miller and van Lookeren consider a system with no heat losses, flow of steam only in the steam zone, and flow of water or oil only in the hot liquid zone (see Fig. 74). Under these conditions, their criterion can be easily obtained from (5.68). Now,

$$\alpha = \frac{[c_{pw}^{(1)} \Delta T + L_v^{(1)}] w_s}{c_{pi}^{(2)} \Delta T w_i^{(2)} + L_v^{(1)} w_s} \quad i=w,0 \quad [\text{compare to (5.42b)}] \text{ and the}$$

inequality (5.68) reduces to

$$\frac{w_s}{\rho_s} \left(\frac{\mu_s}{k_s} \right)^I > \frac{w_i^{(2)}}{\rho_i} \left(\frac{\mu_i}{k_i} \right)^{II} \quad i=w,0 \quad (5.70)$$

for Miller ($i=w$) and van Lookeren ($i=0$), respectively.

If we neglect heat losses, the general stability criterion (5.68) assumes the more conventional form in terms of injection and production flow rates

$$\frac{\left(\frac{w_s^{(1)}}{\rho_s^{(1)}} + \frac{w_w^{(1)}}{\rho_w^{(1)}} + \frac{w_o^{(1)}}{\rho_o^{(1)}} \right)}{\left(\left(\frac{k_{rs}}{\mu_s} \right)^I + \left(\frac{k_{rw}}{\mu_w} \right)^I + \left(\frac{k_{ro}}{\mu_o} \right)^I \right)} > \frac{\left(\frac{w_w^{(2)}}{\rho_w^{(2)}} + \frac{w_o^{(2)}}{\rho_o^{(2)}} \right)}{\left(\left(\frac{k_{rw}}{\mu_w} \right)^{II} + \left(\frac{k_{ro}}{\mu_o} \right)^{II} \right)} \quad (5.71)$$

The latter expression may be used to estimate the stability of the steam front based on the volumetric rates that reach and leave the front (injection and production rates), whereas Equation (5.68) depends on the thermal and dynamic properties of the flowing phases. Although both

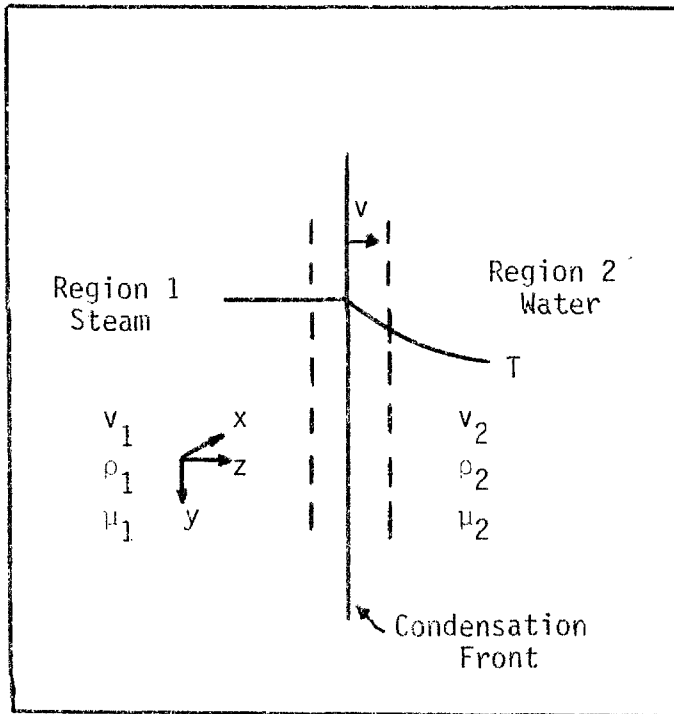


Figure 74. System Considered by Miller (1975).

formulations are derived from the same basic assumptions, the latter formulation, (5.71), may be regarded as a global stability criterion, the former, (5.68), as a local one. The same stability condition is derived from the steam mass Equations (5.57a,b) and the energy equation in radially symmetric geometry, (5.55b).

Returning to Eq. (5.64), we rewrite the slope in dimensional notation:

$$\frac{\partial z}{\partial x} = \frac{\phi_1(t)}{\left[\sum_{i=s,w,0} \frac{\rho_i^{(1)} c_{pi}}{N_i^I} + \frac{\rho_s L_v^{(1)}}{\Delta T} \right]} \cdot \frac{\left[\sum_{i=w,0} \frac{\rho_i^{(2)} c_{pi}}{N_i^{II}} \right] (N-1)}{\left[\sum_{i=w,0} \rho_i^{(2)} c_{pi} \left(\frac{k_{ri}}{\mu_i} \right)^{II} (\rho_i - \rho_s) \right] \text{kg} \Delta T} \quad (5.72)$$

which is very similar to van Lookeren's model for a linear steam drive

$$\frac{\partial z}{\partial x} = \frac{w_s}{\text{kg} \rho_s} \left(\frac{\mu_s}{k_{rs}} \right)^I \cdot \frac{(M^* - 1)}{(\rho_0^{(2)} - \rho_s)} \quad (5.73)$$

with N substituting for $M^* = \left(\frac{\mu_0}{k_{ro}} \right)^{II} \left(\frac{k_{rs}}{\mu_s} \right)^I \frac{w_0^{(2)}}{\rho^{(2)}} \cdot \frac{\rho_s}{w_s}$ and the total heat input substituting for the steam mass injection rate. Working in exactly the same manner for radial geometries, we recover the stable displacement slope:

$$2\pi r_D \frac{\partial z_D}{\partial r_D} = \frac{\phi_{1D}(t_D)(N-1)}{G_{r1}} \quad (5.74)$$

and after integration

$$z_D - 1 = - \frac{\phi_{1D}(t_D)(1-N)}{2\pi G_{r1}} \ln \frac{r}{R_{Fu}(t)} \quad (5.75)$$

Expression (5.75) is slightly different from the one presented by van Lookeren for a radial steam drive due to the different assumptions used. Notice also that in contrast to the parallel displacement obtained for rectangular coordinates, the stable radial drive belongs to the class of separable fronts [see (5.20), (5.21)].

If, instead, we work with the steam mass equation, we get in the two coordinate systems:

$$\frac{\partial z}{\partial x} = \frac{\Phi_2(t) \left[\sum_{i=w,0} \frac{\rho_i^{(2)} c_{pi}}{N_i^{II}} \right] (N-1)}{kg \rho_s L_v^{(1)} \left[\sum_{i=w,0} \rho_i^{(2)} c_{pi} \left(\frac{k_{ri}}{\mu_i} \right)^{II} (\rho_i - \rho_s) \right]} \quad (5.76)$$

and

$$2\pi r_D \frac{\partial z_D}{\partial r_D} = \frac{\Phi_{2D}(t_D)(N-1)}{G_{r2}} \quad (5.77)$$

respectively. The two sets (5.73), (5.74) and (5.76), (5.77) should, in principle, be identical to each other. Within the approximations made, a comparison shows that the two sets are close indeed.

5.7.3 A Viscous Solution Using Lower Bounds for the Heat Losses

The non-linear structure of Eqs. (5.55a,b) calls for a numerical solution. This subject, although very interesting, requires further study and, given the limitations of the present work, will not be discussed any further. Instead, we attempt to develop some simple analytical solutions that arise when the term involving the high derivative in Eqs. (5.55a,b) can be neglected. Conditions that favor this assumption include high injection rates and small thickness. The remaining terms produce a

deformation that is solely due to the difference in viscous forces between the steam and the liquid phases and the heat transfer characteristics

$$\frac{\partial z_D}{\partial t_D} + \frac{\partial}{\partial x_D} \left\{ \left[\frac{z_D^N}{z_D^N + 1 - z_D} - \frac{1}{\beta_1} \right] \phi_D(t_D, x_D) \right\} = 0 \quad (5.78)$$

We solve this equation with the boundary condition that the trailing edge of the steam front is stationary.

Clearly, by dropping the higher order derivative we also eliminate the gravity term, the effect of which we would like to evaluate in the first place. This contradiction in objective is partly removed by the boundary condition of a stationary trailing edge. It is well known from experimental data that due to gravity, steam rises and travels along the top of the steam zone, and subsequently forces the steam zone to propagate along the upper boundary of the reservoir with little or no movement of the trailing edge along the lower boundary. The proposed scheme does account for this effect by the proper selection of the above boundary condition. Other than that, Equation (5.78) generates a solution to the steam front shape which is independent of the acceleration of gravity.

With this approximation,

$$\phi_D(t_D, x_D) = \frac{\phi_{1D}(t_D)}{2} - \frac{\beta_1}{2} [\text{CNHF} + \text{CHL}]_D \quad (5.79)$$

and under constant injection rates, Equation (5.78) reads in both rectangular and radially symmetric geometries

$$\frac{\partial z_D}{\partial t_D} + \frac{\partial}{\partial x_D} \left\{ \left[\frac{z_D^N}{z_D^N + 1 - z_D} - \frac{1}{\beta_1} \right] \left[\frac{1}{2} - \frac{\beta_1}{2} [\text{CNHF} + \text{CHL}]_D \right] \right\} = 0 \quad (5.80)$$

One has still to model the heat losses to the surroundings and the hot liquid zone. To describe the heat fluxes to the overburden, we use the lower bounds derived in Section 3.3. We will also use the quasi-steady state approximation 3.6.1 to model the two-dimensional heat transfer inside the hot liquid zone. We expect the two approximations to give a fairly good idea of the way the steam zone propagates. Then

$$\frac{\partial z_D}{\partial t_D} + \frac{\partial}{\partial x_D} \left\{ \left[\frac{z_D^N}{z_D^N + 1 - z_D} - \frac{1}{\beta_1} \right] \left[\frac{1}{2} - \frac{\beta_1}{4} \cdot \frac{x_D}{\sqrt{t_D}} \right] \right\} = 0 \quad (5.81)$$

$$z_D(0, t_D) = 1.0$$

This is identical to Eq. (4.106) for the saturation distribution in the steam zone in one-dimensional displacement with

$$f_{SD} = \frac{z_D^N}{z_D^N + 1 - z_D}, \quad D = 1, \quad E = \frac{\beta_1}{2}, \quad \frac{\gamma}{\gamma - 1} = \frac{1}{\beta_1} \quad \text{and } S_D$$

substituted by z_D . Hence, the solution will be given by expression (4.112):

$$x_D = \frac{2}{\beta_1} \cdot \frac{\left[1 - \frac{z_D^N}{z_D^N + 1 - z_D} \right]}{\left[\frac{1}{\beta_1} - \frac{z_D^N}{z_D^N + 1 - z_D} \right]} \sqrt{t_D} + \frac{4}{\beta_1^2} \cdot \frac{I(z_D)}{\left[\frac{1}{\beta_1} - \frac{z_D^N}{z_D^N + 1 - z_D} \right]} \quad (5.82)$$

where

$$I(z_D) = \int_1^{z_D} \frac{\left[1 - \frac{\eta^N}{\eta^N + 1 - \eta} \right] d\eta}{\left[\frac{1}{\beta_1} - \frac{\eta^N}{\eta^N + 1 - \eta} \right]} \quad (5.83)$$

Note that $0 < \beta_1 < 1$, as can be easily shown from the definition of β_1 , thus $\frac{1}{\beta_1} > 1$.

The result (5.82) is the steam drive analog of the Dietz (1953) approximation for isothermal, immiscible displacement. This solution can consequently be regarded as an approximation describing a "viscous finger" taking into account that the steam zone rides over the top of the hot liquid zone. Also notice that expression (5.82), equally valid for rectangular and radial displacement as well, is of the separable kind

$$x_D = f(z_D)\sqrt{t_D} + g(z_D)$$

where $f(z_D)$ and $g(z_D)$ are functions to be calculated from (5.83). A check to the legitimacy of the obtained result is obtained by comparing this form of steam zone propagation against inequalities (5.9) cast in dimensionless form. The energy inequality is satisfied as an equality which indicates that the solution is actually an upper bound, in an integral sense, to the steam zone volume. This is to be expected, since we used an upper bound on $\phi_D(t_D, x_D)$. On the other hand, the steam mass inequality is satisfied up until time t_{D3} , where

$$t_{D3} = \frac{4I^2(0)}{\beta_1^2(1-A)^2}$$

The analogy to the one-dimensional upper bounds is clear. We expect the

solution (5.82) to be valid, in an integral sense, for a short time interval extending up until t_{D3} beyond which the solution based on the steam mass balance takes over. Table 15 presents values of t_{D3} for various values of A , for $\beta_1 = 0.9$ and $N = 20, 100$. Comparing to t_{Da} in Table 8 we observe that t_{D3} is here a function of the generalized mobility ratio N . The larger N the smaller t_{D3} is, which indicates that Eq. (5.82) may be used to describe the steam zone growth for a smaller time interval than x_{1D}^+ . If, instead, we work with the steam mass Equations (5.57a,b), we obtain, for small G_{L2} , taking into account that $B = O(10^{-2})$:

$$\frac{\partial}{\partial x_D} \left\{ \frac{z_D^N}{z_D^N + 1 - z_D} \left[\frac{\phi_{2D}'(t_D)}{2} - \frac{\beta_2}{2} \{CNHF + CHL\}_D \right] \right\} + \frac{1}{2} \{CHF + HL\}_D = 0 \quad (5.84)$$

which can be integrated to give the quasi-steady state solution:

$$\frac{z_D^N}{z_D^N + 1 - z_D} = \frac{A - \{CCHF + CHL\}_D}{A - \beta_2 \{CNHF + CHL\}_D} \quad (5.85)$$

In dealing with the heat transfer terms we will approximate CHL by the lower bound expressions, $CNHF$ by the quasi-steady state approximation (3.6.1), and we will consider a negligible conductive heat flux, $CCHF = 0$. Under this approximation, we get an explicit representation for x_D :

$$x_D = \frac{2A}{\beta_2} \frac{\left[1 - \frac{z_D^N}{z_D^N + 1 - z_D} \right]}{\left[\frac{1}{\beta_2} - \frac{z_D^N}{z_D^N + 1 - z_D} \right]} \sqrt{t_D} \quad (5.86)$$

A	t_{D3}	
	<u>N = 100</u>	<u>N = 20</u>
0.25	0.2132	1.0611
0.30	0.2447	1.2181
0.35	0.2838	1.4127
0.40	0.3331	1.6580
0.45	0.4797	1.9731
0.50	0.5922	2.3875
0.55	0.7495	2.9476
0.60	0.9790	3.7305
0.65	1.3326	4.8725
0.70	1.9189	6.6321

Values of t_{D3} for various values of
A and for N = 100, 20. $\beta_1 = 0.9$.

Table 15

which is similar to the quasi-steady state part of (4.112). We expect that Eq. (5.86) is the solution to the steam front shape at large times, when (5.82) fails to satisfy the integral constraints (5.9). In Figure 75 we plot the displacement x_D vs. z_D as obtained from (5.82) for various values of time and $N = 100$. The solution at $t_D = 0.5$ is calculated by Eq. (5.82), while the solution for larger times is based on Eq. (5.86). We observe that, very quickly, a viscous finger is formed, which then propagates along the top of the reservoir leaving unaffected the main core of the original oil in place. In Figure 76 we plot the displacement corresponding to $t_D = 5$ for $N = 1, 10, 100$. The results emphasize the importance of the generalized mobility ratio N to the displacement. As N increases, the override effect is more pronounced and the efficiency of the recovery decreases dramatically.

Slightly different results are obtained when we approximate the heat fluxes by the zero net convection approximation 3.6.2. Then, $\{CNHF\} = \{CCHF\} = \{CHL\}$ and the respective solutions of Eqs. (5.79), (5.85) are:

$$x_D = \frac{1}{\beta_1} \cdot \frac{\left[1 - \frac{z_D^N}{z_D^N + 1 - z_D}\right]}{\left[\frac{1}{\beta_1} - \frac{z_D^N}{z_D^N + 1 - z_D}\right]} \sqrt{t_D} + \frac{1}{\beta_1^2} \cdot \frac{I(z_D)}{\left[\frac{1}{\beta_1} - \frac{z_D^N}{z_D^N + 1 - z_D}\right]} \quad (5.87)$$

and

$$x_D = \frac{A}{\beta_2} \cdot \frac{\left[1 - \frac{z_D^N}{z_D^N + 1 - z_D}\right]}{\left[\frac{1}{\beta_2} - \frac{z_D^N}{z_D^N + 1 - z_D}\right]} \sqrt{t_D} \quad (5.88)$$

The functional interdependence among x_D , t_D , z_D is identical to that of

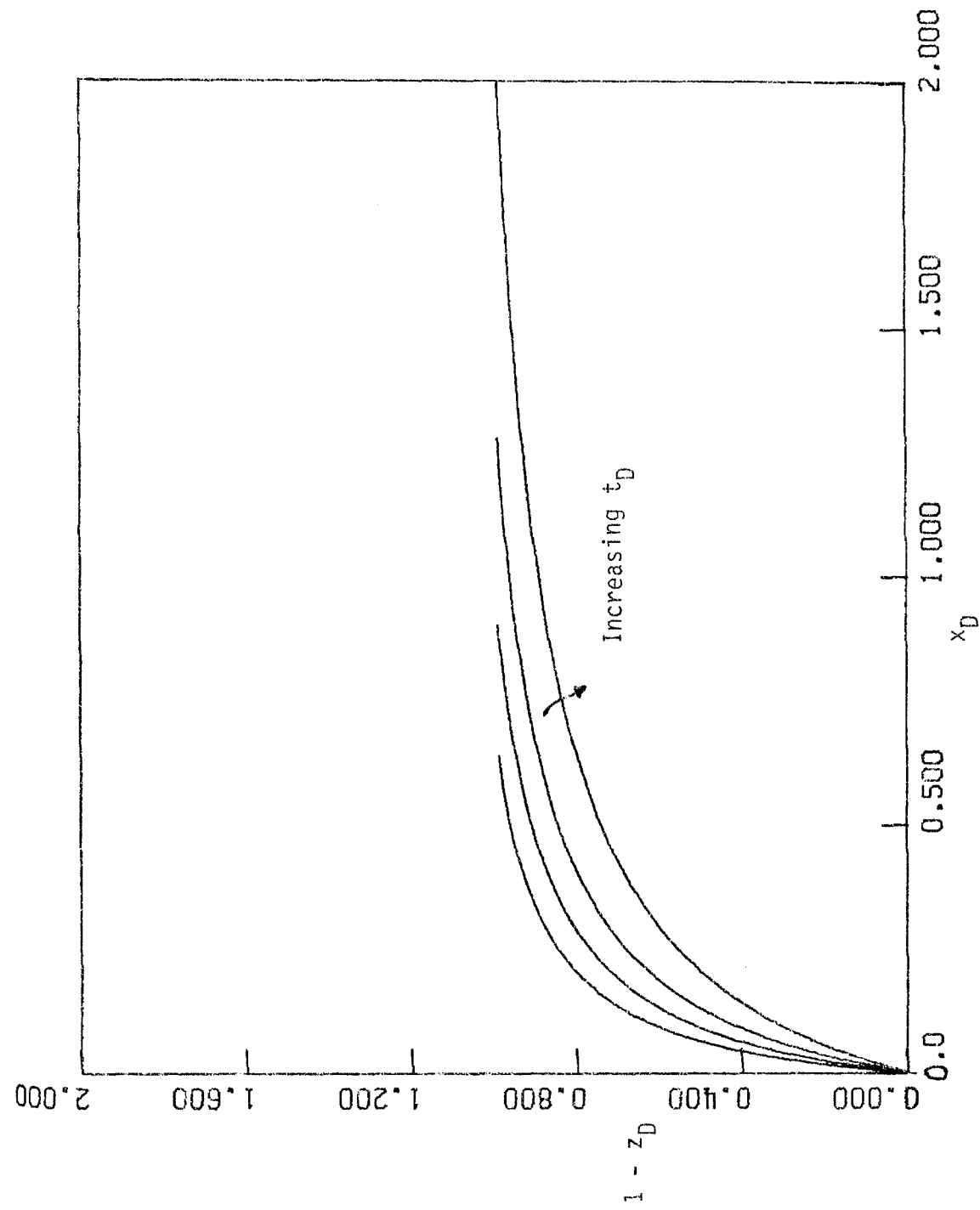


Figure 75. Vertical vs. Horizontal Displacement Based on the Viscous Solution, Eqs. (5.82) and (5.86) for $t_D = 0.5, 1.0, 2.0, 5.0$. $N = 100$, $A = 0.5$, $\beta_1 = 0.9$.

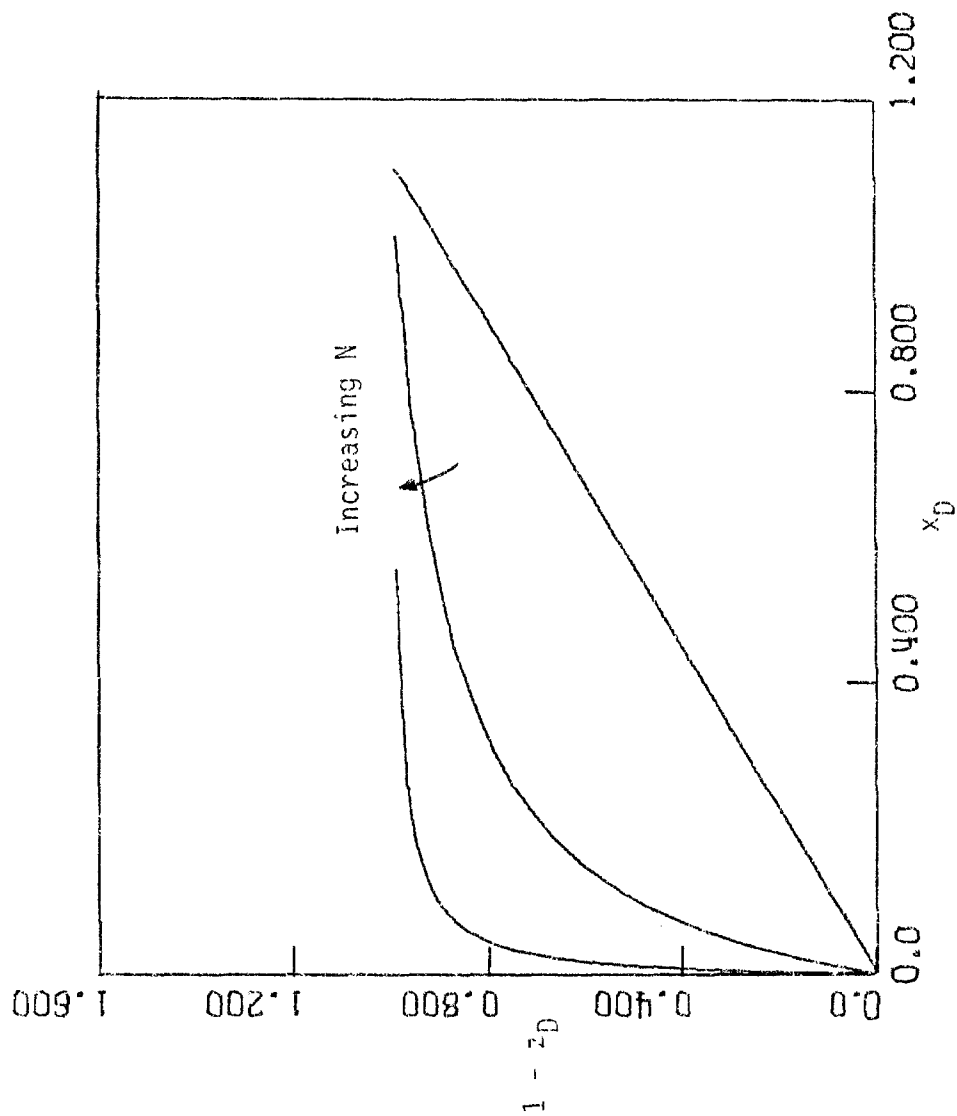


Figure 76. Vertical vs. Horizontal Displacement Based on the Viscous Solution, Eq. (5.86), at $t_D = 5.0$. $N = 1, 10, 100$. $A = 0.5$.

Eqs. (5.82), (5.86) with the exception of a proportionality factor of 2, which is missing from the set of Eqs. (5.87), (5.88).

We finally calculate the interesting index of vertical efficiency, E_v . Initially, E_v is evaluated by using either of (5.82) or (5.88). It is worth noticing that the expressions obtained are identical, regardless of the particular heat transfer model employed (quasi-steady state approximation or zero net convective heat flux assumption). This further suggests that, in terms of estimating indices for the integral performance of a steam drive, the particular heat transfer approximations do not alter the results significantly. At large times, E_v is independent of time and equal to:

$$E_v = \frac{1}{[N(1 - \beta_2) - 1]} \left\{ \frac{N(1 - \beta_2)}{[N(1 - \beta_2) - 1]} \ln [N(1 - \beta_2)] - 1 \right\} \quad (5.89)$$

As shown in Figure 77 the vertical efficiency decreases rapidly, as N increases, in accordance with experimental evidence [Baker (1973)].

Although a rough approximation, the viscous solution of this subsection serves to provide simple analytical expressions, by means of which we can evaluate various interesting integral indices of the performance. The results obtained show, in an approximate but, nevertheless, convincing manner, the important role played by the generalized mobility ratio, N , in the gravity override and the overall performance of a steam-drive. This should become more clear by the complete solution of the general Equation (5.60). The latter should also provide the guidelines for the development of suitable control policies to improve the vertical sweep efficiency. From the foregoing preliminary analysis, it is evident

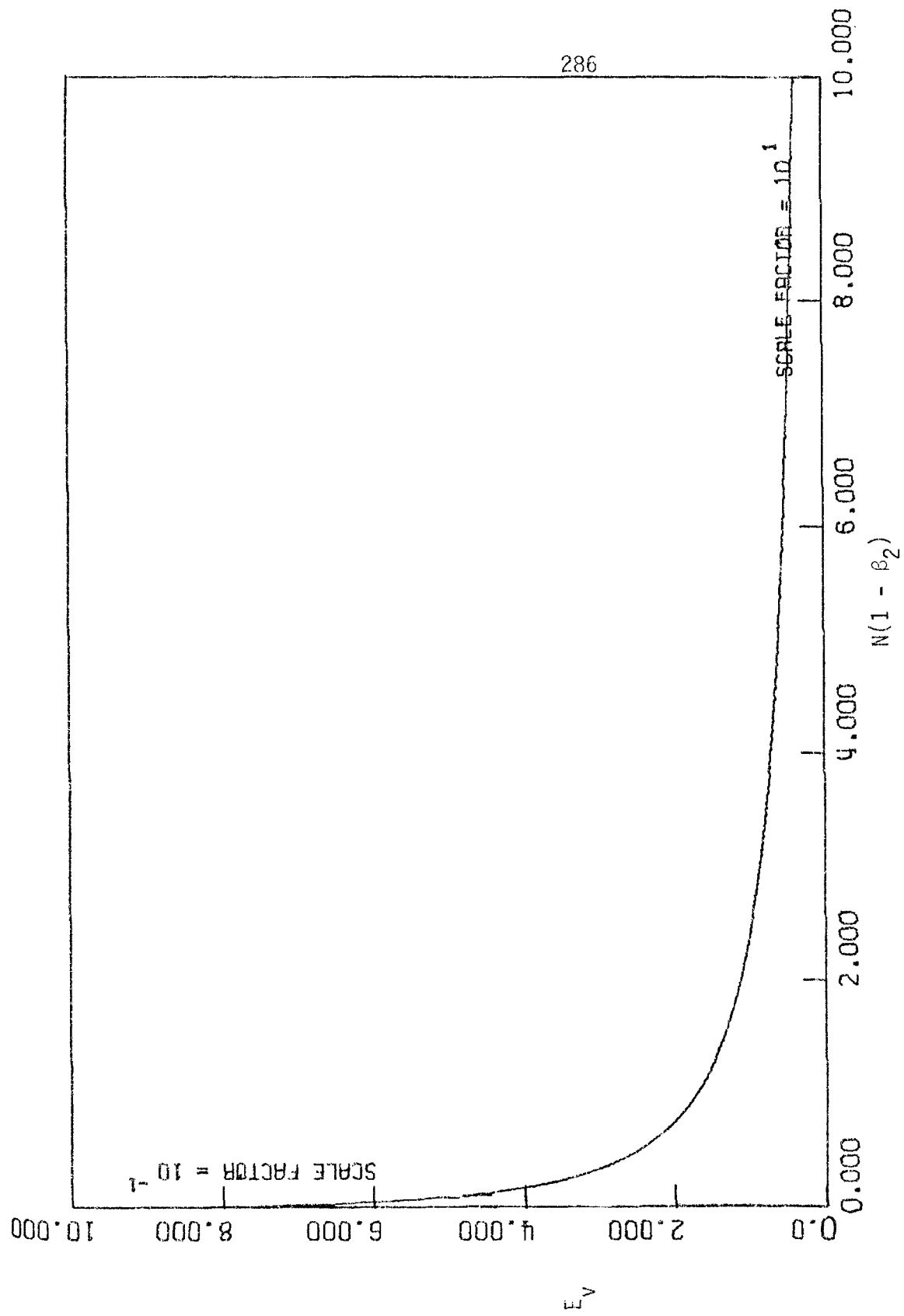


Figure 77. Vertical Sweep Efficiency, E_v , vs. $N(1 - \beta_2)$ Based on the Viscous Solution Eq. (5.88). $\beta_2 = 0.9$.

that in implementing such policies particular attention should be given on the magnitude of N . It is expected that the development of methods that aim to control the magnitude of N at low levels would be of great help in increasing the recovery efficiency of a three-dimensional steam drive.

5.7.4 Neuman's (1975) Model

A final note should be added regarding Neuman's (1975) model, its method of derivation and the range of its validity. In contrast to the present model, Neuman considers injection through a point source at a fixed location (preferably the top of the injection interval). This difference in operating conditions causes the steam zone to expand in a more pronounced way along both the horizontal and the vertical directions, much like the growth of a plume. In spite of this, the approach used by Neuman in modelling the steam zone growth is essentially the integral technique employed here, although with a different set of assumptions. Viewed from our frame of reference, the procedure followed consists of three basic steps. First, a liquid water mass balance over the steam zone is derived. It is our belief that, for the particular modelling purposes, this is equivalent to the following linear combination of Eqs. (2.55), (2.56) and (2.57) of Chapter II:

$$\begin{aligned} & \frac{d}{dt} \int_0^{z(x,t)} (\phi \rho_w S_w + \phi \rho_o S_o) dz + \left[\rho_w^{II} (u_{wn}^{II} - \phi S_w^{II} v_n) + \rho_o^{II} (u_{on}^{II} - \phi S_o^{II} v_n) \right] |\nabla F| \\ &= \frac{\left(-k_{hR} \left(\frac{\partial T_R}{\partial n} \right)^{II} \right)}{L_V^{(1)}} |\nabla F| + \frac{\left(-k_{hf} \left(\frac{\partial T_f}{\partial n} \right)^{II} \right)}{L_V^{(1)}} + \frac{\partial}{\partial x} \left\{ \int_0^{z(x,t)} (\rho_w \hat{u}_{wx} + \rho_o \hat{u}_{ox}) dz \right\} \quad (5.90) \end{aligned}$$

The assumption of zero net convection, 3.5.2, is then introduced. Thus, heat transfer in the hot liquid zone is approximated by one-dimensional heat conduction along the vertical direction, and the net convective flux, $W_F(x,t)$, is considered negligible. By further assuming that heat losses obey a Marx-Langenheim distribution, the following expressions are derived:

$$\left(-k_{hR} \frac{\partial T_R}{\partial n} \right)^{II} |\nabla F| = \sqrt{\frac{k_{hR} M^{(2)}}{\pi}} \frac{\Delta T}{\sqrt{t - \lambda}} \quad (5.91a)$$

$$\left(-k_{hf} \frac{\partial T_f}{\partial n} \right)^{II} = \sqrt{\frac{k_{hf} \rho_f c_{pf}}{\pi}} \frac{\Delta T}{\sqrt{t - \lambda}} \quad (5.91b)$$

[compare to (3.48b) and (3.15)]. Now, the second term on the LHS of (5.90) is approximately equal to $W_F(x,t)$ and, in the spirit of the above approximation, it is considered negligible. The next simplification involves the last term on the RHS of (5.90) which is set equal to zero, assuming negligible flow in the horizontal direction. Combining the above, we get

$$(\phi \rho_W \bar{S}_W + \phi \rho_O \bar{S}_O) \frac{dz}{dt} = \frac{\Delta T}{\sqrt{\pi}} \frac{\left[\sqrt{k_{hR} M^{(2)}} + \sqrt{k_{hf} \rho_f c_{pf}} \right]}{L_V^{(1)} \sqrt{t - \lambda}} \quad (5.92)$$

which gives the rate of growth of the steam zone thickness at any point, in terms of the time elapsed after steam first arrived at the particular point under consideration.

As it was pointed out in the introductory Chapter I, and can be easily confirmed in the above derivation, the model does not differentiate between the mechanisms of growth along the horizontal and the vertical direction. This further indicates that gravity is not actually taken into consideration and this is evidenced by the absence of any gravity terms in the final expression (5.92). It is also clear, that the postulated

mechanism is essentially a balance between the latent heat released by the condensed steam and the thermal resistance to steam zone growth due to heat capacity requirements. In this sense, Neuman's model is closer to the one-dimensional models of Chapter IV than the two-dimensional models of the present chapter.

The above observations suggest that the region of validity of Neuman's model is limited to steam injection processes under low injection rates, and where injection is taking place at a fixed point of the injection interval. As soon as the steam zone reaches the upper and lower boundaries of the reservoir, the postulated mechanism ceases to control the steam zone growth and the model cannot practically be used any further.

5.8 Conclusions

To elucidate the complex three-dimensional steamflood, we followed two different approaches. The first deals with the integral characterization of the steam zone and is an extended version of the one-dimensional method for the derivation of upper bounds. Based on various postulated forms of displacement (separable, parabolic), we developed upper bounds on the volume of the steam zone as a function of time. In contrast to the one-dimensional case, the bounds, hence the actual steam zone volume, depend on a geometric parameter that measures the extent of gravity override. For the frequently occurring case of separable fronts, in particular, we can evaluate the above parameter by means of simplified models for the steam front shape. This gives rise to a reliable method for the estimation of the steam zone growth in terms of the physical

variables of the process. The results obtained warn against the use of the simplified Marx-Langenheim solution, even if it is properly modified to account for gravity segregation.

The second approach involves the study of a finer characteristic of the steam zone, the steam front shape. To develop a suitable model, we employed the integral balance technique of Chapter II, as applied to two-(or three-) dimensional systems, and made use of the Dupuit approximation and proper interfacial conditions at the steam front. Depending on whether we base our calculations on the total energy or the latent heat balance, respectively, we obtain two different partial differential equations that describe the evolution of the steam front shape. In principle, the two equations should be equivalent. Due, however, to the different nature of the approximations that we further employ to approximate heat transfer in the two cases, the respective equations give rise to different solutions, that complement each other in the same sense the two upper bounds in Part A do. A stability analysis of the steam front reveals that a suitably defined generalized mobility ratio determines the stability characteristics of the propagation. Having not solved the detailed partial differential equations, we developed, instead, approximate solutions in the limiting case where viscous forces control the evolution of the steam front. The results indicate that the vertical sweep efficiency is very sensitive to the magnitude of the generalized mobility ratio, rapidly decreasing as the latter increases. The relative significance of the generalized mobility ratio in the performance of the steam drive further suggests that in designing an effective steam injection process, it is imperative to keep its magnitude at low levels. The various

means by which this can be achieved form the topic of another investigation.

Chapter VI. Concluding Remarks

As emphasized in the introductory chapter, the principal objective of the present work was to provide a reliable analytical model for the description of the steam injection process. It was particularly stressed that the desired model should suitably account for the effects of: (1) heat transfer in the hot liquid zone and the surroundings, and (2) gravity segregation, on the performance of a steam drive. To a varying degree of success this task has been accomplished.

We started with a rigorous differential (microscopic) description of the physical phenomena associated with steam injection. We then introduced an integral balance technique, which is essentially a three- (or two-) dimensional averaging procedure and by means of which the basic conservation equations were cast in an integral (macroscopic) form. Based on the assumption that most of the relevant properties of the steam zone have a spatial average which is constant (or slowly varying) with time, the technique can be very effectively applied to determine the rate of growth of the steam zone volume, which is, here, the principal quantity of interest. A check on this assumption was further supplied by a simple iterative scheme: After adopting the method, we solved for the properties distribution and verified the postulated behavior. From a mathematical viewpoint, adoption of the integral balance technique has greatly helped us to simplify the complicated system of non-linear, coupled PDE's in three different regions to a simpler moving boundary problem. As such, we expect that it can be equally well applied to other systems of engineering importance that are marked by similar properties and degree of complexity.

The basic parameters that control the S.Z. growth, in an integral sense, are the heat losses to the surroundings and the fluxes to the H.L.Z. Estimating their magnitude was the topic of a separate analysis dealing exclusively with heat transfer (Chapter III). A subsequent rigorous investigation of the heat transfer in the H.L.Z. produced an interesting new class of heat transfer problems, involving a moving boundary, which are characterized by a novel dimensionless group, R , that expresses the ratio of heat fluxes in orthogonal (conjugate) directions. The key concept in formulating the above problems consisted of two basic elements: simultaneous consideration of heat transfer in both the H.L.Z. and the surroundings (coupling preserved) and separate analysis on the fluid flow and heat transfer in the H.L.Z. (decoupling). Such an approach seems to work pretty well: it renders the problem analytically tractable without altering its nature. The analytical techniques that were further devised for the solution of the resulting moving boundary problems are very helpful not only in the context of steam drive calculations, but also in modelling other in-situ thermal methods. It is, for example, understood that calculating commonly employed integral indices, such as the heat efficiency of the process, can follow in a straightforward way from the presented analysis. It is the author's belief that these techniques may also apply to a variety of other problems of similar nature that involve combined transport by diffusion and convection to two different (orthogonal) regions and a moving boundary. In the same context, it would be interesting to discuss a slightly non-linear version of the examined problem (convective term a function of the dependent variable).

The above considerations were incorporated in the integral formulation of Chapter II and applied to determine the steam zone volume rate of growth in one-dimensional symmetric geometries (Chapter IV). Being unable to develop exact solutions, we concentrated instead on a more explicit representation by deriving new expressions for upper and lower bounds, asymptotic solutions and approximate overall solutions. Each of the derived solutions has its own value and region of validity in different time domains and under different operating conditions. In particular, the upper bounds obtained hold for variable injection rates in contrast to the rest of the solutions which are valid under conditions of constant injection only. Due to the different modes that dominate heat transfer in the H.L.Z. in different time regimes (conductive vs. convective), we did not restrict ourselves in developing one upper bound only, but we rather considered two different bounds which complement each other in defining an overall lower upper bound. The reasoning that dictates such an approach can be briefly summarized as follows: The approximation to the heat transfer terms in the energy balance breaks down at large times due to the change in the heat transfer mechanism. In such a case, we may additionally develop another conservation equation (steam mass balance) the unknown heat transfer terms of which can be better approximated at large times. In other words, we split the problem into two parts that nicely complement each other in different time regions. Of course, had we had an exact representation of the heat transfer in the H.L.Z., the two equations would give rise to identical bounds. We believe that this concept of generating additional conservation equations, in situations where important pieces of information are missing, can be very useful in

many similar fields, not only in providing complementary solutions but also in checking the existing ones.

As also confirmed by the asymptotic expansion results, it is a single dimensionless injection parameter A that regulates the growth of the steam zone. The smaller A , i.e. the smaller the latent heat injected is, the better the description by the bound based on the latent heat balance. This has a significant importance in the context of evaluating the region of validity of the existing Marx-Langenheim model and designing a steam drive. The smaller A is the more the Marx-Langenheim solution deviates from the true solution. In particular, under the frequently occurring conditions of $A < 2/\pi$, one should be careful not to base his predictions on the Marx-Langenheim description, otherwise they are bound to be over-optimistic with all due consequences in the economic sphere. On the other hand, the Marx-Langenheim solution is shown to give reliable results at the beginning of the process, provided that injection rates are sufficiently high. The criterion developed defines a time and physical parameters domain where this occurs, and provides a solid justification on the old confidence on the Marx-Langenheim model for short times.

To obtain a better insight, we developed the asymptotic expansion of the exact solution. We observe that the asymptotic behavior is, at the limit, controlled by a balance between the injected and the dissipated to the surrounding heat alone, and it is solely depending on the parameter A . The latter is decisive in determining how fast the asymptotic behavior is reached. Small values of A favor fast convergence. Another significant conclusion that has been extracted from the asymptotic results deals with horizontal conduction. It is seen that the magnitude of R (hence of

horizontal conduction) plays no role whatsoever in the final expression attained, although it significantly influences the characteristic time for convergence. Although it was not pursued in the text, it is rather easy to construct, based on the asymptotic expressions, a composite approximate solution by appropriate curve fitting. On the other hand, we did develop an approximate solution based on a quasi-steady state approximation to suitably account for heat transfer, which was shown to produce quite reliable results in the investigated regions. Thus, we expect this scheme to hopefully substitute the need for the sophisticated numerical simulators in one-dimensional steam drive calculations. The agreement obtained seems also to solidify the old existing respect to quasi-steady state approximations, both in moving boundary problems and in other fields, as a powerful analytical tool to describe complex phenomena.

A basic question posed in the Introduction was related to the effect that heat transfer in the H.L.Z. has on the S.Z. growth. The foregoing analysis was hopefully quite convincing that this effect is indeed significant in a twofold sense: Firstly, through the heat flux to the H.L.Z. and secondly by virtue of the heat losses from the S.Z. to the surroundings, which, in turn, are depending on the H.L.Z. temperature history in a rather strong coupling. The second effect is seen to affect the heat losses very drastically, as clearly evidenced in the asymptotic expression. A quick comparison with a Marx-Langenheim type of calculation, which is known not to include the aforementioned coupling, supplies additional evidence. Overall, it was shown that heat transport in the H.L.Z. and, by coupling, to the surroundings, will inevitably lead to

lower predictions and, as such, plays a crucial role in heavily influencing the steam-drive performance.

The second basic question introduced in Chapter I was concerned with the effect of gravity on the steam zone growth of a three-dimensional steamflood. This complicated topic was investigated by two different approaches (Chapter V). In the first, we followed the familiar three-dimensional averaging procedure with the objective to set bounds on the steam zone volume. The effect of gravity was reflected in a single parameter that can be evaluated in terms of the physical variables of the problem, by means of reliable simple analytical models for the steam front shape. The resulting expressions constitute a new, simple, reliable, and fast, engineering method to estimate firstly, the severity of gravity segregation and, secondly, its quantitative effect on the steam zone volume. Aiming at a better insight on the mechanism of gravity segregation we attempted to determine the steam front shape. The technique used relies on a two-dimensional averaging approach (integral balances) similar in concept to the three-dimensional averaging. Due to the finer structure (more information) we are seeking after in this case, however, the subsequent handling is more difficult and requires additional approximations. Despite this, we believe that the approach followed gives rise to a reliable first order approximation to the problem of gravity segregation. From the final formulation we produced a set of two novel, non-linear PDE's. In spite of the fact that the two equations are equivalent, the system is not redundant, since the various approximations that are implemented regarding heat transfer are better observed in mutually exclusive regions. Thus, we expect the two equations to complement each other in two

different regions, in an analogous way that the two previously derived bounds do. Due to time limitations, the rigorous solution of the resulting PDE's has not yet been achieved. Instead, a preliminary stability analysis and limiting solutions under the assumption of predominantly viscous flow have emphasized the importance of the newly defined generalized mobility ratio in the performance of a steam drive. These results are expected to be corroborated by the rigorous solution of the PDE's derived. This aspect is certainly fresh ground for future research. To further advance on the subject one has, in addition, to proceed with a more detailed analysis of the heat transfer inside the H.L.Z. The models derived in Chapter III, under various approximations, certainly provide a first step towards a better understanding. A careful look should also be given to the generalized mobility ratio in order to single out the exact parameters that determine its value. It is imperative, if any progress at all is to be made regarding gravity override control, to be able to develop appropriate control policies on the magnitude of N .

A final question that has not been previously raised and deserves particular attention concerns the effect of viscosity reduction on the steam drive performance. As emphatically stressed in the Introduction, the principal advantage of thermal methods, over other EOR methods, lies in the very mechanism of viscosity reduction. By contrast, the majority of the herein derived results do not touch upon this subject. This is seemingly contradictory, but it becomes clearly consistent after the following considerations: As repeatedly noted, here we are mainly concerned with the steam zone volume growth. Due to the postulated decoupling of fluid flow and heat transfer in the H.L.Z., the S.Z. volume rate of

growth is slightly, if at all, affected by viscosity reduction and the same is true for the heat transfer in the H.L.Z. What is influenced by viscosity reduction is the saturation distribution inside the H.L.Z. The preceding analysis is based on the assumption of constant total volumetric flow in the H.L.Z., but nevertheless allows saturations to vary. The effect of temperature on the saturation distribution should be carried out further by a separate analysis, which, in turn, would make use of the already obtained heat transfer results. The new results are expected to indicate a strong influence of viscosity reduction on the saturation distribution, the oil recovery rates and only slightly, if at all, affect the heat transfer mechanism. Such a topic will further complement the one-dimensional modelling by providing the much desired oil recovery rates as a function of steam injected. By analogy to one-dimensional, isothermal, immiscible displacement and recalling concepts of non-linear wave propagation, we expect the oil recovery to be an increasing function of the S.Z. volume rate of growth.

References

- Abdalla, A. and Coats, K. H.: "A Three-Phase, Experimental and Numerical Simulation Study of the Steam Flood Process", paper SPE 3600 presented at the SPE-AIME 46th Annual Fall Meeting, New Orleans, Oct. 3-6, 1971.
- Abramowitz, M. and Stegun, I. A.: "Handbook of Mathematical Functions", Dover Publications, Inc., New York (1965).
- Ames, W. F.: "Nonlinear Partial Differential Equations in Engineering", Vol. II, Academic Press, Inc., New York (1972) 6.
- Aris, R.: "Vectors, Tensors, and the Basic Equations of Fluid Mechanics", Prentice-Hall, Inc., Englewood Cliffs, N.J. (1962).
- Avdonin, N. A.: "Some Formulas for Calculating the Temperature Field of a Stratum Subject to Thermal Injection", Neft'i Gaz, (1964) Vol. 7, 37.
- Baker, P. E.: "An Experimental Study of Heat Flow in Steam Flooding", Soc. Pet. Eng. J. (March, 1969) 89-99; Trans., AIME, Vol. 246.
- Baker, P. E.: "Effect of Pressure and Rate on Steam-Zone Development in Steamflooding", Soc. Pet. Eng. J. (Oct., 1973) 274-284; Trans., AIME, Vol. 255.
- Bear, J.: "Dynamics of Fluids in Porous Media", American Elsevier Publishing Company, Inc., New York (1972).
- Beckers, H. L.: "The Deformation of an Interface Between Two Fluids in a Porous Medium", Appl. Science Res. Annual (1965), Vol. 14, 101.
- Beckers, H. L. and Harmsen, G. J.: "The Effect of Water Injection on Sustained Combustion in a Porous Medium", Soc. Pet. Eng. J. (June, 1970), 145-163; Trans., AIME, 249.

- Blevins, T. R., Aseltine, R. J., and Kirk, R. S.: "Analysis of a Steam Drive Project, Inglewood Field, California", J. Pet. Tech. (Sept., 1969) 1141.
- Blevins, T. R. and Billingsley, R. H.: "The Ten-Pattern Steamflood, Kern River Field, California", J. Pet. Tech. (Dec., 1975) 1505.
- Boberg, T. C. and Lantz, R. B.: "Calculation of the Production Rate of a Thermally Stimulated Well", J. Pet. Tech. (Dec., 1966) 1613.
- Boyd, A. V.: "Inequalities for Mill's Ratio", Rep. Statist. Appl. Res. Un. Jap. Sci. Engrs. (1959) Vol. 6, 44-46.
- Buckley, S. E. and Leverett, M. C.: "Mechanism of Fluid Displacement in Sands", Trans., AIME (1942), Vol. 146, 107.
- Bursell, C. G.: "Steam Displacement--Kern River Field", J. Pet. Tech. (Oct., 1970) 1225-1231.
- Business Week: "The FEA's Big Push for Tertiary Oil", June 14, 1976, 31.
- Cady, G. V., Bilhartz, H. L., Jr., and Ramey, H. J., Jr.: "Model Studies of Geothermal Steam Production", Water - 1972, AIChE Symposium Series (1972) 445-452.
- Calhoun, J. C., Lewis, M. and Newman, R. C.: "Experiments on the Capillary Properties of Porous Solids", Trans., AIME (1949) Vol. 186, 189.
- Carslaw, H. S. and Jaeger, J. C.: "Conduction of Heat in Solids", 2nd ed., Oxford University Press, London (1959) 387.
- Chase, C. A. and O'Dell, P. M.: "Application of Variational Principles to Cap and Base Rock Heat Losses", Soc. Pet. Eng. J. (Aug., 1973) 200-210; Trans., AIME, Vol. 255.
- Chu, C.: "Pattern Configuration Effect on Steamflood Performance", paper SPE 6728 presented at the SPE-AIME 52nd Annual Fall Meeting, Denver, Oct. 9-12, 1977.

- Chu, C. and Trimble, A. E.: "Numerical Simulation of Steam-Displacement-Field Performance Applications", J. Pet. Tech. (June, 1975) 765-776.
- Chuoque, R. L., van Meurs, P. and van der Poel, C.: "The Instability of Slow Immiscible, Viscous Liquid-Liquid Displacements in Porous Media", Trans., AIME (1959) Vol. 216, 188-194.
- Clossman, P. J. Ratliff, N. W. and Truitt, N. E.: "A Steam-Soak Model for Depletion-Type Reservoirs," J. Pet. Tech. (June, 1970) 757-770; Trans., AIME, Vol. 249.
- Coats, K. H., George, W. D., Chu, C. and Marcum, B. E.: "Three-Dimensional Simulation of Steamflooding", Soc. Pet. Eng. J. (Dec., 1974) 573-592; Trans., AIME, Vol. 257.
- Coats, K. H.: "Simulation of Steamflooding with Distillation and Solution Gas", Soc. Pet. Eng. J. (Oct., 1976) 235-247.
- Davis, H. T.: "Introduction to Nonlinear Differential and Integral Equations", Dover Publications, Inc., New York (1962) 70.
- de Haan, H. J. and Schenk, L.: "Performance Analysis of a Major Steam Drive Project in the Tia Juana Field, Western Venezuela", J. Pet. Tech. (Jan., 1969) 111-119; Trans., AIME, Vol. 246.
- Delhaye, J. M.: "Jump Conditions and Entropy Sources in Two-Phase Systems. Local Instant Formulation", Int. J. Multiphase Flow (1974), Vol. 1, 395-409.
- Dietz, D. N.: "A Theoretical Approach to the Problem of Encroaching and By-Passing Edge Water", Proc. Ned. Akad. Wetensh., (1953), B56, 83.
- Dietz, D. N. and Weijdemans, J.: "Wet and Partially Quenched Combustion", J. Pet. Tech. (April, 1968) 411-413; Trans, AIME, Vol. 243.

- Doscher, T. M. and Ershaghi, I.: "Current Economical Appraisal of Steam and Combustion Drives", Report (March, 1978), Department of Petroleum Engineering, University of Southern California.
- Doscher, T. M. and Wise, F. A.: "Enhanced Crude Oil Recovery Potential-- An Estimate", J. Pet. Tech. (May, 1976) 575-585.
- Edmonson, J. A.: "Effect of Temperature on Waterflooding", J. Cdn. Pet. Tech. (Oct.-Dec., 1965) 236.
- Erdélyi, A. et al.: "Tables of Integral Transforms", Vol. II, McGraw-Hill Book Co., Inc., New York (1954), Ch. 13.2.
- Geertsma, J., Croes, G. A. and Schwarz, N.: "Theory of Dimensionally Scaled Models of Petroleum Reservoirs", Trans. AIME (1956), Vol. 207, 118-127.
- Glasser, D. and Kern, J.: "Bounds and Approximate Solutions to Linear Problems with Nonlinear Boundary Conditions; Solidification of a Slab", AIChE J. (March, 1978), Vol. 24, 161-170.
- Gomaa, E.: "Simplified Method for Predicting Oil Recovery by Steam Flood", Paper SPE 6169 presented at the SPE-AIME 51st Annual Fall Meeting, New Orleans, 1976.
- Goodman, T. R.: "Applications of Integral Methods to Transient Nonlinear Heat Transfer" in "Advances in Heat Transfer", (1964), Vol. 1, 52-120.
- Gottfried, B. S.: "A Mathematical Model of Thermal Oil Recovery in Linear Systems", Soc. Pet. Eng. J. (Sept., 1965) 196-210; Trans., AIME, Vol. 234.
- Hagoort, J., Liejnse, A. and van Poelgeest, F.: "Steam-Strip Drive: A Potential Tertiary Recovery Process", J. Pet. Tech. (Dec., 1976), 1409-1419.

- Hall, A. L. and Bowman, R. W.: "Operation and Performance of the Slocum Field Thermal Recovery Project", J. Pet. Tech. (April, 1973) 402-408.
- Hearn, C. L.: "The El Dorado Steam Drive--A Pilot Tertiary Recovery Test", J. Pet. Tech. (Nov., 1972) 1377-1384.
- Johnson, F. Sam, Walker, C. J., and Bayazeed, A. F.: "Oil Vaporization During Steamflooding", J. Pet. Tech. (June, 1971) 731-742; Trans., AIME, Vol. 251.
- Lauwerier, H. A.: "The Transport of Heat in an Oil Layer Caused by the Injection of Hot Fluid", Appl. Sci. Res. (1955), Vol. 5, Sec. A, 145.
- Le Fur, B. and Sourieau, P.: "Étude de l'Écoulement Diphasique dans une Couche Inclignée et dans un Modèle Rectangulaire de Milieu Poreux", Rev. Inst. Fr. Petrol. (1963), Vol. 18, 325-343.
- Mandl, G. and Volek, C. W.: "Heat and Mass Transport in Steam-Drive Processes", Soc. Pet. Eng. J. (March, 1969) 59-79; Trans., AIME, Vol. 246.
- Marx, J. W. and Langenheim, R. H.: "Reservoir Heating by Hot Fluid Injection", Trans., AIME (1959), Vol. 216, 312-315.
- Martin, J. C.: "Analysis of Internal Steam Drive in Geothermal Reservoirs", J. Pet. Tech. (Dec, 1975) 1493-1499.
- Miller, C. A.: "Stability of Moving Surfaces in Fluid Systems with Heat and Mass Transport. III. Stability of Displacement Fronts in Porous Media", AIChE J. (1975), Vol. 21, 474-479.
- Morel-Seytoux, H. J.: "Two-Phase Flow in Porous Media", in Advan. Hydroscience (1973), Vol. 9, 119-202.

- Mori, A. and Araki, K.: "Methods for Analysis of the Moving Boundary-Surface Problem", International Chemical Engineering (1976), Vol. 16, 734-744.
- Myhill, N. A. and Stegemeier, G. L.: "Steam-Drive Correlation and Prediction", J. Pet. Tech. (Feb., 1978) 173-182.
- N.E.L. (National Engineering Laboratory): "Steam Tables 1964", Her Majesty's Stationary Office, Edinburgh (1964).
- Neuman, C. H.: "A Mathematical Model of the Steam Drive Process-Applications", paper SPE 4757 presented at the 45th Annual California Regional Meeting, Ventura, Calif., April 2-4, 1975.
- Niko, H. and Troost, P.J.P.M.: "Experimental Investigation of Steam Soaking in a Depletion-Type Reservoir", J. Pet. Tech. (Aug, 1971), 1006-1014; Trans., AIME, Vol. 251.
- Ockendon, J. R. and Hodgkins, W. R., editors: "Moving Boundary Problems in Heat Flow and Diffusion", Proceedings of the Conference Held at the University of Oxford, 25-27 March, 1974.
- Oldham, K. B. and Spanier, J.: "The Fractional Calculus; Theory and Applications of Differentiation and Integration to Arbitrary Order", Academic Press, New York (1974).
- Outmans, H. D.: "Nonlinear Theory for Frontal Stability and Viscous Fingering in Porous Media", Soc. Pet. Eng. J. (June, 1962) 165-176; Trans., AIME, Vol. 225.
- Ozen, A. S. and Farouq Ali, S. M., Jr.: "An Investigation of the Recovery of the Bradford Crude by Steam Injection", J. Pet. Tech. (June, 1969) 692.

- Pearson, C. E.: "Handbook of Applied Mathematics", Van Nostrand Reinhold Company, New York (1974), 130.
- Philip, J. R.: "Theory of Infiltration", in Advan. Hydroscience (1969), Vol. 5, 248-267.
- Poots, G.: "An Approximate Treatment of a Heat Conduction Problem Involving a Two-Dimensional Solidification Front", Int. J. Heat Mass Transfer, (1962), Vol. 5, 339-348.
- Poston, S. W., Ysrael, S., Hossain, D.K.M.S., Montgomery, E. F. III, and Ramey, H. J., Jr.: "The Effects of Temperature on Irreducible Water Saturation and Relative Permeability of Unconsolidated Sands", Soc. Pet. Eng. J., (June, 1970), 171-180; Trans., AIME, Vol. 249.
- Prats, M.: "The Heat Efficiency of Thermal Recovery Processes", J. Pet. Tech. (March, 1969) 323-332; Trans., AIME, Vol. 246.
- Prats, M. and Miller, W. C.: "The Role of Technical Publications in the Advancement of Fluid Injection Processes for Oil Recovery", J. Pet. Tech. (Dec., 1973) 1361-1370.
- Ramey, H. J., Jr.: "Discussion on the Paper by Marx and Langenheim", Trans., AIME (1959) Vol. 216, 364.
- Rubin, A. and Schweitzer, S.: "Heat Transfer in Porous Media with Phase Change", Int. J. Heat Mass Transfer, Vol. 15, 43-60, 1972.
- Rubinshtein, L. I.: "The Stefan Problem", American Mathematical Society, Providence, R. I., (1971).
- SPE (Society of Petroleum Engineers):
 "Letter Symbols for Petroleum Reservoir Engineering, Natural Gas Engineering and Well Logging Quantities", J. Pet. Tech. (Dec., 1965) 1463-1495; Trans., AIME, Vol. 234.

- "Supplements to Letter Symbols and Computer Symbols for Petroleum Reservoir Engineering, Natural Gas Engineering and Well Logging Quantities", Trans., AIME, (1972), Vol. 253, 556.
- "The SI Metric System of Units and SPE's Tentative Metric Standard", J. Pet. Tech. (Dec., 1977) 1575-1610.
- "Thermal Recovery Processes", Transaction Reprint Series, Vol. 10, 1972.
- Saffman, P. G. and Taylor, G.: "The Penetration of a Fluid into a Porous Medium or Hele-Shaw Cell Containing a More Viscous Fluid", Proc. Roy. Soc. of London (1958), Vol. 245, 312.
- Schlichting, H.: "Boundary Layer Theory", McGraw-Hill, New York, (1955).
- Sheldon, J. W. and Fayers, F. J.: "The Motion of an Interface Between Two Fluids in a Slightly Dipping Porous Medium", Soc. Pet. Eng. J. (Sep., 1962) 275-282; Trans., AIME, Vol. 225.
- Shutler, N. D.: "Numerical Three-Phase Simulation of the Linear Steam-flood Process", Soc. Pet. Eng. J. (June, 1969) 232-246; Trans., AIME, Vol. 246.
- Shutler, N. D.: "Numerical Three-Phase Model of the Two-Dimensional Steam-flood Process", Soc. Pet. Eng. J. (Dec., 1970) 405-417; Trans., AIME, Vol. 249.
- Shutler, N. D. and Boberg, T. C.: "A One-Dimensional Analytical Technique for Predicting Oil Recovery by Steamflooding", Soc. Pet. Eng. J. (Dec., 1972) 489-498.
- Smith, R. V., Bertuzzi, A. F., Templeton, E. E. and Clampitt, R. L.: "Recovery of Oil by Steam Injection in the Smackover Field, Arkansas", J. Pet. Tech. (Aug., 1973) 883-889.

- Spillette, A. G.: "Heat Transfer During Hot Fluid Injection into an Oil Reservoir", J. Canadian Pet. Tech. (1965), Vol. 4, 213.
- Stakgold, I.: "Boundary Value Problems of Mathematical Physics", Vol. II, MacMillan, New York (1968), Ch. 7.
- Thomas, G. W.: "Approximate Method for Calculating the Temperature Distribution During Hot Fluid Injection", J. Canadian Pet. Tech. (Oct.-Dec., 1967), Vol. 6, 123.
- van Daalen, F. and van Domselaar, H. R.: "Scaled Fluid-Flow Models with Geometry Differing from that of Prototype", Soc. Pet. Eng. J. (June, 1972) 220-228; Trans., AIME, Vol. 253.
- van Dijk, C.: "Steam-Drive Project in the Schoonebeek Field, the Netherlands", J. Pet. Tech. (March, 1968) 295-302; Trans., AIME, Vol. 243.
- van Lookeren, J.: "Calculation Methods for Linear and Radial Steam Flow in Oil Reservoirs", paper SPE 6788 presented at the 52nd Annual Fall Meeting of SPE of AIME, Denver, Colorado, Oct. 9-12, 1977.
- Volek, C. W. and Pryor, J. A.: "Steam Distillation Drive-Brea Field, California", J. Pet. Tech. (August, 1972) 899.
- Weinbrandt, R. M., Ramey, H. J., Jr. and Cassé, F. J.: "The Effect of Temperature on Relative and Absolute Permeability of Sandstones", Soc. Pet. Eng. J. (Oct., 1975) 376-384.
- Weinstein, H. G.: "Semi-Analytical Method for Thermal Coupling of Reservoir and Overburden", Soc. Pet. Eng. J. (Oct., 1972) 439-451; Trans., AIME, Vol. 253.
- Weinstein, H. G.: "Extended Semi-Analytic Method for Increasing and Decreasing Boundary Temperatures", Soc. Pet. Eng. J. (April, 1974) 152-164; Trans., AIME, Vol. 257.

- Whitaker, S.: "Introduction to Fluid Mechanics", Prentice-Hall, Inc., Englewood Cliffs, N.J. (1968) 88.
- Whitaker, S.: "Advances in Theory of Fluid Motion in Porous Media:", in Flow Through Porous Media, American Chemical Society Publications, Washington, D.C. (1970) 31-46.
- Whitham, G. B.: "Linear and Nonlinear Waves", John Wiley & Sons, Inc., New York (1974), Ch. 2.
- Widder, D. V.: "The Heat Equation", Academic Press, New York (1975), Ch. IV.
- Willman, B. T., Valleroy, V. V., Runberg, G. W., Cornelius, A. J. and Powers, L. W.: "Laboratory Studies of Oil Recovery by Steam Injection", J. Pet. Tech. (July, 1961) 681-690; Trans., AIME, Vol. 222.
- Wilson, L. A., Wygal, R. J., Reed, D. W., Gergins, R. L. and Henderson, J. H.: "Fluid Dynamics During an Underground Combustion Process Trans., AIME (1958), Vol. 213, 146-154.
- Wu, C. H.: "A Critical Review of the Steamflood Mechanisms", Paper SPE 6550, presented at the 47th Annual California Regional Meeting of SPE of AIME, Bakersfield, California, April 13-15, 1977.

Nomenclature

- a Asymptotic coefficient of the steam zone volume, defined by Eq. (4.59), dimensionless.
- A Injection parameter, defined by Eq. (4.31), dimensionless.
- A Area, $[L^2]$.
- A_R Geometric parameter for three-dimensional steam flood, defined by Eq. (5.18), dimensionless.
- b Width of the reservoir, $[L]$.
- B_i Parameter related to characteristic time of steam zone growth, $[t^{-1/2}]$.
- B Parameter of the steam zone, defined by Eq. (4.31), dimensionless.
- c Velocity of moving front, dimensionless.
- c_p Specific heat capacity under constant pressure, $[L^2 t^{-2} T^{-1}]$.
- C_i Dimensionless group related to three-dimensional steamflood, defined in Table 14b.
- CCHF Cumulative conductive heat flux to the hot liquid zone, defined by Eq. (5.86), $[mLt^{-3}]$ or $[mL^2 t^{-3}]$.
- CHF Local conductive heat flux to the hot liquid zone, defined by Eq. (5.58a), $[mt^{-3}]$.
- CHL Cumulative heat losses to the surroundings, defined by Eq. (5.49), $[mLt^{-3}]$ or $[mL^2 t^{-3}]$.
- CNHF Cumulative net heat flux to the hot liquid zone, defined by Eq. (5.49), $[mLt^{-3}]$ or $[mL^2 t^{-3}]$.
- d Parameter related to heat losses, defined by Eq. (4.6), $[mL^{-1} t^{-5/2}]$.
- D Dimensionless group related to the steam saturation distribution, defined by Eq. (4.93).

E	Dimensionless group related to the steam saturation distribution, defined by Eq. (4.93).
E_v	Vertical efficiency, defined by Eq. (5.15), dimensionless.
f	Heat capacity term, defined by Eq. (4.6), $[mL^{-1}t^{-2}]$.
f_{st}	Steam quality, dimensionless.
f_i	Fractional volumetric flow of phase i, defined by Eq. (4.89), dimensionless.
g	Acceleration of gravity, $[Lt^{-2}]$.
G	Volume of liquid water generated by steam condensation per unit reservoir volume and time, defined by Eq. (4.83), $[t^{-1}]$.
G_{ij}	Dimensionless group related to three-dimensional steam flood, defined by Eqs. (5.56), (5.59).
h	Thickness of reservoir, $[L]$.
h_i	Specific enthalpy of Phase i, $[L^2t^{-2}]$.
HL	Local heat losses to the surroundings, defined by Eq. (5.50b), $[mt^{-3}]$.
J_i	Dimensionless group related to three-dimensional steamflood, defined in Table 14b.
k	Absolute permeability, $[L^2]$.
k_h	Thermal conductivity, $[mLt^{-3}T^{-1}]$.
k_{ri}	Relative permeability of Phase i, dimensionless.
l	Characteristic length (area) of the steam zone, $[L]$ ($[L^2]$).
L	Length (area), $[L]$ ($[L^2]$).
L_v	Latent heat of vaporization of water, $[L^2t^{-2}]$.
m	Water mass injection rate $[mt^{-1}]$.
M	Volumetric heat capacity, $[mL^{-1}t^{-2}T^{-1}]$.

M_g	Rate of steam condensation per unit reservoir volume and time, defined by Eq. (2.1), $[mL^{-3}t^{-1}]$.
n	Coordinate along the direction normal to a surface, $[L]$.
N	Generalized mobility ratio, defined by Eq. (5.51b), dimensionless.
N_i	Mobility ratio, defined in Table 14b, dimensionless.
NHF	Local net heat flux to the hot liquid zone, defined by Eq. (5.50a), $[mt^{-3}]$.
P	Pressure, $[mL^{-1}t^{-2}]$.
P_{coi}	Capillary pressure between oil and phase i , $[mL^{-1}t^{-2}]$.
Pe	Peclet number, dimensionless.
q	Convective heat flux in radial geometries, defined by Eq. (3.30), $[mLt^{-3}T^{-1}]$.
Q	Conductive heat flux to the hot liquid zone, defined by Eq. (2.49b), $[mt^{-3}T^{-1}]$.
r	Coordinate along the radial direction, $[L]$.
R	Dimensionless group related to heat transfer in the hot liquid zone, defined by Eq. (3.74), dimensionless.
$R(t)$	Radius, $[L]$.
s	Coordinate along the direction parallel to a surface, $[L]$.
S	Saturation, dimensionless.
S_t	Stefan number, dimensionless.
t	Time, $[t]$
T	Temperature, $[T]$.
u	Volumetric velocity per unit reservoir cross section, $[Lt^{-1}]$.
U_o	Volumetric velocity per unit injection area, $[Lt^{-1}]$.
v	Steam front velocity, $[Lt^{-1}]$ or $[L^2t^{-1}]$.
V	Volume, $[L^3]$.

w	Water mass injection rate per unit injection area or unit injection thickness, $[mL^{-2}t^{-1}]$ or $[mL^{-1}t^{-1}]$.
W	Net convective heat flux to the hot liquid zone, defined by Eq. (2.49a), $[mt^{-3}T^{-1}]$.
x	Space coordinate, $[L]$.
X	Steam zone length (area), $[L]$ ($[L^2]$).
y	Space coordinate, $[L]$.
z	Space coordinate, $[L]$.
z_i	Root of Eq. (3.86), dimensionless.
α	Parameter of steam flood, defined by Eq. (5.38), dimensionless.
α_i	Thermal diffusivity of species i , $[L^2t^{-1}]$.
β_i	Parameter of steam flood, defined by Eqs. (5.51a), (5.59a), dimensionless.
γ	Density ratio, ρ_w/ρ_s , dimensionless.
Δ	Entropy source at the steam front, $[mt^{-3}T^{-1}]$.
ΔT	Temperature difference, $T_s - T_i$, $[T]$.
η	Coordinate, $[L]$.
θ	Time coordinate, $[t]$.
Θ	Temperature, $[T]$.
κ	Parameter, defined by Eq. (5.16), dimensionless.
λ	Parameter, defined by Eq. (5.27), dimensionless.
μ	Viscosity, $[mL^{-1}t^{-1}]$.
ξ	Space coordinate, $[L]$.
Π	Perimeter of the steam front.
Π_i	Dimensionless group of steam flood, defined in Table 2.

ρ	Space coordinate, [L].
ρ_i	Density, [mL ⁻³].
σ	Space coordinate, [L].
τ	Time coordinate, [t].
ϕ	Porosity, dimensionless.
$\cdot\phi$	Heat injection rate per unit injection area or unit injection thickness, [mt ⁻³] or [mLt ⁻³].
x	Space coordinate, [L].

Subscripts

D	Refers to dimensionless quantity
f	Rock formation
F	Steam front
Fo,fo	Overburden
Fu,fu	Underburden
i	Initial
inj	Injection point
l	Linear geometry
ML	Related to Marx and Langenheim
n	Normal to a surface
o	Oil
r	Radial geometry
R	Reservoir
s	Steam
w	Water

1	Refers to energy balance
2	Refers to steam balance
α	Refers to a combination of energy and steam balances.
III	Related to Chapter III
IV	Related to Chapter IV

Superscripts

I	Inner side of a surface
II	Outer side of a surface
(1)	Steam zone
(2)	Hot liquid zone
-	Spatial average
0	Stationary
*	Dimensional
+	Upper bounds
-	Lower bounds
^	Refers to uniform notation for both linear and radial geometry.

Script Symbols

A	Area
C	Curve in x,t plane
L	Laplace Transform operator
L_L	Linear operator, defined by Eq. (4.6)
L_{NL}	Non-linear operator, defined by Eq. (4.4)
R	Domain (Reservoir)
V	Volume
Γ	Curve in x,θ plane

APPENDIX I

Consider a fixed arbitrary volume V , enclosing the moving interface $A(t)$, within which the quantity ψ is conserved.

$$\frac{\partial \psi}{\partial t} + \nabla \cdot \underline{q} = 0 \quad (\text{A.1})$$

In the absence of surface sources we integrate (A.1) over V and decompose the resulting integrals to an inner and an outer part, as shown in Figure A-1.

$$\int_V \frac{\partial \psi}{\partial t} dV + \int_{A_t} \underline{q} \cdot \underline{n} dA = 0 \quad (\text{A.2})$$

$$\begin{aligned} \int_{V_1(t)} \frac{\partial \psi}{\partial t} dV + \int_{V_2(t)} \frac{\partial \psi}{\partial t} dV \\ + \int_{A_1(t)} \underline{q}^I \cdot \underline{n} dA + \int_{A_2(t)} \underline{q}^{II} \cdot \underline{n} dA = 0 \end{aligned} \quad (\text{A.3})$$

Applying Leibnitz's rule of integration [Aris (1962)]

$$\int_{V_1(t)} \frac{\partial \psi}{\partial t} dV = \frac{d}{dt} \int_{V_1(t)} \psi dV - \int_{A(t)} \psi \underline{v}_n dA \quad (\text{A.4})$$

$$\int_{V_2(t)} \frac{\partial \psi}{\partial t} dV = \frac{d}{dt} \int_{V_2(t)} \psi dV + \int_{A(t)} \psi^{\text{II}} v_n dA \quad (\text{A.5})$$

and substituting in (A.3) one gets

$$\begin{aligned} \frac{d}{dt} \int_V \psi dV + \int_{A_t} \underline{q} \cdot \underline{n} dA + \int_{A(t)} \underline{q}^{\text{I}} \cdot \underline{n} dA - \int_{A(t)} \underline{q}^{\text{II}} \cdot \underline{n} dA \\ - \int_{A(t)} \psi^{\text{I}} v_n dA + \int_{A(t)} \psi^{\text{II}} v_n dA = 0 \end{aligned} \quad (\text{A.6})$$

For a fixed volume $\frac{d}{dt} \int_V \psi dV = \int_V \frac{\partial \psi}{\partial t} dV$, thus recalling (A.2):

$$\int_{A(t)} \left[\underline{q}_n^{\text{I}} - \psi^{\text{I}} v_n - \underline{q}_n^{\text{II}} + \psi^{\text{II}} v_n \right] dA = 0 \quad (\text{A.7})$$

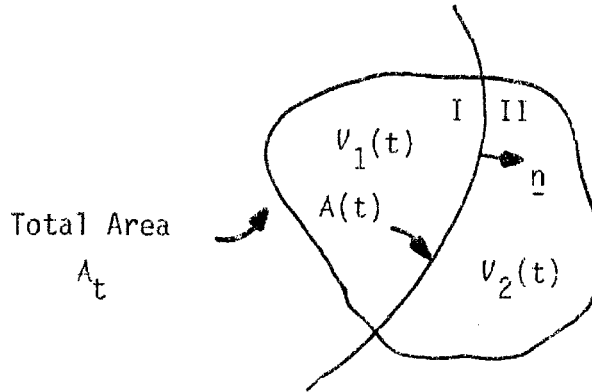


Figure A.1

Now \$V\$ is an arbitrary volume and so is the enclosed area \$A(t)\$. Hence,

(A.7) is valid for any \$A(t)\$, which is possible if and only

$$\underline{q}_n^{\text{I}} - \psi^{\text{I}} v_n = \underline{q}_n^{\text{II}} - \psi^{\text{II}} v_n \quad (\text{A.8})$$

Eq. (A.8) is the desired interfacial condition at any point of the interface.

APPENDIX II

We start the inspectional analysis by considering the partial differential equations and the boundary conditions of Sections 2.3.1, 2.3.2.

Characteristic values for T , S_i , u_{ix} are fixed by the boundary and initial conditions (2.34) - (2.39f).

From the mass balance Eqns. (2.10), (2.3) in combination with the thermodynamic equilibrium expression (2.8) and Darcy's law, we get the non-trivial groups:

$$f_{st} \text{ (steam quality)}, \frac{k_L^{(1)} \left[\rho_s + (\rho_w - \rho_s) f_{st} \right] t^*}{\phi \mu_w \left[L_x^{(1)*} \right]^2}, \frac{\rho_w \rho_s}{\rho_o S_{oi} \left[\rho_s + (\rho_w - \rho_s) f_{st} \right]},$$

$$\text{and the mobility ratios } \left(\frac{\rho_o u_{ox}^*}{\rho_w u_{wx}^*} \right), \left(\frac{u_{wz}^*}{u_{wx}^*} \right), \left(\frac{u_{oz}^*}{u_{wz}^*} \right), \left(\frac{u_{sz}^*}{u_{wz}^*} \right).$$

The energy equations (2.11) and (2.17) produce the groups

$$\left(\frac{w_s L_v^{(1)}}{(w_w + w_s) c_{pw} \Delta T + w_s L_v^{(1)}} \right), \left(\frac{k_{hf} M_1^*}{\rho_f c_{pf} k_{hR}} \right), \left(\frac{c_{po}}{c_{pw}} \right) \quad \text{and}$$

$$\left(\frac{k_{hf} t^*}{(L_z^{(1)*})^2 \rho_f c_{pf}} \right), \frac{\left[(w_w + w_s) c_{pw} \Delta T + w_s L_v^{(1)} \right] t^*}{h L_x^{(1)*} L_z^{(1)*} M_1^* \Delta T}$$

Working on the hot liquid zone equations we derive analogous mobility ratios and the Peclet number inside the hot liquid zone:

$$\frac{(\rho_w c_{pw} u_{wx}^* + \rho_o c_{po} u_{ox}^*) L_x^{(2)*}}{k_{hR}}$$

The interfacial conditons determine the important mobility ratios on both sides of the steam front

$$\left(\frac{\rho_s u_{sn}^I}{\rho_w u_{wn}^I} \right), \quad \left(\frac{\rho_o u_{on}^I}{\rho_w u_{wn}^I} \right), \quad \left(\frac{u_{wn}^{II}}{u_{wn}^I} \right), \quad \left(\frac{\rho_o u_{on}^{II}}{\rho_w u_{wn}^I} \right)$$

and the coupling group at the reservoir-steam zone boundary

$$\left(\frac{k_{hf} \Delta T}{L_z^{(2)*} \rho_s L_v^{(1)*} u_{sz}^*} \right).$$

For scaling purposes we additionally need geometric similarity, constant ϕ and functional similarity in the functions k_{ri} , μ_i , ρ_i , P_{ci} ($i=s,w,o$).

APPENDIX III

Introducing the Weyl transform [Erdélyi et al. (1954)] we rewrite Eq. (3.83) as:

$$\phi(x) = \mu\phi'(x) + \lambda W^{\frac{1}{2}}\{\phi(x)\} \quad (C.1)$$

where $W^{\frac{1}{2}}\{\phi\} \equiv \frac{1}{\sqrt{\pi}} \int_x^\infty \frac{\phi(\sigma)d\sigma}{\sqrt{\sigma-x}}$ is the Weyl transform of ϕ , of order $\frac{1}{2}$.

Let us now take the $W^{\frac{1}{2}}$ transform of (C.1) and rearrange

$$W^{\frac{1}{2}}\{\phi(x)\} = \mu W^{\frac{1}{2}}\{\phi'(x)\} + \lambda \int_x^\infty \phi(\xi)d\xi \quad (C.2)$$

$$\phi(x) - \mu\phi'(x) = \lambda\mu W^{\frac{1}{2}}\{\phi'(x)\} + \lambda^2 \int_x^\infty \phi(\xi)d\xi \quad (C.3)$$

Using the identity

$$\frac{d}{dx} \{W^{\frac{1}{2}}\{\phi(x)\}\} = W^{\frac{1}{2}}\{\phi'(x)\} \quad (C.4)$$

in (C.1) and combining with (C.3) we obtain

$$\phi(x) - \mu\phi'(x) = \mu\left(\phi'(x) - \mu\phi''(x)\right) + \lambda^2 \int_x^\infty \phi(\xi)d\xi \quad (C.5)$$

After differentiation

$$\phi'''(x) - \frac{2}{\mu}\phi''(x) + \frac{1}{\mu^2}\phi'(x) + \frac{\lambda^2}{\mu^2}\phi(x) = 0 \quad (C.6)$$

which is the desired ODE.

APPENDIX IV

Let us consider the general form of the equations discussed in Sections 3.7, 3.8:

$$\frac{\partial T_D}{\partial t_D} + \frac{W_F^0}{|W_F^0|} \cdot \frac{\partial T_D}{\partial x_D} = \frac{1}{R} \cdot \frac{\partial^2 T_D}{\partial x_D^2} - \frac{1}{\sqrt{\pi}} \int_0^{t_D} \frac{\partial T_D}{\partial \tau_D} \cdot \frac{d\tau_D}{\sqrt{t_D - \tau_D}}$$

which can also be rewritten as

$$\frac{\partial T_D}{\partial t_D} + \frac{W_F^0}{|W_F^0|} \cdot \frac{\partial T_D}{\partial x_D} - \frac{1}{R} \cdot \frac{\partial^2 T_D}{\partial x_D^2} = - I^{-1/2} \{T_D\} \quad (D.1)$$

in fractional calculus notation. Since we deal mostly with moving boundary problems, we would like to express the above linear equation under a form which is easier to handle. We operate on both sides of (D.1) with

$$H = \frac{\partial}{\partial t_D} + \frac{W_F^0}{|W_F^0|} \frac{\partial}{\partial x_D} - \frac{1}{R} \frac{\partial^2}{\partial x_D^2}$$

Then,

$$H^2 \{T_D\} = - H I^{-1/2} \{T_D\} \quad (D.2)$$

From known properties of fractional calculus, we can interchange the order of operation in the RHS of (D.2), provided that $T_D(0, x_D) = 0$ [Oldham and Spanier (1974)]. Thus,

$$H^2 \{T_D\} = - I^{-1/2} H \{T_D\} \quad (D.3)$$

and using (D.1) to simplify the RHS of (D.3)

$$H^2 \{T_D\} = I^{-1} \{T_D\} \quad (D.4)$$

or

$$\left[\frac{\partial}{\partial t_D} + \frac{W_F^0}{|W_F^0|} \frac{\partial}{\partial x_D} - \frac{1}{R} \frac{\partial^2}{\partial x_D^2} \right]^2 \{T_D\} = \frac{\partial T_D}{\partial t_D} \quad (D.5)$$

We see that, by increasing the order of the original equation, we are able, due to its convolution character, to get rid of the integral part. Obviously, the two equations (D.1), (D.5) may not be equivalent since every solution of the former satisfies the latter while the opposite may not be true. Nevertheless, a partial differential equation is easier to work with. If we succeed in solving it, we can, then, discard those solutions that do not satisfy the original equation and the boundary conditions.

We can look, for example, at the limiting case $R \rightarrow \infty$ (Section 3.7). Then, (D.5) reduces to:

$$\left(\frac{\partial}{\partial t_D} + \frac{W_F^0}{|W_F^0|} \frac{\partial}{\partial x_D} \right)^2 \{T_D\} = \frac{\partial T_D}{\partial t_D} \quad (D.6)$$

and by the transformation $\chi = x_D$, $\theta = t_D - \frac{W_F^0}{|W_F^0|} x_D$ to

$$\frac{\partial \Theta}{\partial \theta} = \frac{\partial^2 \Theta}{\partial \chi^2}$$

which is exactly Eq. (3.58). To solve the more general Equation (D.5), we attempt a factorization of the form:

$$\left(A \frac{\partial}{\partial t_D} + B \frac{\partial}{\partial x_D} + \frac{\partial^2}{\partial x_D^2} \right) \cdot \left(C \frac{\partial}{\partial t_D} + D \frac{\partial}{\partial x_D} + E \frac{\partial^2}{\partial x_D^2} + F \right) \{T_D\} = 0 \quad (D.7)$$

where A, B, C, D, E, F are constants yet to be determined. It turns out

that this sort of factorization is possible if and only if $R = 1$. Then, (D.7) becomes

$$\left[\frac{\partial}{\partial t_D} + 2 \frac{W_F^0}{|W_F^0|} \frac{\partial}{\partial x_D} - \frac{\partial^2}{\partial x_D^2} - 1 \right] \cdot \left[\frac{\partial}{\partial t_D} - \frac{\partial^2}{\partial x_D^2} \right] \{T_D\} = 0 \quad (D.8)$$

This suggests that for $R = 1$, the dependent variable T_D satisfies either of the two equations

$$\frac{\partial T_D}{\partial t_D} = \frac{\partial^2 T_D}{\partial x_D^2} \quad (D.9a)$$

$$\frac{\partial T_D}{\partial t_D} + 2 \frac{W_F^0}{|W_F^0|} \frac{\partial T_D}{\partial x_D} = \frac{\partial^2 T_D}{\partial x_D^2} + T_D \quad (D.9b)$$

To select the proper solution we check the Laplace Transform, thus confirming that (D.9a) is the governing equation, when $W_F^0 > 0$, while (D.9b) is the proper equation when $W_F^0 < 0$, as indeed postulated in Section 3.8. From (D.5) we can also derive the steady-states obtained in Section 3.8. Other particular solutions, for arbitrary R , may be possible by some ingenious transformation of (D.5).

Useful information about the solution of (D.1) can also be obtained from the use of the Laplace Transform. The transformed variable becomes:

$$L_t\{T_D\} = A(s) \exp \left\{ \frac{R x_D}{2} \left[\frac{W_F^0}{|W_F^0|} - \frac{2}{\sqrt{R}} \left(\frac{R}{4} + \sqrt{s} + s \right)^{1/2} \right] \right\} \quad (D.10)$$

We would like to find a value for R such that, for example,

$$\sqrt{\frac{R}{4} + \sqrt{s} + s} = B + \sqrt{s}$$

with B a constant. Carrying out the calculations, we confirm that this is possible only if $R = 1$. Then, (D.10) becomes

$$L_t\{T_D\} = A(s) \exp \left\{ \frac{x_D}{2} \left[\frac{w_F^0}{|w_F^0|} - 1 \right] - x_D \sqrt{s} \right\} \quad (D.11)$$

which can be inverted to either (D.9a) or (D.9b), as already proved.

The above technique may be employed to the solution of other linear integro-differential equations, as well.

APPENDIX V

Using the defining Equation (4.12) and the inequality (4.11), one obtains, for $j=1,2$

$$\begin{aligned} \frac{d}{dt} \int_0^{X_F(t)} f_j(x, t; X_F(t)) dx + \frac{d}{\sqrt{t}} X_F(t) < \frac{d}{dt} \int_0^{X_j^+(t)} f_j(x, t; X_F(t)) dx \\ + \frac{d}{\sqrt{t}} X_j^+(t) \quad \forall 0 < t \end{aligned} \quad (E.1)$$

Thus,

$$\begin{aligned} \frac{d}{dt} \left[\int_0^{X_j^+(t)} f_j(x, t; X_F(t)) dx - \int_0^{X_F(t)} f_j(x, t; X_F(t)) dx \right] \\ + \frac{d}{\sqrt{t}} (X_j^+(t) - X_F(t)) > 0 \end{aligned} \quad (E.2)$$

Introducing the variables $\tau = \sqrt{t}$, $u(\tau) = X_j^+(t) - X_F(t)$ we get

$$\frac{d}{d\tau} \left[\int_0^{u(\tau)} f_j(x + X_F(\tau), \tau; X_F(\tau)) dx \right] + au(\tau) = g(\tau) > 0 \quad \forall 0 < \tau \quad (E.3)$$

where $a = 2d$ and $g(\tau)$ a positive function $\forall \tau > 0$. By definition

$u(0) = 0$, thus from (E.3) one can easily deduce

$$\left. \frac{d}{d\tau} \left[\int_0^{u(\tau)} f_j(x + X_F(\tau), \tau; X_F(\tau)) dx \right] \right|_{\tau=0} > 0$$

hence, $u(\tau) > 0$ in the neighborhood of $\tau = 0$. We will show that $u(\tau) > 0$

$\forall 0 < \tau$. We integrate (E.3),

$$\int_0^{u(\tau)} f_j(x + X_F(\tau), \tau; X_F(\tau)) dx + a \int_0^\tau u(\lambda) d\lambda = \int_0^\tau g(\lambda) d\lambda > 0 \quad \forall 0 < \tau \quad (\text{E.4})$$

Let us assume for a moment that $u(\tau_c) = 0$ for some $\tau_c > 0$, with $\dot{u}(\tau_c) < 0$. Then for every $\tau' > \tau_c$, in some neighborhood of τ_c , we have $u(\tau') < 0$. It follows then from (E.4)

$$a \int_0^{\tau_c} u(\lambda) d\lambda = \int_0^{\tau_c} g(\lambda) d\lambda > 0 \quad (\text{E.5})$$

$$\int_0^{u(\tau')} f_j(x + X_F(\tau'), \tau'; X_F(\tau')) dx + a \int_0^{\tau'} u(\lambda) d\lambda = \int_0^{\tau'} g(\lambda) d\lambda > 0 \quad (\text{E.6})$$

Rearranging (E.6) and taking into account (E.5):

$$\int_{u(\tau_c)}^{u(\tau')} f_j(x + X_F(\tau'), \tau'; X_F(\tau')) dx + a \int_{\tau_c}^{\tau'} u(\lambda) d\lambda = \int_{\tau_c}^{\tau'} g(\lambda) d\lambda > 0 \quad (\text{E.7})$$

By hypothesis $u(\tau_c) = 0$, $u(\lambda) < 0$ for every $\tau_c < \lambda \leq \tau'$. Also, $f_j > 0$ from physical considerations. Thus, the LHS of (E.7) is negative whereas the RHS is positive, which is incompatible. Therefore the hypothesis is not true; hence, $u(\tau) > 0 \quad \forall 0 < \tau$. In terms of the original variables:

$$X_j^+(t) > X_F(t) \quad \forall 0 < t \quad j=1,2 \quad (\text{E.8})$$

as postulated in Subsection 4.3.1.

APPENDIX VI

Consider the function $f(x)$

$$f(x) = x - 1 + \exp(-x) - \frac{2}{\pi} \left[x - 1 + \exp\left(\frac{\pi x^2}{4}\right) \operatorname{erfc}\left(\frac{\sqrt{\pi}x}{2}\right) \right], \quad 0 < x \quad (\text{F.1})$$

$$f(0) = 0.$$

We will show that $f(x) > 0$, $\forall x > 0$. Successive differentiation of $f(x)$ gives

$$f'(x) = 1 - \exp(-x) - x \exp\left(\frac{\pi x^2}{4}\right) \operatorname{erfc}\left(\frac{\sqrt{\pi}x}{2}\right) \quad (\text{F.2a})$$

$$f'(0) = 0 \quad (\text{F.2b})$$

$$f''(x) = \exp(-x) - \exp\left(\frac{\pi x^2}{4}\right) \operatorname{erfc}\left(\frac{\sqrt{\pi}x}{2}\right) \quad (\text{F.3b})$$

$$- \frac{\pi}{2} x^2 \exp\left(\frac{\pi x^2}{4}\right) \operatorname{erfc}\left(\frac{\sqrt{\pi}x}{2}\right) + x \quad (\text{F.3a})$$

$$f''(0) = 0$$

$$f'''(x) = -\exp(-x) - \frac{3\pi}{2} x \exp\left(\frac{\pi x^2}{4}\right) \operatorname{erfc}\left(\frac{\sqrt{\pi}x}{2}\right) + 2$$

$$- \frac{\pi^2}{4} x^3 \exp\left(\frac{\pi x^2}{4}\right) \operatorname{erfc}\left(\frac{\sqrt{\pi}x}{2}\right) + \frac{\pi}{2} x^2 \quad (\text{F.4a})$$

$$f'''(0) = 1 > 0. \quad (\text{F.4b})$$

From (F.4b), $f(x) > 0$ in the right neighborhood of the origin. Also, it is easily verified that

$$\frac{2}{\pi x} f'(x) - f(x) = 1 - e^{-x} - x + \frac{2}{\pi} (x - 1) + \frac{2}{\pi x} (1 - e^{-x}) \quad (\text{F.5})$$

Therefore,

$$\frac{2}{\pi x} f'(x) - f(x) > 0 \quad 0 < x < x_0 \quad (\text{F.6a})$$

$$\frac{2}{\pi x} f'(x) - f(x) < 0 \quad x_0 < x \quad (\text{F.6b})$$

where x_0 is the positive root of the RHS of (F.5):

$$g(x) \equiv x(x-1) \left(\frac{2}{\pi} - 1 \right) + \frac{2}{\pi} - e^{-x} \left(\frac{2}{\pi} + x \right) \quad (\text{F.7})$$

From a numerical calculation, $x_0 \approx 1.18$.

If $f(x)$ were non-positive for some value of x in $0 < x \leq x_0$, then it would have a positive maximum at some point ξ in $0 < \xi < x_0$ because $f(x)$ is positive in the right neighborhood of the origin and $f(0) = 0$.

Therefore,

$$f'(\xi) = 0, \quad f(\xi) > 0 \quad \text{for some} \quad 0 < \xi < x_0,$$

which contradicts (F.6a). Hence, $f(x) > 0 \quad \forall 0 < x \leq x_0$.

Similarly, if $f(x)$ were non-positive for some value of $x > x_0$, then $f(x)$ would have a negative minimum, since $f(x) \sim x \left(1 - \frac{2}{\pi} \right)$ as $x \rightarrow \infty$. Hence, there would be an η such that

$$f'(\eta) = 0, \quad f(\eta) < 0 \quad \text{for some} \quad x_0 < \eta,$$

which contradicts (F.6b). Therefore $f(x) > 0 \quad \forall x_0 < x$.

We thus proved that

$$f(x) > 0 \quad \forall 0 < x \quad (\text{F.8})$$

Rearranging (F.8), we obtain

$$\exp(x^2)\operatorname{erfc}x < \left(\frac{2x}{\sqrt{\pi}} - 1\right) \left(\frac{\pi}{2} - 1\right) + \frac{\pi}{2} \exp\left(-\frac{2x}{\sqrt{\pi}}\right), \quad \forall x > 0 \quad (\text{F.9})$$

This inequality provides a better upper bound to the function $\exp(x^2)\operatorname{erfc}x$ than the bound reported by Abramowitz and Stegun (1965) in $0 < x < 0.53$ and the bound derived by Boyd (1959) in $0 < x \leq 0.15$.

APPENDIX VII

Using the defining Equation (4.47) and inequality (4.46) one obtains

$$\frac{d}{dt} \left[\int_0^{x_F(t)} f_2(x, t; x_F(t)) dx - \int_0^{x_2^-(t)} f_2(x, t; x_F(t)) dx \right] + d \int_0^t \frac{[\dot{x}_F(\lambda) - \dot{x}_2^-(\lambda)]}{\sqrt{t - \lambda}} d\lambda > 0 \quad (G.1)$$

$$\forall t > t_c$$

where t_c is the time after which (4.46) is valid. Introducing the variable $u(t) = x_F(t) - x_2^-(t)$, we get

$$\frac{d}{dt} \left[\int_0^{u(t)} f_2(x + x_2^-(t), t; x_F(t)) dx \right] + d \int_0^t \frac{\dot{u}(\lambda) d\lambda}{\sqrt{t - \lambda}} = g(t) > 0 \quad (G.2)$$

$$\forall t > t_c$$

where $g(t)$ is positive $\forall t > t_c$. Integrating (G.2) and recalling that $u(0) = 0$, we get

$$\int_0^{u(t)} f_2(x + x_2^-(t), t; x_F(t)) dx + d \int_0^t \frac{u(\lambda) d\lambda}{\sqrt{t - \lambda}} = \int_0^t g(\lambda) d\lambda \quad (G.3)$$

We will show that $u(t) > 0$ for sufficiently large t . Assume that $u(t) < 0 \forall 0 < t$. Then, the LHS of (G.3) is negative while the RHS is positive for sufficiently large t , since

$$\int_0^t g(\lambda) d\lambda = \int_0^{t_c} g(\lambda) d\lambda + \int_{t_c}^t g(\lambda) d\lambda$$

and $g(t) > 0 \quad \forall t > t_c$. Hence, the hypothesis is false. Let us, next, assume that $u(t_a) = 0$, at some time t_a , and remains negative thereafter: $u(t) < 0 \quad \forall t > t_a$. Rearranging (G.3)

$$\begin{aligned} \int_0^{u(t)} f_2(x + x_2^-(t), t; x_F(t)) dx + d \int_{t_c}^t \frac{u(\lambda) d\lambda}{\sqrt{t - \lambda}} \\ = \int_{t_c}^t g(\lambda) d\lambda + \int_0^{t_c} g(\lambda) d\lambda - d \int_0^{t_c} \frac{u(\lambda) d\lambda}{\sqrt{t - \lambda}} \end{aligned} \quad (G.4)$$

By hypothesis, the LHS of (G.4) is negative. The RHS is the sum of a continuously increasing, a constant and a continuously decreasing to zero terms. Therefore, for sufficiently large times, the RHS becomes positive contradicting the hypothesis.

We conclude that there is some time t_b , such that

$$u(t) > 0 \quad \forall t > t_b$$

and in terms of the original variables

$$x_F(t) > x_2^-(t) \quad \forall t > t_b \quad (G.5)$$

as postulated in Section 4.4.

APPENDIX VIII

When $R = 1$, the steam mass balance, Eq. (4.2), reads:

$$2B\dot{\chi}_{FD}(t_D) - \frac{2(1-A)^2}{\pi} \left(\frac{M^{(2)}}{M_1} \right) \frac{\partial T_D}{\partial x_D} + \int_0^{t_D} \left(- \frac{\partial T_f}{\partial n} \right)_D \dot{\chi}_{FD}(\lambda_D) d\lambda_D = A \quad (H.1)$$

Combining (4.57), (3.99), (4.55a,b), (4.56) we get for the temperature in the hot liquid zone:

$$T_D(t_D, x_D) = \operatorname{erfc} \left\{ \frac{\sqrt{\pi}}{2(1-A)} \cdot \frac{x_D}{\sqrt{t_D}} \right\} / \operatorname{erfc} b \quad (H.2)$$

and the conductive heat flux at the origin given by Eq. (3.100) becomes

$$\frac{\partial T_D}{\partial x_D} = - \frac{\exp(-b^2)}{(1-A)\sqrt{t_D} \operatorname{erfc} b} \quad (H.3)$$

In the new notation, Eq. (3.13) is

$$\left(- \frac{\partial T_f}{\partial n} \right)_D = \int_0^{\lambda_D} \frac{\partial T_D}{\partial \tau_D} \cdot \frac{d\tau_D}{\sqrt{t_D - \tau_D}} = I_3(t_D, \lambda_D) \quad (H.4)$$

The integral $I_3(t_D, \lambda_D)$ is evaluated in Appendix IX

$$I_3(t_D, \lambda_D) = \frac{\exp \left\{ -b^2 \frac{\lambda_D}{t_D} \right\}}{\sqrt{t_D}} \cdot \frac{\operatorname{erfc} \left\{ b \sqrt{1 - \frac{\lambda_D}{t_D}} \right\}}{\operatorname{erfc} b} \quad (H.5)$$

Substituting in (H.1), we obtain the integral equation:

$$2B\dot{\chi}_{FD}(t_D) + \frac{2(1-A)}{\pi} \left(\frac{M^{(2)}}{M_1} \right) \frac{\exp(-b^2)}{\operatorname{erfcb}} \cdot \frac{1}{\sqrt{t_D}} + \int_0^{t_D} \dot{\chi}_{FD}(\lambda_D) I_3(t_D, \lambda_D) d\lambda_D = A \quad (\text{H.6})$$

Since we have already assumed $\dot{\chi}_{FD}(t_D) \sim \frac{a}{\sqrt{t_D}}$, (H.6) becomes:

$$2B \frac{a}{\sqrt{t_D}} + \frac{2(1-A)}{\pi R} \left(\frac{M^{(2)}}{M_1} \right) \frac{\exp(-b^2)}{\operatorname{erfcb}} \cdot \frac{1}{\sqrt{t_D}} + a \int_0^{t_D} \frac{I_3(t_D, \lambda_D)}{\sqrt{\lambda_D}} d\lambda_D \sim A \quad (\text{H.7})$$

Collecting terms of the same order:

$$\frac{a \exp(-b^2)}{\operatorname{berfcb}} \int_0^{b^2} \frac{\exp(\omega) \operatorname{erfc}\sqrt{\omega} d\omega}{\sqrt{b^2 - \omega}} = A \quad (\text{H.8})$$

From Appendix IX we obtain

$$I_4 = \int_0^{b^2} \frac{\exp(\omega) \operatorname{erfc}\sqrt{\omega} d\omega}{\sqrt{b^2 - \omega}} = \sqrt{\pi} (1 - \exp(b^2) \operatorname{erfcb}) \quad (\text{H.9})$$

Substituting in (H.8) we find that a satisfies the algebraic equation

$$a = \frac{bA}{\sqrt{\pi}} \left[\frac{\exp(b^2) \operatorname{erfcb}}{1 - \exp(b^2) \operatorname{erfcb}} \right] \quad (\text{H.10})$$

i.e., exactly as in Subsection 4.5.2.1, where $R \rightarrow \infty$.

Here, since $R = O(1)$, the convergence depends primarily on the heat flux to the hot liquid zone. The asymptotic state is reached when

$$\frac{2}{\pi R} \left(\frac{M^{(2)}}{M_1} \right) \frac{1}{\sqrt{t_D}} < \varepsilon.$$

For $\varepsilon = 0.05$, the above imply that the convergence is extremely slow, attained for $t_D > 165$.

APPENDIX IX

Consider the function

$$f(t, x) = \operatorname{erfc} \left\{ \frac{x}{2\sqrt{t-x}} \right\} H(t-x) \quad (I.1)$$

and form the integral

$$J_1(t, \lambda) = \int_0^\lambda \frac{\partial f}{\partial \tau} \frac{d\tau}{\sqrt{t-\tau}} \quad 0 < \lambda < t \quad (I.2)$$

From (I.1), (I.2)

$$J_1(t, \lambda) = \frac{1}{2\sqrt{\pi}} \int_x^\lambda \frac{x}{(\tau-x)^{3/2}} \frac{\exp\left[-\frac{x^2}{4(\tau-x)}\right]}{(t-\tau)^{1/2}} d\tau \quad (I.3)$$

Using the transformation $y = \frac{x^2}{4(\tau-x)}$, (I.3) becomes:

$$J_1(t, \lambda) = \frac{1}{\sqrt{\pi}} \int_{\frac{x^2}{4(\lambda-x)}}^{\infty} \frac{\exp(-y) dy}{\sqrt{t-x} \cdot \sqrt{y - \frac{x^2}{4(t-x)}}} \quad (I.4)$$

and by further setting $z = y - \frac{x^2}{4(t-x)}$ we obtain:

$$\begin{aligned} J_1(t, \lambda) &= \frac{\exp\left[-\frac{x^2}{4(t-x)}\right]}{\sqrt{\pi} \sqrt{t-x}} \int_{\left[\frac{x^2}{4(\lambda-x)} - \frac{x^2}{4(t-x)}\right]}^{\infty} \frac{\exp(-z) dz}{\sqrt{z}} \\ &= \frac{1}{\sqrt{t-x}} \exp\left[-\frac{x^2}{4(t-x)}\right] \operatorname{erfc}\left[\frac{x}{2} \sqrt{\frac{t-\lambda}{(t-x)(\lambda-x)}}\right] \end{aligned} \quad (I.5)$$

By suitably substituting x by $\frac{\pi}{2(1-A)} \frac{M_1}{M(2)} x_D$, t by $\frac{\pi}{4} \left(\frac{M_1}{M(2)}\right)^2 t_D$ and

setting $I_1(t_D, \lambda_D) = \frac{J_1(t, \lambda)}{\text{erfc}b}$ we recover the desired expression (4.64).

Consider, now, the integral

$$J_2(t) = \int_0^t \frac{w(\lambda)}{\sqrt{t-x}} \exp \left[-\frac{x^2}{4(t-x)} \right] \text{erfc} \left[\frac{x}{2} \frac{\sqrt{t-\lambda}}{\sqrt{(t-\lambda)(\lambda-x)}} \right] d\lambda \quad (1.6)$$

where $x = 2\alpha\sqrt{\lambda + \alpha^2} - 2\alpha^2$ is a function of the dummy variable λ and $w(\lambda) = \alpha/\sqrt{\lambda + \alpha^2}$. Introducing the new dummy variable, $\sigma = \frac{x}{2\sqrt{t-x}}$, we find that λ is implicitly defined by the equation

$$\sqrt{\lambda + \alpha^2} = \frac{\alpha^2\lambda + 2\alpha^4 - 2\alpha^2\sigma^2 - t\sigma^2}{2\alpha(\alpha^2 - \sigma^2)} \quad (1.7)$$

and then (1.6) becomes

$$J_2(t) = \int_0^\alpha \frac{\alpha}{\sqrt{\lambda + \alpha^2}} \cdot \frac{\exp(-\sigma^2)}{\sqrt{t-x}} \text{erfc} \left[\sigma \sqrt{\frac{t-\lambda}{\lambda-x}} \right] \frac{d\lambda}{d\sigma} d\sigma \quad (1.8)$$

Using (1.7) to evaluate $\frac{d\lambda}{d\sigma}$, we further obtain

$$J_2(t) = \int_0^\alpha \frac{2\alpha^2}{(x + 2\alpha^2)} \frac{\exp(-\sigma^2)}{\sqrt{t-x}} \text{erfc} \left[\sigma \sqrt{\frac{t-\lambda}{\lambda-x}} \right] \frac{(x + 2\alpha^2)}{2\alpha^2} \frac{4(t-x)^{3/2}}{(2t-x)} d\sigma$$

which simplifies to:

$$J_2(t) = 4 \int_0^\alpha \exp(-\sigma^2) \text{erfc} \left[\sqrt{\alpha^2 - \sigma^2} \right] \frac{(t-x)}{(2t-x)} d\sigma \quad (1.9)$$

Let us define

$$\phi = \frac{t-x}{2t-x} \quad (1.10)$$

Employing (I.7) and substituting for x in terms of λ we get after lengthy calculations

$$\phi = \frac{1}{2} \pm \frac{\sigma}{2\sqrt{\sigma^2 + t}} \quad (\text{I.11})$$

(where the selection of the proper sign is not important in our case) and further

$$J_2(t) = 4 \int_0^\alpha \exp(-\sigma^2) \operatorname{erfc} \left[\sqrt{\alpha^2 - \sigma^2} \right] \left[\frac{1}{2} \pm \frac{\sigma}{2\sqrt{\sigma^2 + t}} \right] d\sigma \quad (\text{I.12})$$

We have, thus, reduced the original expression (I.6) to a single function of t . To evaluate the asymptotic behavior of $J_2(t)$, we note that at sufficiently large t , say $t > 10\alpha^2$, the main contribution to the integral comes from the first term of ϕ . Therefore,

$$J_2(t) \sim 2 \int_0^\alpha \exp(-\sigma^2) \operatorname{erfc} \left[\sqrt{\alpha^2 - \sigma^2} \right] d\sigma \quad t > 10\alpha^2 \quad (\text{I.13})$$

The integral on the RHS is easily evaluated, since

$$\begin{aligned} J_3 &= \int_0^{\alpha^2} \exp(-\sigma^2) \operatorname{erfc} \left[\sqrt{\alpha^2 - \sigma^2} \right] d\sigma \\ &= \frac{1}{2} \exp(-\alpha^2) \int_0^{\alpha^2} \frac{\exp(z) \operatorname{erfc}(\sqrt{z}) dz}{\sqrt{\alpha^2 - z}} \end{aligned} \quad (\text{I.14})$$

and from (I.23), we get

$$\int_0^{\alpha^2} \frac{\exp(z) \operatorname{erfc}(\sqrt{z}) dz}{\sqrt{\alpha^2 - z}} = \sqrt{\pi} \left[1 - \exp(\alpha^2) \operatorname{erfc}(\sqrt{\alpha}) \right] \quad (\text{I.15})$$

Thus, if we substitute (I.15) in (I.14) and (I.13), we conclude that

$$J_2(t) \sim \sqrt{\pi} \exp(-\alpha^2) [1 - \exp(\alpha^2) \operatorname{erfc} \alpha] \quad t > 10\alpha^2 \quad (\text{I.16})$$

The desired expression (4.68) follows directly if we replace x by

$$\frac{\pi}{2(1-A)} \cdot \frac{M_1}{M(2)} x_D, \quad t \text{ by } \frac{\pi}{4} \left(\frac{M_1}{M(2)} \right)^2 t_D, \quad \alpha \text{ by } a \text{ and set } I_2(t_D) = \frac{J_2(t)}{\operatorname{erfc} b}.$$

To evaluate $I_3(t, \lambda)$, we let

$$f(t, \lambda) = \operatorname{erfc} \left(\alpha \sqrt{\frac{\lambda}{t}} \right) \quad \alpha > 0 \quad \lambda < t \quad (\text{I.17})$$

and consider the integral

$$J_3(t, \lambda) = \int_0^\lambda \frac{\partial f}{\partial \tau} \frac{d\tau}{\sqrt{t-\tau}} \quad (\text{I.18})$$

From (I.17), (I.18)

$$J_3(t, \lambda) = \frac{\alpha \sqrt{\lambda}}{\sqrt{\pi}} \int_0^\lambda \frac{\exp[-\alpha^2 \lambda / \tau]}{\tau^{3/2} (t-\tau)^{1/2}} d\tau \quad (\text{I.19})$$

Using the transformation: $\sigma^2 = \alpha^2 \lambda \left(\frac{1}{\tau} - \frac{1}{t} \right)$, we get

$$J_3(t, \lambda) = 2 \exp \left(-\alpha^2 \frac{\lambda}{t} \right) \int_{\alpha \sqrt{1-\frac{\lambda}{t}}}^\infty \exp(-\tau^2) d\tau = \frac{1}{\sqrt{t}} \exp \left(-\alpha^2 \frac{\lambda}{t} \right) \operatorname{erfc} \left(\alpha \sqrt{1-\frac{\lambda}{t}} \right) \quad (\text{I.20})$$

If we, now, substitute x by $2a\sqrt{\lambda_D}$, t by t_D , α by $\frac{\sqrt{\pi}a}{(1-A)}$ and set

$I_3(t_D, \lambda_D) = \frac{J_3(t, \lambda)}{\operatorname{erfc} b}$ we obtain the desired expression (H.5). Finally, let

$$J_4(x) = \int_0^x \frac{\exp(\omega) \operatorname{erfc}(\sqrt{\omega})}{\sqrt{x - \omega}} d\omega \quad (1.21)$$

Taking the Laplace Transform of $J_4(x)$ with respect to x , we have:

$$\bar{J}_4(s) = \frac{\sqrt{\pi}}{s(1 + \sqrt{s})} \quad (1.22)$$

which after inversion leads to:

$$J_4(x) = \sqrt{\pi} [1 - \exp(x) \operatorname{erfc}(\sqrt{x})] \quad (1.23)$$

exactly as in (H.9)

APPENDIX X

Using the defining Equation (5.12) and the dimensionless form of inequality (5.9) one obtains, for $j = 1, 2$

$$2 \frac{B_j}{B_1} \dot{A}_{jD}^+(t_D) + \frac{1}{\sqrt{t_D}} F_D(A_{jD}^+(t_D)) > 2 \frac{B_j}{B_1} \dot{A}_D(t_D) + \frac{1}{\sqrt{t_D}} F_D(A_D(t_D)) \quad (J.1)$$

$\forall 0 < t$

Thus

$$2 \frac{B_j}{B_1} [\dot{A}_{jD}^+(t_D) - \dot{A}_D(t_D)] + \frac{1}{\sqrt{t_D}} [F_D(A_{jD}^+(t_D)) - F_D(A_D(t_D))] > 0 \quad (J.2)$$

$\forall 0 < t$

Introducing the variables $\tau = \frac{B_1}{B_j} \sqrt{t_D}$, $u(\tau) = A_{jD}^+(t_D) - A_D(t_D)$, we get

$$\dot{u}(\tau) + F_D(u(\tau) + A_D(t_D)) - F_D(A_D(t_D)) > 0 \quad \forall 0 < \tau \quad (J.3)$$

By definition, $A_{jD}^+(0) = A_D(0)$, thus from (J.3) one deduces $\dot{u}(0) > 0$ and therefore $u(\tau) > 0$ in the neighborhood of $\tau = 0$. We will show that $u(\tau) > 0 \quad \forall 0 < \tau$.

Assume for a moment that $u(\tau_c) = 0$ for some $\tau_c > 0$, with $\dot{u}(\tau_c) < 0$. Then, for every $\tau' > \tau_c$ in some neighborhood of τ_c , we have $\dot{u}(\tau') < 0$, $\dot{u}(\tau') < 0$. But $F(x)$ is an increasing function of x , therefore

$$F_D(u(\tau') + A_D(t_D)) - F_D(A_D(t_D)) < 0 \quad (J.4)$$

and also $\dot{u}(\tau') < 0$. Hence, the LHS of (J.3) is negative in contradiction with (J.3). This proves that the hypothesis is not true and

$$A_{jD}^+(t_D) > A_D(t_D) \quad \forall 0 < t_D \quad j=1,2 \quad (J.5)$$

as postulated in Subsection 5.3.2.